BIOPHYSICAL CHARACTERIZATION OF PEPTIDE MIMICS OF LUNG SURFACTANT PROTEIN-B

By

VIJAY C. ANTHARAM

A DISSERTATION PRESENTED TO THE GRADUATE SCHOOL
OF THE UNIVERSITY OF FLORIDA IN PARTIAL FULFILLMENT
OF THE REQUIREMENTS FOR THE DEGREE OF
DOCTOR OF PHILOSOPHY

UNIVERSITY OF FLORIDA

2008

To my Mom.

ACKNOWLEDGMENTS

I thank my mentor Dr. Joanna Long for providing me the opportunity for working in her laboratory. I thank her for her support, patience, sense of humor, and kindness. I hope to acquire some of those qualities that she has as I continue to mature and develop. I would also like to offer my gratitude to members of my committee: Dr. Arthur Edison, Dr. Robert McKenna, Dr. Susan Frost and Dr. Ron Castellano. I appreciate their support and their help. I am particularly grateful for Dr. Susan Frost for giving me some extra support with regards to my presentation and for her willingness to afford some of her time to look over my dissertation.

I want to extend my heartfelt gratitude and sincere thanks to members of the laboratory throughout these years. These include Dr. Frank Mills, Dr. Mini-Samuel Landtiser, Dr. Doug Elliott, Seth McNeill, Suzanne Farver, David Fleishmann, Julie Vanni, Joanne Anderson, and Jonathan Lane. I also want to thank some very special people I have met: Sonny Flores, Nelson Klahr, Saurav Chandra, Karen vonDeneen and Mariam Rahmani. I am grateful and fortunate to have known Sonny, Nelson, Jonathan, and especially Mariam--all of them are very special to me.

Lastly, I thank my family members, mainly my mother Urmila Antharam. I feel very blessed and grateful for all that they have done for me.

TABLE OF CONTENTS

page

LIST OF TABLES

LIST OF FIGURES

LIST OF ABBREVIATIONS

AAA	amino acid analysis
AP	alveolar proteinosis
BAL	bronchoalveolar lavage
B_o	external magnetic field
C-D	carbon-deuterium bond
C_p^{max}	maximum heat capacity
CD	circular dichroism
CPAP	continuous positive airway pressure
CPMAS	cross polarization with magic angle spinning
CSA	chemical shift anisotropy
CU	cooperativity unit
D or d	deuterium atom (^2H)
DPPC	1,2-Dipalmitoyl-s*n*-Glycero-3-Phosphocholine
DRAWS	dipolar recoupling with a windowless sequence
DSC	differential scanning calorimetry
E_o	electric field vector
FTIR	Fourier-transform infrared spectroscopy
P	pressure across alveoli
γ_m	gyromagnetic ratio of a NMR nucleus
ΔG^o	change in Gibbs free energy (standard state)
ΔH_{cal}	change in calorimetric enthalpy
ΔH_{vH}	change in van Hoft enthalpy
$\Delta\sigma$	change in shift in ppm
HFOV	high frequency oscillatory ventilation

HPLC	high performance liquid chormatography
ITC	isothermal titration calorimetry
KL_4	KLLLLKLLLLKLLLLKLLLLK (sinapultide)
LUVs	large unilamellar vesicles
L_α	gel phase of phospholipid bilayer
L_β	liquid-crystalline phase of phospholipid bilayer
MLVs	multilamellar vesicles
NMR	nuclear magnetic resonance
P_β	ripple phase of a phospholipid bilayer
PA	palmitic acid
PDB	protein data bank
POPC	1-Palmitoyl-2-Oleoyl-*sn*-Glycero-3-Phosphocholine
POPG	1-Palmitoyl-2-Oleoyl-*sn*-Glycero-3-[Phospho-*rac*-(1-glycerol)]
R	universal gas constant (1.987 cal K^{-1} mol^{-1})
rad	radians
RDS	respiratory distress syndrome
$<S^i_{CD}>$	time averaged order parameter of a C-D bond at position *i*
ssNMR	solid-state NMR
SP-A	Lung surfactant protein A
SP-B	Lung surfactant protein B
SP-C	Lung surfactant protein C
SP-D	Lung surfactant protein D
SUVs	small unilamellar vesicles
ΔS	change in entropy
γ_p	surface tension

T_m	phase transition temperature
$\Delta T_{½}$	peak-width at half height in a DSC trace

Abstract of Dissertation Presented to the Graduate School
of the University of Florida in Partial Fulfillment of the
Requirements for the Degree of Doctor of Philosophy

BIOPHYSICAL CHARACTERIZATION OF PEPTIDE MIMICS OF LUNG SURFACTANT PROTEIN-B

By

Vijay C. Antharam

May 2008

Chair: Joanna R Long
Major: Medical Sciences-Biochemistry and Molecular Biology

Lung surfactant is a lipid rich fluid that coats the inner surface of the alveoli, the primary units of respiration where oxygen diffuses into the bloodstream. Due to the small radii and high curvature of the alveoli, significant pressure is required to overcome surface tension and to inflate the lung. Lung surfactant is a biological coating that lowers surface tension and minimizes the work required for breathing. It is primarily composed of two phospholipids, the zwitterionic 1,2-dipalmitoyl-*sn*-Glycero-3-Phosphocholine (DPPC) and the anionic 1-Palmitoyl-2-Oleoyl-*sn*-Glycero-3-[Phospho-*rac*-(1-glycerol)] (POPG). The 79-amino acid surfactant protein B (SP-B), however, is an absolutely essential component of lung surfactant. Although present at low levels (approximately 1% by weight), mutation or loss of SP-B results in respiratory distress syndrome (RDS).

The design of simple peptides to mimic the charge distribution and the hydrophobic characteristics of SP-B was investigated in the early 1990s. A peptide composed of only the basic residue lysine and hydrophobic leucine systematically repeated (KLLLLKLLLLKLLLLKLLLLK) has demonstrated clinical efficacy in the treatment of RDS when administered with DPPC, POPG and palmitic acid.

In this dissertation, solid-state NMR spectroscopy (ssNMR) was used to examine in detail the phase properties of these lipids and the effects of KL_4 on lipid organization and dynamics. Structural measurements were also performed to determine the secondary structure of KL_4. These studies were carried out using two model lipid systems: 1) 3:1 POPC: POPG, a bilayer system used in many studies probing peptide:lipid interactions, including amphipathic antibiotics of similar size and hydrophobicity to KL_4, and 2) 4:1 DPPC:POPG, which is similar to the lipid composition in the lung. Complementary studies using differential scanning calorimetry (DSC) and circular dichroism (CD) were also carried out. Comparative experiments were also performed on residues 59-80 of SP-B ($SP\text{-}B_{59\text{-}80}$), the C-terminal region upon which the sequence of KL_4 was derived.

Based on these studies, a molecular model incorporating the structure of KL_4 and its interactions with 3:1 POPC:POPG bilayers and 4:1 DPPC:POPG bilayers was developed. This model can serve as a guide for understanding how proteins modulate surface tension and for developing more effective peptide mimetics for clinical use.

CHAPTER 1
DISCOVERY AND HISTORY OF LUNG SURFACTANT

In 1929, Swiss physiologist Kurt von Neergard discovered that the pressure required to fill the lungs with air was much greater than the pressure required to fill the lungs with water. He hypothesized that surface tension was the force responsible for inhibiting the expansion of the lung with air (*1-6*). It was not until two decades later that an absolutely essential surface active material was found in the lungs for overcoming this force and reducing the work of breathing. Research describing the difficulties the lung undergoes during alveolar expansion and contraction can be traced back to 1854, including contributions made by Alexander Graham Bell before he shifted interests and help invent the telephone (*1*). The discovery of lung surfactant as a material that minimizes alveolar surface tension, and its pivotal role in respiratory distress syndrome (RDS) has a history that contains contributions from physicists, physiologists, biochemists, and medical doctors. The knowledge generated by this diverse community has led to an understanding of the mechanics involved in lung function as well as better diagnoses and treatments of RDS.

RDS is a disease prevalent amongst premature infants, but it also occurs in adults and children affected by significant injury or inflammation to their lungs. General treatment of the disease involves mechanical ventilation, a procedure that forces air into the lungs by positive pressure. Epidemiologic estimates indicate that onset of adult respiratory distress occurs in 75 of 100,000 individuals per year (*7*); and the incidence of respiratory distress after delivery is 1% of all newborns. The advent of preventative surfactant instillation therapies has greatly improved survival outcomes, especially in premature infants where mortality decreased by 6% from 1989 to 1990 (*8*). Recent estimates indicate less than a thousand infants annually are diagnosed with RDS as compared to 10,000-15,000 in the 1950s and 1960s (*9*). However, improvements need

to be made in terms of therapy, and basic clinical and scientific questions remain to be answered which can aid in the development of therapeutic agents.

Originally, RDS in infants was incorrectly diagnosed as hyaline membrane disease, based on the mistaken assumption that the strain and grunting noises that occurred when premature infants took their first breath was caused by the inspiration of amniotic fluid or milk, leading to the appearance of glassy membranes found during lung autopsy. In the mid-1950s, however, physicians Dr. Mary Ellen Avery and Dr. Jere Mead found that babies who died from RDS had no residual air in their lungs implying that premature lungs were unable to retain air. At the same time, Dr. John Clements, a physiologist working at the United States Army Chemical Center, designed a surface balance where a movable barrier was allowed to cyclically compress and expand a shallow trough containing minced lung tissue while forces were measured. Such an apparatus, akin to a conventional Langmuir-Wilhelmy balance (*6*), allowed Clements to monitor surface tension as surface area was varied. He found that surface tension rose as the surface area containing lung extracts was expanded, but dropped from 45 to 10mN/m when the layer was compressed without any collapse (*6, 10*). The evidence pointed to a fluid that modulated surface tension in the lung that Clements first referred to as an "anti-atelectasis" factor but was then later renamed (by Clements) as pulmonary surfactant.

Countless research by innumerable investigators contributed to the surmounting evidence of the importance of this surface active material. This has lead to the current and almost indisputable claim that an absence or delayed appearance of pulmonary surfactant material is the prevailing cause of RDS in premature infants.

The Alveoli and Surface Tension

The alveoli are the respiratory units of the lung and contain an air/water interface for oxygen diffusion into the bloodstream. It is estimated that human lungs contain approximately

350 million alveoli with diameters ranging from 75 to 300 microns (*11*). Unique molecular forces arise at interfaces compared to molecules in solution or in a bulk phase. Surfactants are substances that have an energetic preference for interfacial regions and affect intermolecular forces there. A critical force that exists at the alveolar interfacial region is surface tension. Surface tension arises due to unbalanced forces that exist for molecules residing at the surface, particularly since these molecules have diminished interaction with the bulk fluid phase (Figure 1-1). As a result of this imbalance, the surface tends to minimize in area.

Surface tension is the work needed to expand the surface area of a system, in respiration this is the work from expanding the alveolar air sacs. Surface tension is defined as the change in free energy per unit surface area, or equivalently it can be interpreted as work done on a surface, with units of force per distance (mN/m) (*11*).

In the lung, amphipathic phospholipid molecules serve as the surface film that separates the air volume of the alveoli from the fluid layer (Figure 1-2). These lipid surface films have been found to lower surface tension values during *in vitro* dynamic compression experiments. The most abundant lipid in lung surfactant, 1,2-Dipalmitoyl-*sn*-Glycero-3-Phosphocholine (common name and abbreviated DPPC) contains two saturated 16-carbon fatty acid chains esterfied to a zwitterionic phosphatidylcholine headgroup. The rigid nature of the disaturated fatty acyl chains allows DPPC to form tightly packed surface films that can lower surface tension to values of less than 1mN/m (*11*). Hence, the addition of a phospholipid film found in the lung greatly alleviates the surface tension problem faced by the lung.

The essential need of the alveolus to have an inner coating of surfactant becomes clearer when considering the law of Young and Laplace . This law states that the pressure difference normal to surface must be greater than twice (or equal to at equilibrium) the surface tension

divided by the radius of the object: $\Delta p=2 \gamma /r$ (where γ represents surface tension) for inflation to occur (*4*). In terms of expansion and contraction of pulmonary alveoli, the Young-Laplace equation suggests considerable force is required to overcome the surface tension in the highly-curved alveoli. Theoretically, γ values fall to values near 0 upon expiration in the lung, and is estimated to be roughly 30mN/m in the trachea, and about 15mN/m in the airways; consequently, a surface tension gradient exists during exhalation (*12*). Methods to study surface tension *in-vitro* include the Langmuir-Wilhelmy balance, captive bubble surfactometer, and pulsating bubble surfactometer (*13*). Such methods for measuring the properties of surfactant are highly dependant on lung surfactant composition and the buffer salts present in the hypophase chosen to simulate an air/water interface.

Chemical Composition and Origin of Lung Surfactant

Knowing the exact chemical constitution of lung surfactant is important to understanding how it lowers surface tension. Initial analyses using material lavaged from bovine lung indicated the dominant fraction was lecithin (*14*), commonly known as phosphatidylcholine. Of phosphatidylcholine, the primary fraction was the dipalmitoylated form, or DPPC. However, the chemical composition of lung surfactant can best be described as heterogeneous mixture of proteins and lipids with the protein fraction constituting ~8% of the total dry weight and the lipid constituting ~92% of the total dry weight. In the lipid fraction, DPPC is predominant, comprising up to 70%, followed by phosphatidylglycerols, comprising about 8% of the lipid mass (*5, 9*). However, variations amongst species do exist (*15*). In humans, the second most prominent lipid in lung surfactant is palmitoyloleoylphosphatidylglycerol (POPG). With the advent of mass spectrometry and other analytical techniques, quantification of surfactant material after lavage treatment has revealed a far more assorted mixture of lipids (*16*). Table 1 lists the most common lipid and protein species found in lung surfactant. Other surfactant components

include phosphatidylinositols, phosphatidylethanolamines, sphingomyelins, lysophosphatidylcholines, cholesterol, Ca^{+2}, and free fatty acids (*5, 15, 17*). Despite the heterogeneity present in lung surfactant, most artificial formulations used as candidates for clinical treatments contain only a few components, particularly DPPC and a monounsaturated phospholipid (usually POPG) (*18*).

The lipid and protein components of lung surfactant are also evolutionary conserved. Surfactant has been discovered in the Australian lungfish *Neoceratodus forsteri*, which dates back more than 300 million years, raising the question of whether the anti-adhesive properties of surfactant may have served in the primitive respiratory system and led to the evolution of gas-containing organs (*19*). Surfactant still remains one of the most highly conserved systems in vertebrate biology (*17*).

Lung surfactant contains four proteins named in chronology of their discovery: (surfactant protein A) SP-A, SP-B, SP-C and SP-D. Both SP-A and SP-D are large multi-component proteins with an extensive collagenous structure and carbohydrate recognition domains. These two proteins have been implicated in immune surveillance of the alveolar structure of the lung, although SP-A has been found to also have roles in surface activity as well as intracellular surfactant processing (*20*). The presence of SP-A and SP-D and their close structural resemblance to components of the complement system (a glycoprotein cascade found in the blood for clearance of viral and bacterial pathogens) raises interesting questions regarding divergent evolution of the immune system and lung surfactant (*20*). While SP-A is critical to surfactant homeostasis, and SP-D is important to immunological recognition, the focus of this thesis is on factors modulating surface tension, particularly the molecular basis for SP-B changing the phase behavior of lipids in the lung.

Cellular Biology of Lung Surfactant

Pulmonary lung surfactant is synthesized by the highly differentiated type II alveolar epithelial cell derived from the alveolar epithelial lining (*11, 15, 21-23*). These cells are distinguished from type I cells by their flat appearance, apical microvilli, and the presence of lamellar bodies in the cytoplasm. Type II epithelial cells comprise 5% of total alveolar cell surface area, account for 15% of peripheral lung cells, and have a surface area of 250μm^2 per cell (*21*). In addition to producing the four major surfactant proteins, type II alveolar epithelial cells have recently been demonstrated to be an important line of defense in innate immunity. Various anti-microbial and anti-inflammatory substances have been found to be secreted by type II cells, including lysozyme, defensins, cathelicidin, lipocalin 2, as well as SP-A and SP-D which agglutinate fungi, bacteria, and viruses (*21*). Also, since lung surfactant consists of primarily lipids, a high level of lipogenesis occurs in these cells. The upregulation of fatty acid biosynthetic enzymes such as fatty acid synthase, acetyl-CoA carboxylase, ATP citrate lyase, and stearoyl CoA desaturase is stimulated by transcription factors SREBP-1c and C/EBP alpha delta. These transcription factors are in turn upregulated in response to various growth factors, most prominently keratinocyte growth factor (KGF) (*21*). Due to the critical role of the type II cell, it has often been dubbed as the "great pneumocyte" and the "defender of the alveolus" (*22*), since it not only produces the necessary lung surfactant lining the alveoli, but also functions in maintaining sterility within the lung.

Lung surfactant is synthesized *in utero* beginning at 28-32 weeks of gestation and babies born before 35 weeks of gestational age typically suffer from RDS (*11, 24*) due to inadequate levels of lung surfactant. The phospholipid profile in amniotic fluid has historically been used as a diagnostic marker for the onset of lung surfactant synthesis. Tests for predicting the likelihood of RDS typically analyze amniotic fluid for the presence of phosphatidylglycerol, the second

most abundant phospholipids in lung surfactant; its absence is a highly predictive marker for RDS. Historically, preventive measures include stimulation of lung surfactant production by type II cells through treatment with corticosteroids or glucocorticoids, which increase the enzymes necessary for lipogenesis (*15*). Lung surfactant production has been found to be regulated by hormonal agents (*25*) and metabolism of the lipid/protein species are under the control of granulocyte-macrophage colony stimulating factor (GM-CSF) (*26*).

Prior to the development of lung surfactant replacement therapy, the clinical course for the management of newborns with RDS was mechanical ventilation. Variations in ventilatory management give rise to differing outcomes of the disease, and treatments included continuous-positive airway pressure (CPAP) and high-frequency oscillatory ventilation (HFOV). Both methods involve heavy oxygenation of the lung but high frequency-ventilation has become the preferred course due to its advantages of reducing lung distension and minimizing shear forces. In this procedure small volumes airway of gas are pumped into the airways of the lung at rates of 15 Hz (*27*).

Important Surface-Acting Proteins of Lung Surfactant

A fundamental problem associated with air-breathing stems from the dynamic nature of the lung: the need to reduce surface tension in small, gas-containing, aqueous lined structures which are constantly changing in volume. For most mammals, the task of reducing this force is achieved by the proteins SP-B and SP-C, which directly interact with lipids specific to the air-water interface. Initial sequencing of isolated protein showed SP-B to be extraordinarily hydrophobic (~41% to ~52%) with a high relative fraction of the amino acids valine, leucine, isoleucine, alanine, phenylalanine, and tryptophan (*12, 23, 28*). Later studies found the protein to also have a net cationic charge > +6 at physiologic pH (*29, 30*). Based on electrophoretic mobility in sodium-dodecyl polyacrylamide gels, SP-B has a molecular weight of approximately

5-8 kDa (*31*). The native form contains 6 cysteines that form intramolecular disulfide bonds and a seventh cysteine residue that forms an intermolecular disulfide bond (*32*). In the lung, SP-B exists primarily as a 15-18 kDa homodimer with the monomers connected via a disulfide bond at cysteine residue 48 (*23, 30, 31*). The conservation of the 6 cysteines forming intramolecular disulfide bridges, the pattern of disulfide formation, and the high number of hydrophobic residues place SP-B as the most hydrophobic member in the saposin family of proteins. Other proteins in the saposin family include amoebapores from *Entamoeba histolytica*, acid sphingomyelinase, acyloxyacyl hydrolase, and sphingolipid activator proteins A-D (saposins A-D). Saposin family members are important to both lipid homeostasis and lipid physical properties as they can facilitate lipid fusion or bind lipids to increase the activity of lipid modifying enzymes. Saposins have been characterized as being heat-stable, with a helical secondary structure (*33*). What differentiates SP-B from other saposin family members is its hydrophobicity, rendering the protein insoluble in aqueous solutions, and the seventh cysteine residue, used in forming the homodimer, is unique to SP-B (*33*).

The second surface-acting protein in lung surfactant is SP-C. SP-C is a 35 amino acid peptide of molecular weight 4.2 kDa. Its amino acid sequence lacks any known homologs and possesses a high valine, leucine, and isoleucine content. An NMR structure of porcine SP-C determined in organic solvent reveals a helical secondary structure (*29*). Two cysteine residues near the N-terminus are palmitoylated in human SP-C. The protein has an overall hydrophobicity of ~66% and is considered the most hydrophobic protein ever to be found in a biological system (*11, 28, 29*). While SP-C has been deemed essential in respiratory dynamics, mutations in, or of knock-out of, the gene have not been proven to be lethal (*34*). SP-C null mice show normal respiratory kinetics. Nonetheless, mutations in SP-C have been linked to lung

disease and susceptibility to infection (*34*). It has also been shown that genetic knockout of SP-B causes aberrant processing and misfolding of SP-C (*35*) and can lead to structures reminiscent of amyloid fibrils causing pulmonary alveolar proteinosis, a condition in which pathologically high protein levels are found in the airspaces (*36*). Models of the structure and interaction of SP-B and SP-C with lipids are shown in Figure 1-3.

Lung Surfactant Protein B (SP-B) and RDS

The critical role of SP-B has been highlighted by targeted disruption of the gene in mice, as well as the identification of genetic mutations and polymorphisms in humans correlated with respiratory distress (*23, 37, 38*). The difficulty in breathing associated with respiratory distress stems from an altered histopathology seen in the lungs of patients who have inadequate levels of mutated SP-B. Altered morphology of the lung air spaces as well as perturbations in the normal surfactant processing, secretion and storage are seen (*23, 38*). SP-B mutations or deletions lead to disorganization of lamellar bodies and alveolar type II cells, and alterations of the lung surfactant cycle leading to severe disruption of respiratory mechanics. (*30, 39*). Besides the general abnormal morphology of type II cells lacking SP-B, an accumulation of distorted, or irregularly shaped multivesicular bodies in these cells suggests an impairment in lipid packaging and secretion as seen in SP-B(-) mice (Figure 1-4) (*40*). Depletion of SP-B also causes distortion or disorganization of tubular myelin (*23*), resulting in lower lung compliance resulting from the pathological organization of lamellar bodies in the Type II cell. The most prevalent nucleotide mutation of SP-B linked to RDS is an insertion of 2 bases at position 121 leading to a frameshift in the open reading frame (*23, 41*).

The above findings clearly indicate the central importance of SP-B in lipid packaging, cycling and the lung surfactant cycle. Knockout studies and genetic analysis clearly indicate that SP-B is essential in the reorganization and restructuring of lipids at the air/water interface to

allow for respiratory function. While inadequate levels of functional SP-B is linked to respiratory distress, an excess of lung surfactant proteins also leads to the clinical condition known as alveolar proteinosis (AP). Patients afflicted with AP often have 100-fold higher ratios of SP-B to disaturated lipids compared to normal subjects (*42*) and tend to suffer from dyspnea. Typically 75% of individuals with AP are smokers.

To date, only saposin-B of the saposin family has had its structure solved via x-ray crystallography. Recombinant expression of saposin B in *Escherichia coli* gave rise to crystals diffracting to 2.2 Å (*43, 44*). The structure of saposin B revealed an α-helical rich dimer enclosing a hydrophobic cavity (*45*). Structures of saposin-A, saposin-B, and saposin-D have been characterized by ^{15}N solution NMR and also show an α-helical rich fold (*46*). Modeling of one subunit of SP-B based on the sequence of NK-lysin has also been reported (*47*). While these structures provide insight for modeling the conformation of SP-B, its hydrophobicity and tight association with lipids make it an unlikely candidate for either x-ray crystallography or solution (high resolution) NMR, which can yield a more definitive structure as compared to modeling. Efforts to recombinantly express SP-B have been met with limited success (*48*).

SP-B was first isolated in 1986 (*49*). The initially discovered 6 kDa protein fragment, based on Edman sequencing of protein isolated from pig lung lavage, was found to lower surface tension when reconstituted in lipids (*50*). Studies directly linking SP-B to RDS were done in the mid-1990s (*37, 39, 51*). A structural model of how protein reduces surface tension was first predicted in 1993 by Longo (*52*). Isolation and purification procedures for SP-B are rather extensive and time-consuming with low yields; new methods were developed to simplify purification, but many different protocols for SP-B isolation exist in the literature (*53-56*). Isolation of SP-B generally includes a low speed centrifugation of lung lavage fluid to remove

cells, followed by a high speed centrifugation to pellet large surfactant aggregates. The hydrophobic constituents are extracted into chloroform, the lipids are removed using a Sephadex LH-20 column, and a final reverse phase C18 column chromatography step can be used to ensure highest purity (*23, 56*).

Human SP-B is encoded on the short arm of chromosome 2 and the gene has 9500 base pairs and 11 exons. Translation of the protein results in the expression of a precursor protein of 381 amino acids containing both N-terminal and C-terminal signal sequences. The N-terminal signal sequence directs the precursor to the endoplasmic reticulum (ER) while the C-terminal signal, containing a glycosylated asparagine, appears to have no role in the trafficking of the protein (*23*). Cleavage of the precursor protein by proteases in the ER results in mature protein which transits from the ER to the Golgi apparatus where it associates with lipids that self-assemble to form a multi-lamellar concentric structure, called a lamellar body, containing SP-B, SP-C and SP-A (*3*), which act as a functional storage unit of lung surfactant containing both the essential lipids and proteins. Exocytosis from the type II pneumocyte results in unraveling of the lamellar bodies into a meshwork film known as tubular myelin. Electron microscopy images of tubular myelin show an interlocking lattice of lipids (*17*). Tubular myelin is the lipid reservoir from which adsorption and resorption occur at the air/water interface (*23*). Mutations in or deletions of SP-B have been demonstrated to lead to breakdown of the multi-lattice organization of tubular myelin which is essential for the maintenance of this interface (*23, 39*). Functions ascribed to SP-B include the promotion of rapid phospholipid insertion at the air-liquid interface during lung expression, promotion of tubular myelin formation, and an impact on the overall ordering and organization of phospholipids (*5*).

Lipids cannot account for the near zero surface tension seen in lung tissue during exhalation or its surface compression characteristics; the presence at low molar ratios of SP-B and SP-C is required. Direct atomic level measurements on how surfactant proteins associate with lipids to achieve surface tension minimization has previously not been accomplished. Preliminary models of SP-B and SP-C structure and orientation in phospholipid environments are based on examining charge distributions and presumed secondary structures based on FTIR and Raman measurements (*6, 23, 57*). An important consideration in determining structure and interactions of SP-B and SP-C with lipids is the cycle that occurs at the air-water interface during compression and expansion of the alveoli. The interface separating the air space of the alveoli from the adjacent liquid lining is a lipid film that is enriched in DPPC, but its physical composition must be under constant flux between a liquid-expanded phase and a condensed film and there may also be cyclic changes in lipid composition (*58*). The saturated acyl chains of DPPC provide a surface film that can withstand compression of the surface, as would be the case during exhalation, but due to the molecules' poor respreading qualities, requires the assistance of unsaturated lipids to aid in surface expansion that is required during the subsequent inhalation.

Western blots probing for hydrophobic surfactant proteins often show no presence of SP-B from BAL (bronchoalveolar lavage) samples from premature infants with RDS. Some infants with chronic cases of RDS have been found positive for antibody to an aberrant 40-42kDa pro-form of SP-B indicating inadequate proteolytic processing, not just genetic mutation, as a contributor to disease (*41*). A highly sensitive technique employing HPLC in conjunction with Western blotting and light scattering detection on human BAL fluid showed SP-B from normal individuals to be on the order of 740±85 ng/mL. Premature infants with respiratory tract infections or chronic bronchitis have SP-B levels 10-15% of normal (*59*).

Mammalian Lung Surfactant Cycle

A cycle exists that allows for a change of film composition when the surface film in the alveoli expands (inhalation) and contracts (exhalation). The "classical hypothesis" of the lung surfactant cycle has been described in a review by Weaver and Conkright (1991) as well as Veldhuizen and Hagsman (2000) and will be briefly described here: (1) after transit from the ER to the Golgi, lung surfactant proteins SP-A, SP-B and SP-C are packaged with associated lipids to form a concentric organization of lipids known as lamellar bodies, (2) once secreted from type II pneumocytes, lamellar bodies unravel to form an extended mesh structure known as tubular myelin, (3) tubular myelin interacts with the lipid monolayer film at the air/water interface by aiding in the adsorption of DPPC enriched lipids during film expansion, and promoting "selective squeeze out" of non-DPPC lipids occurs during film compression, thus allowing for DPPC enrichment leading to a more stable compressed film, (4) the residual surfactant particle that is "squeezed out" can then (5) undergo catabolism by nearby macrophages, or (6) be taken up by a type II pneumocyte and recycled (Figure 1-5). Data disagreeing with this classical hypothesis exist, most notable is the appearance of lipids undergoing a "buckled structure" at the air/water interface, rather than a complete "selective squeeze out"(*58*). Furthermore, recent fluorescence and Brewster angle microscopy data also seem to contradict the classical hypothesis and support the notion that the interface remains compositionally heterogeneous during film compression and not DPPC enriched as previously believed (*58, 60*).

Exogenous and Artificial Lung Surfactants

As the chemical composition of lung surfactant was elucidated, replacement therapy, or instillation of the most critical components of lung surfactant become another mode of treatment for RDS. Administration of micro-aerosolized DPPC resulted in negative results, while slight changes in breathing profiles were seen by blowing DPPC and PG powders into the trachea of

premature infants (*61*). Better outcomes were observed for instillation of lung surfactant isolated from BAL of animals or animal lung homogenates. The first clinical success using exogenous lung surfactant was reported by Fujiwara, *et al*, who administered bovine lung homogenate via an endotracheal tube. The result was improved oxygenation in 9 of the 10 infants in the trial (*61, 62*). Despite such procedural successes, concerns about viral and other pathogenic contamination from these animal sources remained significant. Furthermore, development of synthetic surfactants for clinical treatment overcomes the expense of isolation and permits better levels of quality control (*32*).

Initial success obtained from administration of exogenous lung surfactant heralded a new avenue of exploration using lung surfactant isolated either from lung lavage or tissue homogenates for the treatment of premature newborns afflicted with respiratory distress. Application of lung tissue homogenates from bovine, porcine sources, or lavage material are now standard treatments for RDS, and formulations are currently marketed by several pharmaceutical companies. A comprehensive list of available lung surfactant formulations used for the treatment of respiratory distress syndrome is compiled in Table 1-2 and includes formulations using derivatized compounds as well as peptide mimetics not found biologically.

The first concept of testing the "bare minimum" components for surface activity came in 1981. Tanaka, et al, tested the surface properties of 25 lipid mixtures in Langmuir trough assays as well as in rabbits to examine the minimum composition necessary to minimize surface tension. His findings concluded that the best and most minimal requirements for a successful administration of artificial lung surfactant (in rabbits and *in vitro*) were DPPC, a saturated fatty acid (either palmitic or stearic), an anionic phospholipid (phosphatidylglycerol or phosphatidylserine), and a yet to be discovered "lipid bound protein" (*18*). The protein referred

to by Tanaka was a not yet fully characterized form of SP-B. Subsequent work has shown that in the presence of DPPC, palmitic acid acts as a "spreading agent" facilitating monolayer expansion as the surface area increases (*63, 64*). The need to assist in monolayer expansion is critical since DPPC itself has poor respreadability and adsorptive characteristics (*60, 63, 65*).

Artificial lung surfactants greatly simplify the problem of studying the underlying biophysical aspects of lung surfactant function against the complicated, heterogeneous background existing *in vivo* and allow the possibility of designing simpler replacements of SP-B with peptide mimetics (*66*). Non-natural peptide analogs of SP-B that exploit the molecule's helical and amphipathic quality, such as KL_4, can circumvent the need to isolate SP-B to sufficient purity. Oligo N-substituted glycines (phenylethyl, 2-butyl, or 4-aminobutyl substituents attached to the nitrogen of glycine), or peptoids, have also been employed to mimic the helicity of SP-B and show potential (*67*). Most lung surfactant formulations have in common DPPC and a chemical agent that facilitates interfacial spreading such as palmitic acid or tyloxepol. The role of palmitic acid in spreading has been investigated by grazing incidence x-ray diffraction and by fluorescence microscopy on DPPC:PA monolayers. It has been found PA enhances membrane fluidity and causes the DPPC chains to be more rigid and ordered. Higher surface tensions of greater than 40mN/m cause phase segregation of PA into condensed domains (*64*).

KL_4 is a 21 amino acid peptide designed to mimic the activities of SP-B. To date, KL_4 has enjoyed the most research focus and clinical success as a replacement for SP-B (*61, 68, 69*). The primary amino acid sequence of KL_4 is KLLLLKLLLLKLLLLKLLLLK with a pattern of hydrophobic leucines punctuated by the basic, hydrophilic lysines. KL_4-based surfactant therapy relies on a formulation of the peptide with DPPC, POPG, and a spreading agent (palmitic acid).

Indicators used to measure improvements in oxygenation after administration of lung surfactant include assaying the ratio of arterial/alveolar partial pressure of oxygen (a/AO_2) (which must not fall below 0.22), the fraction of inspired oxygen (FiO_2), and mean airway pressure (MAP). Declines in MAP, and FiO_2, and an increase in a/AO_2 are markers for improvement in the respiratory status of a premature infant (*69*). KL_4 improves respiratory status and has been found to prevent the appearance of diffuse, granular radiopacity seen in chest radiographs typical of RDS and meconium aspiration syndrome (*69, 70*). A recent antimicrobial function of KL_4 has also been suggested, in line with some other recent reports concerning the anti-bacterial properties of SP-B (*71, 72*). However, the biophysical properties of KL_4 and their relation to alleviating RDS remains the focal point of current investigations, particularly in regard to its structure and organization in lipid environments.

Sections of SP-B have also been assayed for their surface active properties including the C-terminal 21 amino acids. These peptides are amenable to solid-phase peptide synthesis and can circumvent some of the problems associated with isolation of the full-length mature protein; the C-terminal segment has demonstrated surface activity and an effect on surface tension values in phospholipids films (*67, 73*). Figure 1-6 shows the primary amino acid sequence of SP-B and KL_4 which was designed based on the charge distribution in $SP\text{-}B_{59\text{-}80}$.

In this thesis, the effects of KL_4 and $SP\text{-}B_{59\text{-}80}$ on the biophysical properties of two lipid systems, DPPC:POPG MLVs and POPC:POPG MLVs, are described based on an array of techniques for biophysical characterization of both the peptides and the lipids. DPPC:POPG in a 4:1 molar ratio was chosen as a model lipid system because it represents the native lipid profile in lung surfactant and artificial lung surfactants. POPC:POPG in a 3:1 molar ratio was chosen as a second model system because it has convenient physical properties and has been used in

characterizing other amphipathic peptides. The POPC:POPG phase transition temperature is below 0^{o}C allowing for easy manipulation of samples at room temperature; furthermore, the composition of PC and PG headgroups in this ratio is typically found in eukaryotic and prokaryotic membranes. Differential scanning calorimetry (DSC), circular dichroism (CD), and a variety of solid-state NMR (ssNMR) techniques were employed to assess the structure of these peptides in solution and bound to lipids, and their impact on lipid self-assembly. A model of these peptides interacting with both these lipid systems is presented and described in the following chapters. The integration of the structure of these peptides with their orientations in the lipid bilayer is a critical first step towards obtaining an atomic level understanding of how lung surfactant functions and may lead to development of more potent peptide mimetics. The power of ssNMR in examining biomolecules in heterogeneous environments was critical in the development of this model. Such measurements were previously unattainable using x-ray crystallography, where peptide:lipid complexes are typically not amenable to the crystallization process. Furthermore, solution state NMR, where purity and size of the complex place limitations on samples, was unsuitable.

Chapter 2 discusses background and theory behind the biophysical techniques used in these experiments. Chapter 3 describes ^{2}H NMR, ^{31}P NMR and DSC studies of the lipid systems and the effects of KL_4 on their properties. Chapter 4 discusses structural studies of KL_4 interacting with phospholipids by applying ssNMR techniques to isotopically ^{13}C labeled KL_4 peptides, as well as circular dichroism. The results discussed in Chapter 4 were done in collaboration with Professor Joanna Long and Dr. Douglas Elliott. Chapter 5 introduces DSC, ^{2}H and ^{31}P NMR data taken on SP-B_{59-80}, the C-terminal 21 amino acids of SP-B from which KL_4 was derived, and compares these results to results for KL_4. Finally, Chapter 6 provides

conclusions regarding this work, thoughts on future experiments, and questions that stem from these studies.

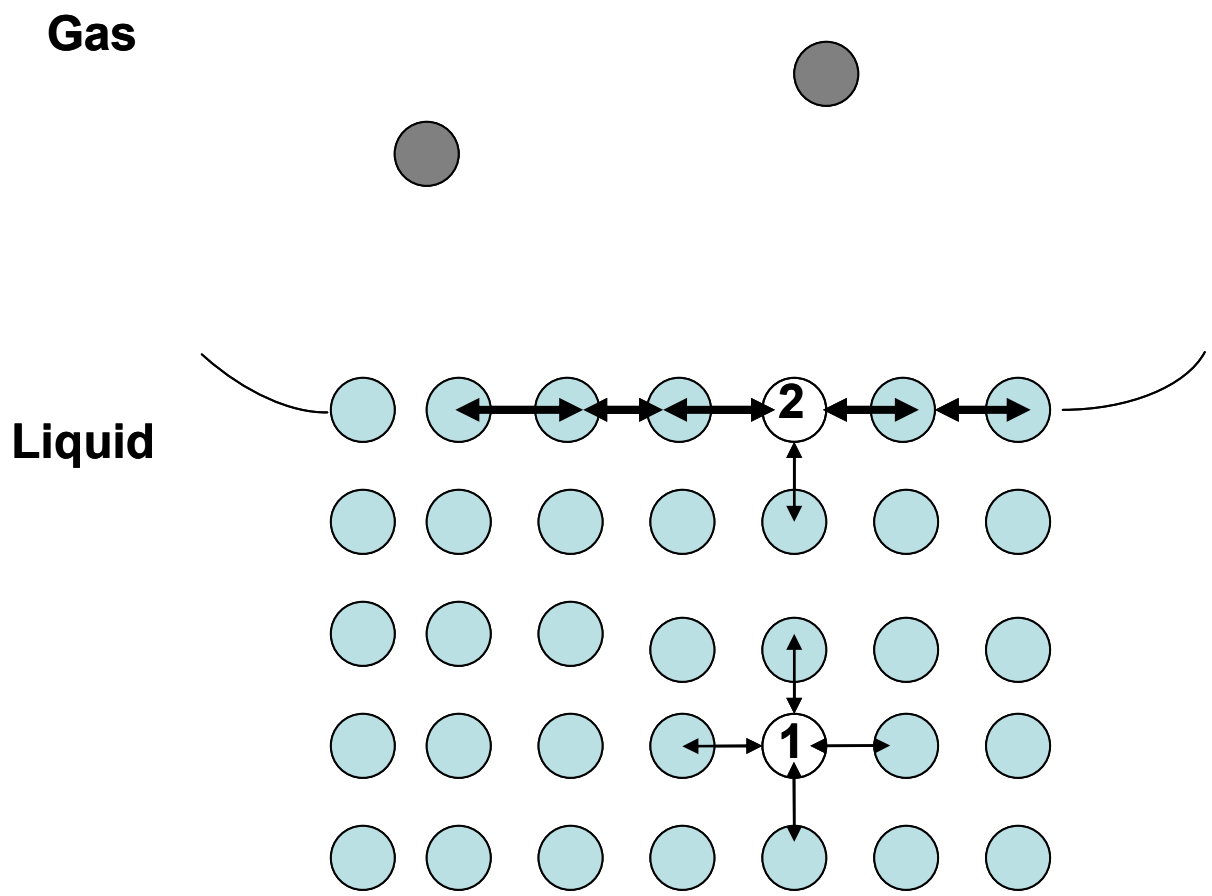

Figure 1-1. Cartoon illustration of surface tension. Molecules at the surface experience an enhanced attraction (shown as the darkened arrows near molecule 2) The result is net attractive inward force causing the surface to curve seeking a minimal area, thus generating surface tension.

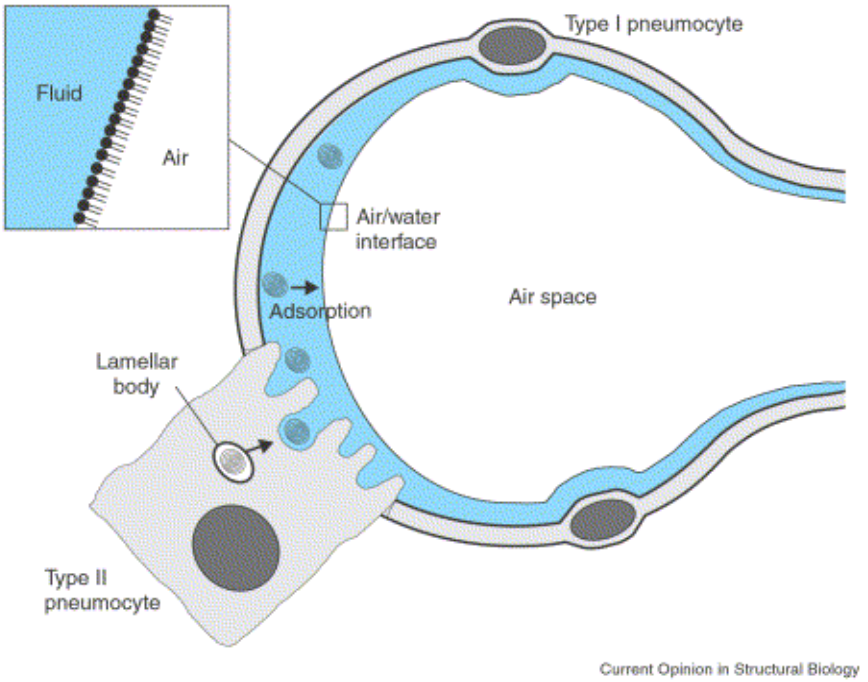

Figure 1-2. The alveolar environment. In the alveoli, fluid coats the inner surface of the alveoli. The air/fluid interface is demarcated by a monolayer enriched in DPPC as shown in the inset. The periphery is composed of 95% Type I pneumocytes and 5% Type II pneumocytes. The type II pneumocytes secrete lung surfactant. Reproduced with permission from Current Opinion in Structural Biology 2002 Aug,12(4):487-94.

Table 1-1. Approximate weight percentages of lipids in mammalian lung surfactant (Adapted from Lung Surfactants: Basic Science and Clinical Applications by Robert H. Notter)

Lipid^	Lavaged lung surfactant
Phosphatidylcholine	80.0 ±0.9
Phosphatidylglycerol	6.8±1.4
Phosphatidylinositol & Phosphatidylserine	5.4±1.3
Phosphatidylethanolamine	3.7±0.4
Sphingomyelin	2.0±0.3
Other	2.0±0.3
Protein*	
SP-A	5%
SP-B	1-2%
SP-C	1-2%

^ Percent weight of total lipid *Percent weight of total lung surfactant. Lung surfactant proteins constitute approximately 10% by weight of lung surfactant

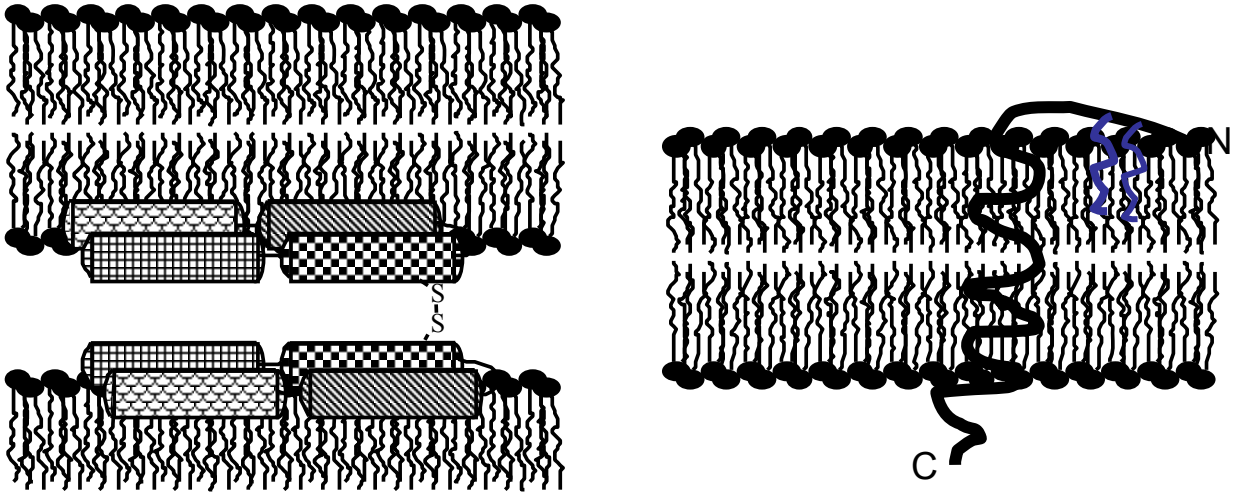

Figure 1-3. Hypothesized interactions of SP-B and SP-C with lipid lamellae. Left: SP-B is a homodimer with the two monomers lining adjacent lamellae. Right: SP-C is believed to exist as a transmembrane helix within DPPC bilayers. SP-C is palmitoylated at cysteine residues near the N-terminus.

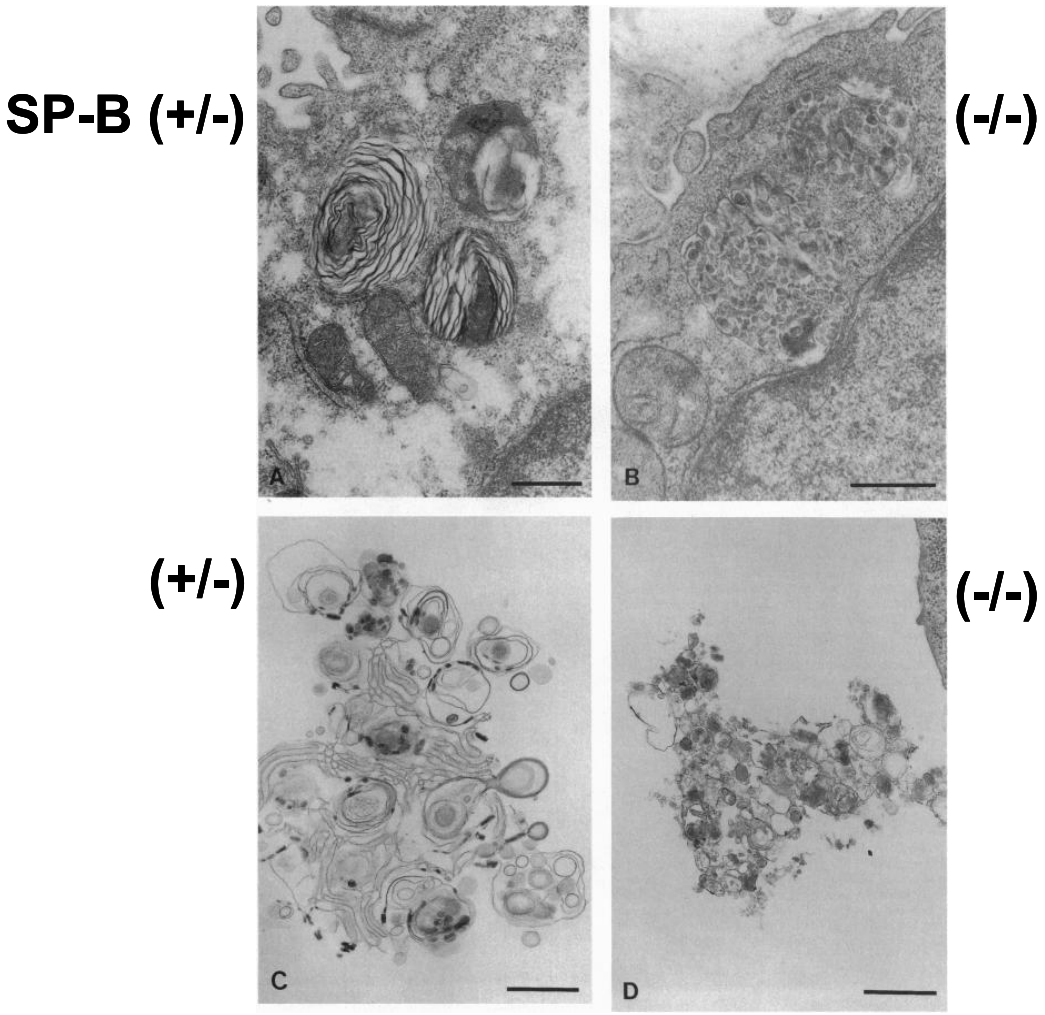

Figure 1-4 Histology of SP-B mutation. Figure taken with permission from JC Clark, originally appearing in PNAS 92(17):7794-8. Lung surfactant from mice heterozygous (+/-) for SP-B is shown in the left column while lung surfactant from SP-B knockout mice (-/-) is shown to the right. Clearly seen is the loss of lamellar bodies and tubular myelin in homozygous (-/-) knock-out mice.

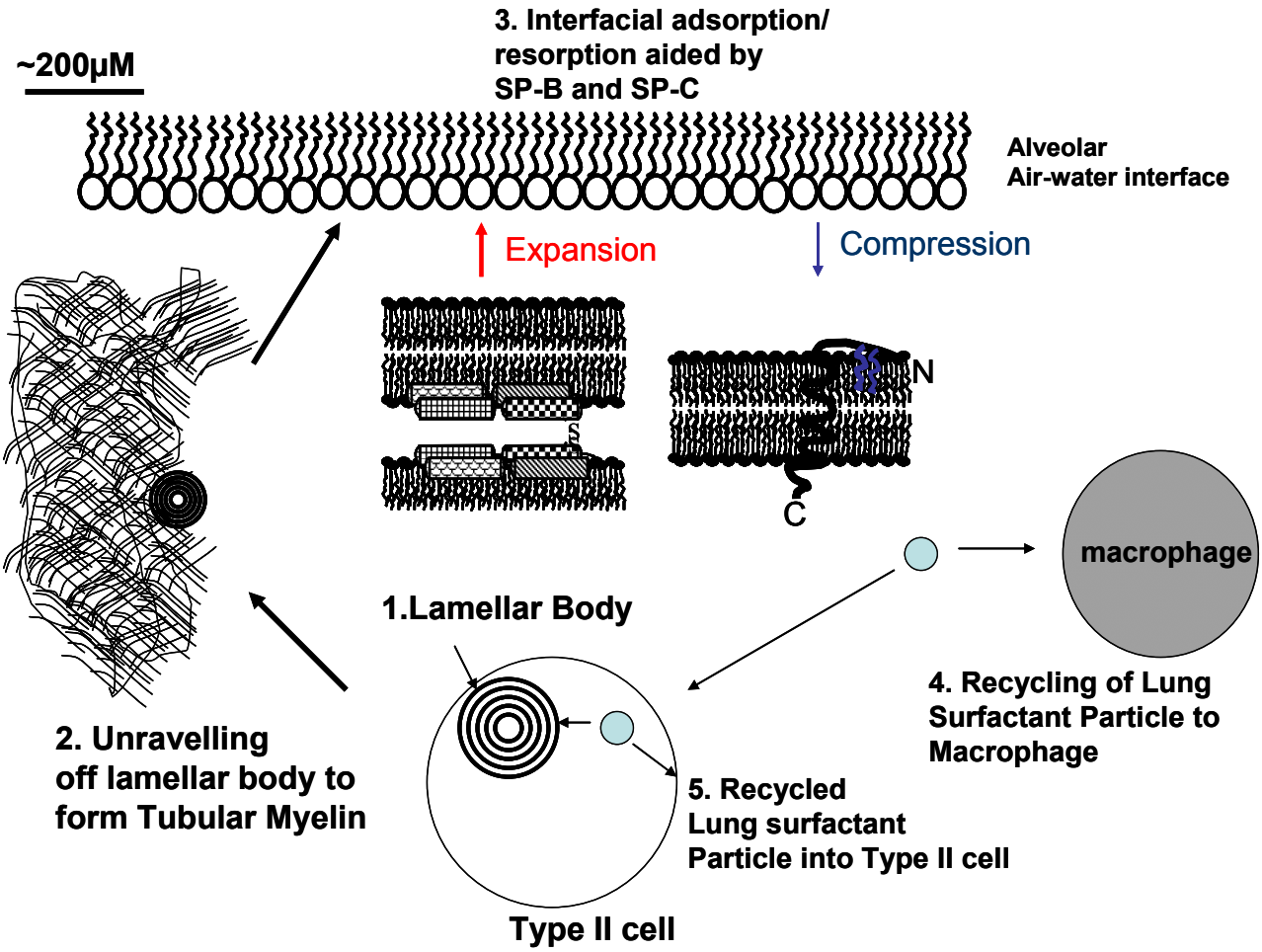

Figure 1-5. Mammalian lung surfactant homeostasis: (1) Lung surfactant is packaged into its the functional storage unit, lamellar bodies, in Type II pneumocytes, (2) lamellar bodies are excreted and unravel to form a network of lipids known as tubular myelin, (3) lipids adsorb to the air-fluid interface, (4) non-DPPC lipids resorb into the hypophase to be degraded by macrophages or (5) type II cells recycle lung surfactant material to reinitiate lamellar body formation.

Table 1-2..Table of artificial lung surfactants used clinically. With permission from TA Merritt. Reproduced from Acta Paediatr. 2006 Sep;95(9):1036-48.

Brand Name	Generic Name	Source/constituents	Company
Protein containing			
Alveofact	SF-RI 1	Bovine-lung lavage	Boehringer (Germany)
BLES	Bovine lipid extract surfactant	Bovine-lung lavage	BLES Biochem (Canada)
Curosurf	Poractant alfa	Porcine-lung lavage	Chiesi Pharmaceuticals (Italy) Dey, LP (USA)
HL-10	–	Porcine-lung tissue	Leo Pharmaceutical (Denmark)
Human amniotic fluid surfactant	NA	Human amniotic fluid at term	University of California, San Diego, USA, Univesity of Helsinki, Finland
Infasurf	Calfactant CLSE	Bovine-lung (calf) lavage	Forest Pharmaceuticals (USA)
Newfacten	–	Bovine-lung	Yuhan (Korea)
Surfacten	Surfactant-TA	Bovine-lung homogenate	Mitsubishi Pharma (Japan, Korea)
Surfaxin	Lucinactant	Synthetic (DPPC, POPG, PA, KL_4 peptide)	Discovery Laboratories (USA)
Survanta	Beractant	Bovine-lung tissue	Abbot Laboratories (USA)
Venticute	rSP-C surfactant	Synthetic (DPPC, POPG, PA, rSP-C)	Altana Pharmaceuticals (UK)
Non-protein containing			
Adsurf	Pumactant (ALEC: artificial lung-expanding compound)	Synthetic (DPPC, PG)	Britannia Pharmaceuticals (UK)
Exosurf	Colfosceril palmitate	Synthetic (DPPC, hexadecanol, tyloxepol)	GlaxoSmithKline (UK)

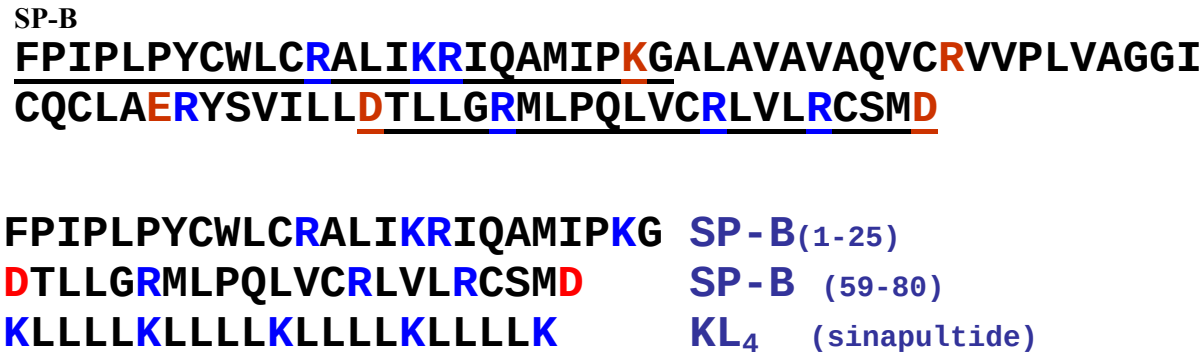

Figure 1-6. Primary amino acid sequence of SP-B and KL_4. KL_4 is modeled after the charge distribution in residues 59-80 of SP-B. KL_4, SP-B(1-25), and SP-B(59-80) affect the surface activity in lipid monolayers at air/water interfaces. Basic residues are highlighted in blue and acidic residues are highlighted in red.

CHAPTER 2
BIOPHYSICAL TECHNIQUES TO PROBE PEPTIDE STRUCTURE AND PEPTIDE-LIPID INTERACTIONS

This chapter details biophysical techniques used in this thesis to study peptide-lipid interactions. These techniques have also been applied in the study of membrane proteins, aggregated proteins (amyloid fibrils), and other complex biomolecular systems. The following descriptions are by no means comprehensive treatments on the rich and detailed history, intricacies, and science behind each technique, but are intended as primers on the information obtainable from each technique in its application to understanding molecular interactions and structure in lung surfactant; references are included for the reader wishing to obtain a more thorough understanding.

Circular Dichroism

Circular dichroism (CD) represents a straightforward method to assess global secondary structure in proteins via detecting the interaction of polarized electromagnetic waves (light) with the chiral protein backbone. Typically, the light source is circularly polarized light generated by a xenon or a helium lamp and filtered to select a particular circular polarization. Light waves are composed of electric and magnetic field waves propagating perpendicularly to each other. Circularly polarized light requires two of these waves (of equal magnitude and frequency) traveling together but 90^{o} out of plane, allowing the magnitude of the electric field to remain constant but its direction to trace the path of a circle. This polarized light differentially excites electronic transitions in proteins leading to CD spectra that are reflective of these excitation energies with both positive and negative absorption. When light passes through an optically active chiral solution, such as amino acids in a protein, the right handed and left handed circularly polarized light are absorbed to different levels at each wavelength.

The differential absorption of left handed and right handed circular polarized light is characterized by

$$\Delta\varepsilon = \varepsilon_L - \varepsilon_R \qquad (2\text{-}1)$$

and gives rise to the CD signal (*74-77*) . The raw CD signal is denoted as ellipticity (in units of millidegrees). The CD signal normalized to the protein concentration is denoted as molar ellipticity m_e and is given by the following equation:

$$m_\varepsilon = \frac{m\deg}{\#AA \cdot [M] \cdot l} \qquad (2\text{-}2)$$

where #AA is the number of amino acids in the protein, [M] is the molar concentration of the protein, *m*deg is the raw CD signal in millidegrees, and *l* is the path length of the sample cell cuvette (in centimeters).

Protein secondary structures such as α-helices, β-sheets, and turns have spectra of distinctive shape and magnitude in the far-UV region. The overall shape of the spectra is due to the periodicity of the amide bonds inherent in each type of secondary structure. For instance, the CD spectrum for an alpha helix has a minimum absorption at ~190nm representing the excitation of π (nb) to π* as well as double minima at ~205 to ~220nm reflecting the excitation of a lone pair oxygen electron to the π* state (*76*). Typical signature CD spectra found for α helix, β-sheet and random coil conformations are shown in Figure 2-1.

CD spectra have been used extensively to monitor secondary structure in proteins free in solution as well as for proteins bound to lipid vesicles at lipid concentrations of 2-10mM (*78-80*). Factors such as the concentration of the protein, path length, buffer composition, and dielectric constant of the buffer, temperature and pH play a role in determining the resultant CD spectra obtained. Helical secondary structure can often be induced in unfolded or random coil

protein by addition of "helix-enhancing" solvents such as fluoro or alkyl alcohols including trifluoroethanol (TFE) and hexafluoroisopropanol (HFIP) (*81*).

Differential Scanning Calorimetry (DSC)

Differential scanning calorimetry (DSC) is a technique used to study the temperature dependent phase behavior of lipids, due to their tendency to self-assemble in both model and biological systems (*82*). The technique has been used to examine the thermally induced transition of lipids from an ordered crystalline state (L_β) to the disordered liquid-crystalline state (L_α), which occurs at a characteristic temperature T_m for a particular lipid or lipid mixture (*82, 83*). Such a transition is characterized by an increase in the *trans-gauche* isomerization rates along the fatty acyl chains, a decrease in bilayer thickness, the onset of axial diffusion, and an increase in the lateral cross section occupied by the phospholipid molecules (*82, 84*). Pure phospholipids have sharp symmetric phase transitions indicating the gel-liquid crystalline transition is a first order process; the T_m at which this transition occurs depends on the headgroup composition, fatty acyl chain lengths, and the degree of saturation in the fatty acyl chains. Broad, asymmetric DSC peaks are commonly seen in biological membranes where appreciable headgroup and acyl chain heterogeneity is present. While the L_β to L_α transition is the most common transition measured by DSC, other phase changes such as pre-melting transitions, liquid-liquid phase separations, and domain formations have been seen and characterized by this technique (*15, 82, 85, 86*).

The principle of DSC is relatively straightforward (Figure 2-2). A sample cell (containing sample) and a reference cell (containing solvent) are heated at very controlled rates. As the temperature is increased linearly, the temperature difference between the reference and sample cell is kept at zero via a feedback loop. This is done by heaters connected to the sample and reference cell. When the sample undergoes a thermally-induced event, such as a phase

transition, a temperature differential is sensed between the reference and sample cell and corrected by varying the power input to the individual cells. The power required to maintain both cells at the same temperature scan rate is measured. This raw differential power signal is converted to heat capacity at constant pressure (C_p) and graphed versus the sample temperature (*82, 87, 88*). More accurately denoted, the DSC instrument measures the *excess* specific heat, the amount by which the apparent specific heat of a particular solute transition exceeds the baseline specific heat required for heating the reference cell. Figure 2-3 illustrates the output generated after the excess specific heat is converted to heat capacity by the DSC instrument.

DSC thermograms can be analyzed to extract the thermodynamic parameters for a lipid phase transition. The calorimetric enthalpy ΔH_{cal} of a transition is obtained by integration of the peak related to the transition peak: (*84*)

$$\Delta H_{cal} = \int_{T_1}^{T_2} C_p \, d\tau \qquad (2\text{-}3)$$

The van't Hoff enthalpy is the enthalpy calculated as a function of T_m; assuming a two-state process, the formula for ΔH_{vH} is: (*89*)

$$\Delta H_{vH} = 4RT_m^2 \frac{C_p^{\max}}{\Delta H_{cal}} \qquad (2\text{-}4)$$

where R is the universal gas constant and C_p^{max} is the peak heat capacity measured for the transition.

Another parameter which can be extracted is the cooperativity of the transition between phases. In some cases the phase transition can be instantaneous and the DSC thermogram will be highly dependant on the scan rate. In other scenarios, the process might first be initiated by domains or "islands" of lipids and gradually spread throughout the sample as the temperature is changed. The cooperativity can be assayed by comparing the values of the derived enthalpies

ΔH_{cal} and ΔH_{vH} (*89*) and evaluating their ratio $\Delta H_{vH} / \Delta H_{cal}$. When this ratio is less than unity, intermolecular cooperation dominates the transition mechanism; however, when the ratio is greater than unity, intermediate states are significantly populated.

The effects that exogenous agents such as cholesterol, proteins and antimicrobial peptides have on the T_m of model lipid systems have been extensively investigated using DSC (*79, 90-92*). DSC has also been used to delineate peptide induction of alternative lipid polymorphisms, such as the H_{II} phase, which has been shown to occur when transmembrane α-helices enriched in the amino acid leucine are added to lipids (*93*). (This is of particular importance since the peptide under study (KL_4) has a high percentage of leucines). Thus, DSC is a powerful tool to study the effects peptides have on the thermotropic phase behavior of lipid systems.

It should be noted that the "pre-transition" peak often seen in DSC on pure lipids (such as that seen in Figure 2-4) has been fully evaluated in terms of the structural changes within the bilayers. For phosphatidylcholines, the pretransition occurs in the range of ~5^o below the main phase transition temperature and has been denoted the P_β or "ripple" phase. Since it is due to a transformation from a pure lamellar phase to a two-dimensional monoclinic lattice, in which the bilayer contains undulations (*86, 88, 94*). Addition of peptides or other exogenous agents have been shown to abolish or modulate the appearance of this pre-transition phase. Also shown in Figure 2-4a is the information content yielded from a DSC thermogram. The T_m corresponds to the temperature where the maximal heat capacity C_p^{max} of the system is observed for each transition; the integration of any peak reflects ΔH_{cal}, and the PWHH or $\Delta T_{1/2}$ measures how broad the phase transition is. A broad peak (which implies a large PWHH and hence a greater temperature span or $\Delta T_{1/2}$) indicates less lipid cooperativity during the phase transition. Adding

monounsaturated lipids to pure DPPC has consequences in terms of thermodynamics, lipid cooperativity and phase transition temperature (Figure 2-4b).

Solid state NMR Spectroscopy

Solid state NMR spectroscopy (ssNMR) has advanced significantly as a tool to study the structure and dynamics of solid systems ranging from glasses to polymers to catalysts. Advances and progress in the field have now been increasingly focused on developing methodologies for complicated biomolecules such as membrane proteins (*95, 96*). Unlike solution NMR, where narrow resonances result due to rapid reorientation of molecules and averaging of anisotropic interactions, ssNMR must deal with unaveraged interactions (*97, 98*).

On the NMR time scale (Figure 2-5), interactions such as chemical shielding, dipole-dipole coupling, and quadrupole coupling are time averaged in the solution state by the rapid reorientation of the molecule. Slower motions of molecules in the solid state give rise to a superposition of many overlapping resonances representing the many possible orientations of the molecules with respect to the magnetic field; the resulting broad spectrum can be referred to as a powder pattern (*96, 98*). These powder patterns observed in ssNMR spectra suffer from low resolution, low sensitivity, and (for the most part) very little extractable structural information. However, magic angle spinning (MAS), described briefly below, can yield liquid-like spectra from solid-state experiments; and clever pulse sequences during MAS can be used to re-introduce and to measure anisotropic information (*99*). A discussion of time scales used to measure molecular processes by NMR is detailed later in this chapter.

Spin Interactions Commonly Seen in ssNMR

Chemical shift

When placed in a strong magnetic field, nuclei in different parts of a molecule experience varying fields due to their electronic environment. This phenomenon is referred to as chemical

shielding and is caused by the external magnetic field ($\mathbf{B_0}$) generating currents in the molecule's electron cloud, which in turn generates induced fields. The magnitude of this induced field at a given nuclear site depends on the orientation of the molecule with respect to $\mathbf{B_0}$ and on the location of the nuclear spin within the molecule. This variation in chemical shielding leads to different nuclei of the same isotope resonating at different frequencies or chemical shifts.

In liquids the chemical shielding is averaged and is referred to as the isotropic chemical shift. This chemical shift depends upon the gyromagnetic ratio of the nuclear spin, the shielding by local electron currents, and the influence of local low-lying electronic ground states (*100*).

For a single crystal sample, the NMR spectrum looks similar to a solution NMR spectrum in resolution (neglecting dipole-dipole couplings) but chemical shifts depend on the orientation of the crystal with respect to $\mathbf{B_0}$. Therefore, by rotating the crystal relative to the magnetic field, the resonance positions change. In powder samples, where all such orientations are present, the chemical shift spectrum is broad reflecting that it is a superposition of spectra from each crystallite. This is described in more detail below.

Dipole-dipole couplings

The interaction of nuclear spins with one another also affects NMR spectra. Since each NMR active nucleus has a magnetic moment, each spin experiences the field generated by other nuclear spins nearby. This interaction is called the (direct) dipolar coupling.

Dipolar couplings (d) are through-space interactions and provide important structural information. The dipolar coupling is directly proportional to the gyromagnetic ratio of each participating spins (γ_1 and γ_2) and inversely proportional to the cube of the distance between the spins (r) (*100*). The spatial dependence of the dipolar coupling with respect to the external magnetic field is accounted for in the angular term $\frac{3\cos^2\theta - 1}{2}$:

$$d = \frac{1}{2}\frac{\gamma_1\gamma_2(3\cos^2\theta - 1)}{r^3} \qquad (2\text{-}13)$$

The gyromagnetic ratio describes the size of the Zeeman interaction for a spin with respect to the magnetic field and determines its Larmor frequency. For example, the γ value for a ^{1}H spin is 2.68x10^8 rad/sec/Tesla (*101*), corresponding to 600MHz in a 14.1T field. In a powdered NMR samples, dipolar, quadrupolar, and (in part) chemical shift interactions scale by a factor of -0.5 to 1 based on the angular dependence of these interactions on the term $(3\cos^2\theta\text{-}1)/2$ (*102, 103*).

Quadrupole couplings

Quadrupole couplings represent the interactions of spin $> \frac{1}{2}$ nuclei with the electric fields from their non-spherical nuclear charge distribution. The measure of a nucleus's effective ellipsoidal shape is called its quadrupole moment (*Q*, often reported as *eQ*). The strength of the quadrupole coupling is a good measure of a nucleus's mobility. For example, in this study, spin 1 deuterium (^{2}H) has a quadrupolar coupling constant: $\frac{e^2qQ}{h}$ used to assess the mobility of lipid acyl chains where *e* is the charge of an electron, *q* is the principle component of the electric field gradient tensor, and *h* is Plank's constant.

Applications and Methodologies in Solid-State NMR

Pake Powder Pattern

Large biomolecular systems such as membrane proteins, polymers, or inorganic complexes give rise to difficulties in structure determination because the orientation dependencies of the NMR interactions described above are not time averaged. Resultant NMR spectra yield broad lineshapes known as *Pake powder patterns* or *powder spectra* (*104*), after George Pake who derived the equations for these patterns in the late 1940s. A typical ^{31}P chemical shift spectrum for the phospholipid DPPC above it's T_m is shown in Figure 2-6 and shows a powder pattern

over a range of frequencies covered due to multiple orientations of the lipids with respect to the external magnetic field (*98, 105*). Below a phospholipids T_m, the motion of the phospholipid is non-axial and results in a spectrum shown in Figure 2-7. In lipid dispersions taken above the phase transition temperature the onset of motion about an axis of symmetry leads to a lineshape that has distinct parallel edge and perpendicular edges relative to the static magnetic field. All other intermediate orientations of the symmetry axis relative to magnetic field are also enveloped in the powder pattern. The relative intensity at each point in the pattern is based on the probability distribution of that orientation. For a phospholipid dispersion, the powder pattern can take different lineshapes, not only dependant on T_m, but also dependent on the dynamics present for various lipid polymorphisms, such as hexagonal or inverted hexagonal phases (Figure 2-9).

Chemical Shift Anisotropy (CSA)

In an unoriented sample, many orientations of a particular molecule to the magnetic field are present. The chemical shifts seen are dependent on the distribution of orientations in the sample. It is the chemical shift anisotropy that determines the ^{31}P spectra in this work.

The chemical shift anisotropy for a spin ½ nucleus (such as ^{31}P) can be described in its principle axis system by three values, designated as σ_{11}, σ_{22}, and σ_{33} (Figure 2-7). By convention, σ_{33} has the largest difference from the isotropic value and lower intensity and corresponds to the parallel edge in the powder pattern, σ_{22} corresponds to the highest intensity of the powder pattern, and σ_{11} has an intermediate intensity and corresponds to the perpendicular edge in a powder pattern. The isotropic peak, σ_{iso}, seen in MAS spectra and solution NMR, is equal to the average of the principal values. These values are dependent on the electronic field surrounding the nucleus, which shields the nucleus from the external magnetic field. Since the shielding is three dimensional, it is represented by a second rank tensor where the principal values correspond to the diagonal elements in a principal axis system (PAS), where this 3x3

matrix is diagonalized. This interaction tensor can be visualized as an ellipsoid whose center is the active NMR nucleus of interest and the axes of the ellipsoid coincide with the principal values of the CSA tensor in Cartesian space. If the molecular orientation changes with respect to the magnetic field, then so does the nucleus and its corresponding CSA tensor (*98*) (Figure 2-8).

For phospholipid bilayer assemblies, a symmetry axis due to rotational averaging around the director axis perpendicular to the plane of the bilayer, (or the "bilayer normal") avereages the ^{31}P CSA leading to axial symmetry where $\sigma_{11} = \sigma_{22}$ as shown in Figure 2-5 (*94*). This onset of motion causes rotational averaging of the ^{31}P CSA tensor around the director axis and as a result, the z-axis of the time averaged CSA, or σ_{33}^{PAS}, coincides with the bilayer normal and remains unchanged. In such a scenario, $<\sigma^{PAS}_{11}> = <\sigma^{PAS}_{22}> \neq <\sigma^{PAS}_{33}>$. The isotropic chemical shift σ_{iso} is defined as the average of the three main components of the tensor

$$\sigma_{iso} = \frac{1}{3}(\sigma_{11} + \sigma_{22} + \sigma_{33}) \quad (94, 98) \qquad (2\text{-}14)$$

and corresponds to the frequency if the sample were tumbling isotropically in solution. The lower than usual signal at $\sigma_{\parallel}$ seen in Figure 2-6 is due to the fact that DPPC lamellae orient in high magnetic fields which is addressed below.

Magic Angle Spinning NMR

If the NMR sample is spun at a "magic" angle (54.74^{o}) relative to the magnetic field, the orientation dependent term, ($3\cos^2\theta$-1), is zero. At fast enough spinning speeds, dipolar couplings and chemical shift anisotropies (CSA) can be completely averaged, thus removing their anisotropic effects in resulting NMR spectra (*95*). MAS thus improves resolution and subsequently the applicability of ssNMR to complicated biomolecular spectra (*99*).
Figure 2-10 illustrates the phenomenon of MAS and its effects on a chemical shift spectra (*106*). However, with the averaging of dipolar couplings, important structural information is lost. But

dipolar couplings that are averaged under MAS conditions can still be observed by the introduction of radiofrequency pulses synchronized with the spinning of the sample (dipolar recoupling). Pulse sequences such as DRAMA (dipolar recovery at the magic angle) use $\pi/2$ RF pulses applied twice per rotation period to interrupt the averaging of the dipolar coupling caused by MAS (*95*). A variation of the DRAMA sequence called DRAWS (dipolar recoupling with a windowless sequence) uses additional pulses to retain more of the dipolar interactions, while still averaging CSA interactions. DRAWS is therefore more effective for nuclei with large CSAs such as carbonyls (Figure 2-11).

Structural aspects of the molecule in question can also be determined independent of the application of external RF pulses, simply by modulating the speed of the spinning rotor while the sample is under MAS conditions. The presence of spinning side bands at spin rates of 3000-4000 Hz allows the determination of CSAs. Thus observation of any molecular motions of peptides in lipid MLVs as a function of sample composition is possible.

Range of NMR Time Scales

While solid state NMR is used to look at molecules that are slowly tumbling on the NMR time scale, it is important to realize that NMR can probe molecular motion over a wide array of time scales ranging from picoseconds to several seconds. The following section serves as a brief primer on the vast ranges of frequencies that an NMR experiment can detect.

The internal dynamics of molecules allow nuclei to oscillate to a net average position. These molecular vibrations are on the order of picoseconds or shorter. Internal dynamics within the molecule allow for large rotation of substituents within the molecule as well, such as a methyl group or an amine. If the substituent has an axis of symmetry such as around a local three-fold axis existing in a $-CH_3$ group, then such motion can be on the order of internal molecular vibrations (picoseconds), but if the same $-CH_3$ group is hindered by another nearby substituent,

as can be expected during the folding of a protein or in a lipid bilayer environment, then such rotational motion can occur on the timescale of milliseconds to seconds. Hence, the boon of NMR stems from its ability to detect molecular motions as well as the number of molecules in different states (*100*).

Time scales which can be probed using NMR experiments are vast—from hundreds of picoseconds (molecular rotations), to many seconds (macroscopic diffusion and chemical exchange processes) (Figure 2-5). Depending on the sampling time during signal acquisition, one can discriminate between types of motion being measured. Very fast motions in the picosecond to nanosecond timescale are on the order of the Larmor frequency representing the shortest time available to specifically encode information—anything faster is encoded as an average. However, NMR is not generally sampled this quickly and the totality of different actions must also be considered. For example, vibrational motion and molecular rotation can average out direct dipole-dipole couplings (often in the millisecond domain) in liquids (*100*). Motions on this timescale often form the basis for T_1 relaxation measurements.

Motional time ranges on the order of microsecond to milliseconds affect the typical spectral timescale strongly. As a result, lineshape perturbations such as a broadening, are seen. An example of the changes in NMR spectra within this regime is hindered rotation. In this type of experiment, a molecule has two (or more) non-equivalent conformations with a significant energy barrier between them. The first NMR experiment is run "cold" and shows each conformation as a distinct resonance—indicating that their intraconversion is slow on the timescale. As the temperature is raised, the spectra first broaden and then coalesce into a single peak—indicating that their intraconversion is fast on the timescale.

Lastly, molecular motion that ranges from milliseconds to seconds can also be probed from NMR. Macroscopic diffusion or flow occurs via the transport of molecules from one region of space to another occurs on this timescale. Such a phenomenon forms the basis of diffusion NMR, whereby an inhomogenous magnetic field is generated and used to quantitate molecular diffusion and flow.

Depending on what frequency of motion one is interested in examining, the NMR experiment can be correspondingly devised. For natural abundance ^{31}P NMR experiments, the timescale of motion being probed are on the order of 10^{-9} to 10^{-11} seconds. The frequency range of a ^{31}P CSA span is 50 ppm or approximately 30,000 Hz for an NMR experiment run at 600MHz. Headgroup vibrations, lateral diffusion, and rotational motion along the lipid axis are faster than this, so their effects are seen as primarily narrowing the spectra to an average value. Likewise, the frequency range of quadrupolar interaction are on the order of approximately 167,000 Hz. The ^{2}H NMR experiments, looking at the dynamics of the acyl chain also involve motions that are faster than the spectral frequency so again, averaging of the spectra components are seen. Finally, in solids there is incomplete motional averaging of the internal spin interactions, so both intramolecular and intermolecular spin interactions retain their dependence on the orientation of the sample with respect to the magnetic field (*100*).

NMR-Active Nuclei and Importance to Biological Molecules

^{31}P (Phosphorus) NMR

Phosphorous is the spin ½ NMR-active nucleus that gives rise to the powder lineshape mentioned above. ^{31}P NMR is one of the tools that can be used as a non-perturbing probe to measure the orientation and conformation of the phosphate headgroup in a lipid molecule (*94*). Another advantage of ^{31}P NMR is that no isotopic incorporation is necessary since the target nucleus is 100% naturally abundant. Furthermore, dipole-dipole interactions between ^{31}P and ^{1}H

in phosphates are very small, and can easily be decoupled. As detailed above, lipid geometries important in membrane-membrane mediated events such as the lamellar and hexagonal phase, are sensitive to the onset of axial diffusion and molecular motion. These can be discriminated by ^{31}P NMR; also, the technique is sensitive to headgroup orientation and charge interaction effects. ^{31}P NMR spectra of small, sonicated vesicles have a single resonance at their isotropic chemical shift. This is due to the vesicles being small enough to tumble rapidly on the NMR timescale. The tumbling rate of 4000 lipid molecules in a 30-50nm small unilamellar vesicle of radius 250Å has been estimated to be ~1MHz. This is in stark contrast to lamellae which have a tumbling frequency estimated at <1Hz (*107*). Sharp peaks at the isotropic chemical shift seen in NMR spectra of vesicles are also due to a small radius of curvature and lateral diffusion (*107*). The types of lipid polymorphisms described above have had their spectra distinguished and characterized by ^{31}P NMR (*108*). Lipid phases seen by ^{31}P NMR are essentially field independent; however, orientation of lipid assemblies can cause variations in the relative intensities of $\sigma_{\parallel}$ and $\sigma_{\perp}$ edges with higher B_o fields (*94*).

While ^{31}P NMR of phospholipids ensembles yield specific lineshapes due to CSA interactions, it is also critical to mention that sharp, nearly Lorentzian lineshapes at a particular resonance frequency can occur on hydrated phospholipids if the assemblies are highly ordered with respect to the magnetic field. Similarly, single crystals of phospholipids produce single Lorenztian lines, which when the crystal is rotated with respect to the magnetic field, change their resonance position. In fact, this has been exploited by many research labs that create oriented bilayers on glass plates, giving rise to a single orientation of the bilayers. The glass plates can then be placed in the magnet with the director axis perpendicular to the B_o yielding a single resonance at the perpendicular edge of the oriented lineshape. This approach has also been pivotal in using

^{15}N spectroscopy to determine the orientation of ^{15}N backbone labeled peptides in bilayers (*106, 109-111*).

The potential detergent and lytic properties of antibiotics and anti-microbial peptides have also been examined by ^{31}P NMR. Addition of molar percentages of down to 4 mol% of these molecules have been found to lead to an appearance of an isotropic peak in ^{31}P spectra indicating significant membrane degradation or perturbation (*112, 113*). In addition to assessing the geometry and polymorphisms of phospholipids phases, ^{31}P NMR has found use in a multitude of applications including muscle and tissue research diagnosing epilepsy, and in specific sectors of the food industry (*114-116*).

An unoriented static ^{31}P NMR spectrum of a phospholipid is due to the CSA of the ^{31}P nucleus in the phosphate headgroup. CSA values have been measured for various phospholipid headgroups in crystallized lipids (*94*). Furthermore, the size and sign of the phosphate CSAs can differentiate between different lipid geometries. As discussed above, lamellar phase lipids have asymmetric spectra below their T_m due to restricted motion, and above their T_m, have axially symmetric lineshapes which are approximately 50 ppm broad. Another lipid mesophase, the hexagonal phase, has an additional axis about which the averaging of the CSA occurs.

The hexagonal phase describes lipids packed as elongated cylindrical structures. It is divided into two types: the H_I and H_{II} phase. The H_I phase contains a cylindrical array of lipid molecules with the polar head group facing an aqueous exterior and the acyl chains facing inward. In the H_{II} phase, or inverted hexagonal phase, the headgroup face an inner aqueous cavity of water and the acyl chains face outward stacked in a tubular form (*15, 94*). Figure 2-9 shows lipids in lamellar and H_{II} phases and their resulting ^{31}P NMR spectra. Lipids arranged in a hexagonal phase have the same motions as lamellar phases, and an additional degree of motional averaging

occurs due to lateral diffusion of the lipids about the cylindrical axes (*94*). The spectral lineshape for a hexagonal phase is half the width and opposite in sign to the corresponding lamellar phase since this motion is perpendicular to the axial diffusion of the individual molecules.

^{2}H (Deuterium) NMR

Deuterium (^{2}H or D) is a spin 1 nucleus with a natural abundance of 0.016%. Hence, any NMR signal obtained from sample unambiguously belongs to deuterons specifically incorporated into the molecule of interest — provided deuterium free solvents were used (*107, 117*). Due to the spin 1 nature of the deuterium nucleus, ^{2}H NMR powder spectra are characterized by two overlapping and opposite in sign lineshapes, due to the two possible transitions -1 → 0 and 0 → 1. These lead to characteristically symmetric perpendicular peaks, often referred to as the "Pake" doublet (*102*). Deuterium spectra of acyl chain deuterated lipids provide structural information since averaging of the Pake powder patterns depends on motions of the individual methylene segments (*118*).

The time averaged order parameter $\langle S_{CD} \rangle$ can be assigned for each C-D bond along the length of the acyl chain. This order parameter is a discrete value assigned for the collective ensemble motions that occur for each C-D bond and average the powder spectrum for that position. Such a value provides information on the internal motions of the fatty acyl chain. Motions of phospholipids pertinent to the NMR time scale (10^{-5} seconds) which average the quadrupolar interaction include oscillatory motions of bond lengths, bond angles, and torsion angles (10^{-12} seconds), gauche/trans isomerizations (10^{-10} seconds), axial diffusion (10^{-8} to 10^{-9} seconds), fluctuations of the director axis known as "wobble" (10^{-8} seconds), and translational diffusion along bilayer surfaces (10^{-7} seconds) (*84, 107*). The motion of a phospholipid molecule can be approximated as a cylinder that axially rotates (*119*) with each C-D bond wobbling as a

cone along the length of the acyl chain (Figure 2-12) and determines overall averaging of the ^{2}H patterns at all positions along the acyl chain. Additional gauche/trans isomerization motions affect the averaging at each C-D along the acyl chain differently, since there is less steric hindrance encountered by methylene segments going toward the methyl terminus. The order parameter for a specific methylene position labeled *i* is defined with a second order Legendre polynomial

$$S_i = \frac{1}{2} < 3\cos^2 \theta_i - 1 > \qquad (2\text{-}15)$$

where θ_i is the angle between the symmetry axis of the molecule and the C-D chemical bond. The brackets indicate a time-average ensemble of all molecular motions of the C-D bond that are fast on the NMR time scale (*107, 119-122*). The bilayer normal is coincident with the symmetry axis for lipids in a fluid lipid bilayer due to the fast axial rotation of the individual molecules (*84*).

The deuterium NMR spectra of lipids with perdeuterated acyl chains contain powder patterns from all the positions in the acyl chains. Full deuteration of both the sn-1 and sn-2 acyl chains of DPPC results in 30 ^{2}H NMR lineshapes correlating to each methylene position in each of the acyl chains. Each lineshape is also symmetric, with a Pake doublet or quadrupolar splitting ($\Delta\nu_q$, measured in kHz) that can be used to calculate the order parameter for that particular acyl position (Figure 2-13).

The frequency splitting $\Delta\nu_q$ for each C-D position is used to calculate the time averaged order parameter $<S_{CD}>$ for the position according to the following simple relation:

$$\Delta\nu_q = \frac{3 \cdot 167 kHz}{2} < S_{CD} > \qquad (2\text{-}16)$$

The quadrupolar coupling constant expected for a deuterium atom in a saturated C-D bond in the static limit is 167kHz (*84*). This value was determined by measuring deuterium quadrupolar coupling constants on deuterated paraffins such as ethane and butane at low temperatures (*123*). A numerical procedure, termed dePaking, is used to deconvolute the spectra. The methylene positions can then be easily assigned since they give rise to single resonances rather than lineshapes. These assignments can then be used to create an order parameter profile. Resonance assignments for each position were initially done by selectively deuterating individual positions along the acyl chain and measuring the NMR spectra (*117, 118*). From the dePaked ^{2}H NMR spectra, a characteristic order parameter profile is generated by graphing the calculated $\langle S_{CD}^i \rangle$ values against the methylene positions in the acyl chain (Figure 2-14). The order parameters decrease as the carbon number of the acyl chain is increased reflecting the increased motional freedom of the acyl chains near the center of the bilayer (*121, 124*).

DePaking

As stated above, dePaking is a numerical deconvolution procedure that takes the lineshape arising from randomly oriented molecules and converts it to an "oriented spectrum". The procedure can be applied to any lineshape resulting from the spatial dependence of the spectrum having the form of a second order Legendre polynomial, i.e. $(\frac{3\cos^2\theta - 1}{2})$. Through a mathematical transform, the spatial component is removed resulting in an "oriented spectrum" in which the signal is refocused at the frequency corresponding to the parallel edge of the powder lineshape (*125*). For our work, the dePaking procedure employs an algorithm provided by Edward Sternin and colleagues at Brock University, which has been used to generate both $\langle S_{CD} \rangle$ profiles and determined the extent of spontaneous magnetic field orientation of lipids (*102, 103*). The result of the transform is a frequency spectrum

corresponding to when the lipid bilayer normal is parallel to B_o (*126, 127*). This is the equivalent to the parallel edge for each C-D powder pattern in ^2H NMR and likewise the parallel edge for each lipid phosphorous moiety in ^{31}P NMR. An example of dePaked ^2H and ^{31}P spectra are shown for 4:1 DPPC(d-62):POPG in Figure 2-13b and Figure 2-15 respectively. By measuring the dePaked frequency as a function of added agent such as a peptide, the extent and level of interaction of the lipids with the additive can be probed.

Magnetic Field Orientation

An additional complexity arising when interpreting NMR spectra for lipids being placed in large magnetic fields is macroscopic lipid alignment, particularly for lamellar phase lipids. The macroscopic orientation is due to the negative diamagnetic susceptibility ($\Delta\chi<1$) of phospholipid molecule assemblies (*128*). The phenomenon of a preferred orientational alignment has been well documented in the literature for many phospholipids classes, ranging from synthetic to biological extracts from *E.coli* and has been observed at field strengths as low as 7T (300 MHz for ^1H) (*103, 129-132*). This complicates analysis of NMR spectra, particularly dePaking algorithms, since the typical powder distribution of angles no longer holds. The formulae and mathematical procedures involved when the powder pattern is distorted by lipid alignment are discussed in Chapter 3. When multilamellar vesicles orient, the spherical shape becomes distorted to a geometry that is ellipsoidal (Figure 2-16). The dePaking algorithms used take into account the fact that the probability distribution of the bilayer normal vector is no longer proportional to $\sin(\theta)$, as it would be for a totally random distribution of MLVs. To account for this discrepancy, the dePaking algorithm written by Professor Edward Sternin generates a orientation parameter, K_ε, which accounts for the extent of spontaneous orientation of the lipid vesicles in the magnetic field B_o, assuming the MLVs deform to more ellipsoidal geometries.

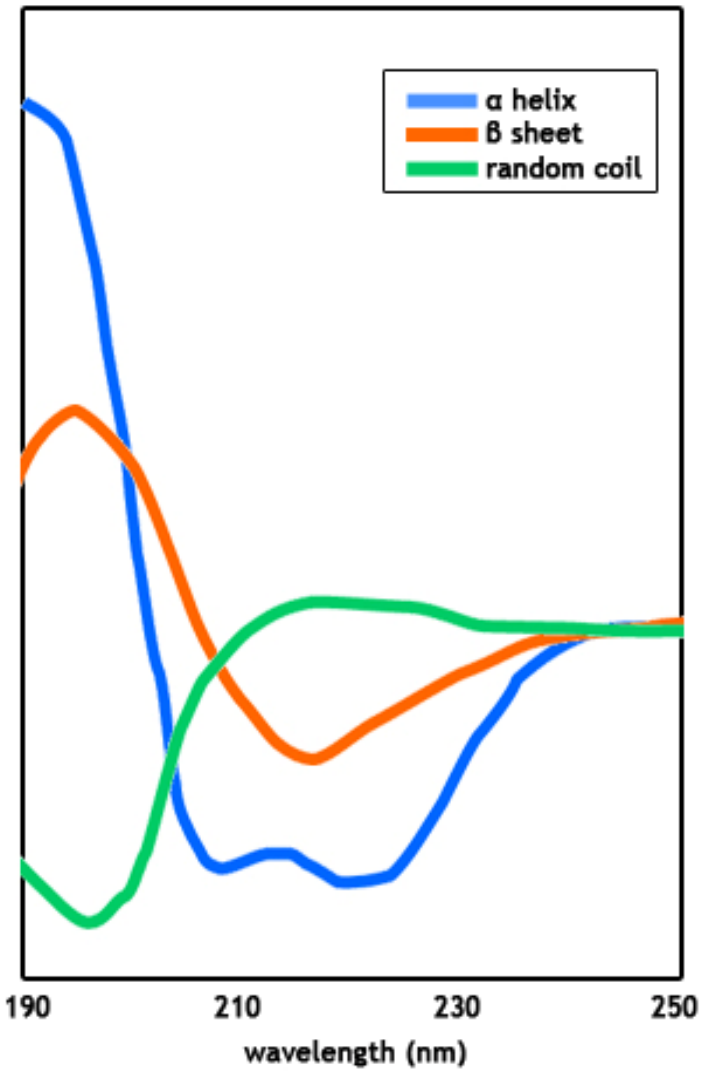

Figure 2-1 CD spectra from various secondary structure elements. Reproduced with permission from Omjoy K. Ganesh.

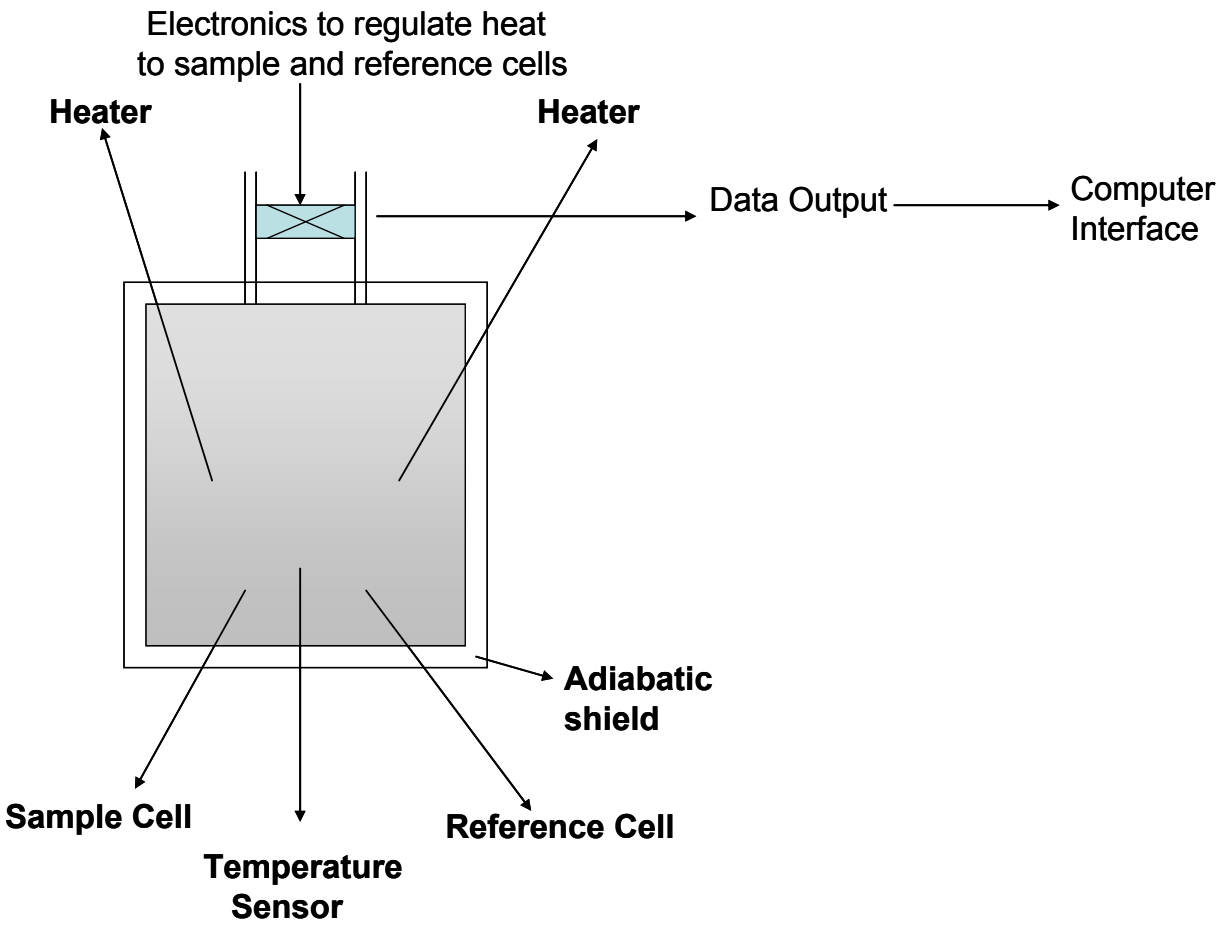

Figure 2-2. Schematic of a differential scanning calorimeter (DSC). Information pertaining to its operation and output are described in Chapter 2.

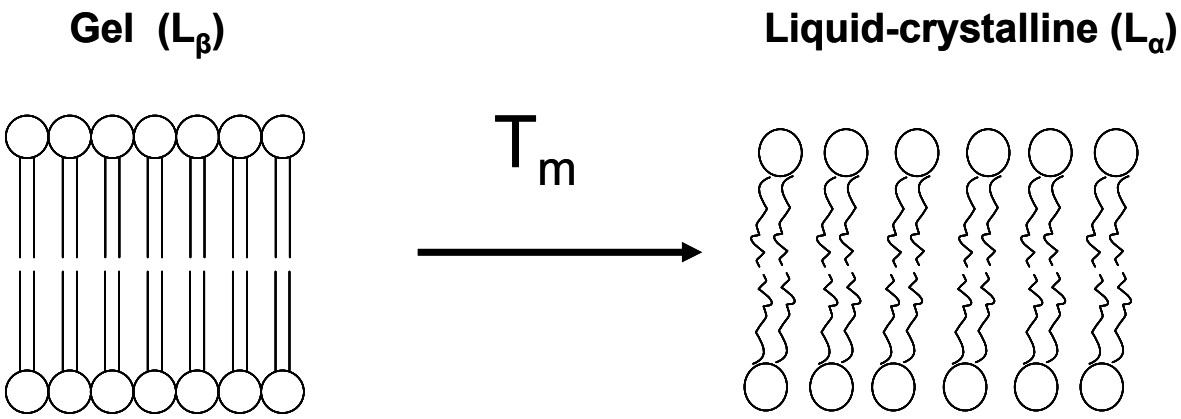

Figure 2-3. The gel to liquid-crystalline phase transition of phospholipids bilayers. When the temperature of a phospholipid dispersion is above its characteristic main phase transition temperature, T_m, the acyl chains acquire additional degrees of freedom causing the individual molecules to freely rotate and an expansion of the bilayer volume occurs.

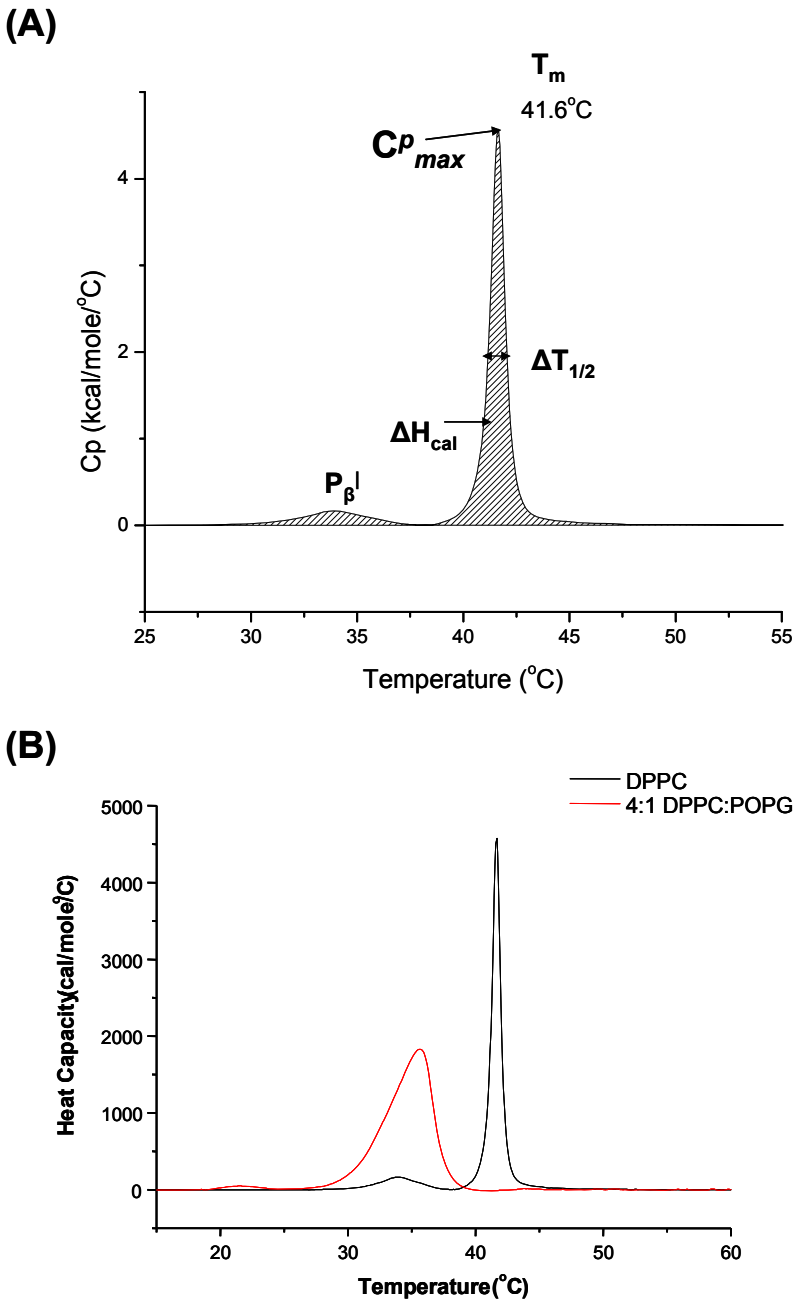

Figure 2-4 A) DSC thermogram of 2mM DPPC large unilamellar vesicles (LUVs) dispensed in 5mM HEPES pH 7.4. Scan rate was at 1 degree per minute and temperature scans were from 10 to 70 degrees Celsius. The phase transition at 41°C indicating the L_β to L_α is clearly shown. The pre-transition or the P'β phase is also shown. B) The effect on the DSC thermogram by the addition of monounsaturated POPG to DPPC LUVs.

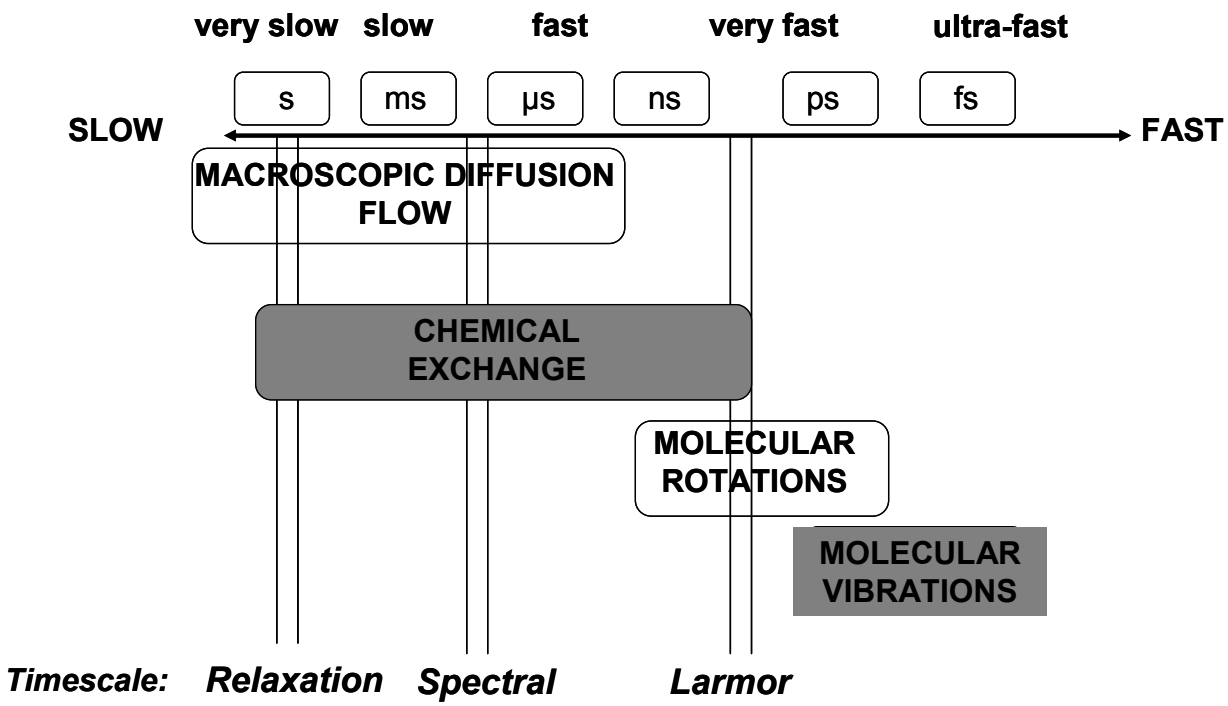

Figure 2-5. Time scale of motional processes for nuclear spins in NMR.

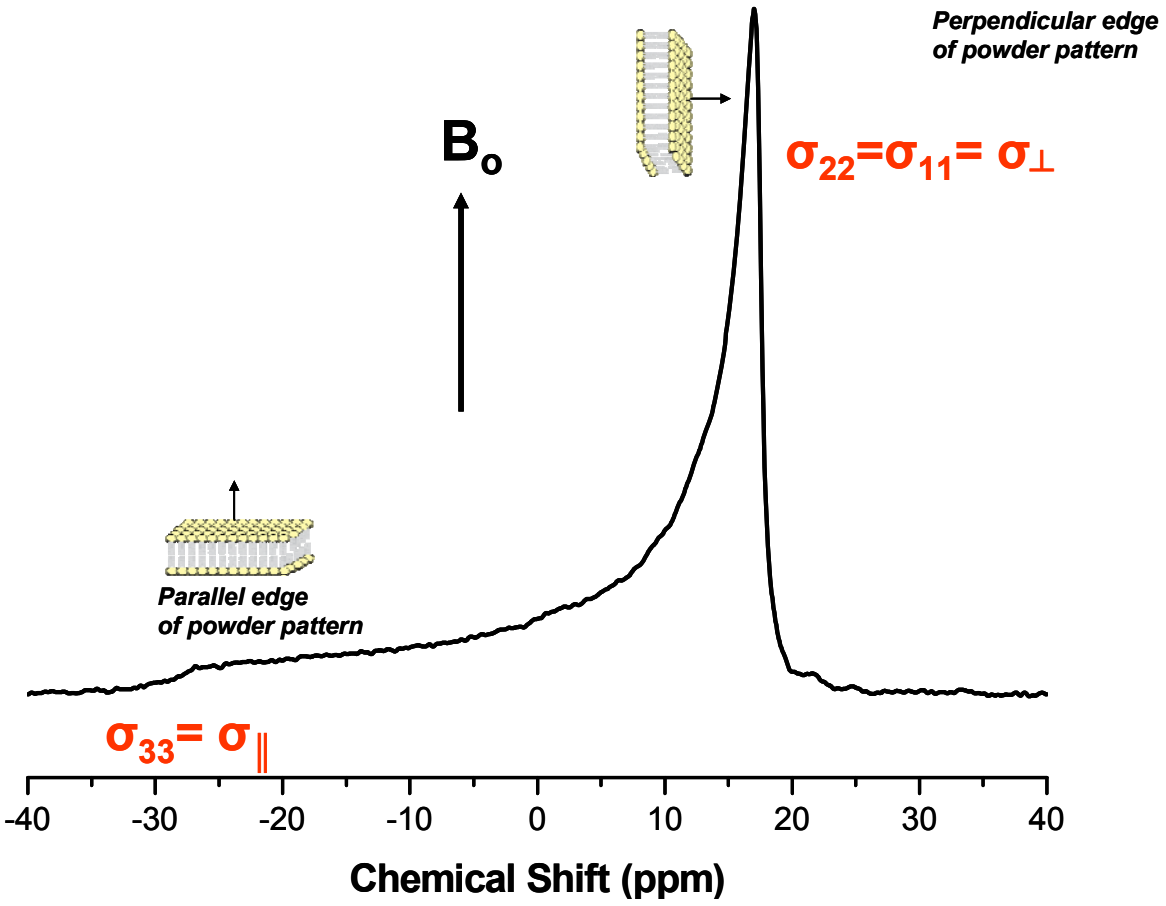

Figure 2-6. ^{31}P NMR static spectrum of DPPC hydrated vesicles (approximately 60mg). The spectrum was taken at 44 degrees on a 600MHz Bruker instrument with 1024 scans. Above its phase transition, T_m, the powder pattern takes on a shape with axial symmetry. A clear perpendicular and parallel edge are seen.

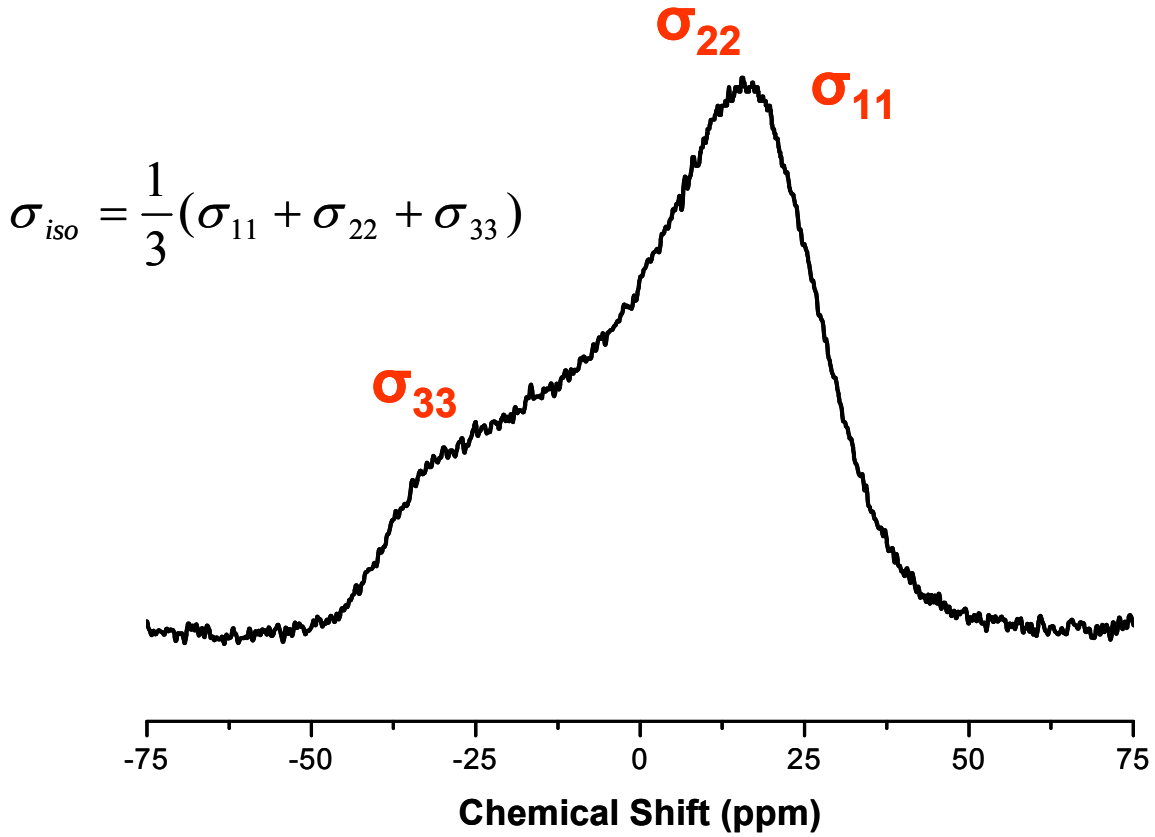

Figure 2-7. ^{31}P NMR of static hydrated DPPC vesicles (approximately 60mg) taken on a 600 MHz Bruker instrument (1024 scans) at 24^{0}C, well below its phase transition temperature, $T_{m.}$ Below T_m, the powder pattern reflects incomplete averaging of the asymmetric ^{31}P CSA tensor. Shown are the principal values of the CSA.

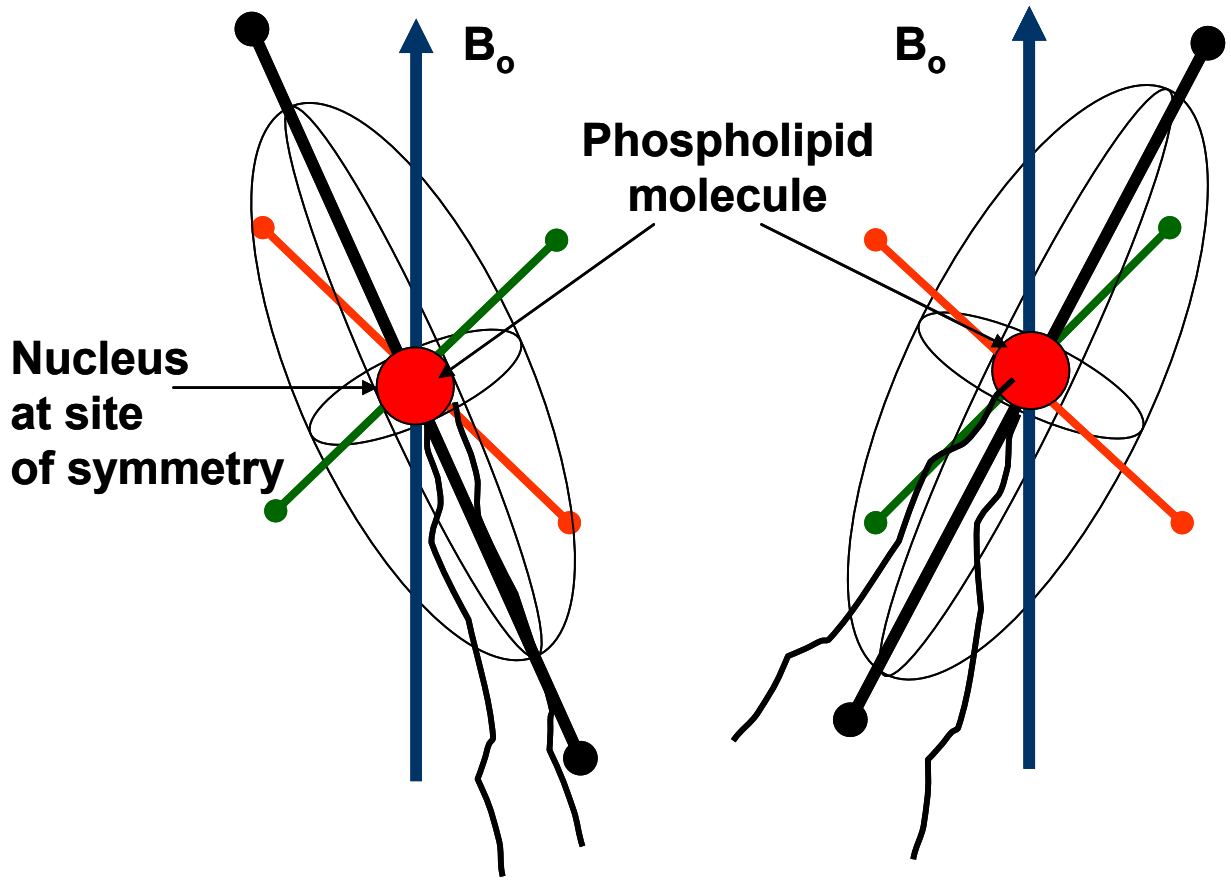

Figure 2-8. Graphical depiction of shielding tensor for a nucleus with an axis of symmetry. The CSA tensor is illustrated as an ellipsoid with the center being at the nucleus of interest, in this case the phosphate headgroup of a phospholipid. When the molecular orientation changes, so does the orientation of the interaction tensor with respect to the magnetic field. For liquid-crystalline phospholipids in a lamellar phase, the symmetry axis is the bilayer normal. Shown in orange and green are principal axes of the ellipsoid, while the dark black line is the axis of rotation. The phosphate headgroup is shown as a red sphere and wavy lines represent the acyl chains.

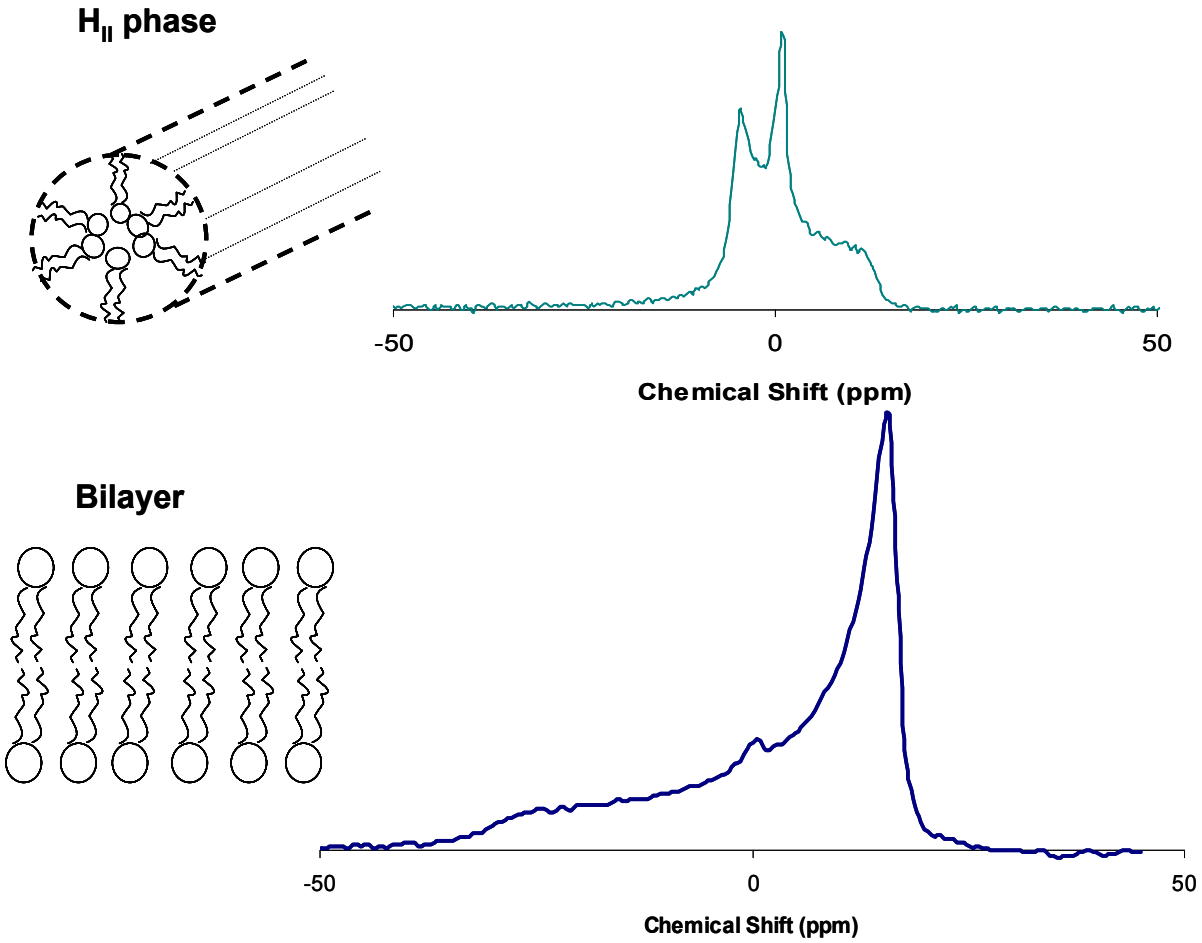

Figure 2-9. Phosphorous NMR lineshape patterns for lipid mesophases. Shown above is the lineshape for an inverted H_{II} hexagonal phase common in many lipid-lipid mediated events. The isotropic peak at 0 frequency represents partial degradation of the sample. Below is the standard powder pattern seen in the bilayer lamellar phase.

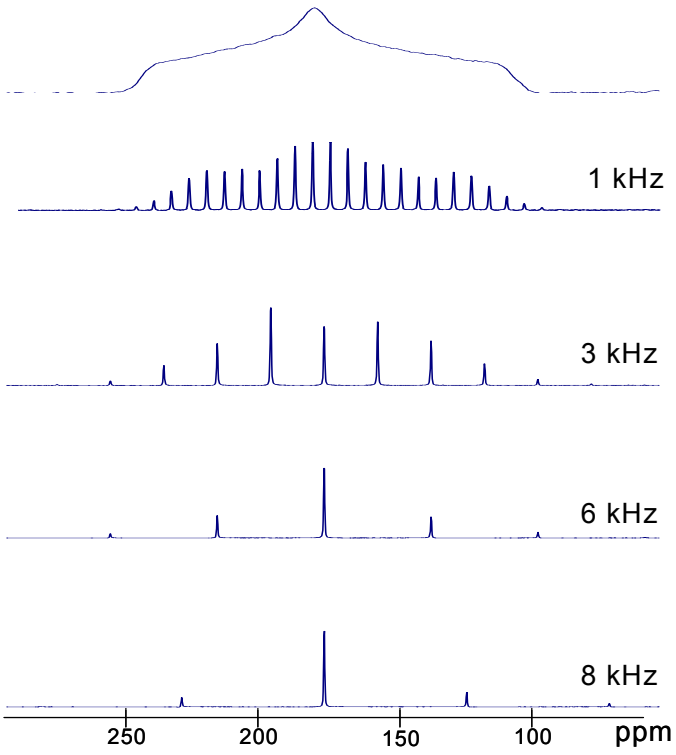

Figure 2-10. Magic angle spinning (MAS) spectra of the $^{13}C'$ nucleus in glycine. Sample was packed in a rotor and spun at the magic angle of 54.74 degrees at spin speeds between 1 and 8kHz. Clearly seen are the "spinning side bands" which gradually disappear as the spin speed becomes comparable with the CSA; the isotropic peak is seen in the center. Data provided with permission from Dr. Manish Mehta.

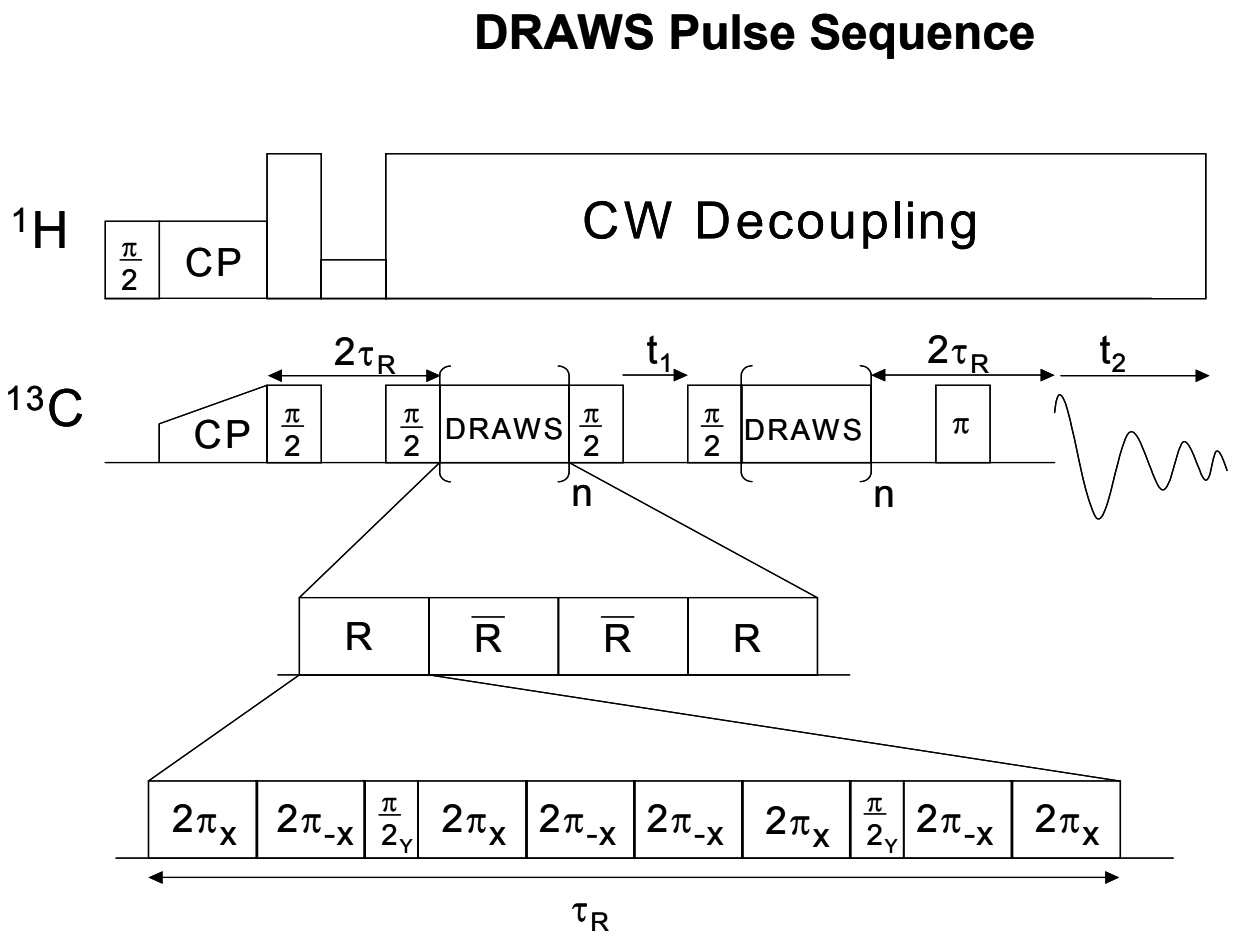

Figure 2-11. DRAWS pulse sequence of DRAWS employed during MAS for dipolar recoupling. Each rectangle represents a RF pulse that rotates the magnetization either 90 or 360 degrees. CP is cross-polarization, the transfer of magnetization from protons to lower gamma ^{13}C nuclei. τ_R and R corresponds to a MAS rotor period.

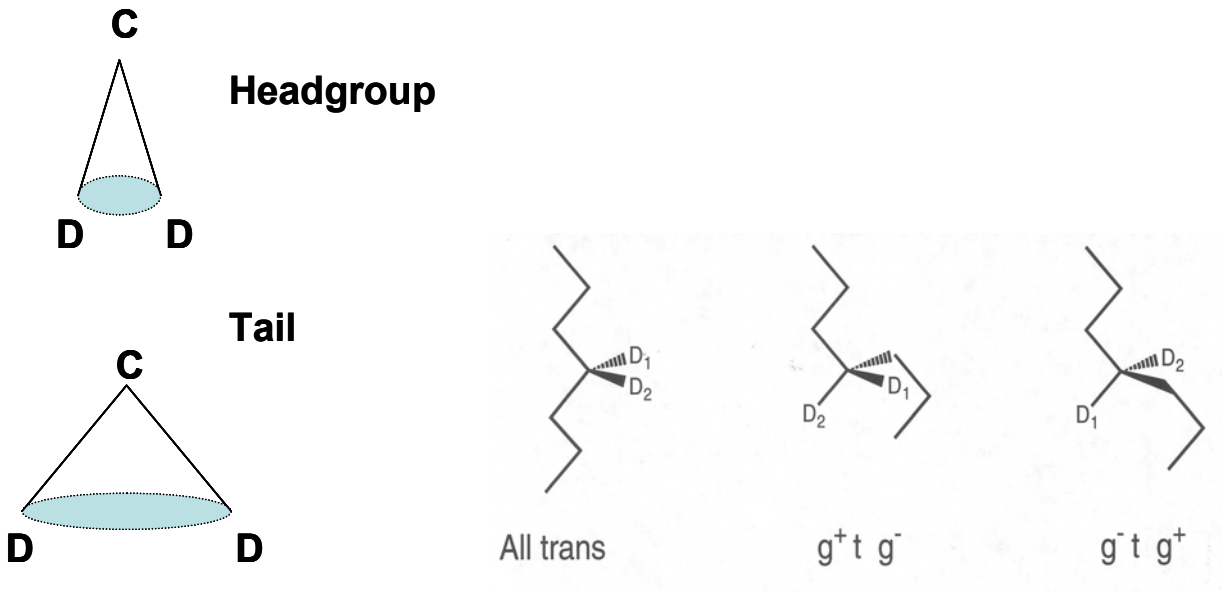

Figure 2-12. Collective motions of each methylene position along the acyl chain roughly averages out to a conicall shape. The methylenes near the headgroup trace out a cone of smaller radius while due to greater motional freedom and lack of steric interference, the acyl chains at the terminal end trace out a cone of larger radius. Shown on the right are the difference orientations of one C-D bond. With respect to other carbons in the chain the C-D bonds can be all trans or gauche-trans-gauche.

(A)

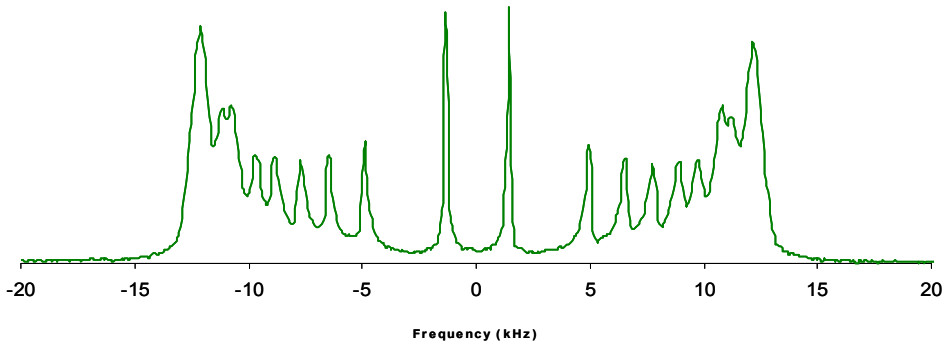

(B)

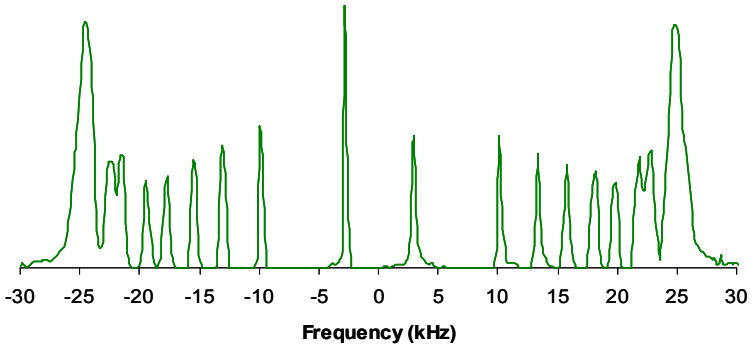

Figure 2-13. Deuterium spectra of (4:1) DPPC:POPG(d-31) (mol/mol) with POPG fully deuterated on the sn-1 acyl chain. Spectrum was taken on a 600 MHz Bruker instrument with 1024 scans. Each pair of peaks corresponds to the perpendicular edges of a powder pattern for a methylene position along the acyl chain. The most intense peaks near 0 frequency correspond to the terminal methyl group while overlapping peaks with the largest quadrupolar splitting corresponds to C-D bonds near the headgroup region. B) The corresponding dePaked spectrum allowing clear determination of the order parameter at each methylene position.

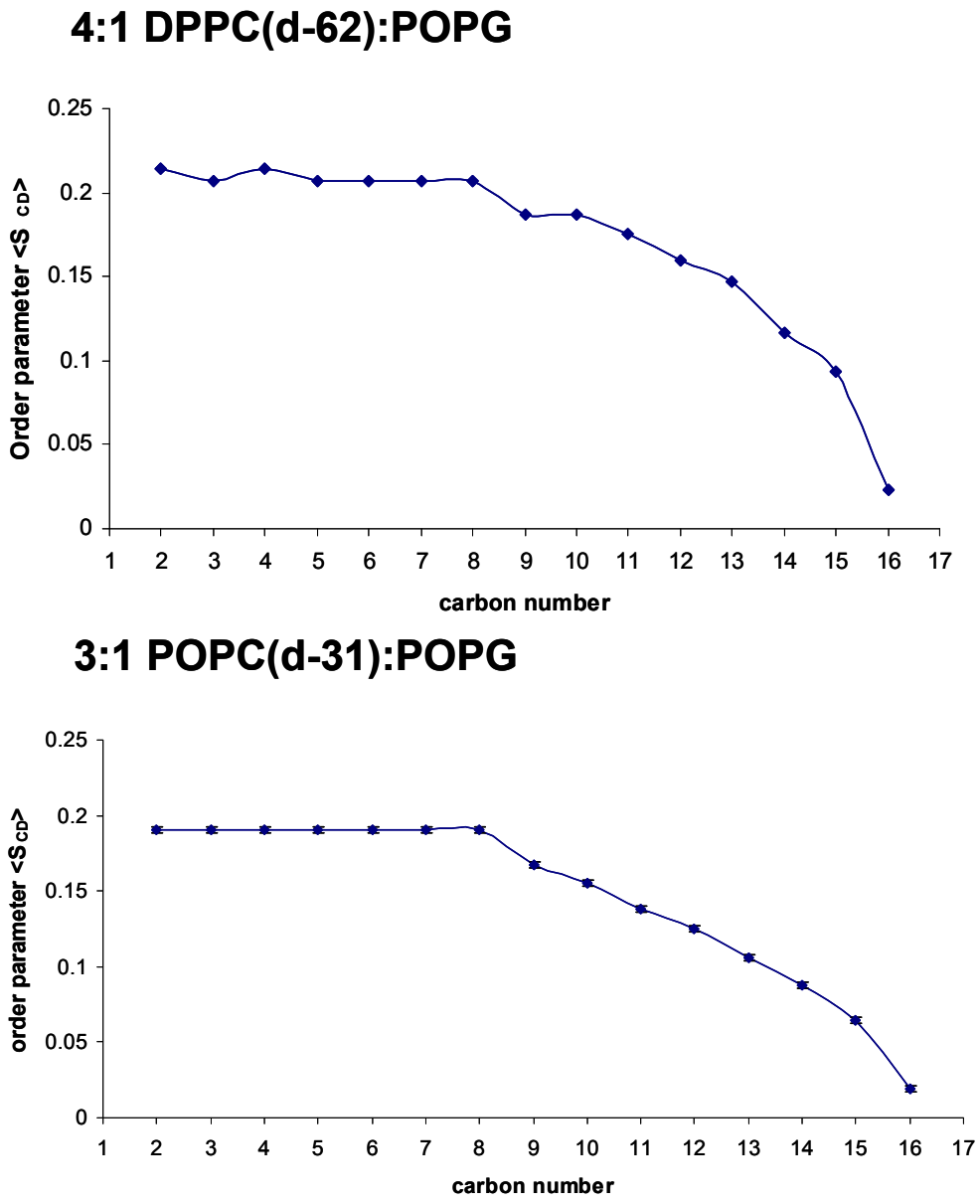

Figure 2-14. Example of order parameter profile generated from dePaking ^{2}H NMR spectra, for perdeuterated acyl chains. The time averaged order parameter for each methylene along the fatty acyl chains were calculated from spectra of 4:1 DPPC(d-62):POPG (above) and 3:1 POPC(d-31):POPG) (below). The order parameter profile for the sn-2 chain of DPPC is shown although both chains were deuterated. Only the sn-1 chain of POPC shown was deuterated.

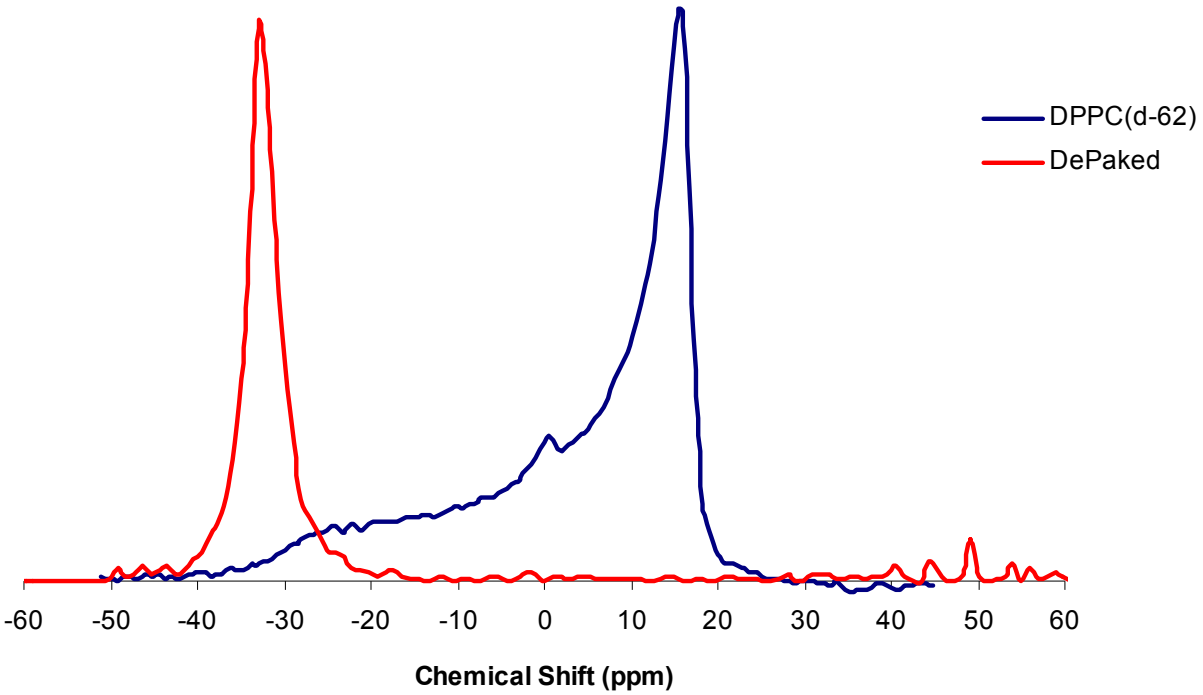

Figure 2-15. Example of ^{31}P NMR (blue) and the dePaked result (red). From the dePaking, a single frequency, corresponding to the parallel edge of the powder pattern, is generated. This spectrum was collected on 25mg of DPPC(d-62) on a 500MHz spectrometer with 3072 scans at 44 degrees.

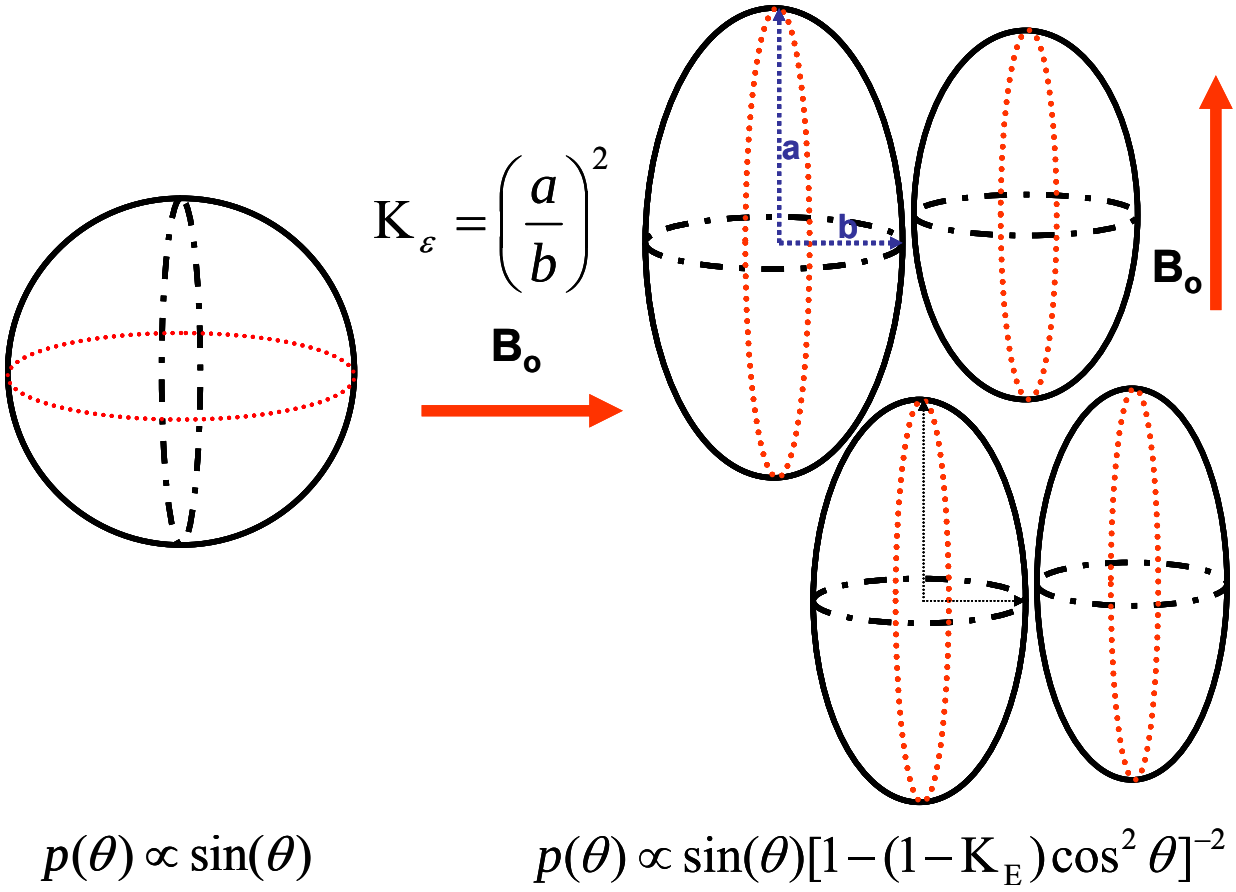

Figure 2-16. Lipid vesicles when placed in a magnetic field can deform to form an ellipsoidal shape. An orientational order parameter designated K_ε is the square of the ratio of the minor to major axis of the ellipsoid and yields information pertaining to the extent of magnetic field alignment by phospholipid molecules. A random distribution, as seen in a classic powder pattern, gives rise to intensities proportional to sin(θ), where θ is the angle between the bilayer normal and B_o. When lipids align, the probability of finding a particular bilayer normal orientation relative to B_o changes and is proportional to the orientational order parameter, according to the equation shown at the bottom. Equations taken from Sternin E in J Magn Reson. 2001 Mar;149(1):110-3.

CHAPTER 3
SURFACTANT PEPTIDE KL_4 DIFFERENTIALLY MODULATES LIPID COOPERATIVITY AND ORDER IN DPPC: POPG AND POPC: POPG LIPID VESICLES

The following is a manuscript in preparation to be submitted to the journal *Biochemistry*. The final version submitted may differ from what is presented in this dissertation due to revisions and corrections during the peer review process and journal format specifications.

KL_4 is a 21-residue peptide employed as a functional mimic of lung surfactant protein SP-B, an essential protein which lowers surface tension in the alveoli. In this study, ^{31}P and ^{2}H NMR were utilized to study the effects of KL_4 on lipid organization in 3:1 POPC: POPG and 4:1 DPPC: POPG MLVs. NMR spectra recorded at 14.1T indicate a high degree of lipid alignment, particularly for DPPC: POPG MLVs. The addition of KL_4 decreases this alignment in a concentration dependent manner. ^{31}P NMR spectra of the phospholipids clearly indicate KL_4 affects the orientation of the anionic headgroups in a concentration dependant manner. ^{2}H NMR spectra of the deuterated lipid acyl chains clearly show KL_4 effects the ordering of the bilayer interior in a manner which is dependant on the degree of saturation in the fatty acid tails. Substantial increases in the acyl chain order parameters were observed in ^{2}H NMR spectra of DPPC(d-62):POPG MLVs with increasing levels of KL_4. The largest changes in order occur at carbon acyl position 9-15 suggesting the peptide deeply penetrates into DPPC:POPG bilayers. Conversely, ^{2}H spectra of POPC(d-31):POPG, DPPC:POPG(d-31), and POPC:POPG(d-31) MLVs showed smaller but measurable decreases in the acyl chain order parameter on addition of KL_4. Thus, fatty acid saturation has a marked effect on the insertion depth of KL_4 into phospholipid MLVs and lipid miscibility. The effects are seen to be approximately linear with KL_4 concentrations up to 3mol% peptide, the highest percentage studied. The influence of KL_4 on lipid phase transitions was also monitored for 4:1 DPPC:POPG MLVs via DSC. Addition of KL_4 led to slightly higher lipid phase transition temperatures, supporting NMR data suggesting

the peptide causes lipid domain separation in a concentration dependant manner. Based on these findings, a model of how KL_4 interacts with these lipids is presented.

Relevance of KL_4 to Lung Surfactant Biology

Lung surfactant is a lipid-rich substance containing key proteins that lines the inner layer of the alveoli. The primary functions of lung surfactant are to minimize surface tension at the alveolar air-fluid interface and to provide a barrier against disease (*2, 15, 60, 133-135*). Inadequate protein levels are a leading cause of respiratory distress syndrome (RDS) in premature infants as well as in adults and children experiencing lung trauma or respiratory infections (*39, 51, 66*). Current therapies for RDS primarily rely on administration of lung surfactant from exogenous sources (*1, 136*). This reliance on xenogenic surfactant is due to the critical role of SP-B, a highly hydrophobic, 79 residue protein which functions as a homodimer containing 7 disulfide bridges (*29*). In mice, deletion of SP-B at the genetic level is lethal (*16*) and disruption via mutation causes respiratory failure (*39, 137*). Peptide-based lung surfactant replacements designed to replicate the properties of SP-B have received noticeable attention (*67, 138*) as the use of synthetic analogs would remove the immunologic risks associated with animal-derived surfactant and allow for greater therapeutic consistency (*136*).

The lipid constitution in mammalian lung surfactant is heterogeneous, but is dominated by zwitterionic DPPC (dipalmitoylphosphatidylcholine) (~60%) and anionic POPG (palmitoyloleoylphosphatidylglycerol) (~10%). Levels of the lipids are relatively conserved in the lungs of vertebrates (*4, 16, 29*). SP-B is present at low levels, 0.7-1.0% by weight or a molar percentage of <0.2% relative to the lipids (*16*). A multitude of roles for SP-B in surface tension minimization, intracellular and extracellular surfactant trafficking and respiratory dynamics in general have been proposed and experimentally established (*23*). Lung surfactant undergoes a cycle of lipid adsorption and resorption at the air-fluid interface which is postulated to be

facilitated by SP-B (*23*). Lipid polymorphisms that change the geometry and arrangement of lipid headgroups have also been posited as critical for the functional properties of lung surfactant, as well as in other membrane-membrane mediated events (*15*, *108, 139*). Molecular level information on how synthetic peptides, unrelated at the primary amino acid level to SP-B, can modulate surface tension in alveolar compartments is lacking, yet KL_4 in combination with POPG, DPPC, and PA (palmitic acid) has been approved as an agent for treatment of RDS due to its efficacy (*136*). *In-vitro* assays as well as animal studies have shown the ability of KL_4 to lower surface tension in different lipid systems (*133, 134*). Clinically, administration of a KL_4 surfactant preparation (lucinactant) to very premature infants was markedly more effective in treating RDS than other commercially available formulations (*140*). Thus, understanding how KL_4 affects the molecular and biophysical properties of the lipids is of particular relevance to the treatment of various forms of RDS.

Peptide mimics which rely on a presumption of helicity and amphipathicity have been pursued both therapeutically and as model systems for understanding the unique properties of SP-B. For example, KL_4 was designed based on the charge distribution of the C-terminal residues 59-80 (*133*, *134*). Of particular interest is that KL_4 retains many of the macroscopic and biophysical properties of SP-B despite bearing little resemblance to the primary sequence of the protein other than a similarity in charge distribution at the C-terminus.

The use of differential scanning calorimetry in combination with NMR can provide insight into how KL_4 induces changes in lipid phase properties and/or geometric arrangement. In this study, ^{2}H NMR, ^{31}P NMR, and DSC were employed to investigate the properties of 4:1 DPPC:POPG and 3:1 POPC:POPG lipid vesicles on addition of KL_4. The former composition was selected to mimic the composition of lung surfactant while the latter composition is similar

to formulations used in numerous NMR studies of membrane-active antimicrobial peptides, allowing us to compare the properties of KL_4 to other amphipathic, helical peptides.

Methodology to Study KL_4 with Lipids

Synthesis of KL_4: KL_4 (KLLLLKLLLLKLLLLKLLLLK) was synthesized via automated solid-phase peptide synthesis on a Wang resin (ABI 430, ICBR, UF). The peptide was cleaved from the resin with 90% TFA/5% triisopropyl-silane/5% water and ether precipitated. The crude product was purified by RP-HPLC using an acetonitrile/water gradient and purity was verified by mass spectrometry.

Dried peptide was weighed and dissolved in methanol to a stock concentration of approximately 1mM. Aliquots were analyzed by amino acid analysis to allow for a more accurate determination of concentration (Molecular Structure Facility, UC Davis).

Preparation of Peptide:Lipid Samples for DSC: DPPC and POPG were purchased (Avanti Polar Lipids, Alabaster, AL) as chloroform solutions and concentrations were verified by phosphate analysis. The lipids were mixed at a molar ratio of 4:1 DPPC:POPG in chloroform, aliquoted, and a methanol solution of KL_4 was added as needed to make samples with peptide:lipid ratios ranging from <1:1000 to >1:50. The peptide-lipid samples were dried, dissolved in cyclohexane and freeze-dried overnight to remove residual solvent. Each resultant peptide-lipid powder was solubilized in 5mM HEPES buffer at pH 7.4, with 140mM NaCl, 1mM EDTA, and 5mM $CaCl_2$ to a final lipid concentration of approximately 3mM. Samples were placed in a 50^{o}C water bath to facilitate solubilization accompanies by 3-5 freeze thaw cycles to facilitate solubilization and equilibration. Peptide:lipid MLVs were extruded through 100nm filters (AvantiPolar Lipids, Alabaster, AL) to form LUVs and degassed just prior to DSC. DSC experiments were conducted over a range of 10-70^{o}C at a scan rate of 1^{o}C/min and run in triplicate. Following DSC, aliquots of each sample were removed and assayed by phosphate

analysis to determine final phospholipid concentration. All assayed concentrations were within 10% of initial estimated concentrations.

Data analysis was performed with Origin v6.0. For heat capacity measurements, the molar lipid concentration in the DSC sample cell was based on inorganic phosphate assays. ΔH_{cal} was determined by integration of the phase transition peaks in the DSC thermograms after baseline correction. The van't Hoff derived enthalpy (ΔH_{vH}), an enthalpic parameter utilizing the phase transition temperature (T_m) of the lipid, was determined by equation (3-1) (*86*):

$$\Delta H_{vH} = 4RT_m^2 \frac{C_p^{\max}}{\Delta H_{cal}} \qquad (3\text{-}1)$$

Lipid cooperativity was assessed by both measuring the peak width at half height ($\Delta T_{½}$) and by calculating the cooperativity unit based on the ratio of the van't Hoff enthalpy to the calorimetric enthalpy.

Solid state NMR sample preparation: A methanol solution of KL_4 was added to chloroform solutions of 4:1 DPPC(d-62):POPG, 4:1 DPPC:POPG(d-31), 3:1 POPC(d-31):POPG, 3:1 POPC:POPG(d-31), DPPC(d-62), POPC(d-31), and POPG(d-31) to make a series of samples with final peptide to lipid ratios ranging from <1:1000 to >1:50. The MeOH and $CHCl_3$ were evaporated under nitrogen and the peptide/lipid film was dissolved in cyclohexane and lyophilized overnight to remove residual solvent. Approximately 25mg of each sample was then placed in a 5mm diameter NMR tube and 300µL of buffer containing 5mM HEPES buffer at pH 7.4,140mM NaCl, and 1mM EDTA in ^2H depleted water (Cambridge Isotope Laboratories, Andover MA) was added. NMR samples were then subjected to 3-5 freeze-thaw cycles to form MLVs.

Phosphorous (^{31}P) NMR: ^{31}P NMR data were collected on a 600 MHz Bruker Avance system (Billerica, MA) using a standard 5mm BBO probe and a standard pulse-acquire sequence with 25 kHz proton decoupling during acquisition. Spectra were acquired at 3 temperatures (39, 44 and 49^{o}C) with 1024-2048 scans for each spectrum and a 5 second recycle delay between scans to minimize RF heating of the samples.

The transform of a powder lineshape to an oriented spectrum at a single frequency is termed dePaking. The dePaking of NMR spectra was performed using an algorithm provided by Professor Edward Sternin. The algorithm employed a Tikhonov regularization method (*102, 103, 105*) to simultaneously determine the extent of macroscopic ordering in partially aligned lipid spectra and the dePaked frequencies (*103*).

Deuterium (^{2}H) NMR: ^{2}H NMR data were collected on a 500MHz Bruker Avance System (Billerica, MA) using a standard 5mm BBO probe and quad echo sequence with a B_1 field of 40 kHz. Spectra were acquired at 3 temperatures (39, 44 and 49^{o}C) with 1024-2048 scans and 0.5 second recycle delay.

The dePaking of ^{2}H NMR data was performed using the same algorithms as for the ^{31}P NMR spectra. Individual assignments of peaks were made based on work by Petrache, *et al* (*104, 117, 124*) and Seelig (*104*).

KL_4 Affects Lipid Phase Behavior

The dynamic air-fluid interface in the lung requires lung surfactant to possess specific attributes to lower surface tension and allow rapid respreading. Lipid-rich surfactant relies on relatively low levels of lung surfactant proteins B and C (<0.2mol%) to alter the structure, dynamics, and phase properties of the lipids to achieve the characteristic properties of lung surfactant. The peptide KL_4 similarly affects the macroscopic properties of the lipids and thus has been pursued as a replacement for SP-B in therapeutic formulations (*137, 140*).

The size and shape of the ^{31}P chemical shift anisotropy in phospholipid headgroups can identify the existence of hexagonal, lamellar, or other lipid phases (*108*), and in lamellar phases the size of the anisotropy is primarily dependant on the average orientation of the phosphate headgroups relative to the bilayer normal. Furthermore, ^{2}H NMR spectra of lipid systems where the palmitoyl chains of either the phosphatidylcholines or the phosphatidylglycerol are deuterated can determine the effects and insertion depth of KL_4. The role of KL_4 in lipid phase behavior can also be observed using ^{31}P NMR.

Calorimetric data at increasing concentrations of KL_4 also assesses the effect of the peptide on the thermodynamics and cooperativity of the L_β to L_α lipid phase transition in DPPC:POPG vesicles. The DSC data for 4:1 DPPC:POPG vesicles containing KL_4 show a concentration dependent effect of the peptide on the main phase transition (Figure 3-1). Adding POPG to DPPC in a 1:4 ratio shifts the T_m for DPPC from 42°C to below 36°C due to the monounsaturated fatty acid group in POPG. Addition of the peptide shifts the T_m back to higher temperatures in a concentration dependant manner. Small amounts of peptide increase the T_m slightly by 2-3°C; ΔH_{cal}, and ΔH_{vH} remain relatively the same except for a slight increase at 0.75 mol% of peptide. At 0.75 mol % KL_4, the shape of the thermogram noticeably bifurcates, providing indirect evidence of lipid domain separation. This bifurcation becomes more pronounced at higher concentrations of peptide, most noticeably 1.5 and 2.2 mol%, agreeing well with the observation of domain formation via Langmuir trough studies of KL_4 interacting with fluorescently labeled DPPC in a DPPC:POPG:PA system (*141*). This bifurcation has also been seen by Saenz, *et al*, at a lower peptide ratio (0.5 mol%) in 3:1 (w/w) DPPC:POPG MLVs (*142*). This correlates well with postulated domain formation mediated via electrostatic interactions between anionic phospholipids (such as POPG) and cationic peptides (such as KL_4) (*85*). This

behavior may be important to the function of the peptide *in vivo* during the lipid resorption/adsorption cycle (*23*). Table 3-1 summarizes the thermodynamic behavior of DPPC:POPG as a function of peptide concentration.

^{31}P NMR: Addition of KL_4 Leads to Changes in Orientation of the PG Headgroups

^{31}P NMR spectra of 3:1 POPC:POPG and 4:1 DPPC:POPG preparations show orientation of the lipid bilayers in the magnetic field leading to distorted axially symmetric spectra with higher than expected intensities at the perpendicular edges (Figure 3-2 and Figure 3-4). Overlapping lineshapes resulting from the PC and PG headgroups are easily distinguished at this field. Lipid alignment in high magnetic fields has been observed previously and is caused by the negative diamagnetic susceptibility inherent to phospholipids (*129, 130, 143*). In lipid bilayers, the cooperative alignment of the magnetic moments of individual lipid molecules leads to a large bulk magnetic susceptibility and an overall macroscopic ordering of the sample within a magnetic field (*132*). Increasing amounts of KL_4 disrupts this alignment in a concentration dependent manner, as evidenced by the gradual increase in the parallel edges of the ^{31}P spectra. The reduction in alignment of the lipid lamellae on addition of KL_4 suggests the peptide disrupts lipid-lipid interactions and dissipates the ellipsoidal distortion of the vesicles in the magnetic field; the degree of alignment seen is similar for all lipids within the sample. When dePaking the NMR spectra the ellipsoidal parameter (K_ε) provides a measure of decreases in alignment with increasing KL_4.

DePaking of the ^{31}P NMR spectra for 3:1 POPC(d-31):POPG and 4:1 DPPC(d-62):POPG clearly show changes in the PG headgroup orientations based on the shifts in the POPG peak on addition of KL_4 while the DPPC anisotropy remains constant (Figure 3-3 and Figure 3-5). When the POPG acyl chains are deuterated, the results are the same as expected since the deuteration

should have little effect on the headgroup of the lipid. These results strongly support a concentration dependant ionic interaction between the cationic KL_4 peptide and electronegative PG moiety. Table 3-2 lists the ^{31}P CSA span for the headgroups and a general reduction in span with increased KL_4 concentration is seen for POPG in both lipid systems. Figures 3-6 and Figure 3-8 show the static ^{31}P NMR spectra of lipids with deuterated POPG and Figure 3-7 and 3-9 show the corresponding dePaked spectra. The shift in the POPG parallel edge frequency is consistently seen throughout all lipid systems studied regardless of which lipid was deuterated. Figure 3-10 shows the $\Delta\sigma$ (change in CSA) for DPPC and POPG in DPPC:POPG(d-31).

To assess the underlying causes of the changes in POPG CSAs and the ordering of the acyl chains in the binary lipid mixtures, ^{31}P and ^{2}H NMR spectra were collected on individual lipids alone and with 1.5mol% KL_4. ^{31}P NMR spectra are shown in Figure 3-11 and the corresponding dePaked spectra are shown in Figure 3-12. Only small changes in CSA are seen on addition of KL_4. However, the CSA for POPG alone is significantly smaller than observed for 4:1 DPPC:POPG or 3:1 POPC:POPG mixtures prior to the addition of KL_4. However, for the binary lipid mixtures with higher amounts of KL4, the ^{31}P CSAs are more similar to those expected based on the spectra of the neat lipids. Thus, KL_4 is clearly affecting the interactions of the PC and PG lipids as well as their miscibility. This is in agreement with the DSC data showing phase separation or lipid sequestration on addition of KL_4. Hence one important role possibly mediated by the peptide is lipid demixing via interactions of KL_4 with the PG headgroups.

KL_4 Effects on Lipid Acyl Chain Ordering Dependent on the Saturation of the Acyl Chains

Deuterium solid state NMR can serve as a sensitive non-perturbing probe for investigating dynamic processes of proteins and lipids. The size of the ^{2}H quadrupolar interaction is well-matched to the time scale of many dynamic processes occurring in membranes and proteins, particularly for fatty acid chains in lipid systems (*144*). The extent of peptide interaction with

the bilayer can easily be monitored by determining the time averaged order parameters, $<S_{CD}>$, for each position in the fatty acid chain and monitoring their changes with addition of peptide.

The order parameter encapsulates motions of the lipids, including axial rotation around the lipid long axis, undulations or reorientations of the lipids with respect to the bilayer normal known as "wobbling", and trans-gauche isomerization at individual methylene positions along the acyl chains (*119*). The order parameter reflects the collective averaging of these motions on the NMR timescale (10^{-5} seconds), which also includes lateral diffusion of the lipid molecule. Typical $<S_{CD}>$ values are on the order of 0.2 for fatty acyl chains in individual lipids near the headgroup (*145*). The effect of KL_4 on motions at each individual C-D bond methylene position, and on lipid motions in general can thus be quantitatively determined.

NMR spectra taken for binary lipid systems with palmitoyl chains deuterated on different lipids are shown in Figures 3-13 to 3-17 along with their dePaked spectra.
As with ^{31}P NMR data, some lipid alignment in the static field is seen. Spectra taken with different deuterated acyl chains were taken to determine whether and how the peptide interacts with the acyl region of a particular lipid.

A recent reevaluation of deuterium order parameters on a series of disaturated PC headgroups was performed by Petrache, *et al* at different temperatures (*124*) which were extrapolated to 44°C to assign the sn-1 and sn-2 positions in DPPC spectra. Using this and the acyl chain assignments from Seelig (*104*) as a guide, assignments and order parameter calculations were made. The calculated order parameters (using Equation 2-14) from $\Delta\nu_q$ values for each lipid system studied can be found in the Appendices. Furthermore, ^2H NMR spectra of neat lipids DPPC(d-62), POPC(d-31), and POPG(d-31) with and without 1.5mol% KL_4 were also collected, dePaked and assigned (Figure 3-18) unfortunately, the poor signal to noise ratio

obtained from these measurements prevented clear assignments for each methylene position after dePaking.

The order parameters profiles obtained for 4:1 DPPC(d-62):POPG , 4:1 DPPC:POPG (d-31), 3:1 POPC(d-31):POPG and 3:1 POPC:POPG(d-31) demonstrate that the peptide interacts with the two lipids in a manner that is dependant on the degree of saturation in the fatty acid chains. Figure 3-19 shows the calculated order parameters as a function of carbon number for the sn-1 and sn-2 chains of DPPC from spectra of 4:1 DPPC(d-62):POPG. KL_4 clearly affects the acyl chain dynamics of DPPC at positions 9-15 in a concentration dependant manner and increases their ordering. Similar concentrations of peptide added to 3:1 POPC(d-31):POPG MLVs lead to only small changes in order parameters (Figure 3-20). Smaller, negative changes in order are seen for corresponding regions in the sn-1 chain of POPC in 3:1 POPC(d-31):POPG bilayers suggesting a more peripheral interaction with the lipids or preferential interaction with POPG as was found from ^{31}P NMR. Hence, the degree of saturation and lipid system has an effect on mode of binding of KL_4.

The data shown above are more pronounced when the observations are viewed as the percent change in order parameter $\delta\langle S_{CD}^{i}\rangle$ at each position along the acyl chain. Shown are the changes in $\langle S_{CD}^{i}\rangle$ at a particular methylene *i* for 4:1 DPPC(d-62):POPG (Figure 3-21) and 3:1 POPC(d-31):POPG (Figure 3-22). Changes in the order parameter, relative to lipids alone, are shown for C-D bond representing the plateau region (carbon 3), middle of the acyl chain, and the terminal ends. Significant changes in $\delta\langle S_{CD}^{i}\rangle$ occur for both sn-1 and sn-2 chains of DPPC, with increases of up to 10% for carbon 10 and 12 and 8.5% for carbon 8. This high degree of ordering suggests KL_4 is penetrating deep into the bilayer and decreasing the mobility of the acyl chains. This increase in ordering at the middle and ends of the acyl chains from deuterium data

for DPPC(d-62):POPG argue for a deep penetration of the peptide, but the lack of similar changes in positions 2-3 suggest the peptide does not adopt a transmembrane orientation. Thus KL_4 lodges into the hydrophobic region of the bilayer, while maintaining a perpendicular orientation to the bilayer normal. Quantitatively, the calculated $\delta<S_{CD}^{i}>$ for 3:1 POPC(d-31):POPG, decrease in magnitude by up to 4-6% indicating the acyl chains have increased mobility. The order parameter shifts are not obvious in the order parameter profiles shown in Figure 3-22 because the difference in their order parameter values are very small, but their percent changes make this distinction possible (Appendix A-D).

In experiments where the palmitoyl chain of POPG were deuterated; 3:1 POPC:POPG (d-31) and 4:1 DPPC:POPG(d-31), show an overall decrease in ordering of the POPG acyl chains on addition of KL_4 (Figure 3-23 and Figure 3-24). Decreases in the order parameters are seen at all the acyl positions in POPG. These results further corroborate ^{31}P NMR findings that show an association with KL_4 and the PG headgroup.

KL_4 in Relation to other Peptides of Similar Size, Composition and Length

A possible explanation for how KL_4 inserts into the bilayers is that it may form a structure in which the lysines lie on one side of a helix. The "snorkeling" of these lysine sidechains would allow an amphipathic helical conformation of KL_4 to deeply penetrate the bilayer while still having electrostatic interactions between the lysine sidechains and the lipid phosphate groups. The snorkeling of lysine residues have previously been postulated to provide negative curvature strain in the context of the transmembrane WALP and KALP peptides (*146*). Of particular interest to the snorkeling model is a molecular simulation study of the 22 amino acid peptide KKLLKLLLLLLLLLKLLLLKK which was found to have a transmembrane orientation and "snorkel" in POPC membranes (*147*). This peptide bears striking homology to KL_4 in both

amino acid content and hydrophobic to hydrophilic ratio, but the lysines are distributed more toward the ends of the peptide leading to a transmembrane configuration.

If KL_4 adopts a helical structure in the lipid environment which is perpendicular to the membrane normal, it cannot form a canonical α-helix as this would place the lysines evenly around the helix rather than in an amphipathic configuration. Nonetheless, FT-IR measurements indicate KL_4 is helical in lipid bilayers, and sits on top of the membrane (*148, 149*). Lysine and leucine rich peptides have been known to adapt to different amphiphathic secondary structures at the air-water interface and on polymer surfaces based on the amino acid pattern of the residues (*149, 150*). Similar driving forces would exist at the lipid bilayer surface and peptides of varying ratios of lysine and leucine residues have been used to modulate the peptide helicity and topology in bilayer systems (*93*). Amphipathic α-helices with specific ratios of L to K that generate a greater hydrophobic face to the helix have been demonstrated to perturb lipid bilayers and aggregate, causing micelle formation (*151*). No indication of micelle formation by KL_4 addition has been found again suggesting its structure and mechanism is different from amphipathic α-helices. The structure of KL_4 will be further discussed in Chapter 4.

The ability of peptides to affect lipid magnetic field alignment has previously been noted (*130, 132, 143, 152*), particularly for amphipathic peptides. One example is the synthetic alamethicin derivatives. In these studies 14 and 21 residue helical peptides with crown ether side chains were studied by ^{31}P NMR to probe peptide induced lipid polymorphism. These findings indicate the peptide changing the elastic properties of the membrane and causing a deformation of the bilayer. Synthetic peptides such KIGAKI, designed to be an amphiphillic beta-sheet, have also been found to change the ratios of the perpendicular to parallel edges in static ^{31}P spectra of POPC:POPG MLVs (*153*). The opposite phenomenon--alignment of lipid bilayers on addition

of peptide--has also been observed by ^{31}P NMR. Studies of the effect of melittin on DPPC/cholesterol bilayers show the ordering of the lipids on addition of peptide (*154*), high amounts of magainin antibiotics was found to magnetically orient POPC bilayers (*112*), and the opioid peptide dynorphin was also demonstrated to increase alignment of DMPC MLVs (*155*). Furthermore, the antimicrobial peptides found in Australian tree frogs, caerin 1.1 and maculatin 1.1 have been demonstrated to increase molecular order in bicelles, but the shorter peptides aurein 1.2 and citropin 1.1 do not (*156*). Hence, the influence of peptides on the magnetic properties of lipids has been shown to exist across a broad spectrum of peptides of similar size and length. Though the primary amino acid sequence of these peptides differs markedly, the results indicate that the decrease in macroscopic lipid alignment mediated by KL_4 may not be entirely unique. The differences in alignment properties are suggestive of different effects on the lipid organizational properties. Unfortunately, the diversity in lipid composition, peptide concentration and experimental conditions precludes a systematic evaluation of how peptide sequences and length affects lipid organization.

A recent study does show antimicrobial activity for KL_4 in hypoxic-injured mice infected with lipopolysacharride (*72*). Cationic, leucine-rich amphipathic α-helical peptides have been pursued as antimicrobial agents since their positive charge leads to preferential targeting of the anionic rich membranes typical to prokaryotes (*80, 146*). These peptides are designed to be amphipathic α-helices based on naturally occurring antimicrobial peptides which are thought to disrupt the membranes on binding through the formation of toroidal or barrel stave pores structure(*79, 157*). However, these peptides have significantly higher percentage of charged residues (>50% compared to <25% for KL_4) and in all probability a different secondary structure.

KL_4 Shares Many Properties with Cholesterol and Transmembrane Helices in DPPC

Ordering of DPPC by KL_4 interacting with bilayers is a phenomenon commonly associated with molecules that penetrate the hydrophobic region of the bilayer, such as cholesterol, or span it, such as transmembrane helices (*127, 158-160*). Much like KL_4, cholesterol has also been shown to decrease magnetic alignment of DMPC lipids at 20 mol% levels (*159*). ^2H NMR studies also indicate increased order of DPPC acyl chains, decreased area per lipid molecule, and domain separation mediated by cholesterol on the range of roughly 15-25mol%, (*161-163*). Raman spectroscopy studies reveal that higher amounts of cholesterol induce a "liquid-ordered" (l_o) phase on DPPC, a state which has limited acyl chain flexibility but a greater degree of lipid mobility (*164*). This raises the interesting possibility of KL_4 acting in a similar capacity to cholesterol but at significantly lower mol%. The $<S_{CD}>$ values for DPPC alone from the literature or in DPPC:POPG vesicles are very similar (*124*); addition of KL_4 increases S_{CD} values in a manner that has been seen for cholesterol. The resultant ordering seen could be the consequence of phase separation as suggested by the DSC thermograms (Figure 3-1), but complete segregation is unlikely given that S_{CD} of DPPC with KL_4 >S_{CD} of neat DPPC. In comparison to 4:1 DPPC(d-62):POPG MLVs, the ^2H spectra of 3:1 POPC(d-31):POPG MLVs only show small downward shifts in the order parameter profiles on KL_4 addition, suggesting only an electrostatic interaction of KL_4 with POPC and a more shallow interaction with the bilayer.

Molecular Model of KL_4 with POPC:POPG and DPPC:POPG

Based on the assumption of helicity for KL_4, with the lysines on one side of the helix, a molecular model of its potential orientation and penetration based on our data is shown in Figure 3-25. The peptide was modeled based on data presented in Chapter 4 and PDB files to simulate a lipid bilayer milieu were based on published values from Professor Scott Feller *et al* (71).

Based on the thickness of the bilayer and the length of the peptide, a transmembrane orientation of the peptide is not likely due to the periodic placement of the lysine residues as well as the lack of a shift in $<S_{CD}>$ parameters for the lipid plateau region on addition of KL_4 (*146, 165*). This peripheral orientation has been verified by infrared reflection-absorption spectroscopy (IRRAS) taken on KL_4 with DPPC and 7/3 DPPC:POPG bilayers. In these measurements, a beta-sheet structure at the membrane interface in a Langmuir trough arrangement was determined (*166*). However, our data supports the conclusion that KL_4 is helical with the lysine side chains aligned to allow them to "snorkel" to the phosphate headgroups in the DPPC:POPG bilayer. Lysine snorkeling is supported by the $<S_{CD}>$ values we observed, particularly at acyl chain positions 8-15. This maximizes electrostatic interactions between the amino groups and the phosphate headgroups. Such snorkeling, which has been reported for many short, lysine capped peptides, can allow for a much greater penetration of the peptide while allowing it to remain perpendicular to the bilayer normal. The thermodynamic penalty imposed by placing KL_4 in a transmembrane orientation would be prohibitive since it would result in charged amino acids partitioned into the hydrophobic core. Also, a transmembrane orientation of the peptide would cause more ordering of the positions 2-8 in the acyl chains than we see, as has been shown for more hydrophobic α-helical peptides with a high distribution of leucines (*167*). The binding of KL_4 to model POPC:POPG lipids are more peripheral based on ^2H NMR derived $<S_{CD}>$ values and ^{31}P NMR. Derivatives of magainin antibiotics, peptides which have an orientation perpendicular to the bilayer normal, also cause a decrease in order parameters that decrease upon addition of 3mol% of peptide, though the downward shifts in order parameter seen are significantly higher than what is seen in this work (*79*). This is probably due to the toroidal pore mechanism of cell lysis attributed to these peptide types. Order parameters seen for KL_4 with POPC(d-31):POPG

similarly decrease indicating a mostly peripheral interaction with the lipid; however, the comparatively smaller decrease in $<S_{CD}>$ values presumably reflects KL_4 facilitating lipid-lipid interaction, and not cellular degradation as would be the case for the magainin family of peptides.

The snorkeling model of KL_4 within DPPC:POPG lipid multilamellar vesicles could have important consequences for membrane structure and function. For the most part, this represents a novel peptide-lipid interaction that is unique in comparison to what has been seen for amphipathic α-helical antimicrobial peptides. Most antimicrobial peptides tend to bind peripherally and destroy bacterial cell membranes via a toroidal pore or carpet mechanism (*79, 113*). While the binding of KL_4 to POPC:POPG vesicles suggest it could bind to these lipids in a manner similar to antibiotic peptides, its ability to snorkel in DPPC:POPG lipids would have a different effect on lipid biophysics. Some of the thermodynamic costs of peptide penetration can be relieved by the formation of alternative non-lamellar structures, such as hexagonal phases (*160, 165*). The inverted H_{II} phase, in which the headgroups invert and follow an aqueous channel can form if peptide lipid hydrophobic mismatch occurs. Such inverted isotropic phases have been shown to exist in phosphatidylcholine membranes at concentrations greater than 3mol% (*168*), the maximum concentration used in these studies. The formation of alternative lipid geometries, specifically, the inverted H_{II} phase, has been found to be important in the proper formation lung surfactant (*139*). The model depicted suggests that KL_4 could facilitate formation of non-lamellar lipid phases and/or induce a curvature strain as its role in lung surfactant. Alternatively, lipid geometry could be critical during fusion of lipids to the air-surfactant interface and KL_4 snorkeling could be essential feature for the proper shuttling of lipids.

In conclusion, DSC, ^{31}P and ^{2}H data indicate KL_4 binds peripherally to 3:1 POPC:POPG lipids through electrostatic interaction of the lipid phosphates with the positively charged lysines. A different interaction is seen with 4:1 DPPC:POPG lipids suggesting the peptide penetrates to a far greater depth in the bilayer. Thus, both peptide structure and acyl chain saturation play an important role in determining the insertion level of KL_4. The DSC and ^{31}P NMR results show KL_4 having similar attributes to cholesterol in terms of lipid ordering and DSC peak broadening, as well the peptide displaying an electrostatic interaction with the PG headgroups when POPG is added to DPPC and POPC lipid systems. ^{31}P NMR spectra indicate spontaneous lipid alignment to the magnetic field which is abrogated by the addition of increasing levels of peptide. A decrease in lipid-lipid association is also seen from our ^{31}P NMR data as peptide is added. With the findings presented here, a more thorough structural model can be established for how this small peptide mimics lung surfactant protein B and drive the development of future mimetics.

ACKNOWLEDGMENTS: The authors of this paper thank Dr. Alfred Chung for synthesis of peptide KL_4, and the Molecular Structure Facility at University of California, Davis for AAA analysis. The research herein was funded by NIH 1R01HL076586 awarded to Dr. Joanna R. Long and UF, MBI.

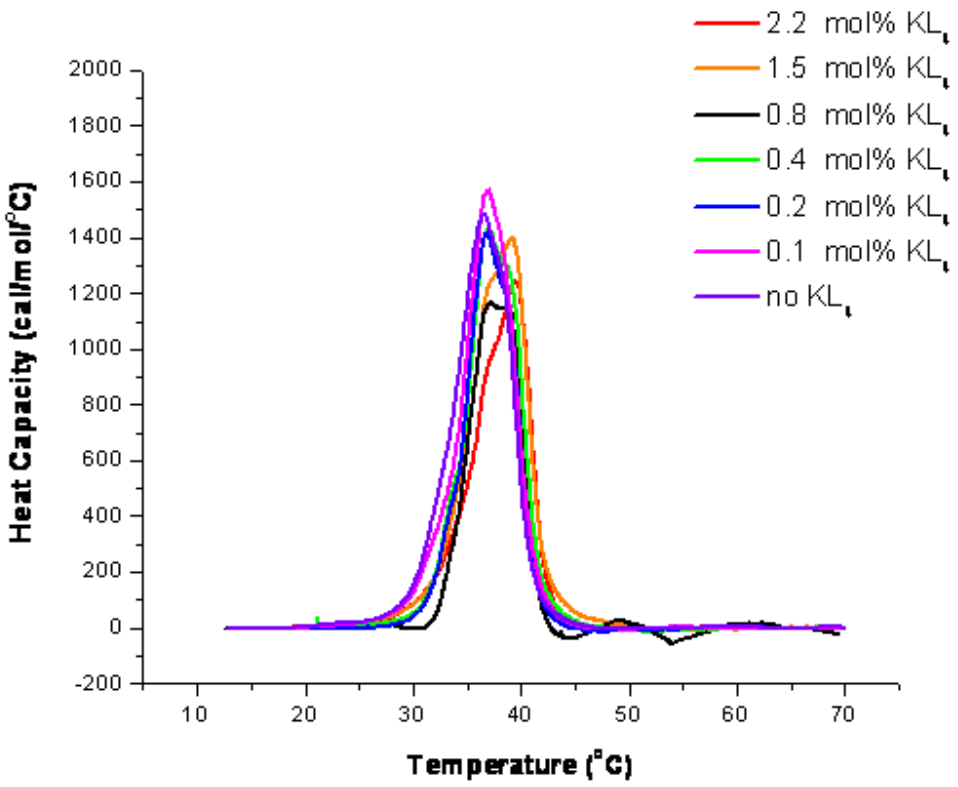

Figure 3-1. Differential scanning calorimetry on KL_4 with 4:1 DPPC:POPG vesicles with KL_4 at the indicated molar percentages. Shown is clear phase separation on addition of peptide. DSC scans on each sample were performed in triplicate at a scan rate of 1 degree per from 10-70°C.

Table 3-1. Thermodynamic parameters obtained from DSC thermograms.

Main Transition	T_m (^oC)	ΔH_{cal} (kcal/mol)	ΔH_{vH} (energy/mol)	ΔS (cal/mol/K)	$\Delta T_{1/2}$	CU*	C_p^{max} kcal/mol/^oC
DPPC:POPG	36.4 ± 0.2	10.0 ± 1.3	115 ± 12	32± 4	6.0 ± 0.4	12 ± 3	1.6 ± 0.1
0.1% KL_4	36.9 ± 0.1	9.7 ± 0.3	124 ± 2	31 ± 1	5.2 ± 0.1	13 ± 1	1.6 ± 0.1
0.2% KL_4	36.7±0.2	8.0 ±0.9	133 ± 1	26 ± 3	5.5 ± 0.1	17 ± 1	1.4 ± 0.1
0.4% KL_4	36.8 ± 0.2	9.0 ±0.7	121 ± 2	29 ± 2	5.5 ± 0.2	14 ± 1	1.4 ± 0.1
0.8% KL_4**	37.1	6.7	113 ± 4	22	5.6	17	1.1
1.5% KL_4	39.20 ± 0.03	9.5 ± 0.4	115 ± 3	30 ± 1	5.84 ± 0.04	12 ± 1	1.4 ± 0.1
2.3% KL_4	39.50 ± 0.04	7.9 ± 0.1	122 ± 1	25 ± 1	5.5 ± 0.1	12 ± 2	1.2 ± 0.1

* cooperativity unit (ΔH_{vH}/ ΔH_{cal}) ** sample only run once in the DSC instrument

Table 3-2. CSA span for phosphate headgroup in 3:1 POPC:POPG and 4:1 DPPC:POPG MLVs with and without KL_4. The greatest change occurs in PG headgroups in 4:1 DPPC:POPG MLVs indicating a preferential interaction of this lipid with the peptide. A change in the PG ^{31}P CSA span is also seen in the 3:1 POPC:POPG MLVs on addition of peptide.

	3:1 POPC:POPG		4:1 DPPC:POPG	
KL4 concentration	POPC	POPG	DPPC	POPG
0	-33.9	-26.9	-42.2	-33.2
0.1	-35.1	-26.9	-42.2	-32.3
0.2	-35.1	-27.6	-41.4	-32.4
0.4	-28.2	-20.7	-43.0	-32.4
0.8	-36.4	-27.6	-43.7	-30.9
1.5	-35.8	-26.3	-43.0	-28.6
2.3	-33.9	-23.2	-42.4	-26.4

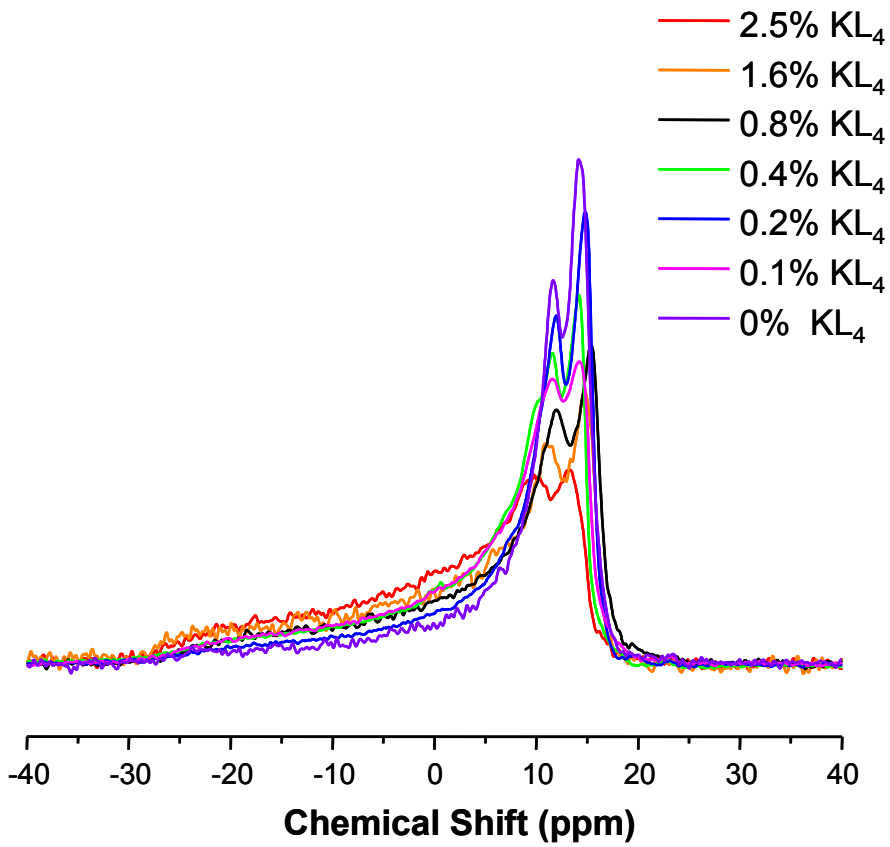

Figure 3-2. Static ^{31}P NMR spectra of 3:1 POPC(d-31):POPG MLVs with the increasing addition of KL_4. As peptide levels increase, signal increases at the parallel edge suggesting KL_4 reduces macroscopic alignment of the lipids. Spectra taken with 1024 scans in a 600MHz Bruker instrument at 44^{o}C.

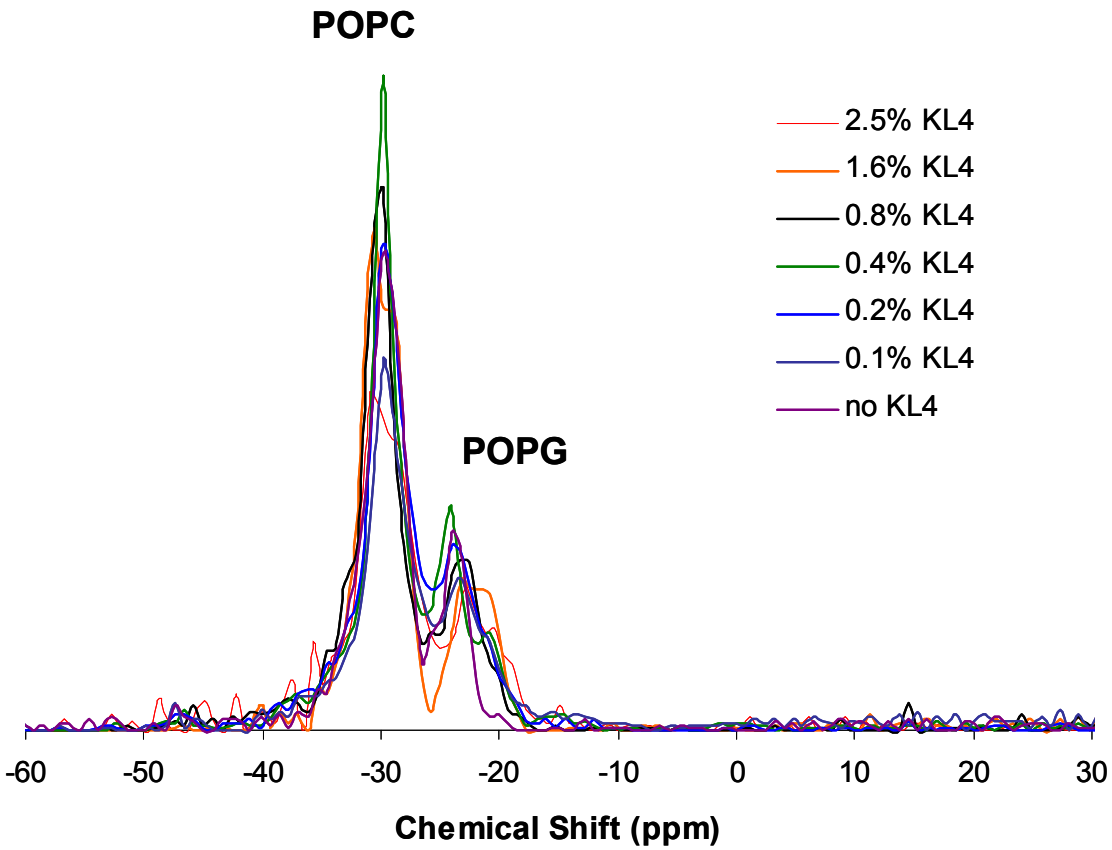

Figure 3-3. Static ^{31}P dePaked NMR spectra of 3:1 POPC(d-31):POPG with increasing amounts of KL_4. The movement of the POPG peak upon addition of peptide is clearly visible.

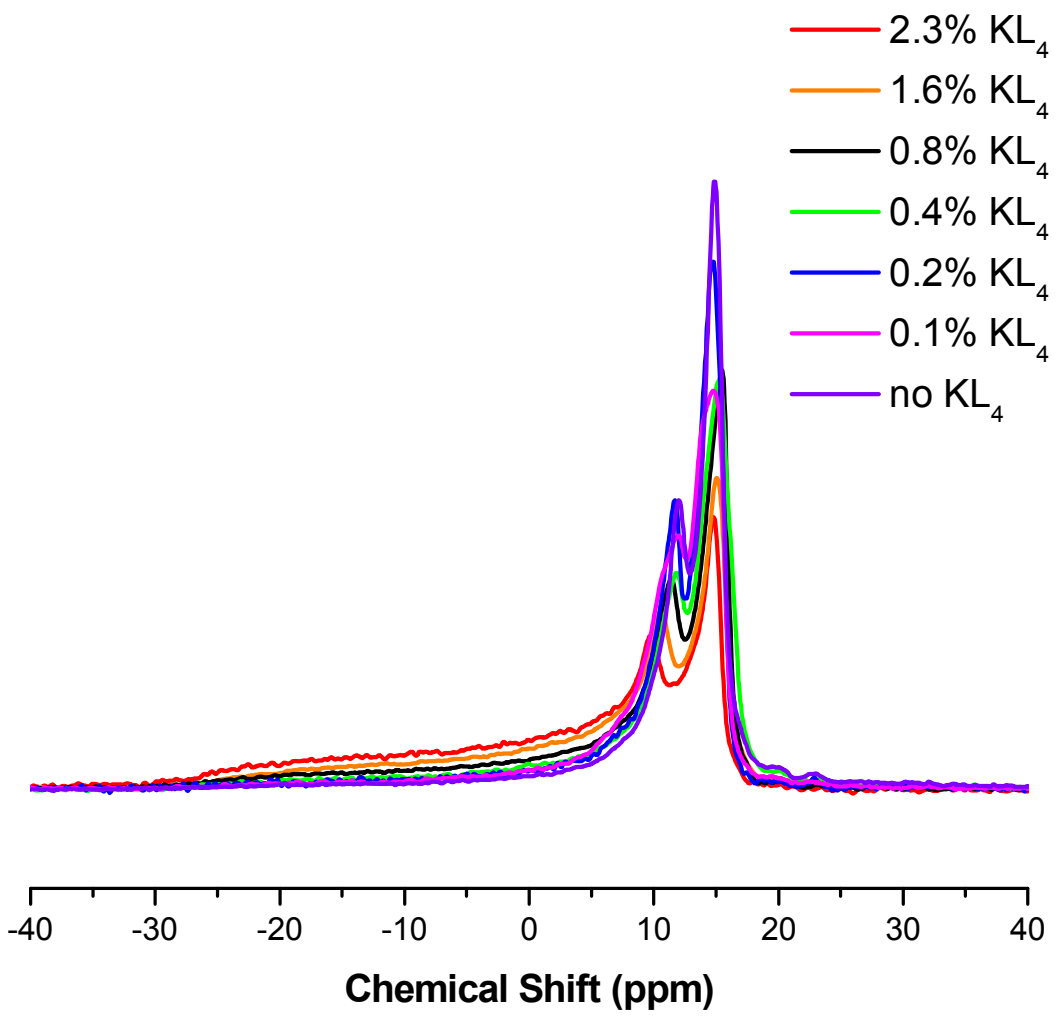

Figure 3-4. Static ^{31}P NMR spectra of 4:1 DPPC(d-62):POPG MLVs with increasing addition of KL_4. As peptide levels increase, signal increases at the parallel edge as seen for 3:1 POPC:POPG MLVs.

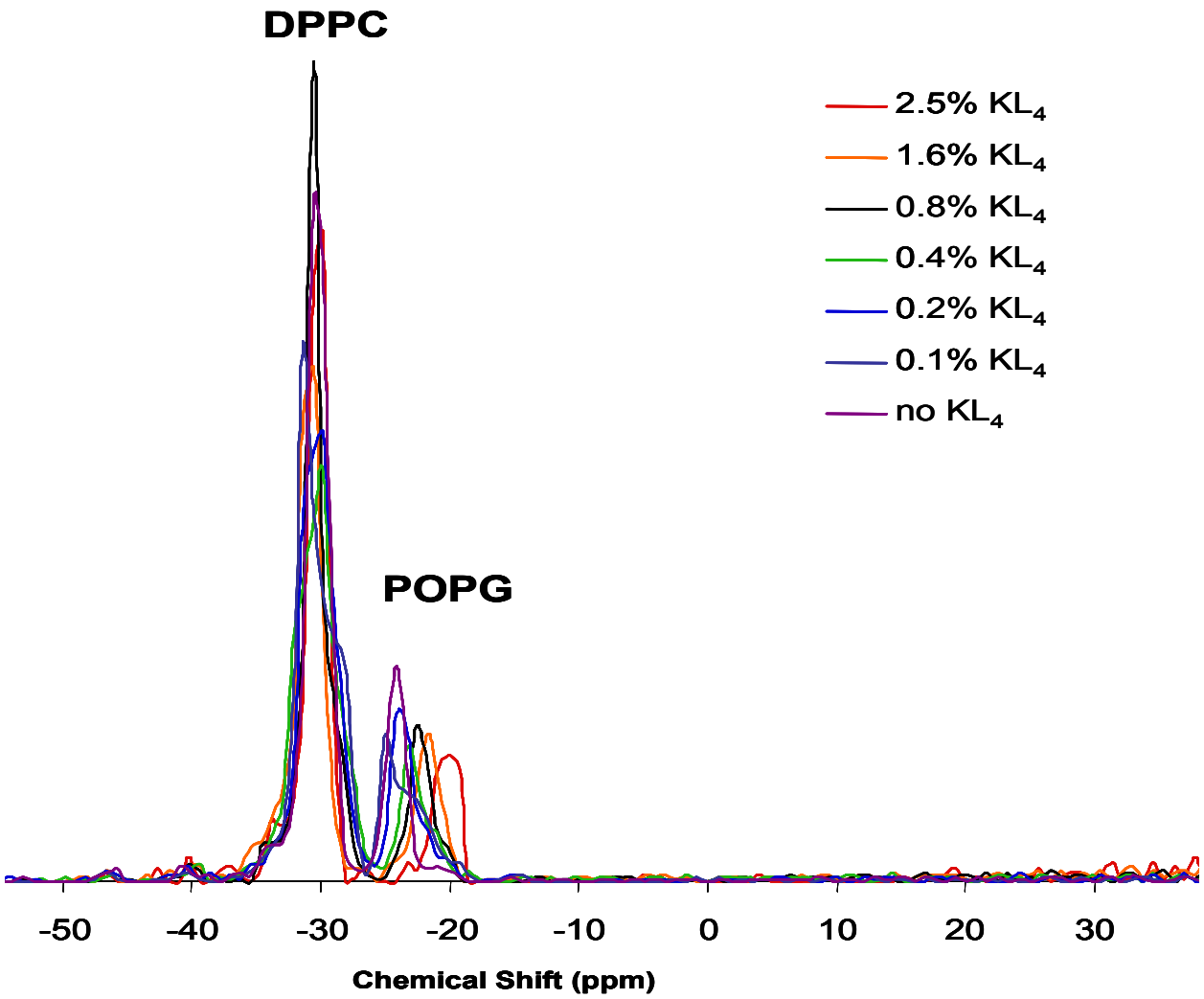

Figure 3-5. Static ^{31}P dePaked NMR spectra of 4:1 DPPC(d-62):POPG with increasing amounts of KL_4. The movement of the POPG peak upon addition of peptide is clearly visible.

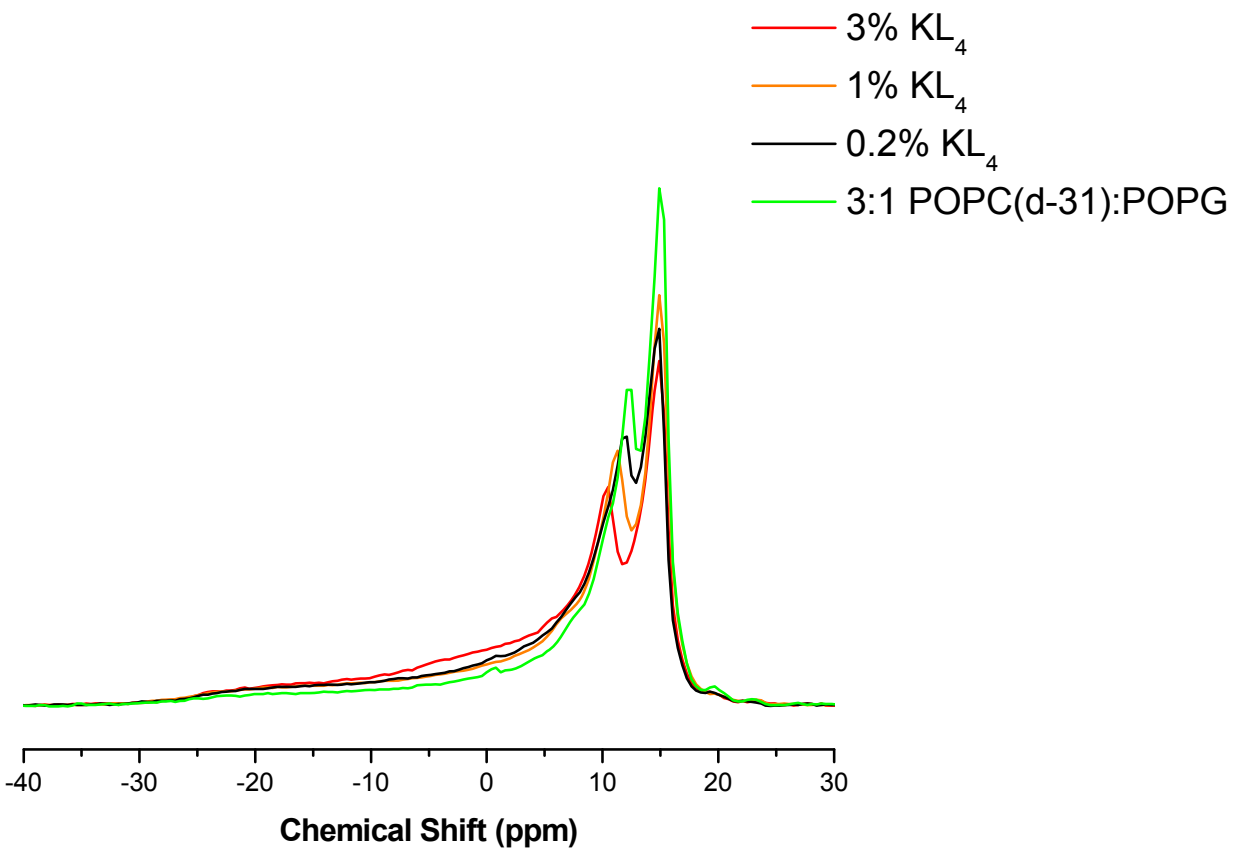

Figure 3-6. Static ^{31}P NMR spectra of 3:1 POPC:POPG(d-31) MLVs with increasing amounts of KL_4.

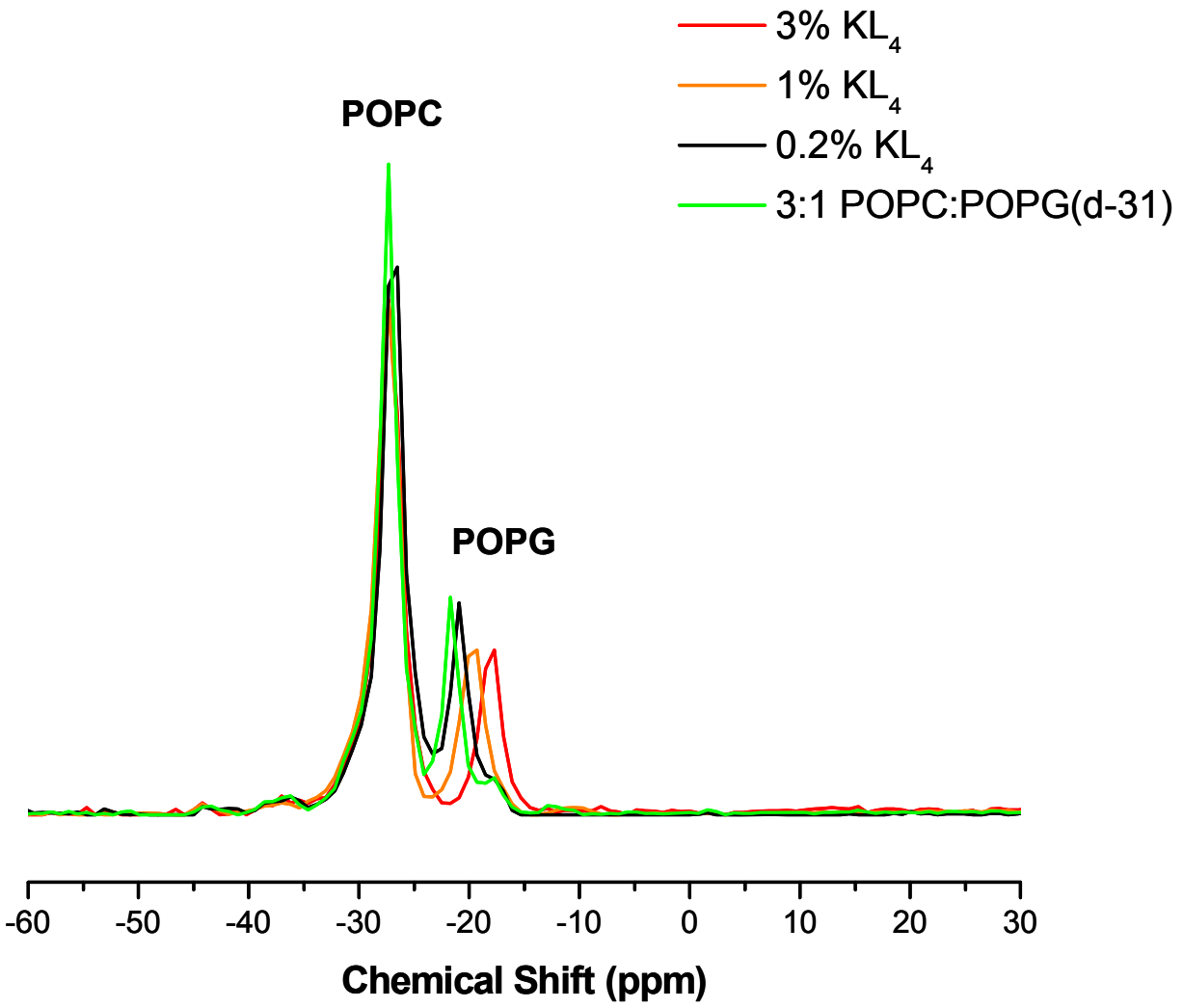

Figure 3-7. DePaked ^{31}P NMR spectra of 3:1 POPC:POPG(d-31) with increasing amounts of KL_4. The movement of the POPG peak upon addition of peptide is clearly visible.

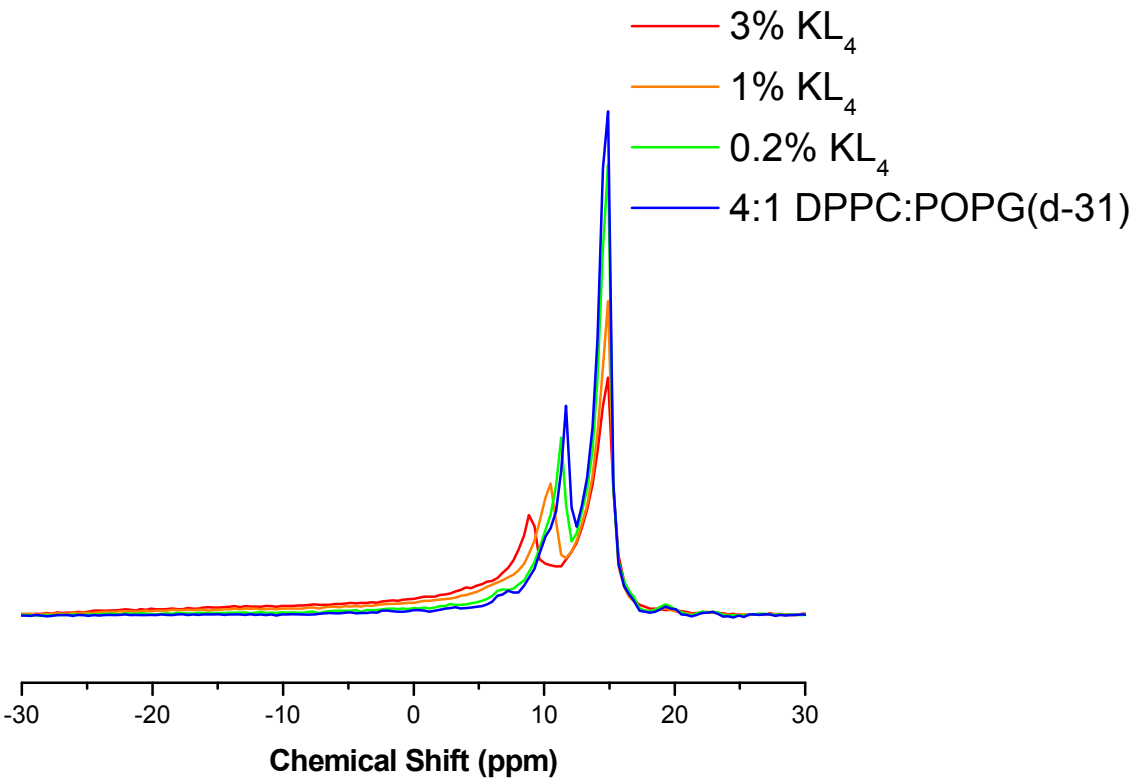

Figure 3-8. Static ^{31}P NMR spectra of 4:1 DPPC:POPG(d-31) MLVs with increasing amounts of KL_4.

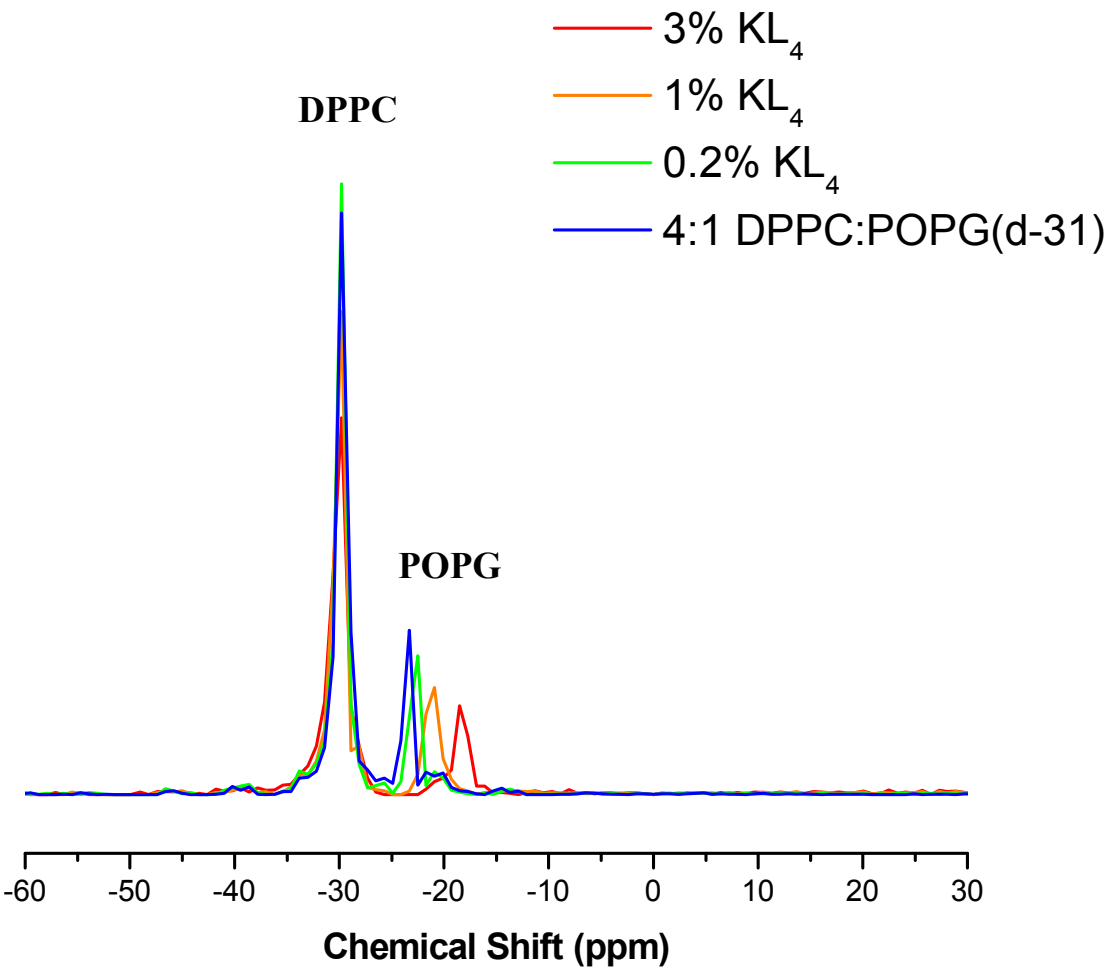

Figure 3-9. DePaked ^{31}P NMR spectra of 4:1 DPPC:POPG(d-31) with increasing amounts of KL_4. The movement of the POPG peak upon addition of peptide is clearly visible

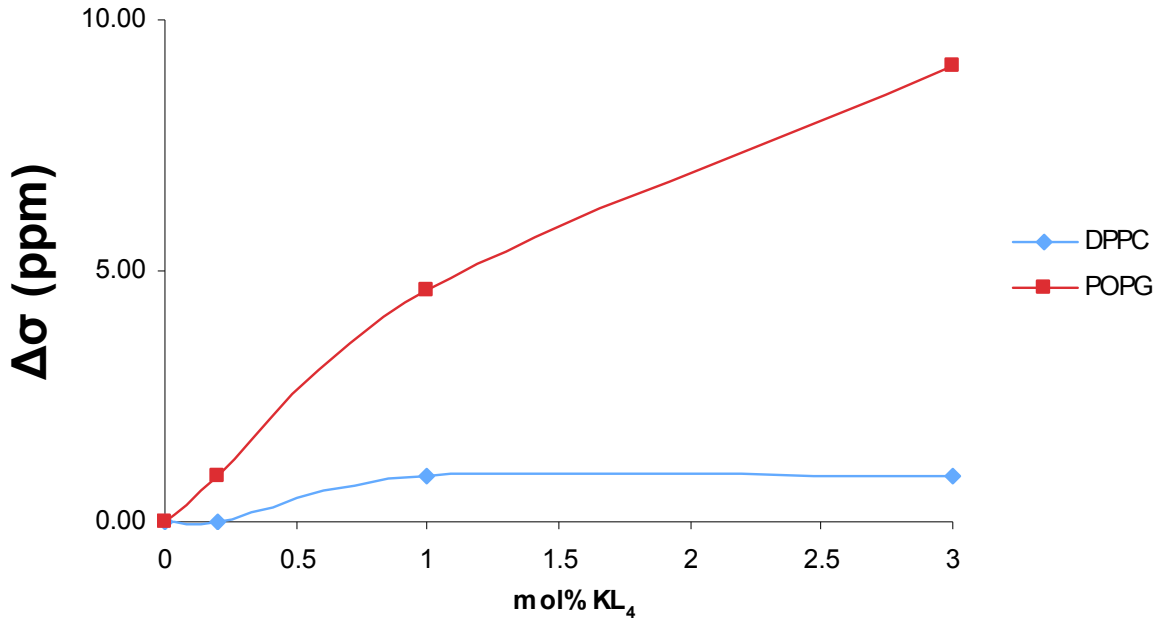

Figure 3-10. The shift in dePaked frequency in ppm (Δσ) for DPPC and POPG (in ppm) by KL_4 in 4:1 DPPC:POPG(d-31).

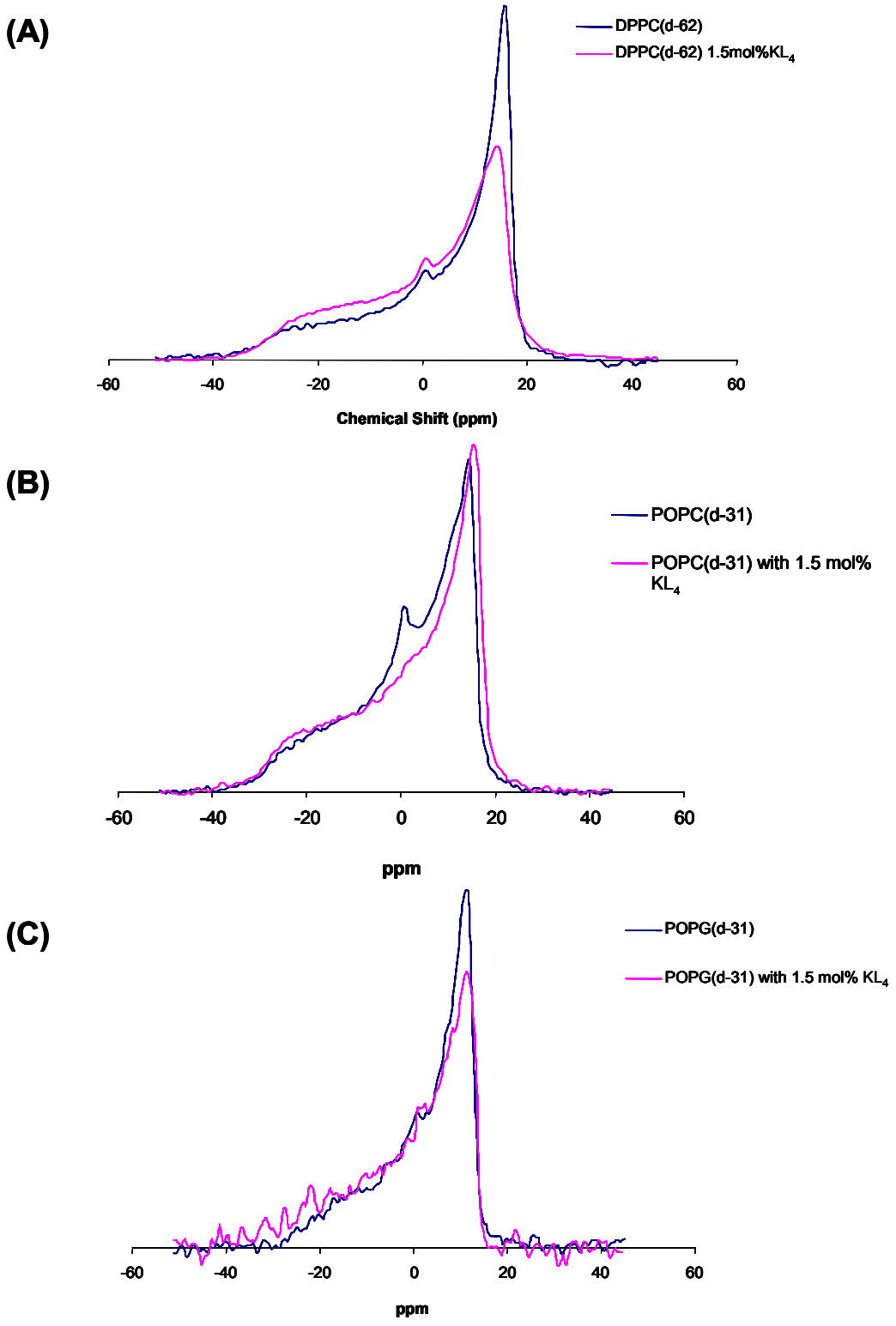

Figure 3-11. Static ^{31}P NMR spectra of single lipid and lipid with 1.5 mol% KL_4 A: DPPC(d-62), B: POPC(d-31) and C: POPG(d-31).

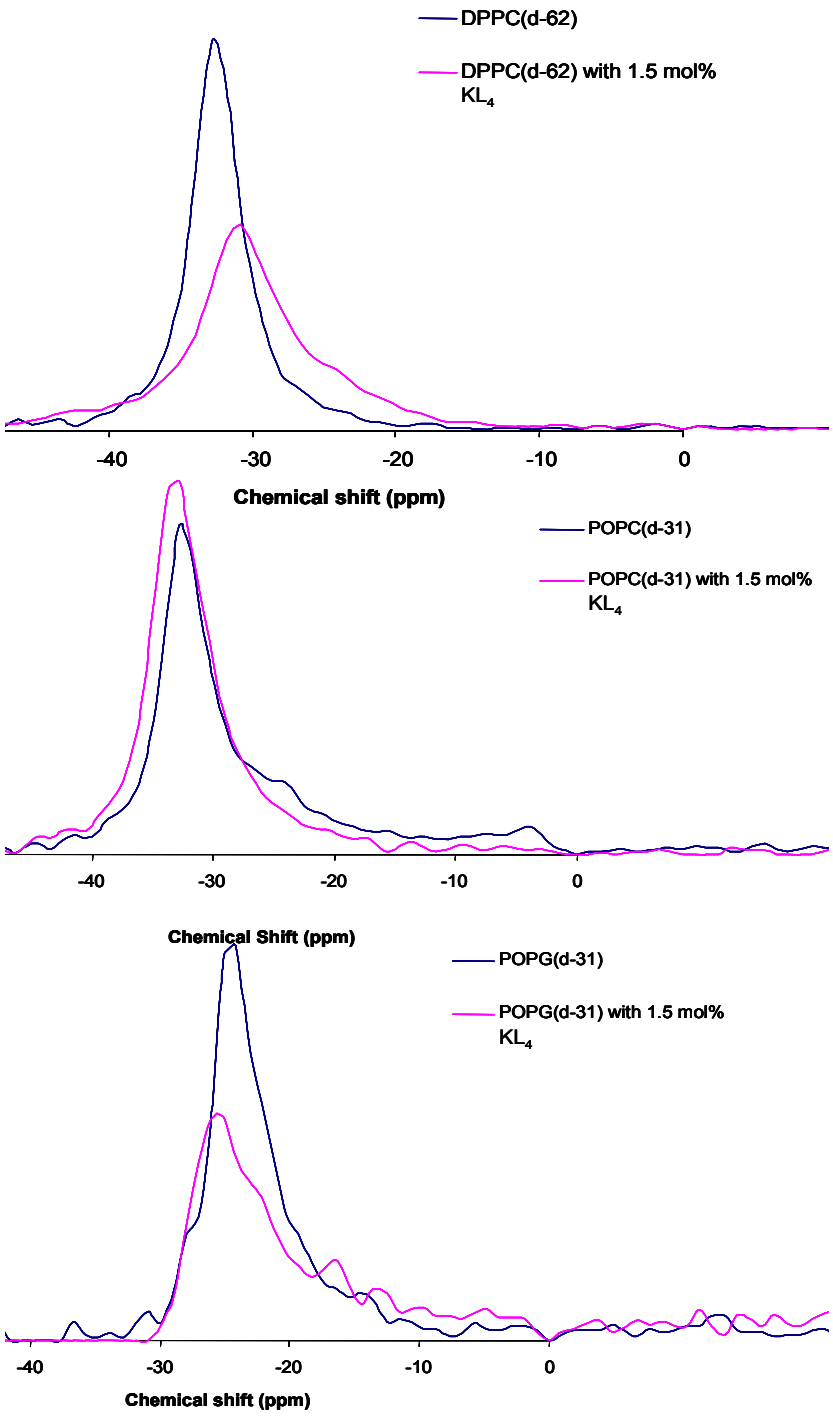

Figure 3-12. DePaked ^{31}P spectra for (Top) DPPC(d-62), (Middle) POPC(d-31) and (Bottom) POPG(d-31) with and without 1.5mol% KL_4.

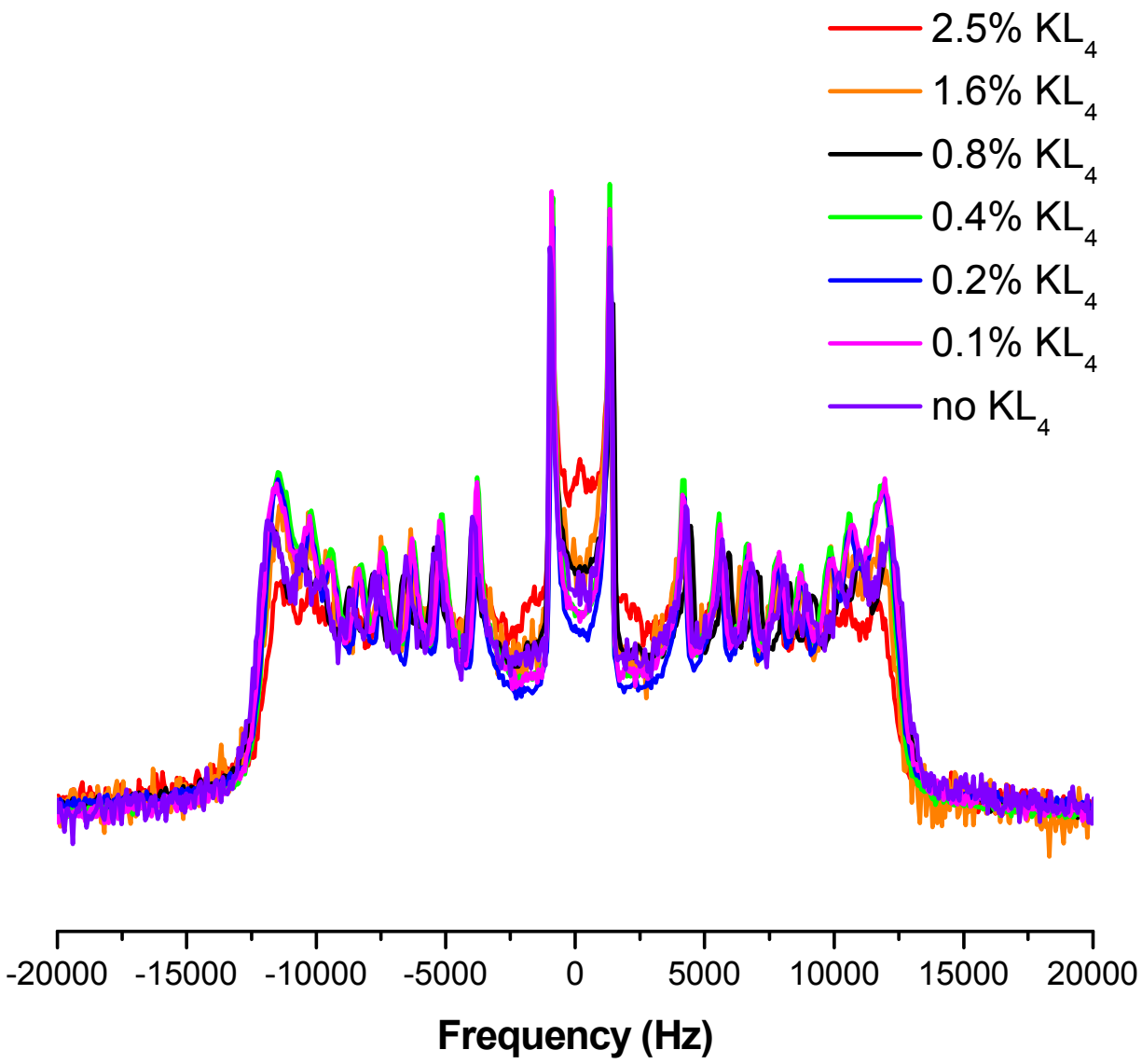

Figure 3-13. ^{2}H spectra of 3:1 POPC(d-31):POPG MLVs with increasing amounts of KL_4. The ^{2}H spectra overlap indicating very little change in this lipid system as a function of KL_4.

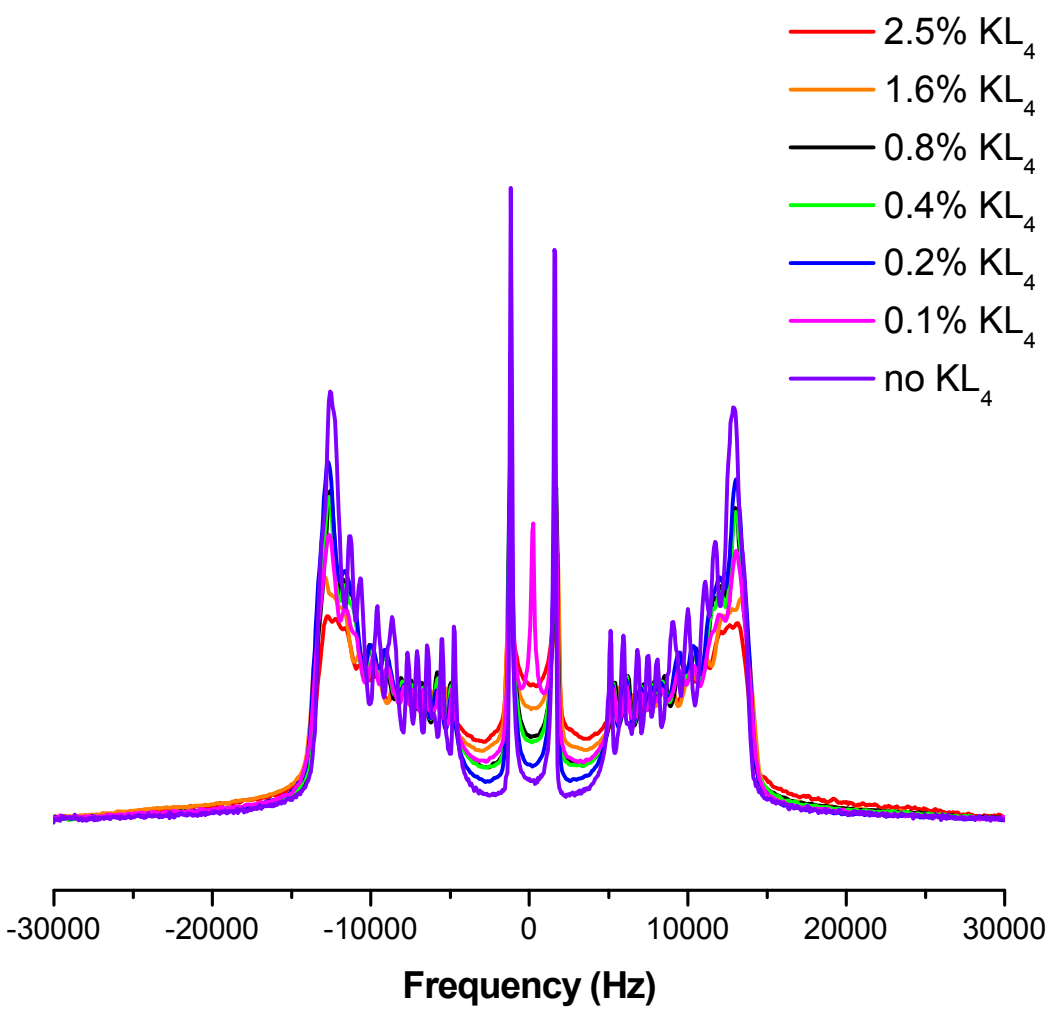

Figure 3-14. ^{2}H NMR spectra of 4:1 DPPC(d-62):POPG with increasing amounts of KL_4.

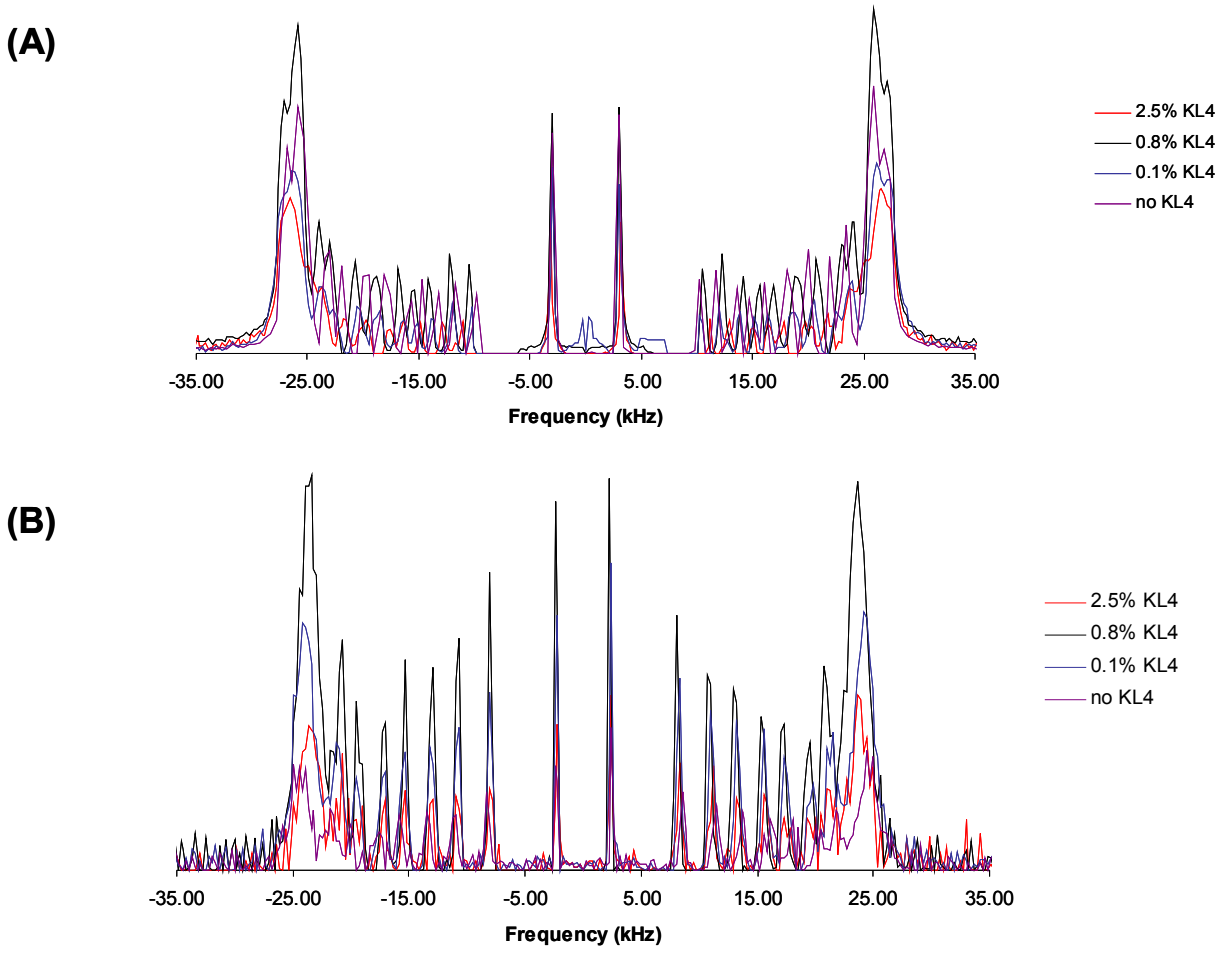

Figure 3-15 DePaked 2H spectra for (A) 4:1 DPPC(d-62):POPG MLVs and (B) 3:1 POPC(d-31):POPG MLVs with increasing amounts of KL4.

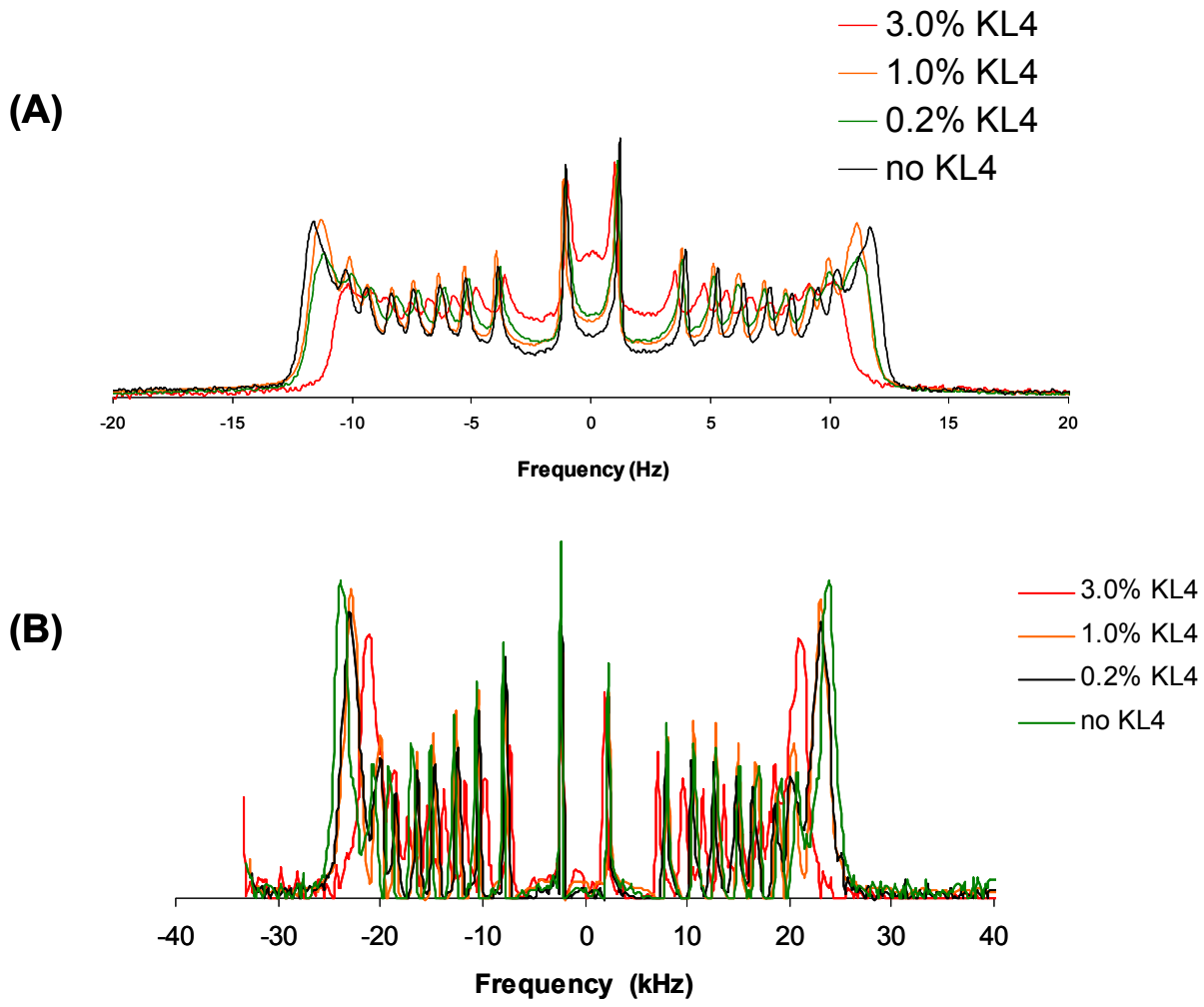

Figure 3-16 Deuterium NMR spectra for (A) 3:1 POPC:POPG(d-31) MLVs and (B) DePaked spectra with increasing amounts of KL_4.

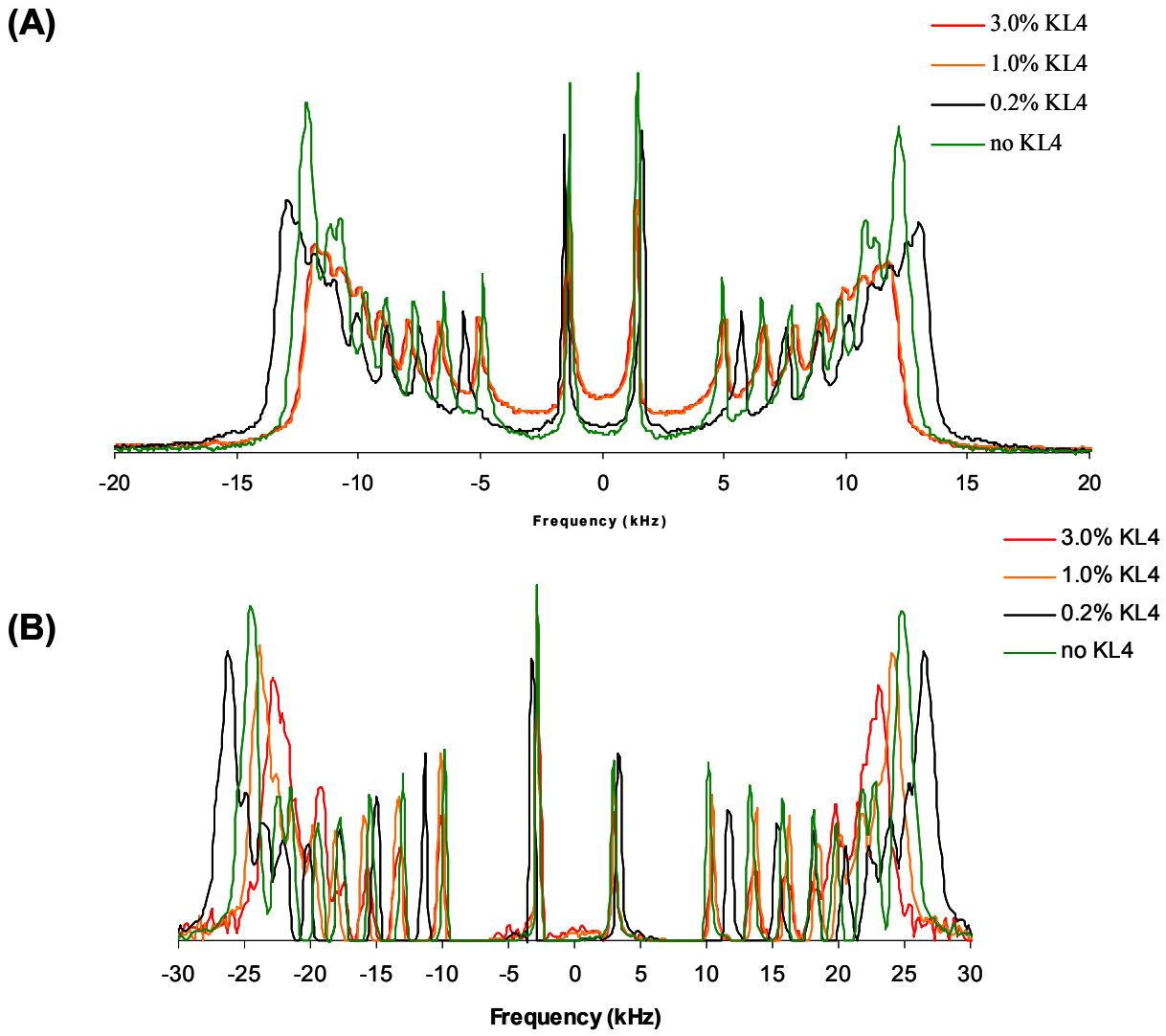

Figure 3-17. Static ^{2}H spectra for (A) 4:1 DPPC:POPG(d-31) MLVs and (B) DePaked spectra with increasing amounts of KL_4.

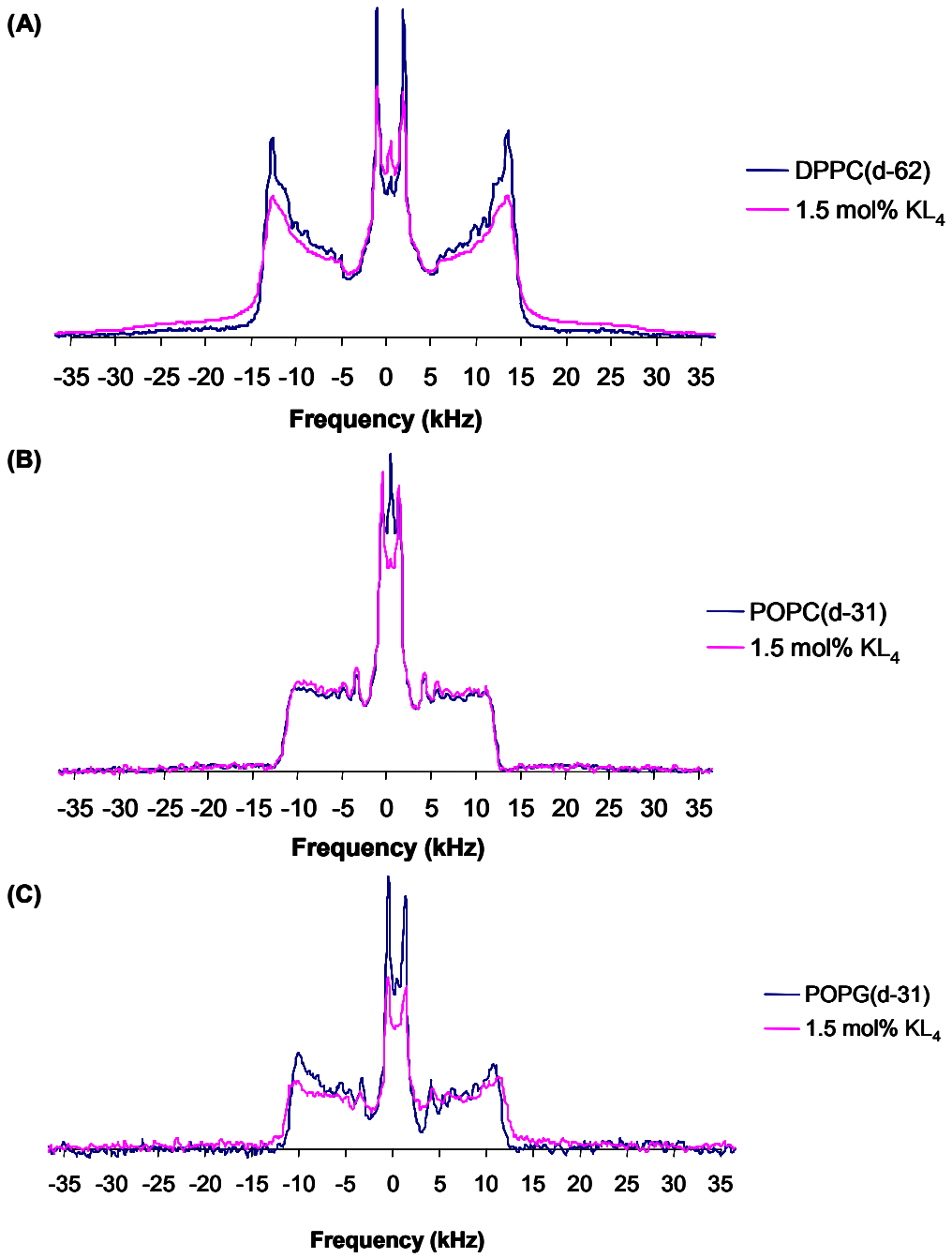

Figure 3-18. Static 2H NMR spectra of single lipid MLVs with and without 1.5mol% KL4. Blue spectrum is single lipid, pink spectrum is lipid with 1.5mol% KL4. (A) DPPC(d-62), (B) POPC(d-31) and (C) POPG (d-31).

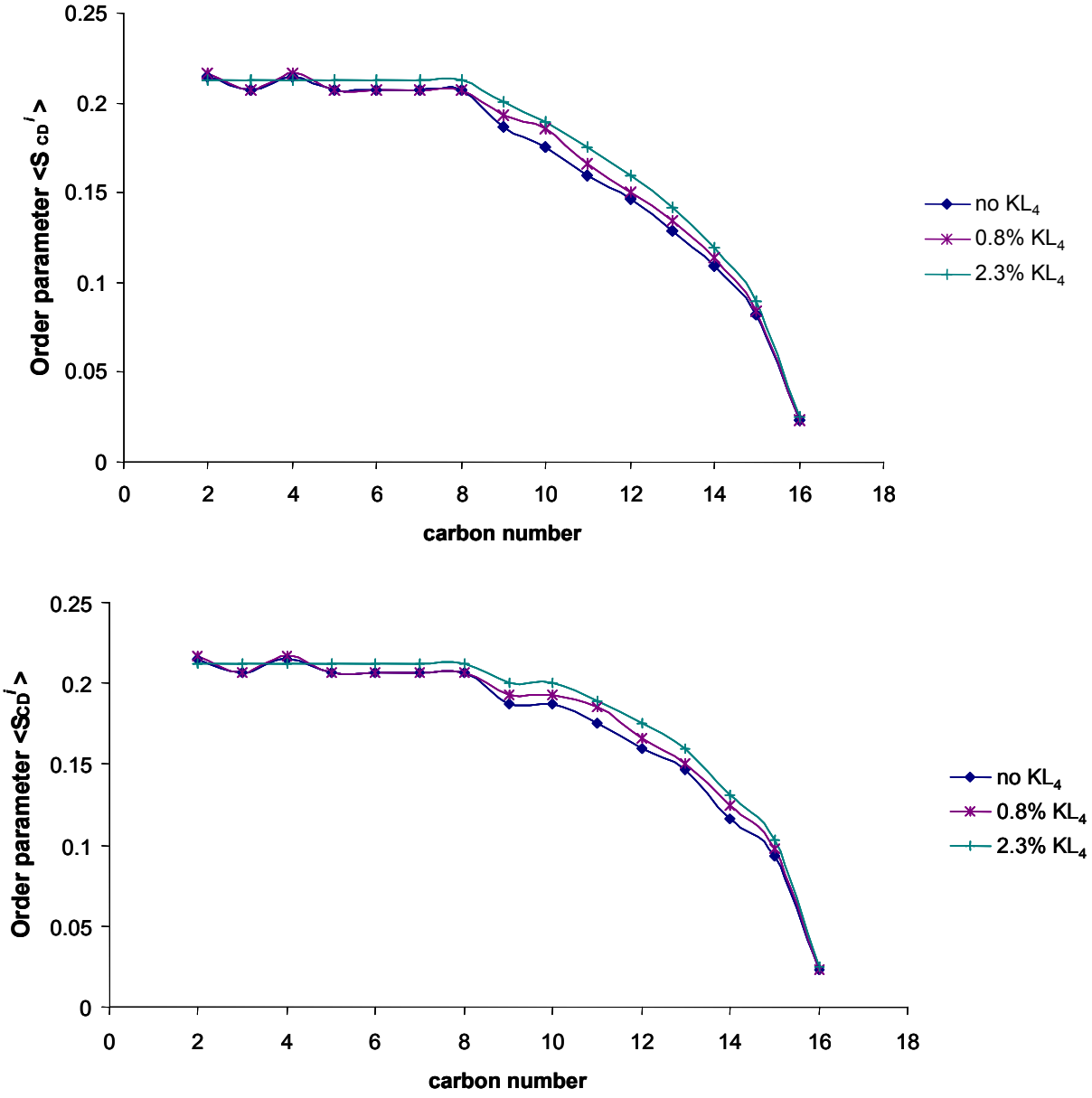

Figure 3-19. Order parameter profiles for (4:1) DPPC(d-62):POPG MLVs with and without KL_4. Top:sn-1 chain Bottom: sn-2 chain

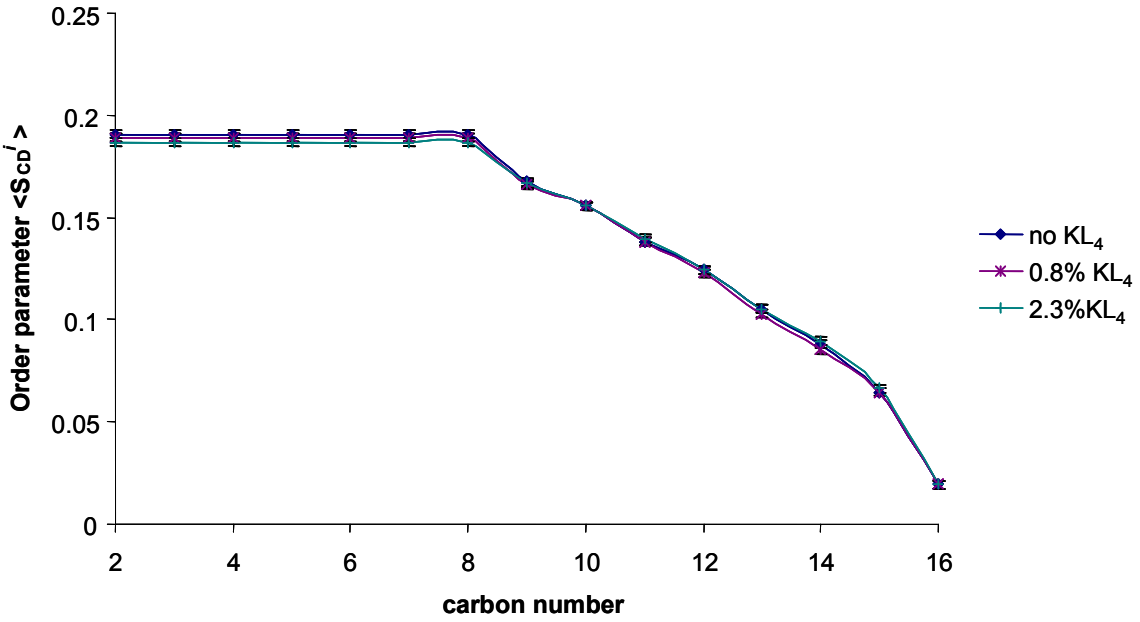

Figure 3-20. Order parameter profile for the sn-1 chain of 3:1 POPC(d-31):POPG MLVs with and without KL_4

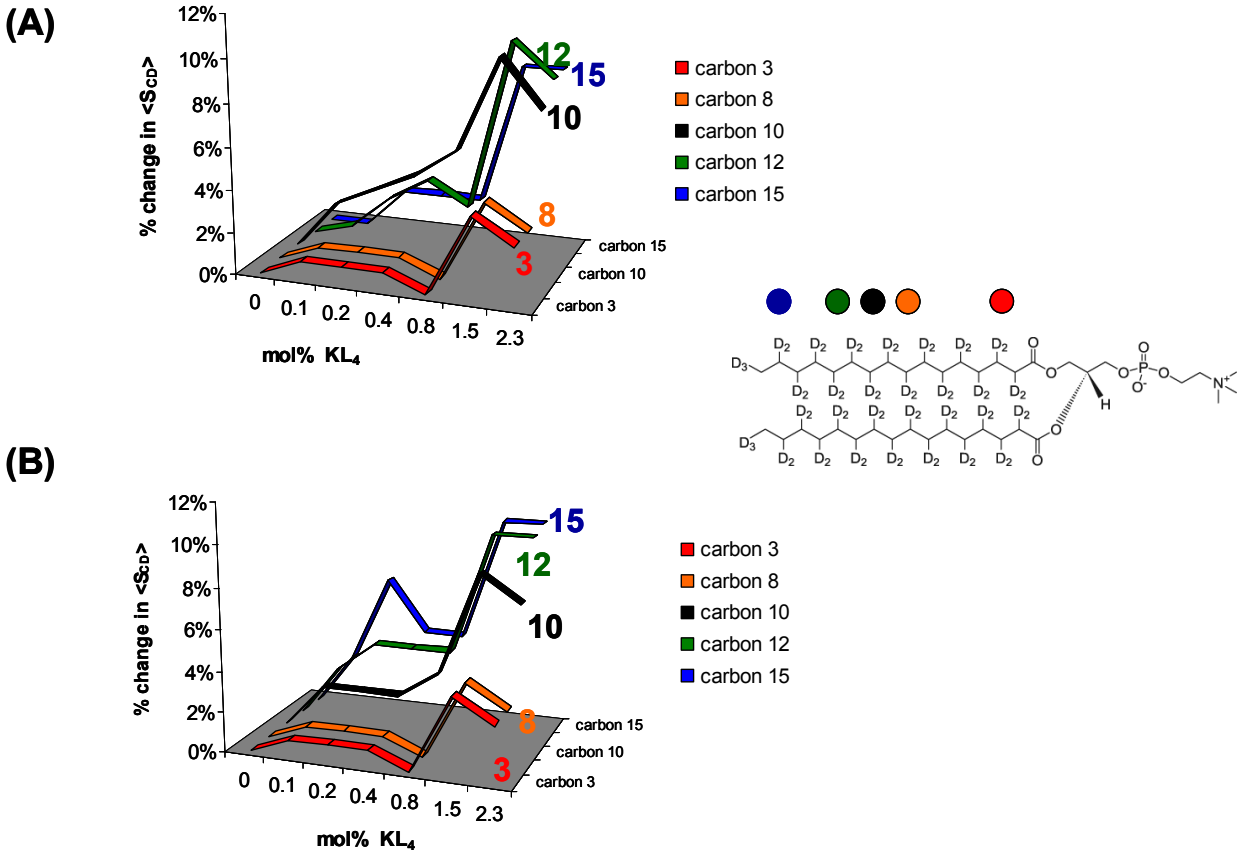

Figure 3-21. Three dimensional plot of change in order parameter for DPPC(d-62):POPG MLVs as a function of mole percentage of KL4. The change in order parameter is color-coded for individual carbons. The top graph is for the sn-1 chain and the bottom graph is for the sn-2 chain.

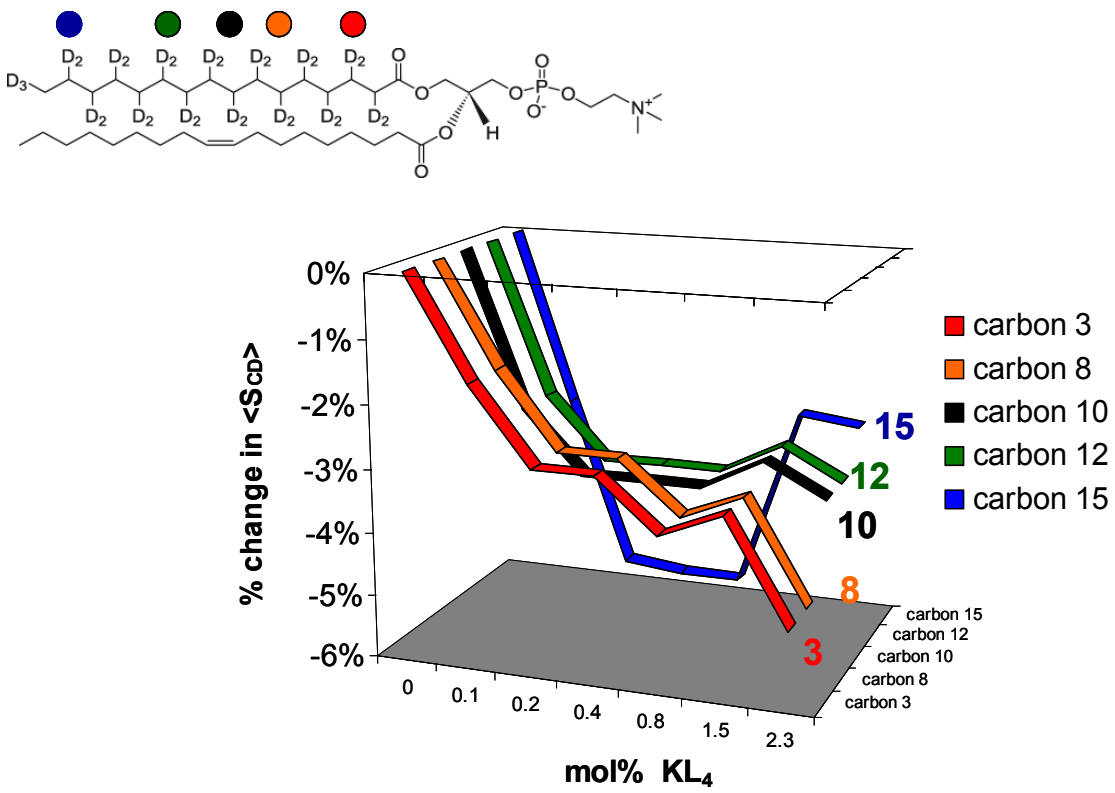

Figure 3-22. Three dimensional plot of change in time averaged order parameter for 3:1 POPC(d-31):POPG MLVs as a function of mole percentage of KL4. The change in order parameter is color-coded for individual carbons.

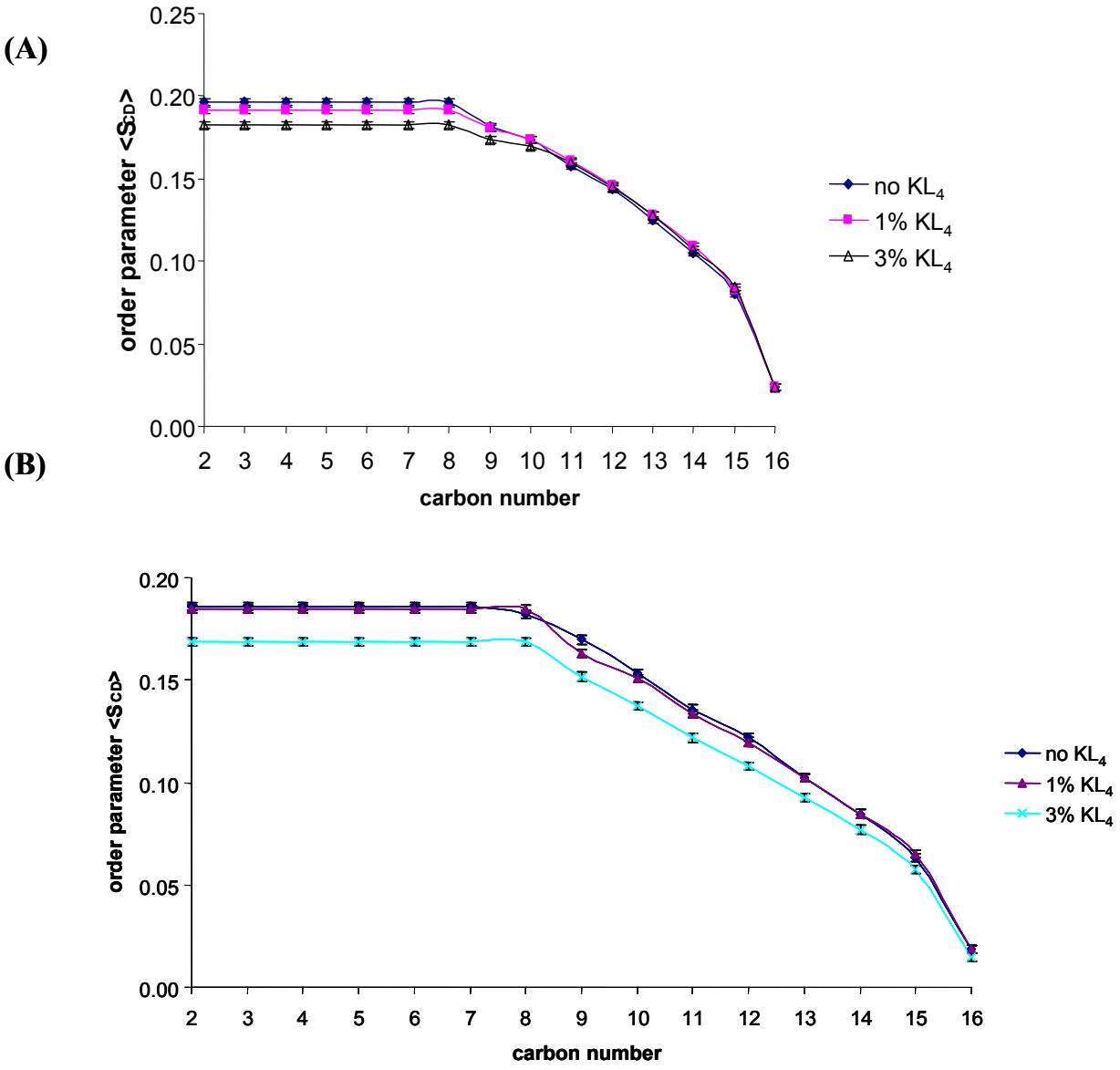

Figure 3-23. Order parameter profile for A) 4:1 DPPC:POPG(d-31) MLVs and B) 3:1 POPC:POPG(d-31) MLVs with varying amounts of KL4.

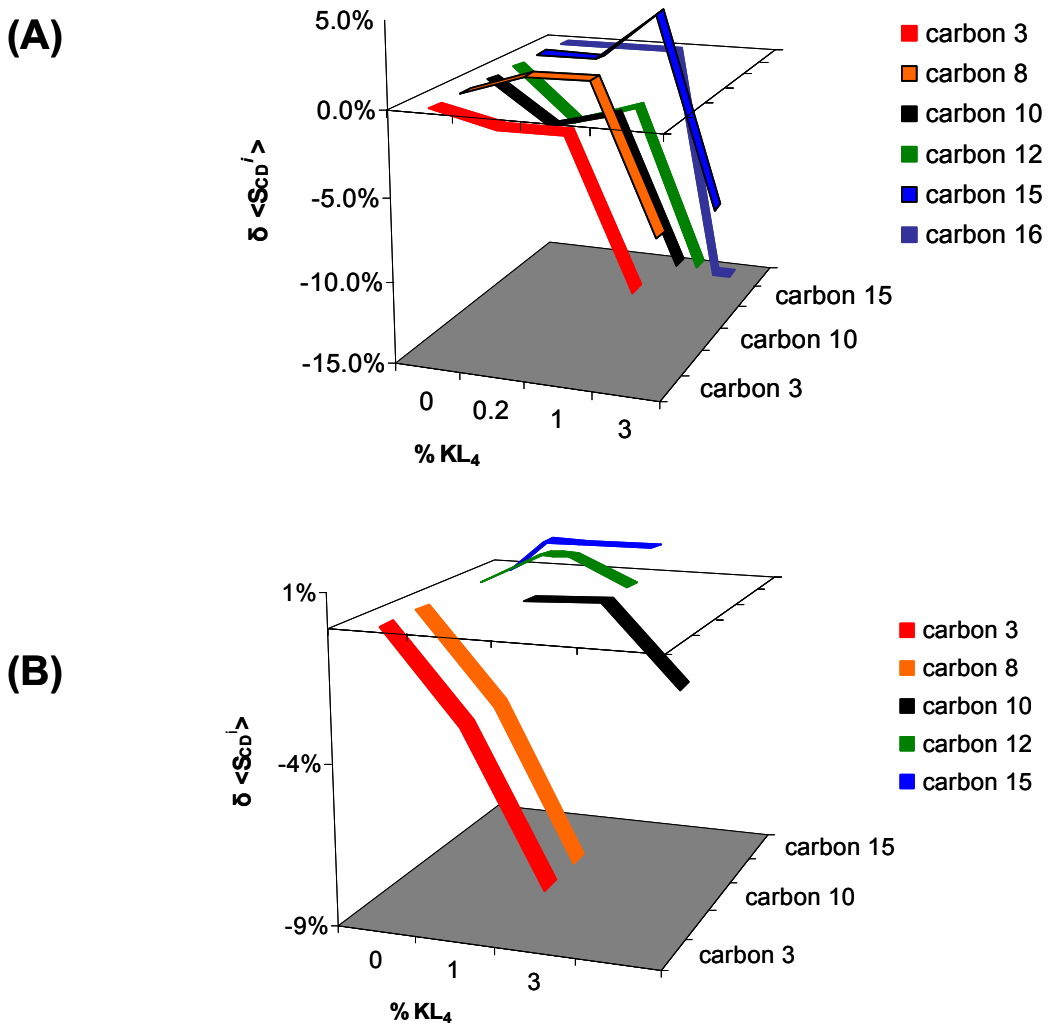

Figure 3-24. Change in order parameter values on (A) POPC:POPG(d-31) and (B) DPPC:POPG(d-31) upon addition of KL_4.

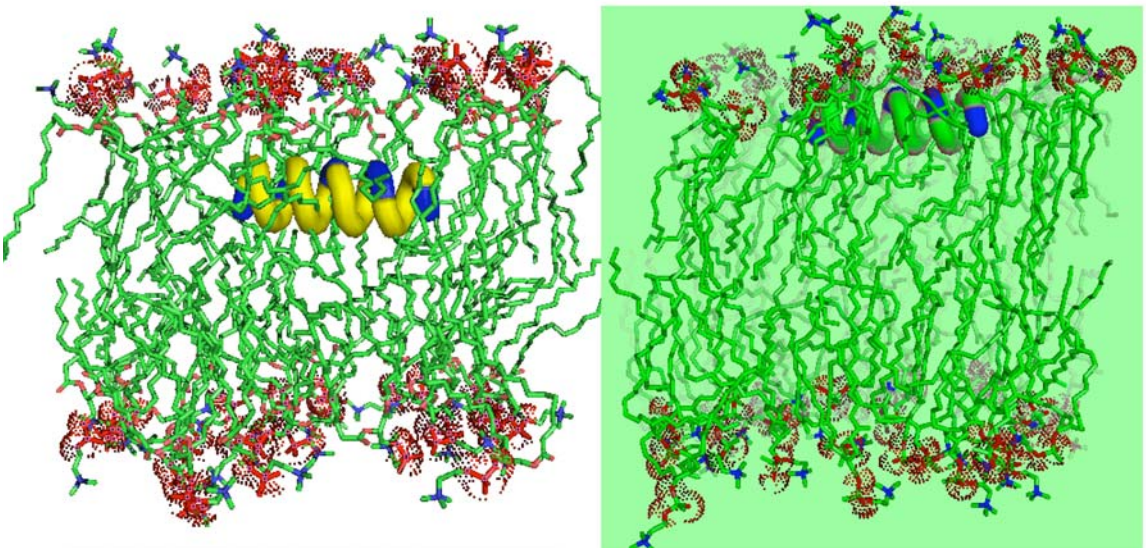

Figure 3-25. Model of KL_4 penetration in two lipid environments. Based on ^2H NMR data, KL_4 appears to "snorkel" in 4:1 DPPC:POPG lipid vesicles. This snorkeling may have consequences in the lung, where these lipids are the most prevalent, since it may help facilitate lipid shuttling and/or promote formation of different lipid phases. In contrast, in 3:1 POPC:POPG MLVs lipids, a more peripheral interaction of KL_4 with the headgroup region is seen

CHAPTER 4
STRUCTURAL STUDIES OF KL_4

This chapter describes structural measurements of KL_4 in a heterogeneous lipid environment using CD and ssNMR. This work was done in collaboration with Dr. Douglas Elliot and Professor Joanna Long.

Characterization of KL_4 Secondary Structure

In vitro and clinical studies show that KL_4 minimizes surface tension and provides for relief from respiratory distress. The linear charge distribution of KL_4 is based on charge distribution in the C-terminus of SP-B with the presumption that both SP-B_{59-80} and KL4 form amphipathic helices. In Chapter 3, the effects of KL_4 on lipid dynamics and order were measured using ^{31}P and ^{2}H NMR. ^{31}P NMR spectroscopy indicated the peptide predominantly interacting with the PG headgroup and having small negative effects on acyl chain order parameters in POPC:POPG. The opposite effects were found in DPPC:POPG LUVs where deuterium-derived order parameters indicate KL_4 ordering the fatty acyl chains. We postulated this increase in deuterium order parameters as being due to KL_4 penetrating deeper into DPPC:POPG bilayers as opposed to POPC:POPG bilayers. While the different effects on one lipid system compared to the other is interesting, the question remains as to the secondary structure of the peptide is when bound to DPPC:POPG and POPC:POPG and how its structure allows shallower or deeper penetration. In Figure 3-25, it is assumed in the molecular models that KL_4 is helical and that it is superficial in one lipid system while embedded in the other. The assumption of KL_4 being helical in both membrane milieus is an assumption based on findings that SP-B and SP-C are helical; particularly, SP-B_{59-80}, which has been purported to be an amphipathic alpha helix (*11*). However, even though SP-B_{59-80} is presumed helical, it does not necessarily implicate KL_4 as being an α-helix in a lipid environment. Furthermore, the structure

of KL_4 in phospholipid bilayers has not been definitively resolved and may be contingent on lipid composition. Infrared studies (*148, 166*) involving the orientation of the peptide in different lipid environments give conflicting secondary structure adaptations. One IR study shows KL_4 being a transmembrane helix in 7:3 DPPC:PG bilayers (*148*); the other study, combining IR measurements with surface pressure isotherms, postulated the peptide to be an anti-parallel beta sheet in a 7:3 DPPC:DPPG membrane environment (*166*). Thus, even when the lipid composition is constant, disagreements exists in the literature. The simple assumption of KL_4 being helical, based on sequence periodicity and charge distribution, cannot be readily accepted and other biophysical methods need to validate the IR measurements and higher resolution measurements could provide even more insight.

In this chapter, circular dichroism and ssNMR studies are described which were undertaken to determine the structure of KL_4 in the lipid environments of 3:1 POPC:POPG and 4:1 DPPC:POPG LUVs as well as neat lipids. Circular dichroism represents the simplest and most effective qualitative measure of global secondary structure in solution and in the presence of LUVs. Under optimized CD conditions, one can rule out β-sheet or α-helical structures for a peptide interacting with different lipid moieties. We undertook a systematic CD study of KL_4 in the presence of differing concentrations of POPC:POPG and DPPC:POPG LUVs. These are the two lipid systems where different topologies of KL_4 were postulated in Chapter 3 based on NMR studies examining phospholipid dynamics. As part of these experiments characterizing the structure of the peptide, CD experiments were also performed to assess the influence of aqueous buffer or helix-inducing solvents on the gross secondary structure of the peptide in the absence of lipids.

In collaboration with Professor Joanna Long and Dr. Douglas Elliot, ssNMR studies were performed on ^{13}C-labeled KL_4 peptides using the DQ-DRAWS pulse sequence (detailed in Chapter 2). ^{13}C labels were enriched in adjacent carbonyl leucines of KL_4 to determine backbone torsion angles phi (φ) and psi (ψ). Each ^{13}C-labeled peptide was complexed to lipids and the DQ-DRAWS sequence was used to first determine the torsion angle φ and then the torsion angle ψ. The technique provides for a more detailed structural characterization of KL_4 in the lipid environments. These structural studies can provide insight into the IR results and possibly explain their discrepancies. They also demonstrate the utility of ssNMR in resolving peptide secondary structures in complex environments; in this case, mixtures of phospholipids are used to simulate eukaryotic membranes and membranes from the lung.

Materials and Methodology

Peptide synthesis*:* KL_4 was synthesized via automated solid-phase peptide synthesis (ABI 430, ICBR, UF) on a Wang resin. Peptide was cleaved from the resin with 90% TFA/5% triisopropyl-silane/5% water and ether precipitated. The crude product was purified by RP-HPLC using an acetonitrile/water gradient and purity was presence of KL_4 was verified by mass spectrometry with a m/z ratio of 2471. Finally, the product was lyophilized and stored at –30 ^{o}C until used in sample preparation.

Preparation of KL_4 in buffer: Dried peptide was weighed and solublized in 1:1 methanol:water to an estimated stock concentration of ~200μM. This ensured full dissociation of the peptide and prevented any unwanted formation of aggregates. The solution of 1:1 methanol:water was placed under a stream of nitrogen to remove the methanol and then concentrated HEPES buffer was added to achieve a final concentration of ~100μM of KL_4 in 5mM HEPES, pH 7.4.

Preparation of POPC:POPG and DPPC:POPG Vesicles For CD Measurements with KL_4: DPPC, POPC and POPG lipids dissolved in chloroform were purchased from Avanti Polar Lipids (Alabaster, AL). The lipids were mixed at molar ratios of 3:1::POPC:POPG and 4:1:: DPPC:POPG and the $CHCl_3$ was removed under a nitrogen stream. The dried lipid films were dissolved in cyclohexane and lyophilized to remove residual chloroform. The lipids were then reconstituted in 5mM HEPES, pH 7.4, and subjected to 3 freeze-thaw cycles to facilitate the formation of multilamellar vesicles (MLVs). Large unilamellar liposomes (LUVs) were prepared by extrusion of the MLVs through 100 nm polycarbonate filters (Avanti Polar Lipids) at room temperature. Extrusion of DPPC:POPG LUVs took place above the mixture's phase transition temperature.

Preparation of solution CD samples: CD spectra were collected on 150μM KL_4 in 1:1 methanol:water as well as hexafluroisopropanol. Since the helical content of KL_4 is unknown in solution, a spectrum of 40μM KL_4 in the helix-inducing solvent trifluoroethanol (TFE) (*81*) was also collected to generate a baseline CD spectrum for the purely helical peptide. In this preparation, stock KL_4 (498μM +/- 3μM) in methanol solution was dried under compressed nitrogen gas and the peptide film was solubilized in 1mL TFE to a final peptide concentration of 40μM. The spectrum for KL_4 in TFE was run at 45^{o}C and subtracted from a spectrum of only TFE.

Preparation of KL_4/lipid samples in organic solvent for CD: A stock concentration of KL_4 in methanol (498μM +/- 3μM) was added to chloroform solution of lipids at 1, 2 and 3mol% peptide relative to lipids. The peptide-lipid mixtures were allowed to dry overnight before being dissolved with cyclohexane and lyophilized overnight. Samples were hydrated in 10mM HEPES

pH 7.4, 140mM NaCl and freeze-thawed 3-5 times over the course of 48 hours before extrusion. Extrusion to generate LUVs were done as described above.

Preparation of CD samples with peptides and lipids mixed in buffer: 100μM KL_4 in HEPES buffer was added to extruded DPPC, POPC, POPG, 4:1 DPPC:POPG, 3:1 POPC:POPG vesicles in the same HEPES buffer. For samples containing DPPC, samples were extruded at 50°C, and 100μM KL_4 stock, prepared as above, was added to freshly extruded vesicles to achieve a final peptide:lipid ratio of 1:33. The final concentration of peptide in these samples was 40μM and the final concentration of lipid was 1.33mM. CD spectra on these samples were recorded at 45°C.

Collection of CD spectra*:* CD experiments were performed on an Aviv Model 215 at a wavelength range 195-260nm with a step size of 1nm for 10-20 scans. The averaging time for each sample was 1 second. The settling time for each time was 0.3-0.6 seconds. All CD spectra were buffer subtracted.

CD shows KL_4 to be helical

Circular dichroism provides a simple qualitative method for determining peptide secondary structure in solution as well as for peptide bound to lipid. As an initial assessment of global secondary structure, CD was performed on KL_4 in 5mM HEPES pH 7.4. At three different concentrations in 5mM HEPES buffer at pH 7.4, the peptide displayed spectra that are characteristics of a helical peptide, although some other secondary structure elements can also be seen (Figure 4-1). CD performed on KL_4 at 150μM, still show a minimum at 208nm, however the appreciable loss of signal at 222nm may indicate the onset of aggregation of the peptide. Given the highly hydrophobic nature of the peptide, aggregation or higher order peptide structures is highly possible. In the presence of the helix-inducing organic solvent hexafluoroisopropanol (HFIP), the CD spectrum of 150μM KL_4 indicates helical structure

(Figure 4-2). These initial CD experiments indicate that KL_4 is helical in buffer and HFIP induces further helicity. At higher concentrations in buffer, peptide aggregation most likely occurs. In methanol and water a reduced helical signature is seen. We then undertook CD experiments to examine the secondary structure of KL_4 when it is interacting with LUVs to answer the question of whether lipid bilayers can serve as a substrate to induce secondary structure formation.

Figure 4-3 shows CD measurements taken of 40μM KL_4 interacting with 1.33mM lipid LUVs in which both peptide and LUVs were reconstituted separately in 10mM HEPES buffer and then mixed. Helicity was assessed by examining the ellipticity at 208 and 222nm. KL_4 added to neat POPG and DPPC LUVs yielded spectra with adsorption minima at 208nm and 222nm indicative of helical secondary structure. The mixture of 4:1 DPPC:POPG LUVs with 3mol% peptide also showed a pronounced helical CD spectrum (Figure 4-3). CD recorded of KL_4 in the presence of neat POPC lipids resulted in a noisy spectrum with poor signal; however when the same amount of peptide was added to 3:1 POPC:POPG LUVs, signal with clear helical tendencies was recaptured (Figure 4-3). The following observations from CD supports ^{31}P NMR data that reflect an affinity of the peptide with the anionic phosphatidylglycerol lipid. Since KL_4 shows helical propensity in solution and is clearly not unstructured (Figure 4-1), the role of POPG may not necessarily involve folding of the peptide, yet the presence of the lipid clearly results in changes in ellipticity at 222nm strongly implicating the modulation of helical content by this phospholipid species. Solution CD of KL_4 in 10mM HEPES buffer, pH 7.4 and 140mM NaCl show a double minima that is characteristic of some helical qualities of the peptide, but the CD spectrum indicates the peptide is not 100% helical, especially when compared to peptide in TFE (Figure 4-4).

Ellipticity at 222nm (θ_{222}) has been found to increase linearly with the extent of helix formation (*169, 170*). Shown in Table 4-1 are the θ_{222} values obtained by adding peptide to pre-formed LUVs. Negative ellipticities at 222nm were found when KL_4 was interacting with DPPC, POPG and DPPC:POPG LUVs. When viewed as the dichroic ratio of $\theta_{222}/\theta_{208}$, the two wavelengths that yield double minima in an alpha helical CD spectrum, it is clear that the helical signatures of the peptide are changing relative to the peptide in solution. The CD data strongly implicate PG headgroups and saturated PC lipids in enhancing the helical propensity of the peptide.

Peptide and lipid mixed together in organic solvent and reconstituted also result in helical CD spectra typified by the minima at 208nm and 222nm. Shown in Figure 4-4 are spectra for 40μM KL_4 in the presence of POPC:POPG and DPPC:POPG LUVs at a peptide molar ratio of 1%. To determine if we can discern structural changes in KL_4 as a function of concentration, samples of 40μM KL_4 which was either at 2mol% and 3mol% with respect to the lipids were also run. At 2mol% peptide, the double minima in both DPPC:POPG and POPC:POPG can be seen, although the signal is degraded by light scattering from the lipids (Figure 4-5). 40μM KL_4 with POPC:POPG LUVs shows a CD spectrum that displays significant overlap in signal to 40μM KL_4 in HEPES/NaCl solution. In an environment of POPC:POPG LUVs, the peptide is in a state that is helical but less so than in TFE. In comparison, the double minima at 208nm and 222nm is prominent at 2mol% peptide in DPPC:POPG LUVs. (Figure 4-5). At 3 mol% peptide, the CD signal from KL_4 is barely discernable when interacting with POPC:POPG LUVs, suggesting it is disturbing the lipid phase properties leading to light scattering, but the double minima is still prominent in DPPC:POPG LUVs (Figure 4-6). The data clearly indicate concentration and lipid dependence in CD signal and can help explain the differing dynamics and

lipid ordering seen from ^{2}H and ^{31}P NMR based on KL_4 studied in POPC:POPG versus DPPC:POPG vesicles. Figure 4-7 shows the CD signal generated as peptide levels are increased in DPPC:POPG LUVs and POPC:POPG LUVs. The helical signature seen for KL_4 in DPPC:POPG bilayers, where we postulated the peptide is more embedded, is seen in Figure 4-7. The signals at 208nm and 222nm seen in DPPC:POPG LUVs could also be a result of contributions from other types of helices such as a π-helix that do not make such contributions in POPC:POPG LUVs. Table 4-2 shows the raw CD ellipticity (in millidegrees) of DPPC:POPG and POPC:POPG at different molar percentages of KL_4. Comparing the ellipticity values amongst the lipid systems, we find that helical signatures in DPPC:POPG at higher peptide levels than in POPC:POPG. However, it is not known if the changes seen in ellipticity are representing changes at the residue level of KL_4 or entire sections of the peptide are assuming different helical conformations as concentration increases relative to the lipids. If the spectrum of KL_4 in TFE assumes complete helicity, then the CD data indicate that both lipid systems increase helical content of KL_4 relative to that in solution. Comparing KL_4 in buffer relative to that in TFE solvent, it is clear that KL_4 contains a mixture of secondary structures rather than a purely α-helical motif. These experiments were performed with 10-20 scans for signal averaging; it is not known if an increase in the number of scans would allow better comparison of KL_4 samples in an embedded bilayer relative to bound to the headgroup regions. It can be seen however that differences can be seen when KL_4 binds DPPC:POPG versus POPC:POPG LUVs.

While the typical double minima characteristic of α-helices are seen in CD spectra of KL_4 both with and without lipid, it is important to realize that such a method is only sensitive to average properties of a molecule, and the distribution of helical and non-helical residues cannot

be determined (*169*). Additionally, CD does not allow clear distinction between different types of helices. The peptide in combination with lipids may have signal due to formation of non-standard helices. Our data do show, however, that KL_4 has helical characteristics both in solution and when interacting with DPPC, POPG, DPPC:POPG and POPC:POPG LUVs.

CD indicates that KL_4 is helical in solution; however, the periodic placement of lysines would make an α-helical conformation favorable in buffer, but not at a lipid interface where amphipathic structures are favored. Placement of KL_4 in helical wheel diagrams for different types of helices show that in order for the peptide to bind to an amphipathic substrate, such as a lipid interface, the peptide might form *i, i+5* hydrogen bonds (Figure 4-8). Such a helical wheel diagram suggests that a π helix has a favorable alignment of the hydrophobic leucine residues and hydrophilic lysine residues for snorkeling into a lipid bilayer. Whereas modeling KL_4 as a $i \rightarrow i+4$ helix shows hydrophilic lysines around the periphery of the helical wheel. This secondary structure should be favored in the solution-state, where interactions occur isotropically, but is disfavored in a lipid environment. This begs the question whether the peptide adapts a canonical $i \rightarrow i+4$ helix or another helix with a different hydrogen bonding pattern in the context of a lipid environment. Torsion angle measurements using ssNMR were used to answer this question.

Different Types of Helices KL_4 May Adapt in a Lipid Bilayer

A standard $i \rightarrow i+4$ helix has 3.6 residues per turn providing for the most stable atomic arrangement thermodynamically, accounting for roughly 30% of secondary structure found in proteins (*171*). Torsion angles used to define the backbone conformation at C_α-N bond (defined as the angle psi: ψ), at the C_α-C' bond (defined as the angle phi: φ) are -57^o (φ) and -47^o (ψ) for a classic α-helix. However, variations do exist, and on average values of $\varphi=-65^o$ and $\psi=-45^o$ are seen in x-ray structures of crystalline proteins (*172*). Given the nature of lysine side chains

spaced every five residues in KL_4, hydrogen bonds to residues in an $i \rightarrow i+5$ arrangement cannot be disqualified as a resulting helical fold in the lipid environment. This can give the helix a tighter coil which may help the peptide interact with heterogeneous environments and facilitate the "snorkeling" model envisaged in Chapter 3. An $i \rightarrow i+5$ hydrogen bond pattern results in a helix with 4.4 residues per turn and is termed a π helix (*171*) with 16 atoms between the hydrogen bonds. This type of helix is considered to be thermodynamically unfavorable in free solution (*173*).

Solid-State NMR Studies of KL_4 in POPC:POPG and DPPC:POPG

Work in determining the helical nature of KL_4 was undertaken by Professor Joanna Long and Dr. Douglas Elliott. In these studies, KL_4 was synthesized with ^{13}C enrichment at specific leucine C′ positions in the peptide and the peptide was complexed with 3:1 POPC:POPG MLVs for CPMAS experiments. Using the DRAWS pulse sequence, the double quantum (DQ) state between the ^{13} C′ spins was excited during mixing times in the pulse sequence. The mixing time it takes to generate the DQ coherence is dependant on the distance between the spins.

Distances between adjacent $^{13}C'$ spins were determined by a least squares fit of DQ buildup curves to numerical simulations (Figure 4-9). As can be seen in this figure, the build-up curve is consistent with a φ angle of -100^o to -105^o. Using a 2D-DRAWS experiment, the relative orientations of the amide planes were measured and compared to simulations. The χ^2-fitting of the ψ torsion angle based on comparison of experimental data to numerical simulations is shown and the best fit torsion angles from these simulations were $\varphi = -105^o$, $\psi = -26^o$ and $\varphi = -105^o$, $\psi = 132^o$ (Figure 4-10).

Using torsion angles of -105^o and -26^o in the molecular graphics program PYMOL renders a helix where all the charged lysines lie on one side of the helix (Figure 4-11). Such a configuration would indeed have biological implications; particularly in terms of the peptide

being able to embed to the membrane. However, the splaying of the lysines suggest it would not be deeply embedded. From the deuterium NMR data performed in Chapter 3, POPC and POPG acyl chain order parameters decreased slightly in the presence of KL_4 corroborating this model. Similar experiments performed by Professor Joanna Long on KL_4 in DPPC:POPG LUVs reveal backbone torsion angles of φ =-65 and ψ =-78. Placement of these torsion angles into the molecular graphics program PYMOL also yields a helix (Figure 4-12). However, unlike what was seen for the peptide bound to POPC:POPG vesicles, it is found that the lysine residues are more aligned along one side of the helix. Comparing Figure 4-11 and Figure 4-12 one sees that in POPC:POPG MLVs, the lysine residues have a more radial distribution around the axis of the helix as compared to in DPPC:POPG MLVs. In POPC:POPG MLVs, the side chain lysines face preferentially one side of the helix, but the first and last lysine residue are particularly out of phase. In DPPC:POPG MLVs, the first and fifth lysine side chains are more parallel and in phase with each other. The argument presented for lysine snorkeling in Chapter 3 from deuterium NMR data corroborates nicely with the structure Professor Long found for the ^{13}C labeled peptide in DPPC:POPG. The helical structure obtained from DQ-DRAWS aids in explaining the increase in deuterium NMR order parameters found in the middle to the end of the acyl chain. If the lysine residues of KL_4 are more aligned in DPPC:POPG, the peptide can bury itself deep into the bilayer, while the long side chains of lysine can extend out into the interface and form a favorable electrostatic interaction with the phosphate headgroups. In POPC:POPG, where the acyl chains become less ordered in the presence of peptide, the lack of lysine alignment seen in the structure found from DQ-DRAWS measurements strongly implicate a peripheral interaction of the peptide with the headgroup only. This is seen from our CD data where in POPC:POPG the helical signature was lost at 3mol% peptide but can still be discerned

in DPPC:POPG. The CD data also rules out φ =-105 and ψ =132 as one of the torsion angles obtained from Professor Long's 2D-DRAWS simulations since such backbone torsion angles would predict a β-sheet for the peptide. Hence, the findings from Professor Long and Dr. Elliott show that headgroup conformation and acyl chain dynamics clearly affect the type of helix KL_4 adapts in a lipid bilayer setting. Our deuterium NMR and CD data with the ssNMR data from Professor Long show that in DPPC:POPG, KL_4 adapts a structure that has more qualities of a π helix. Based on CD and ssNMR torsion angle measurements, in POPC:POPG, KL_4 adapts into a structure that is helical but intermediate between an α-helix and a β-sheet.

Fodje and Karadaghi recently re-evaluated the proteins in the PDB (*171*), and according to their criterion, have found an underestimation in the amount of π helices accounted for. Based on their algorithms, the authors have come up with mean dihedral angles (φ,ψ) of -76° and -41°, which are in stark contrast to previous measurements of -57° and -70° (*171, 172*) but in good agreement with the DPPC:POPG structure. Furthermore, Fodje and Karadaghi found significant differences in dihedral angles from the *i-4* to the *i+4*, residues within the helix. Hence it seems probable that KL_4 has characteristics (particularly in the middle of the sequence) similar to a π helix, offering the advantages of partitioning the charged lysine side chains to adapt to a lipid environment and reducing the surface area and volume occupied by the peptide (*171*) which would be entropically favorable. π helix formation may be modulated by amphilicity and may also help to stabilize lipid-water or air-water interfaces (*174*). Thus, the types of helix resulting from ssNMR data of KL_4 represent non-canonical structures due to residues changing alignment in the presence of amphiphilic lipid substrates such as 3:1 POPC:POPG and 4:1 DPPC:POPG and could indicate how KL_4 modulates lipid dynamics in the lung. The CD data show different secondary structure signals contingent on the different lipid system which agree nicely with ^{31}P

and ^{2}H NMR data. Professor Long's structural measurements of the peptide in DPPC:POPG and POPC:POPG clearly indicate the peptide has a different structure in each environment underscoring the observation that the peptide's structure, orientation, and depth penetration is dependant on the saturation level of the acyl chains.

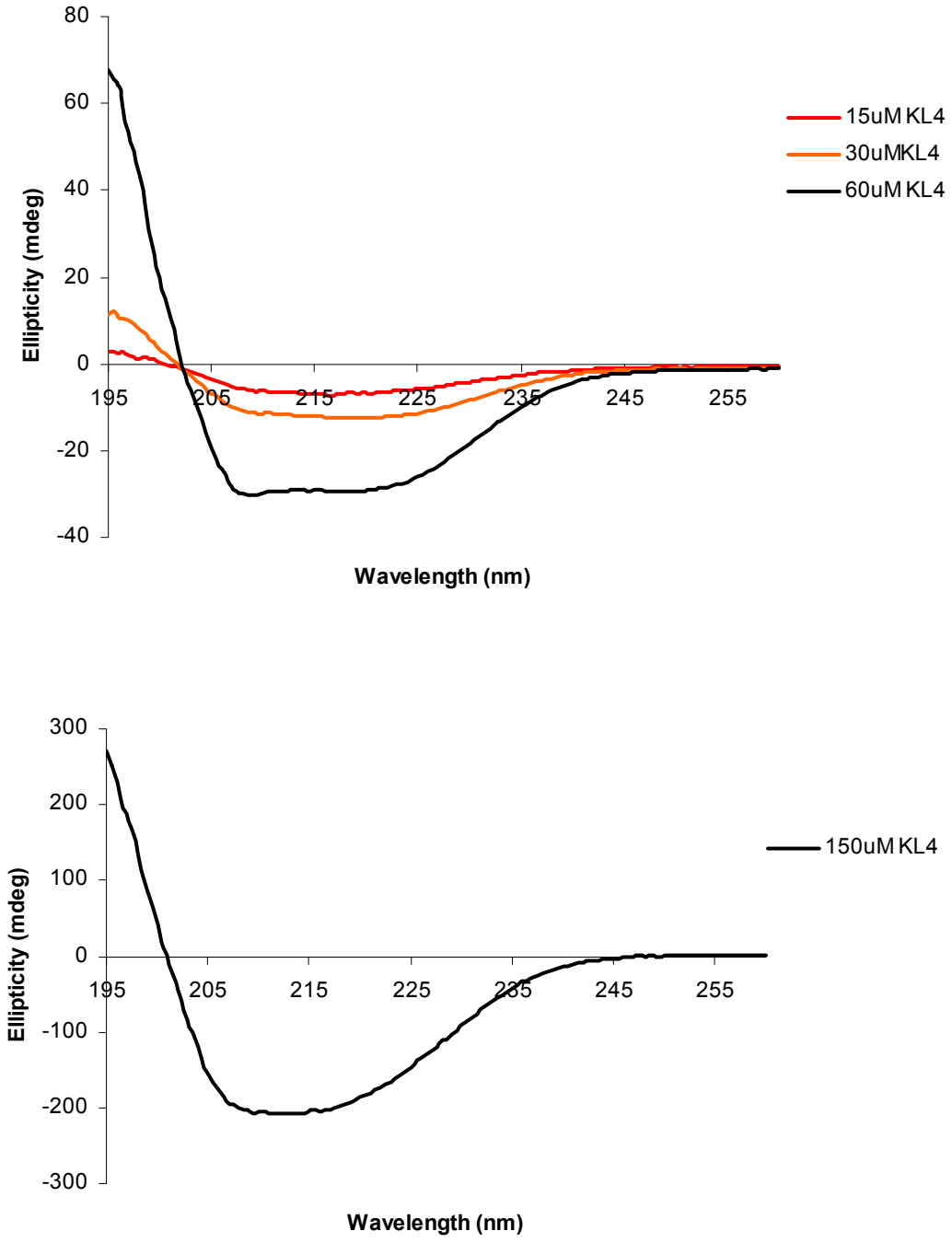

Figure 4-1. CD Spectra of KL_4 in 5mM HEPES at pH 7.4. Below is a spectrum of 150µM KL_4 indicating potential aggregation.

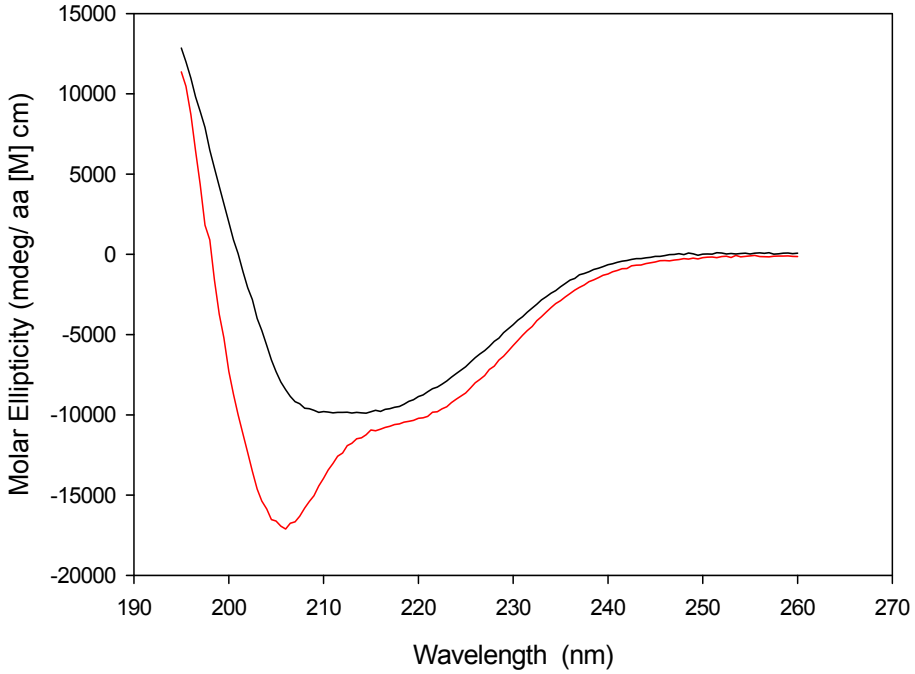

Figure 4-2 CD spectra of KL_4 in organic solvents. Red is a spectrum of peptide in 150µM hexafluroisopropanol and black is a spectrum in 50:50 MeOH:dH_20.

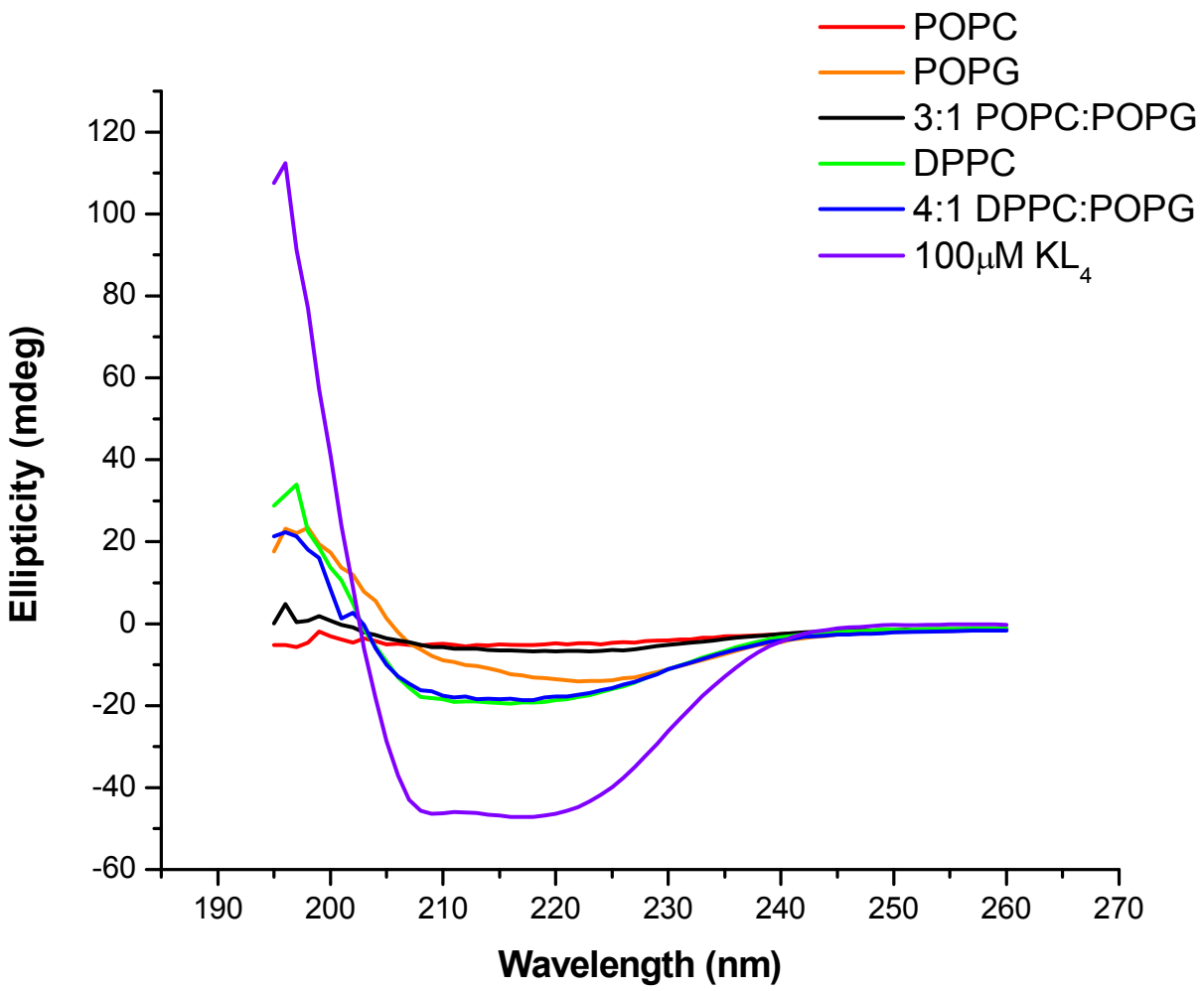

Figure 4-3. CD Spectra of 40μM KL_4 added to 1.33mM LUVs. DPPC containing samples were run at 45°C. Remaining samples were run at room temperature. Samples were in 10mM HEPES pH 7.4 and 140mM NaCl.

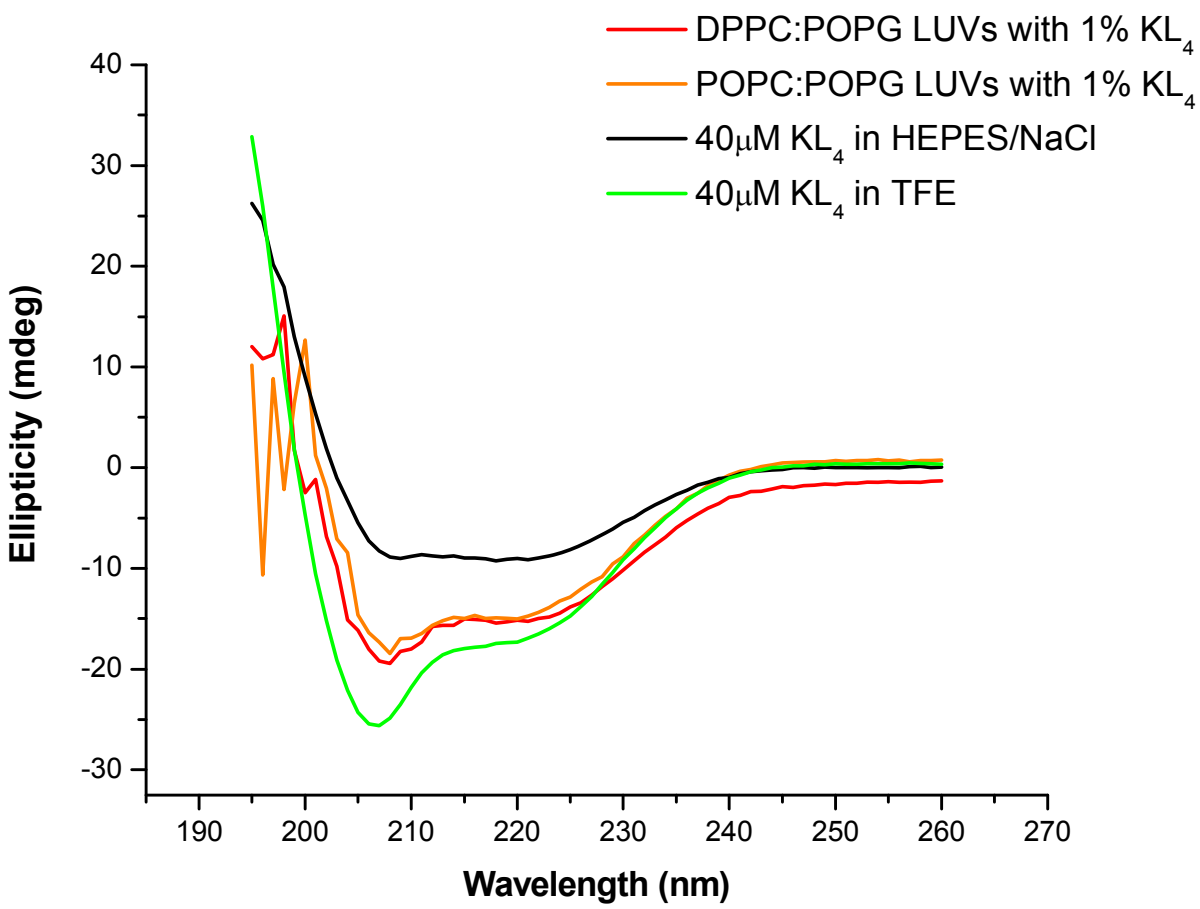

Figure 4-4. CD spectra of 40μM KL_4 reconstituted in 4mM 4:1 DPPC:POPG and 3:1 POPC:POPG LUVs. Shown in comparison is 40μM KL4 in 10mM HEPES, 140mM NaCl and in TFE.

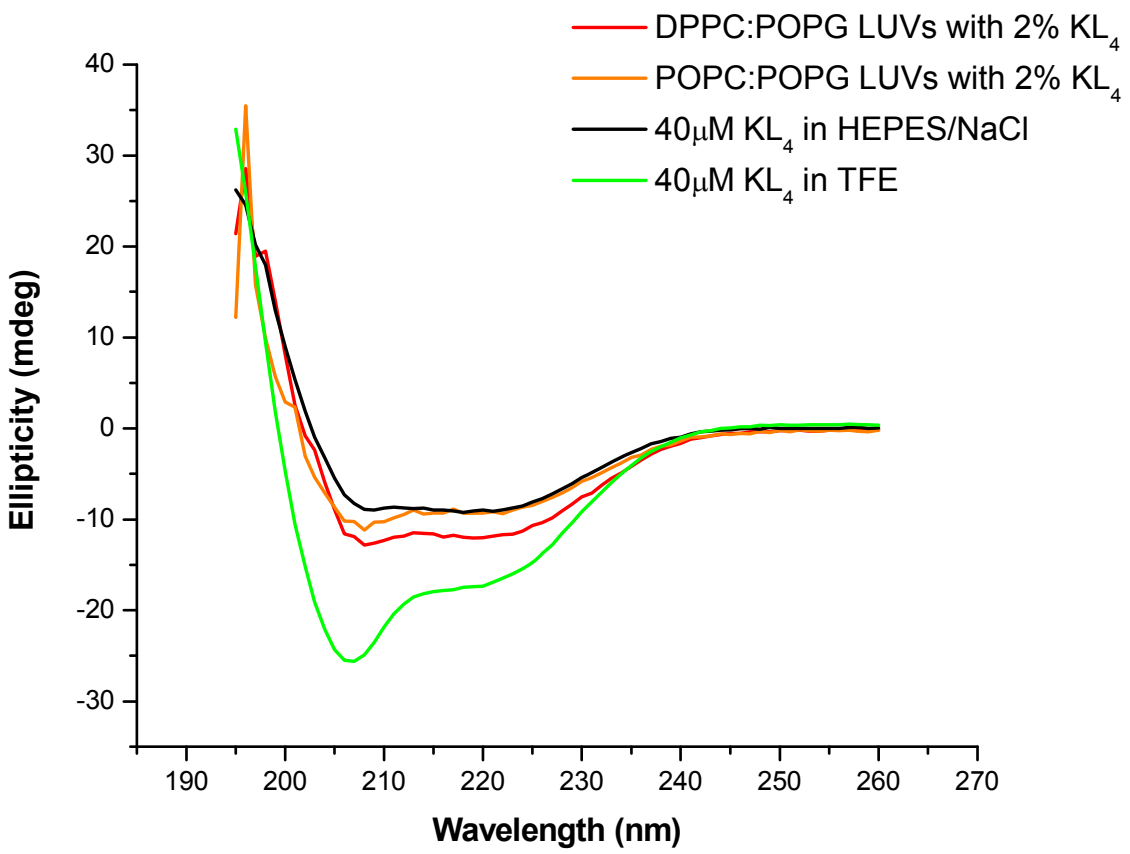

Figure 4-5. CD spectra of 40μM KL_4 reconstituted in 2mM 4:1 DPPC:POPG and 3:1 POPC:POPG LUVs. Shown in comparison is 40μM KL_4 in 10mM HEPES, 140mM NaCl and in TFE.

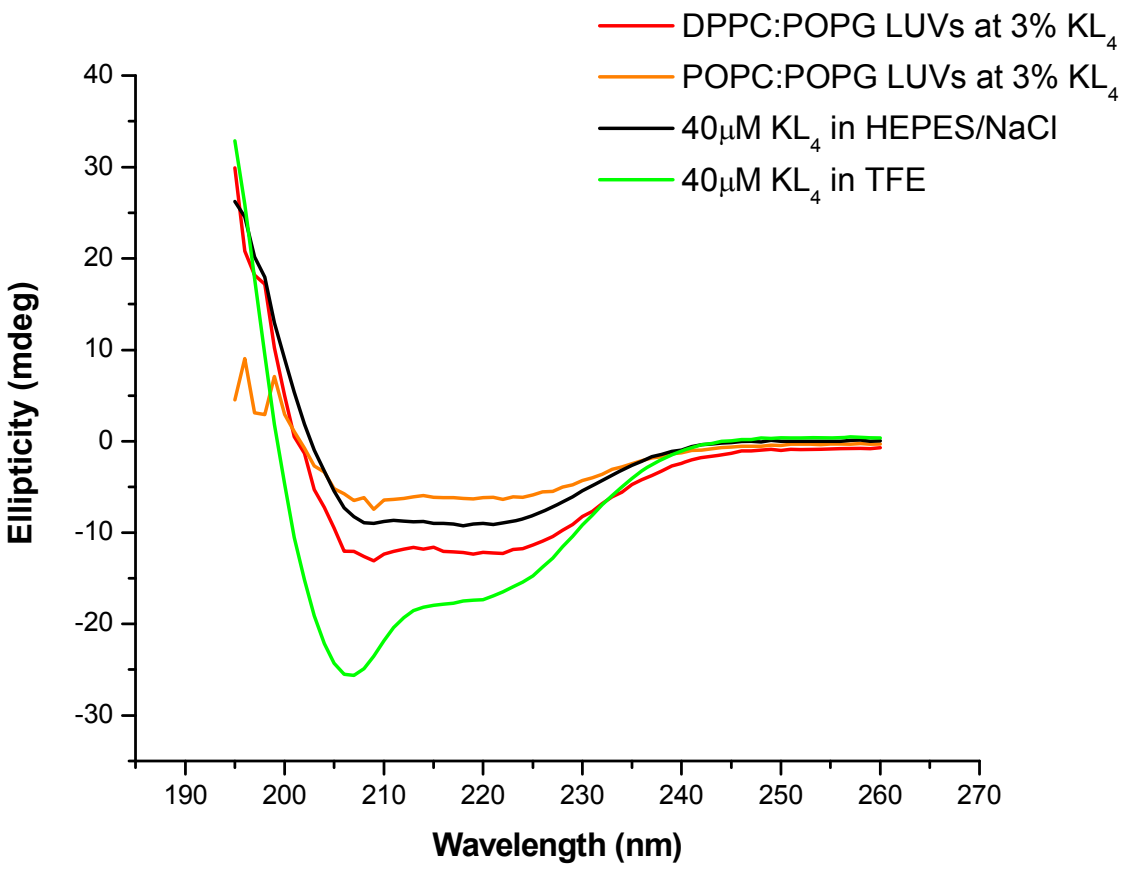

Figure 4-6. CD spectra of 40μM KL4 reconstituted in 1.33mM 4:1 DPPC:POPG and 3:1 POPC:POPG LUVs. Shown in comparison is 40μM KL4 in 10mM HEPES, 140mM NaCl and in TFE.

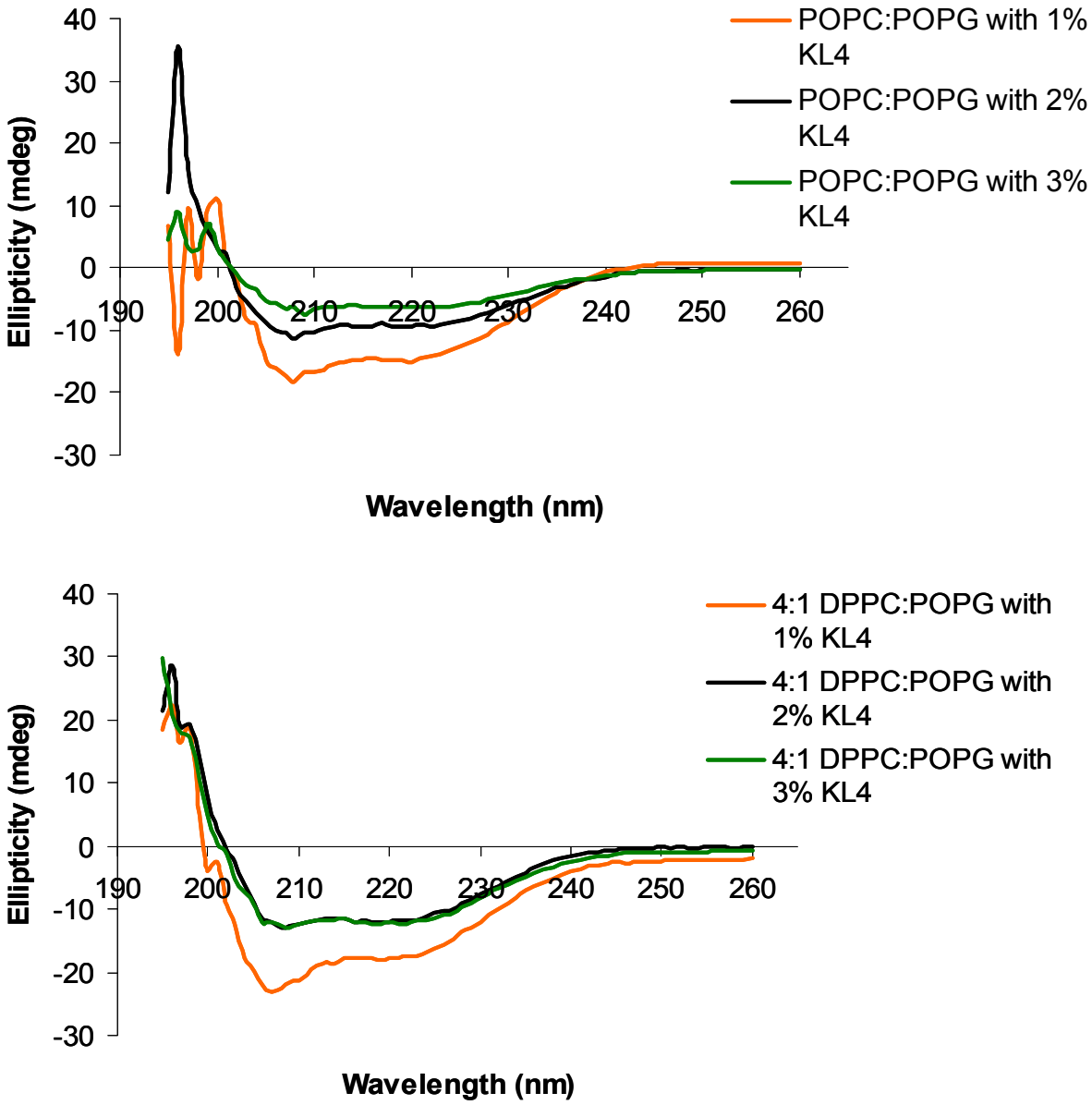

Figure 4-7. CD Spectra of (Top) POPC:POPG LUVs and (Bottom) DPPC:POPG LUVs with increasing mol% of KL_4.

Table 4-1. Ellipticity (in mdeg) of KL_4 at 222nm and 208nm and ratio of helical signatures 222nm and 208nm

	208nm	222nm	222nm/ 208nm
40μM KL_4 in			
POPC	-5.4	-4.8	0.9
POPG	-6.4	-14.1	2.2
3:1 POPC:POPG	-5.2	-6.7	1.3
DPPC	-17.9	-17.9	1.0
4:1 DPPC:POPG	-16.3	-17.3	1.1
100μM KL_4 in solution	-45.7	-9.5	0.2

Table 4-2. Ellipticity (in mdeg) of 40μM KL_4 reconstituted in LUVs from organic solvent.

	208nm	222nm	222nm/208nm
4:1 DPPC:POPG			
1% KL_4	-22.5	-16.1	0.7
2% KL_4	-15.4	-13.5	0.9
3% KL_4	-17.4	-15.2	0.9
3:1 POPC:POPG			
1% KL_4	-20.6	-16.2	0.8
2% KL_4	-11.2	-9.4	0.8
3% KL_4	-10.9	-9.6	0.9
40μM KL_4 (in 10mM HEPES, 140mM NaCl)	-8.9	-9.0	1.0
40μM KL_4 (in TFE)	-24.9	-16.5	0.7

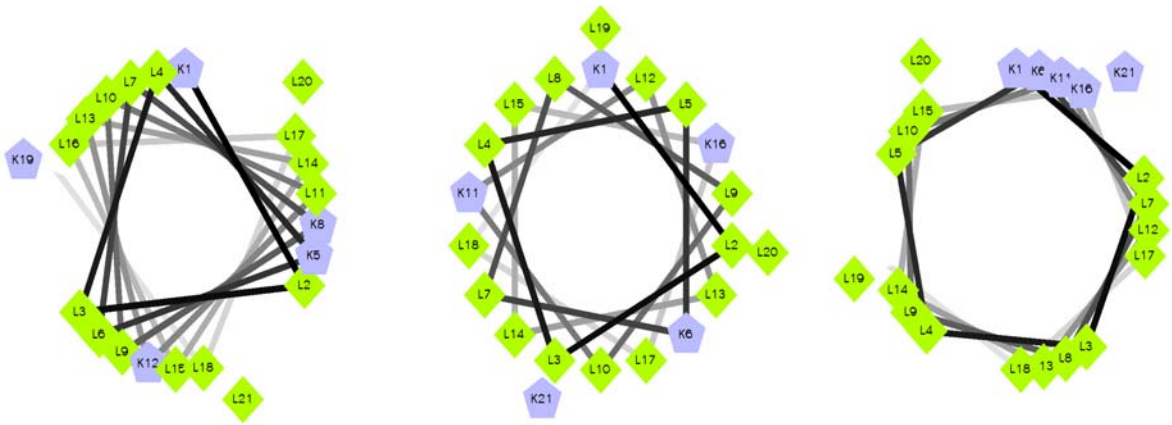

Figure 4-8. Helical wheel projections of KL_4 as: (left) 3_{10} helix, (middle) standard α-helix, and (right) π helix.

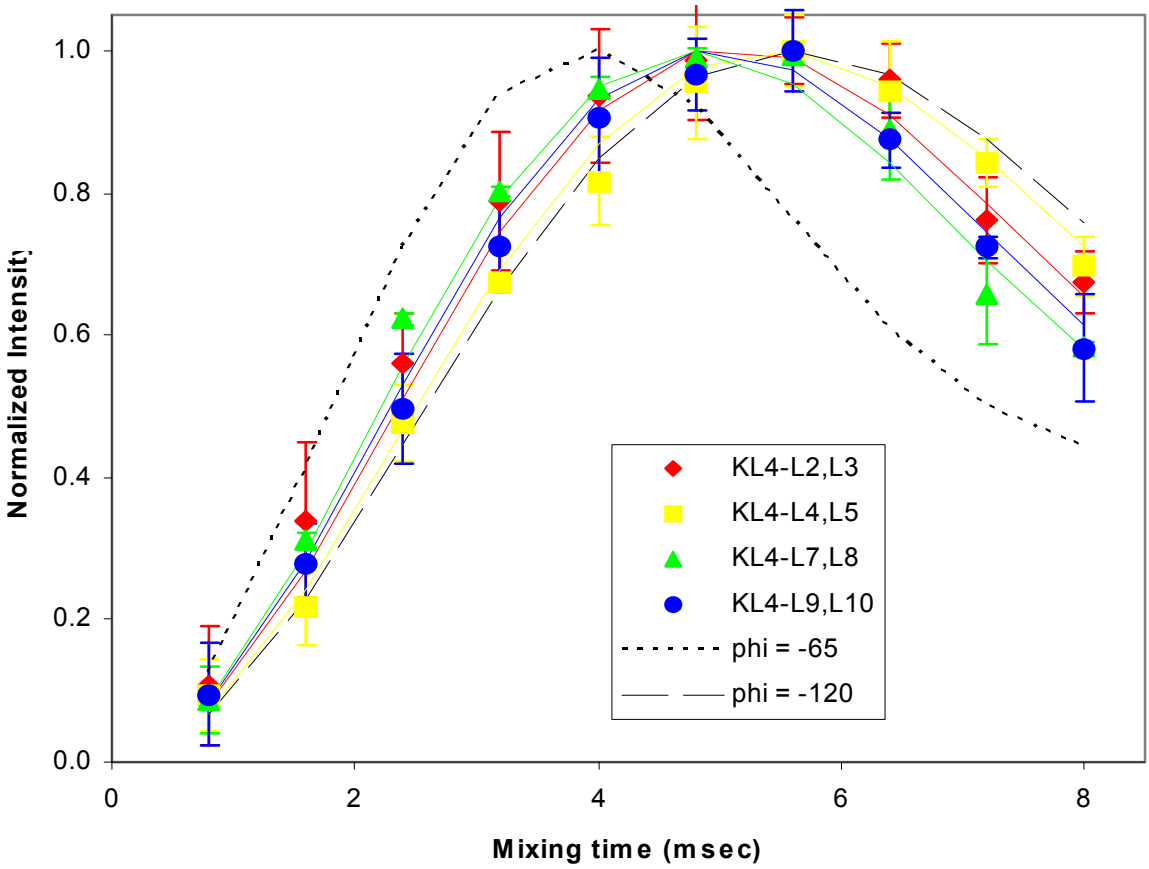

Figure 4-9. DQ-DRAWS buildup curves generated from spectra on ^{13}C labeled KL_4 with POPC:POPG (3:1). Data taken with permission from Professor Joanna Long.

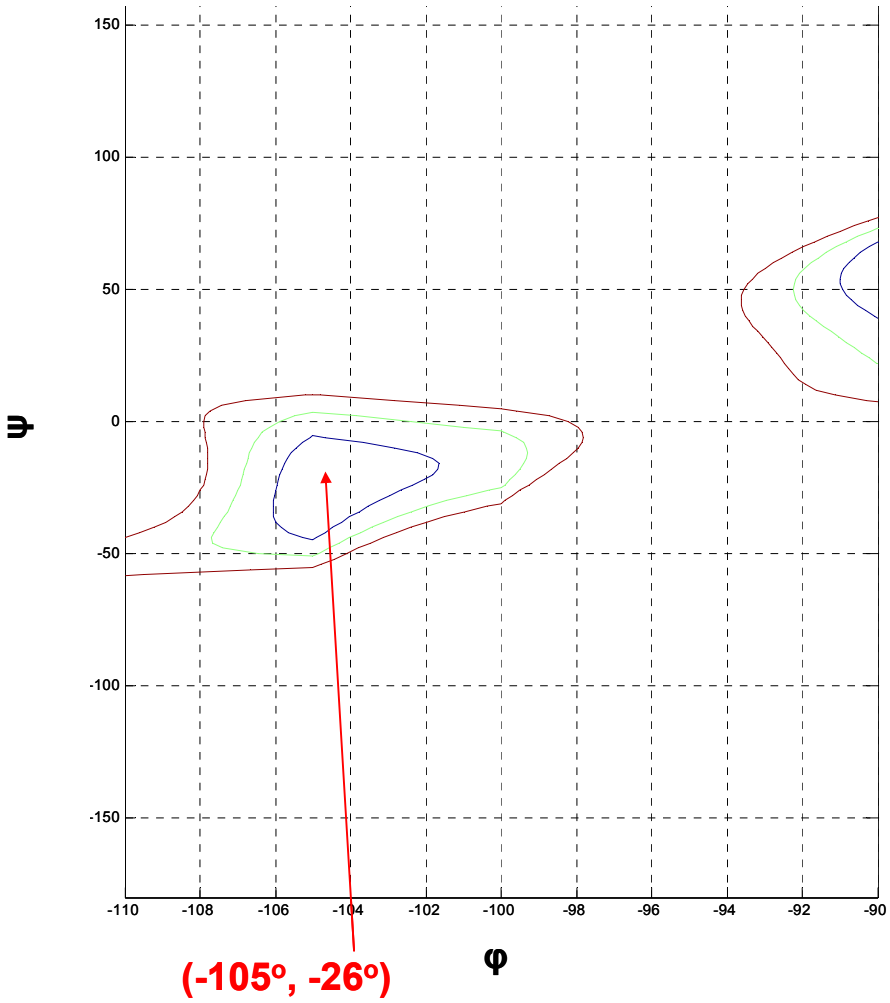

Figure 4-10. Ramachandran plot showing a χ^2 minimum at φ=-105 and ψ=-26 for KL_4 in 3:1 POPC:POPG. Contours shown in blue, green and brown are 1,2, and 3 standard deviations away from the minima. Data taken with permission from Professor Joanna R. Long.

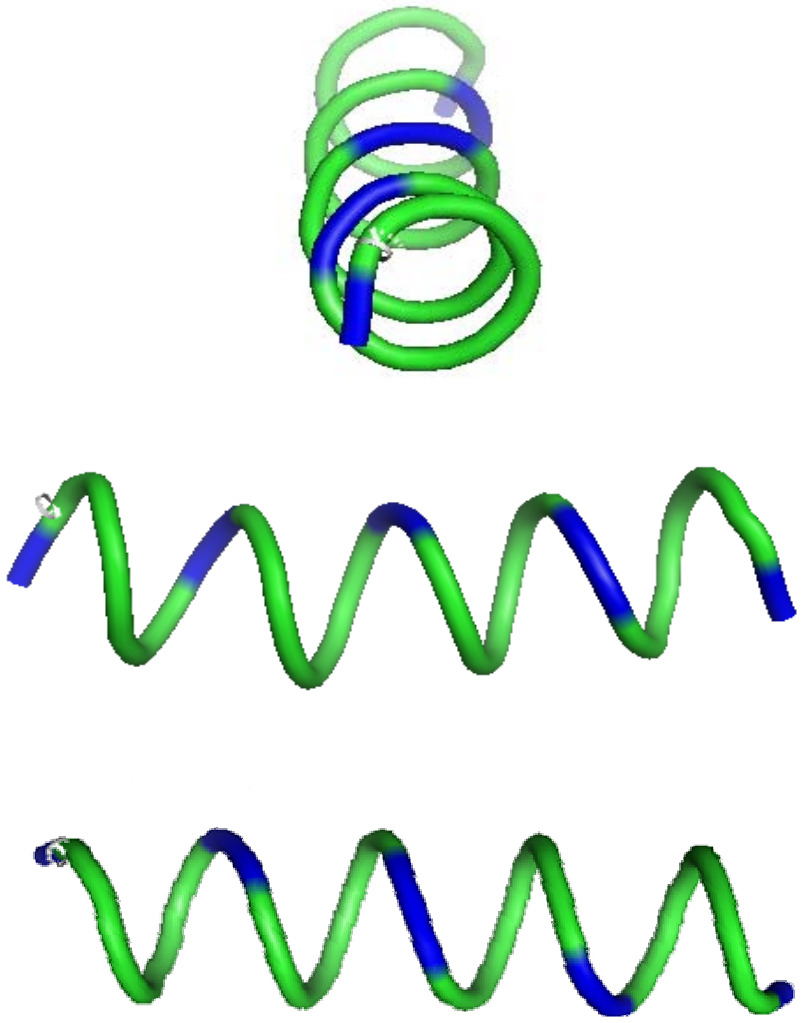

Figure 4-11. Model of KL_4 based on torsion angles obtained from the 2D-DRAWS experiments. The charged lysines (shown in blue) line up along one side of the helix.

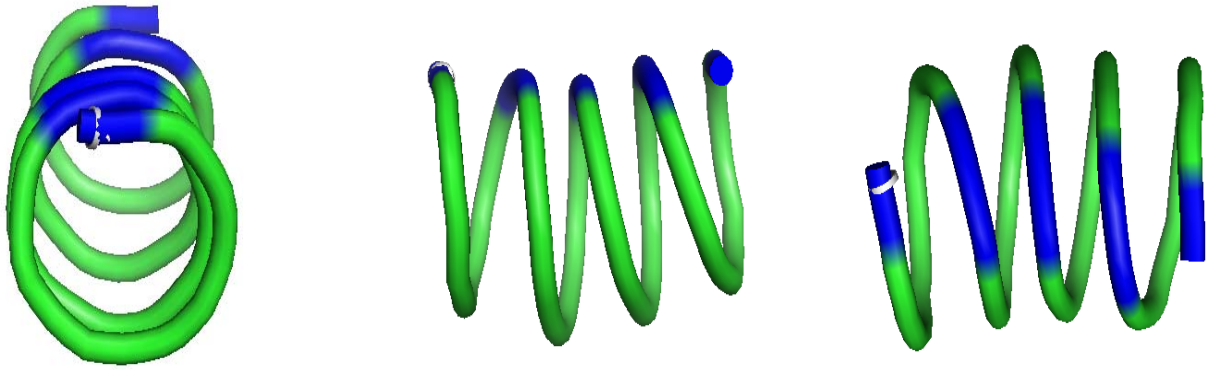

Figure 4-12. KL_4 with torsion angles of φ = -65, ψ= -78 obtained from ssNMR studies of KL4 in a DPPC:POPG lipid environment. Different views of the peptide indicate the lysine side chains line up along one side of the helix. In comparison, in POPC:POPG the lysine side chains splay radially along the helical axis. Data taken with permission from Joanna R. Long.

CHAPTER 5
COMPARATIVE BIOPHYSICAL STUDIES OF SP-B_{59-80}

This chapter describes ^{2}H and ^{31}P NMR studies of 4:1 DPPC(d-62):POPG and 3:1 POPC(d-31):POPG lipid systems on incorporation of $SP\text{-}B_{59-80}$, the C-terminus of SP-B.

Fragments of SP-B have biophysical activity

While the entire 80 amino acid SP-B protein is essential for lung surfactant organization, lung dynamics and respiration, subfragments of the native sequence have also shown significant biophysical function, particularly peptides corresponding to the N-terminal and C-terminal 20-25 amino acids. While both ends of protein have interesting biophysical properties, to date, the N-terminal region of the peptide has been more extensively studied in terms of functional properties and possible structural adaptation in different lipid environments.

The N-terminal 25 residues of SP-B ($SP\text{-}B_{1-25}$) have been shown to interact with specific anionic lipids to facilitate squeeze-out of lipids based on surface-film studies (*52*). $SP\text{-}B_{1-25}$ has also been shown to mediate mixing of lipid vesicles. Fourier-transform infrared measurements and CD studies of the N-terminal peptide in methanol, SDS micelles, and egg yolk lecithin (phosphatidylcholine) indicate the peptide has a high helical content. Spin-labeling of the first phenylalanine residue for electron spin resonance studies show that the N-terminus of the peptide retains mobility when bound to lipid (*175*). Recent molecular dynamics simulations of the peptide in DPPC monolayers indicate that the most likely equilibrium conformation is an α-helix parallel to the interface (*176*). However, the N-terminal fragment of SP-B has not been used in any formulations of artificial lung surfactants in clinical use indicating that while the role of the N-terminus may be of importance, it does not convey all the functionality needed for the protein component of lung surfactant.

The C-terminal fragment of SP-B, specifically residues 59-80 ($SP\text{-}B_{59\text{-}80}$), has shown potential in *in vitro* assays measuring surface tension such as pulsating bubble surfactometry. Isotherms relating surface pressure to surface area show that this peptide imparts lipid monolayer stability under compression, preventing collapse at pressures where monolayers of lipids alone collapse (*133*). Of particular clinical interest, the last 22 amino acids of SP-B served as the template for designing KL_4 as discussed in Chapters 3 and 4 (*67, 133*). The basis of the design for KL_4 was modeling the charge distribution and hydrophilic/hydrophobic ratio of the primary sequence of $SP\text{-}B_{59\text{-}80}$. As with the N-terminus, the C-terminal peptide is believed to form an amphipathic helix involved in headgroup ordering, but direct structural measurements in varying lipid contexts have to date not been documented. Nonetheless, a solution NMR study of the C-terminus of SP-B (residues 63-78) reconstituted in either SDS micelles or the organic solvent HFIP was recently published. This study was unable to see structure in the first five residues, but established that the rest of the sequence formed a helix in both SDS micelles and organic solvent (*177*). Unlike $SP\text{-}B_{1\text{-}25}$, FTIR or CD studies of $SP\text{-}B_{59\text{-}80}$ interacting with lipids are not documented and molecular dynamic simulations of $SP\text{-}B_{59\text{-}80}$ do not exist. A previous CD study (*178*) using TFE and SDS micelles and the solution NMR study are the only current structural assessment of the C-terminal region of SP-B. Despite the scarcity of literature pertaining to residues 59-80 of SP-B, it is widely believed that many *in vivo* activities of SP-B are fulfilled by the C-terminal end based on *in vitro* studies (*134, 177*).

Interestingly, both N and C-terminal ends of the peptide have been reported to be cationic, amphipathic helices which could serve in a functional role by interacting with anionic lipids, particularly PG headgroups (*11*). Placement of $SP\text{-}B_{59\text{-}80}$ in helical wheels based on standard α-helical geometries as well as a 3_{10} and π helix are shown in Figure 5-1. While solution NMR

measurements indicate, and the helical wheel diagrams depicted in Figure 5-1 assume regular periodicity to the helix, it should be noted that this may not be its exact structural adaptation in a lipid environment. Also, an α-helical conformation leads to unfavorable placement of the charged residues in a lipid milieu

Of particular interest to us, the KL_4 sequence originates from the primary sequence residues 59-80 of SP-B. However, if KL_4 provides an essential function to artificial lung surfactant, as the clinical studies suggest, a significant question that is raised is whether the peptide behaves like SP-B_{59-80} or SP-C. From infrared studies, SP-C was found to be a transmembrane helix that can perfectly span the width of a DPPC bilayer and an FTIR study of KL_4 in lipids yielded similar results (*5, 11, 148*). However, our data described in Chapter 3 show that KL_4 is not transmembrane in DPPC:POPG and POPC:POPG bilayers, and therefore would not orient in the same manner as SP-C.

Nonetheless, a significant question remaining is whether KL_4 and SP-B_{59-80} act similarly, despite clear deviations at the primary amino acid level. One key to answering this is to determine if both peptides orient similarly in model lipid membranes with similar effects on their dynamic properties using ^{2}H and ^{31}P NMR experiments. Additionally, one can compare their effects on lipid phase transitions with DSC. The following studies were undertaken to determine whether the biophysical activity of the native sequence closely followed that of KL_4.

Materials and Methodology

Synthesis of SP-B residues 59-80: SP-B_{59-80}, (sequence from the N to C-terminus: DTLLGRMLPQLVCRLVLRCSMD) was synthesized via solid-phase peptide synthesis by Dr. Alfred Chung at the University of Florida and cleaved from the resin with 90% TFA/5% triisopropyl-silane/5% water and ether precipitated. The cleaved product was purified via a HPLC with C18 Vydac column using a water/acetonitrile gradient with 0.3% TFA

(trifluoroacetic acid). The fractions corresponding to SP-B_{59-80} were collected and purity of the product was verified by mass spectrometry with a mass to charge ratio of (m/z) of 2533.

DSC on 4:1 DPPC(d-62):POPG LUVs with SP-B_{59-80}: DSC measurements were taken on DPPC(d-62):POPG LUVs with varying levels of SP-B_{59-80}. Samples were prepared by drying peptide:lipid complex from chloroform:methanol mixtures at a specific molar ratio, drying and dissolution in cyclohexane. After lyophilization overnight, samples were hydrated with 5mM HEPES buffer pH 7.4 containing 1mM EDTA and 140mM NaCl in a water bath maintained at 50^{o}C. The samples underwent multiple freeze-thaw cycles to facilitate MLV formation and then were extruded through 100nm filters a minimum of 15 times to generate LUVs Each sample was run in triplicate at a temperature range of 10-70^{o}C and a scan rate of 1^{o}C/min.

Solid-state NMR **sample preparation:** Samples for ssNMR were prepared in an identical manner to KL_4 detailed in the Materials section of Chapter 3. Briefly, SP-B_{59-80} peptide was dissolved in MeOH to a stock concentration of 1mM. DPPC(d-62), POPC(d-31), and POPG were purchased from Avanti Polar Lipids (Alabaster, AL) in chloroform solutions and mixed to the desired molar ratios. 4:1 DPPC(d-62):POPG and 3:1 POPC(d-31):POPG solutions were mixed with the peptide in MeOH solution to create a range of samples containing 0-3mol% SP-B_{59-80}. After mixing corresponding amounts of peptide and lipids to the desired molar percentage, the samples were reconstituted by drying peptide/lipid mixture to a film under compressed nitrogen gas, solubilizing them in 2mL cyclohexane and freeze-drying overnight. The next day, approximately 20-30 mg each of dried sample was packed into a standard 5mm NMR tube (Wilmad, Buena NJ) and hydrated with 150-200μL 5mM HEPES buffer pH 7.4, containing 1mM EDTA, and 140mM NaCl. NMR samples were freeze-thawed 3-5 times to

facilitate MLV formation. For samples containing DPPC:POPG, the samples were thawed in a water bath maintained at 50°C.

The ^{31}P NMR data were collected on a 600 MHz Bruker Avance system (Billerica, MA) using a standard 5 mm BBO probe, and 25 kHz proton decoupling during acquisition. Spectra were acquired at 3 temperatures with 1024-2048 scans for each spectrum and a 5 second recycle delay between scans to minimize RF heating of the samples. ^{2}H NMR data were collected on a 600 MHz Bruker Avance System (Billerica, MA) using a standard 5mm BBO probe and quad echo sequence with a B_1 field of 40 kHz. Spectra were acquired at 3 temperatures with 1024-2048 scans and 0.5 second recycle delay. Depaking of ^{31}P and ^{2}H NMR spectra was performed using a Tikhonov regularization method that takes into account macroscopic lipid alignment. This algorithm was provided by Professor Edward Sternin (*103, 124*).

DSC Studies on SP-B_{59-80} with DPPC:POPG LUVs

DSC thermograms for DPPC(d-62):POPG LUVs with varying amounts of SP-B_{59-80} are shown in Figure 5-2. Overall, in a concentration dependant manner, SP-B_{59-80} increases C^{p}_{max} and ΔH_{cal} for the phase transition from the L_β to the L_α state in DPPC:POPG LUVs. In comparison to Figure 3-1, where DSC thermograms performed on similar 4:1 DPPC:POPG LUVs with varying levels of KL_4 indicate domain formation, a clear formation of 2 lipid phases on addition of SP-B_{59-80} is not seen. However, it is evident that SP-B_{59-80} causes an ordering of the lipids by the increased amplitude of the transition seen in the DSC curves. This becomes manifest when comparing ΔH_{cal}, the integration of each DSC peak, for no peptide and with 3% peptide. ΔH_{cal} is approximately 2-3 times greater with 3% SP-B_{59-80} than without any peptide (Table 5-1). The phase transition temperature is not dramatically influenced by SP-B_{59-80}, staying relatively constant at 32°C.

Table 5-1 displays a thermodynamic evaluation of the effects of SP-B_{59-80} on the DPPC(d-62):POPG phase transition. The most interesting and unexpected finding stemming from these DSC studies is that, unlike KL_4, SP-B_{59-80} does not produce phase separation in 4:1 DPPC:POPG. In a concentration dependant manner we see an increase in the enthalpy of the DSC curves upon more addition of peptide. DSC studies on KL_4, at a similar concentration range, show a drop in enthalpy at concentrations where phase separation or domain formation became obvious, which were at 1.5 and 2.2mol%. At 1.5mol% KL_4, the DSC curve bifurcated and was characterized by two T_m values, with one T_m value shifted towards the phase transition of DPPC (Figure 3-1) suggesting lipid sequestration or phase separation by the peptide. No such bifurcation or change in the appearance of the DSC curve occurred with addition of SP-B_{59-80} in similar concentration ranges. The increase in enthalpies (both ΔH_{cal} and ΔH_{vH}) seen as more peptide is added, suggest SP-B_{59-80} orders the lipids and stabilizes the DPPC:POPG L_α state. This is corroborated by the finding that $\Delta H >> \Delta S$ indicating that the phase transition is enthalpic, not entropic in nature. While addition of peptide seems to order the lipids and stabilize a particular state, it has no substantial effect on cooperativity other than at 0.5% of peptide (Table 5-1). We cannot explain the sudden increase in peak-width at half height seen only at 0.5mol% of peptide. However, the broadened lineshapes seen in the DSC curves strongly indicate that the phase transition of the lipids in the presence of SP-B_{59-80} is not a highly cooperative process. However, with the exception of 0.5mol% peptide, SP-B_{59-80} seems to decrease the cooperativity of lipid motions and no phase separation is seen when the peptide is added to 4:1 DPPC:POPG LUVs. This is also verified from DSC calculations that measure indirectly the extent of cooperativity by comparison of the Van Hoft and calorimetric enthalpies where it is seen that their ratio decreases slightly on addition of peptide.

It is known that the addition of monounsaturated lipids markedly reduces the T_m when added to saturated phospholipid dispersions, such as DPPC, thus aiding such mixtures to be more fluid. This is important in lung surfactant because without such molecules, the enriched amount of DPPC in the lungs would cause the monolayer to exist as rigid gel. In our DSC results with SP-B_{59-80}, we see an increase in the energy required for 4:1 DPPC:POPG to shift to any other state or transition. By keeping the thermodynamic barrier high for any such temperature dependant transitions of 4:1 DPPC:POPG it is possible to hypothesize that SP-B_{59-80} is destabilizing the fluidizing properties of the monounsaturated lipids, particularly POPG. This would be beneficial in situations where DPPC needs to be selectively enriched, such as would occur when the alveolar lipid monolayer needs to be compressed. However, the exact implication of ordering of lipids by residues 59-80 of SP-B, as seen by DSC, is complex especially with regard to the complicated lipid environment in the lung as well as in DPPC:POPG. Still unanswered is whether the ordering seen is due to SP-B_{59-80} interacting with DPPC, with POPG, or by stabilizing the mixed state of both species. Since there was no significant shift in phase transition temperature (T_m) of the binary lipid system with SP-B_{59-80}, the exact role of the C-terminus of the peptide in altering lipid biophysics is not easy to interpret based on DSC data.

^{31}P NMR of Lipid MLVs Containing SP-B_{59-80} Show POPG Interacting with the Peptide

Natural abundance phosphorous NMR for 4:1 DPPC:POPG and 3:1 POPC:POPG MLVs with varying levels SP-B_{59-80} were collected to assess the effect of this peptide on lipid phases and headgroup dynamics in comparison to KL_4 (Chapter 3). Shown in Figure 5-3 are ^{31}P NMR spectra for the DPPC(d-62):POPG samples. Only lamellar phases are observed and the resonance for the POPG lipids moves with addition of peptide. Like the experiments with KL_4, macroscopic lipid alignment is seen and the extent of alignment was accounted for by the

dePaking algorithm. As with KL_4, SP-B_{59-80} reduces this macroscopic alignment and generates spectra that are more powder-like in nature. This is apparent by the concentration dependent change in the intensity of the double-singularity seen in the compiled spectra (Figure 5-3). DePaking the series of spectra (Figure 5-4) yields the parallel component of the powder spectra for DPPC and POPG and allows a quantitative measurement of the change in ^{31}P CSAs. Plotting these changes relative to lipids alone reveals that addition of peptide causes a decrease in the POPG ^{31}P CSA by up to 10% but does not affect the DPPC ^{31}P CSA (Figure 5-5). This is similar to behavior seen for DPPC:POPG MLVs on addition of KL_4 and argues strongly for a similar interaction of the two peptides with the anionic POPG headgroups.

The ^{31}P spectra for 3:1 POPC(d-31):POPG MLVs show that a lamellar phase is also observed (Figure 5-6). Although the spectrum at 3% peptide potentially shows the onset of other phase behavior; however, it has not been fully characterized. Examination of the dePaked ^{31}P spectra show that changes in the POPG peak occur upon increasing levels of peptide (Figure 5-7). The dePaked spectra stacked together show that the PC headgroup remains largely invariant while significant ppm shifts are seen in the PG headgroup (Figure 5-8). Interpretation of the dePaked spectrum for the sample with 3mol% SP-B_{59-80} is not straightforward and the shape of the spectrum indicates a drastic change in headgroup dynamics at this specific concentration. As with KL_4, we did not see an inverted H_{II} phase upon addition of peptide. However, at a higher percentage of SP-B_{59-80}, this might be observed. Also, similar to the non-natural peptide analog, there seems to be a preferential electrostatic interaction with the PG headgroup. However, we also see SP-B_{59-80} affecting the dynamics of POPC at higher concentrations, though the physiological amount of SP-B believed to be in the lung is much lower (~0.2mol% relative to the lipids) than the levels where these dynamics are seen by our ^{31}P NMR measurements.

^{2}H NMR Indicates that the Properties of KL_4 are Similar to SP-B_{59-80}.

Deuterium NMR was performed on DPPC(d-62):POPG and POPC(d-31):POPG MLVs with varying levels of SP-B_{59-80} (Figure 5-9) to assess how the peptide affects the acyl chain dynamics in the two lipid systems. If increasing order is seen, then it can be assumed that SP-B_{59-80} penetrates deeply into the lipid bilayer much like the findings reported with KL_4. Time averaged deuterium order parameters $\langle S_{CD} \rangle$, calculated after dePaking (Figure 5-10) and assigning each C-D bond in the acyl chain, show that, just as with KL_4, SP-B_{59-80} increases order in acyl chains of DPPC in 4:1 DPPC(d-62):POPG MLVs (Figure 5-11). These large scale effects in ordering are not equal over the entirety of the acyl chain, which can be seen from the change in order parameter profiles depicted in Figure 5-11; the largest shifts in $\langle S_{CD} \rangle$ are seen from the middle to the end of the acyl chains. Regions corresponding to the plateau region (carbons 2-8) (*145*) have order parameter values changing on the order of 4% even at SP-B_{59-80} levels of 2 mol%. Positions 9-15 show ordering even at 0.1 mol% peptide. In 4:1 DPPC(d-62):POPG MLVs, the largest change in time averaged order parameter $\langle \delta S_{CD} \rangle$ occurs in C-D bonds at positions 10-13 which show increases up to 10% in C-D bonds 10-12, and up to a 15% increase for the C-D bond at position 13. This is seen in both the sn-1 and sn-2 chains of DPPC(d-62) in the context of 4:1 DPPC:POPG MLVs.

Similar experiments were run on 3:1 POPC(d-31):POPG MLVs containing SP-B_{59-80} (Figure 5-12) and dePaked (Figure 5-13) for calculation of order parameters. Looking at the same sn-1 C-D positions 10-13 for POPC(d-31) in 3:1 POPC:POPG, we find that changes in order parameters are negative and the ordering goes down by as much as 13-16%, with a 16% decrease in ordering seen for position 13 (Figure 5-14). This strongly correlates to SP-B_{59-80} having minimal to little interaction with the acyl chains of POPC in 3:1 POPC(d-31):POPG MLVs. Conversely, the peptide displays profound ordering of DPPC(d-62) in 4:1 DPPC(d-

62):POPG MLVs. Since only the middle carbons seem to be ordered on addition of peptide (Figure 5-11), a transmembrane orientation of SP-B_{59-80} is unlikely. If SP-B_{59-80} were indeed transmembrane in any of our lipid systems, we would expect ordering of the plateau carbons as well as the middle and tail ends of acyl chains. This is what is seen for helical transmembrane peptides including the WALP and KALP synthetic peptides (*79, 127*). More intriguing is the finding that, like KL_4, we see that when acyl chains of the PC lipids are deuterated, SP-B_{59-80} causes changes in order of the acyl regions dependent on whether the lipid is saturated or monounsaturated.

The derived order parameters for each acyl chain C-D bond from ^2H NMR spectra seem to contradict literature ^2H data studying the effects of full-length SP-B on DPPG (*d*-62) and DPPC (*d*-62) lipids. These studies concluded that there was little effect of SP-B on the orientational order parameters for perdeuterated acyl chains examined in the liquid crystalline state (*179, 180*). In these papers, it was argued that SP-B perturbation was not localized at a particular depth along the bilayer at concentrations of up to 11% by weight. However, they used concentrated, non-physiological levels of SP-B to determine its effects and orientation in various lipid environments. More recent findings by the same group indicate that full length SP-B can reduce chain order in DPPC(d-62) (*181*) which even further contradicts our ^2H data which shows an ordering of the lipid in the presence of POPG. However, there are several plausible explanations for these discrepancies. It should be noted that in these published works, order parameters are not reported for each carbon along the acyl chain, which correspond to a more discrete, quantitative measure of order derived from the dePaked spectra. Instead, a first spectral moment (M_1) is reported as a function of temperature. While the spectral moment reported is proportional to the overall average orientational order parameter, it does not yield a thorough

analysis of the change in the order at each carbon of the acyl chain, and thus changes at particular positions would be averaged out, or not seen, by such an analysis. It also cannot be discounted that the sample preparation choices may have given rise to these conflicting findings. Although Morrow, *et al*, and our preparations both involve reconstitution from organic solvents, we used substantially lower concentrations of peptide in our experiments, which more closely reflect physiologic levels and prevent aggregation of the peptide. Their findings that SP-B has no effect on acyl chain order in DPPC and DPPG may stem from the amount of SP-B used in these experiments. In one study, concentrations of 6-17 weight percent of full length SP-B were used (*182*). At these levels, protein aggregation is highly possible, especially given the hydrophobicity inherent within the full length protein. Higher order intermolecular complexes such as dimers, tetramers and multimers cannot be ruled out at these concentration ranges used for their NMR experiments. This may explain the little to no perturbation caused by the peptide on DPPC acyl chains. The potential of full-length SP-B at these high, non-physiologic concentrations to form higher order aggregates has not been fully addressed by the authors and any minimal interaction seen with the acyl chain may thus reflect this. In our studies, we are seeing dramatic effects on acyl chain order in DPPC with as little as 0.5mol% of the C-terminal end of the peptide. Aggregation of SP-$B_{59\text{-}80}$ at the levels of peptide we use is unlikely given the concentration dependent effects on lipid ordering and disordering in this range; if aggregation were indeed a concern we would expect minimal perturbation of these chains in a concentration dependant manner. However, we cannot completely reconcile their findings with ours since our studies used SP-$B_{59\text{-}80}$ in binary lipid systems mimicking the lung and Morrow, *et al* used full length protein SP-B in neat lipid systems. Also, we cannot rule out the regulation of activity by the C-terminal end of SP-B by the full length protein; it also provides evidence that SP-B is

sensitive in its function to the lipids it is in complex with. Thus, our studies as well as those of Morrow *et al*, and numerous others clearly underscore the vital notion that membrane protein form and function is highly contingent on the lipid environment used to study it.

Evidence of Alternative Dynamics at High Concentrations of SP-B_{59-80}?

In 3:1 POPC(d-31):POPG vesicles, the deuterium NMR order parameters decrease in a concentration dependent manner (Figure 5-14). The downward sloping $<\delta S_{CD}>$ values seen in Figure 5-14 are similar to the trends found for KL_4. However, the changes seen with SP-B_{59-80} are larger. In conjunction with ^{31}P NMR, these findings indicate that the SP-B_{59-80} is clearly stationed at the headgroup region of these lipids. However, at the highest concentration used in these studies, we found a clear deviation in the typical powder spectrum in 3:1 POPC(d-31):POPG. With 3mol% SP-B_{59-80} complexed to 3:1 POPC(d-31):POPG, the ^{2}H NMR spectrum shows a large coalesced peak in the center of the spectrum (Figure 5-12). The dePaked spectra for 3:1 POPC(d-31):POPG MLVs are shown in Figure 5-13, and while all spectra were readily dePaked, the spectrum taken with 3% SP-B_{59-80} has less definition. The ^{31}P NMR spectrum for the sample with this concentration of peptide also resulted in a poor quality dePaked spectrum that was uninterpretable (Figure 5-7). One possibility emerging from the ^{2}H NMR and ^{31}P NMR data is that at 3mol% SP-B_{59-80}, the formation of a second, non-bilayer lipid phase is occurring. This averaging seen at this peptide concentration is due to additional fast motions of the lipid acyl chains which could occur in a non-lamellar phase, such as an inverted H_{II} phase, addressed briefly in Chapter 2 or due the formation of small vesicles which tumble quickly on the NMR timescale.

These results indicate that higher concentrations of SP-B_{59-80}, the dynamics and motion of the acyl chain are significantly affected. Not only is the finding shown in Figure 5-12 a possible indicator of an inverted H_{II} phase, but it may also implicate SP-B_{59-80} in lipid shuttling, lysis or

degradation. Lipid lysis and degradation has been reported to be one of the putative functions attributed to SP-B that could be necessary for effective surfactant recycling and remediation. Some reports implicate SP-B in anti-microbial function which could help explain and corroborate the striking dynamics seen here, which should be of no surprise since SP-B is classified into the saposin family of proteins (*23, 30, 33, 71*). However, further studies are needed to differentiate between a role for SP-B_{59-80} in lipid degradation or alternative phase formation. Surprisingly, we only saw this effect in 3:1 POPC(d-31):POPG, and not in DPPC(d-62):POPG at 3 mol% SP-B_{59-80}. If the above finding is indeed reproducible, it would represent an exciting discovery of an activity for SP-B_{59-80} that can discriminate based on saturation level of the acyl chain.

Comparisons of SP-B_{59-80} and KL_4

Even though the sequence of KL_4 is based on SP-B_{59-80}, there are some differences seen from our data. First, the most striking difference is seen in the DSC data. In the same concentration ranges, SP-B_{59-80} does not seem to influence the phase properties of DPPC(d-62):POPG as markedly as KL_4. While SP-B_{59-80} clearly affects the thermodynamic properties of these LUVs, we saw clear affects of KL_4 in the lipid miscibility and overall mixing properties in DPPC(d-62):POPG LUVs and MLVs. Our data showed that during the initial stages of lipid sequestration, KL_4 lowered the C_p^{max} and ΔH_{cal} of the peptide-lipid system, seen at 1.5 and 2.2mol% peptide in MLVs. Clear phase separation was also seen with KL_4 added to 4:1 DPPC(d-62):POPG LUVs (Figure 3-1). SP-B_{59-80} does not cause similar behavior. ^{31}P and ^{2}H static NMR data show that KL_4 and SP-B_{59-80} behave similarly in 4:1 DPPC(d-62):POPG lipid environments. ^{31}P NMR data show that, after dePaking, very little change occurs in DPPC parallel edge frequency, while some modest changes occur in POPG parallel edge frequency. While an interaction of SP-B_{59-80} with anionic PG headgroup occurs is

seen, the placement of lysines in KL_4 could allow for a more enhanced interaction with PG than with SP-B_{59-80}, which does not possess the distinct charge periodicity found in KL_4 and whose peptide sequence contains negative charges as well. The most striking changes seen on addition of either peptide is in deuterium order parameters which indicate significant changes in the middle to the tail end of the acyl chain corresponding to carbons 8-15. Increases in ordering of these regions while a lack of ordering in the carbons 2-8 were seen on addition of both peptides to DPPC:POPG MLVs. These findings discount a transmembrane orientation of either peptide and predispose them to adapting a more peripheral orientation. In this regard, our observations implicate KL_4 and SP-B_{59-80} to orient similarly in DPPC(d-62):POPG lipid environments.

The ^2H NMR data also show the KL_4 and SP-B_{59-80} behave similarly in 3:1 POPC(d-31):POPG MLVs up to a concentration range of 3mol%. The substantial decrease in time averaged order parameters indicate very little effect on the motional freedom of the POPC sn-1 acyl chains mediated by both KL_4 and SP-B_{59-80}. In 3 mol% peptide, SP-B_{59-80} seems to facilitate additional lipid dynamics which needs to be addressed for reproducibility by ^{31}P and ^2H NMR. If indeed the observations at 3 mol% are valid, SP-B_{59-80} changes the dynamics of lipid systems based on the saturation of the PC acyl chains. This was seen with KL_4 as well, however, the possibility of peptide-mediated change in lipid properties at high molar percentages of SP-B_{59-80} is a novel distinguishing feature relative to KL_4.

Static ^{31}P NMR data reveal that in 4:1 DPPC:POPG MLVs, both SP-B_{59-80} and KL_4 interact with the PG headgroup. Both peptides displayed no predilection for an inverted H_{II} phase though as-of-yet uncharacterized dynamics were seen at 3 mol% SP-B_{59-80}. In KL_4, we reconciled interaction with DPPC acyl chains and the POPG headgroup with domain formation that stemmed from our DSC studies with the peptide. However, since we did not see any phase

separation from our DSC studies with SP-B_{59-80}, we have no data correlating SP-B_{59-80} interacting with DPPC acyl chains at the same time interacting with the PG headgroup. One way to reconcile these findings is to conduct experiments with deuterated PG acyl chains, *i.e* 4:1 DPPC:POPG(d-31) and 3:1 POPC:POPG(d-31). If the deuterium order parameters for each C-D bond increase, clearly the peptide is buried deep within the bilayer of the two lipids. If the $<S_{CD}>$ values decrease, then a more complicated molecular picture must be occurring whereby the peptide somehow is buried with DPPC without facilitating de-mixing of the lipids. While KL_4 has proven to be a clinically functional and potent peptide for replacing SP-B in treating respiratory distress and conventional lung surfactant formulations contain SP-B in full form, no formulation currently used contains either the N or C-terminal peptide as a substitute for SP-B. This raises the possibility that while SP-B_{59-80} and KL_4 may have similar structural topologies in lipid environments, KL_4 may have additional functions that SP-B_{59-80} lacks due to the flexibility imparted by using only leucines and lysines in the peptide.

Preliminary Molecular Model of SP-B59-80 with Lipids

With ^{31}P NMR data looking at headgroup dynamics and ^{2}H NMR data examining acyl chain ordering, a low resolution molecular picture of SP-B_{59-80} interacting with lipid systems can be hypothesized derived from NMR spectroscopy and DSC. It should be noted the following model contains the important assumption that SP-B_{59-80} is helical in a lipid environment. This estimation is valid given the findings in the literature pertaining to the helical nature of SP-B particularly at the C-terminal region; models describing this region as being helical are well documented in the literature (*87, 133, 134, 177*). However, as seen with KL_4, the type of helix and the derived torsion angles may be non-canonical and deviate from those seen for an *i, i+4* helix. To answer the question of the type of helix SP-B forms in a lipid environment, MAS NMR experiments on ^{13}C labeled peptide in complex with lipids need to be performed in

conjunction with the DQ-DRAWS pulse sequence. The laboratory of Professor Joanna Long is currently testing various conditions for the expression of SP-B_{59-80} in a DNA vector for production by *E. coli* using recombinant molecular biology techniques. Once optimal conditions for expression are found, bacteria expressing the construct can be grown in isotopically enriched ^{13}C medium for incorporation into the growing polypeptide chain for NMR experiments

With the assumption that SP-B_{59-80} is helical in lipid systems, Figure 5-15 displays a preliminary orientation of the peptide in lipid environment. It is important to realize that the following model is theoretical and is only used to display the presumed orientation of the peptide based on ^{2}H and ^{31}P NMR data. Since we saw an increase in ordering in 4:1 DPPC:POPG, we assume the peptide buries in DPPC acyl chains. In 3:1 POPC:POPG, the disordering in the acyl chains and increased ordering of the headgroup region indicates that the peptide is peripheral in this lipid system. Unlike KL_4, which had its leucine content buried in a hydrophobic environment, we predict that the acidic aspartic acid residues in SP-B_{59-80} point toward the aqueous interface away from the phosphate headgroups. With the valid assumption of helicity for SP-B_{59-80}, we predict that the peptide is more peripheral in POPC:POPG than KL_4.

The results of SP-B_{59-80} in DPPC:POPG may indicate snorkeling, which we postulated occurs for KL_4. The snorkeling hypothesis as predicted for KL_4 appears valid given it's periodicity in primary amino acid sequence. However, despite the periodic charge distribution inherent in SP-B_{59-80}, we cannot account for snorkeling for the peptide unless we assume that the long chain of aspartic acid, glutamine, and arginine extend to the interface to interact with the phosphate headgroup. As of this moment, more experiments are needed utilizing NMR and EPR on ^{13}C labeled and spin labeled peptide in complex with lipid. This will yield more accurate information in terms of orientation and depth penetration of the peptide.

.

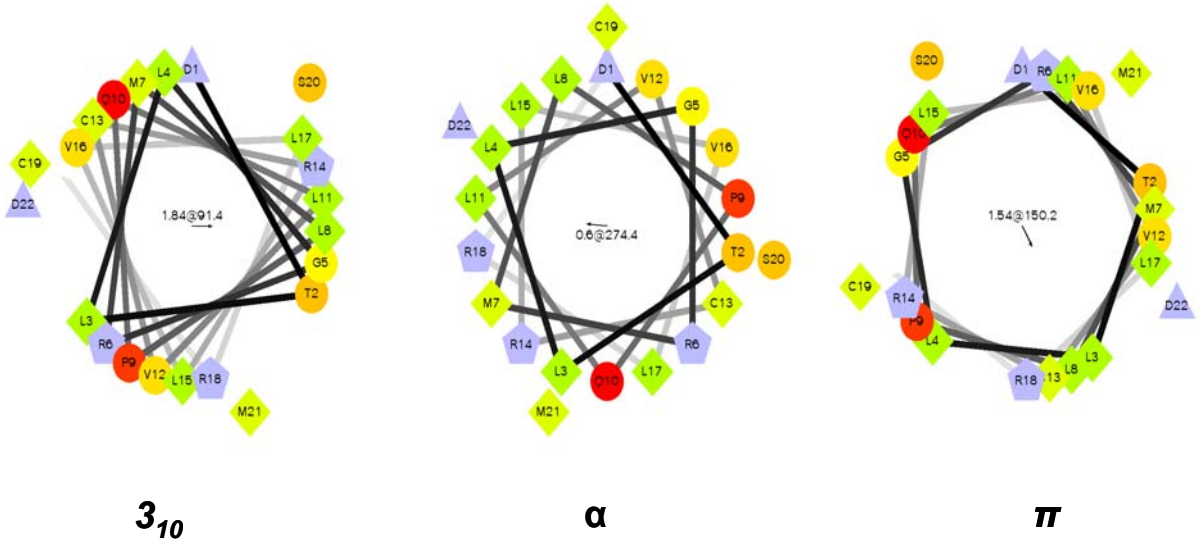

Figure 5-1 Putative helical wheel for each type of helix rendered for the C-terminal residues 59-80 of SP-B.

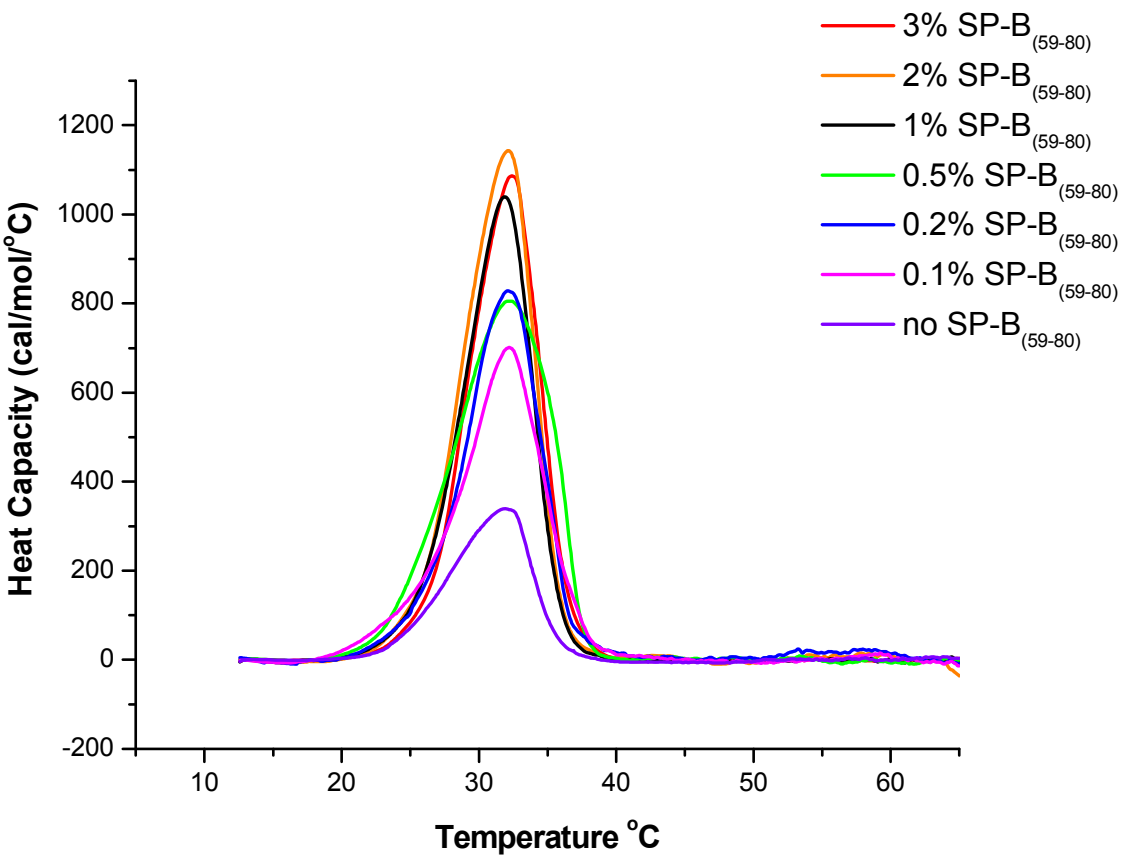

Figure 5-2. DSC thermograms of 4:1 DPPC:POPG LUVs with varying molar percentages of residues SP-B_{59-80}.

Table 5-1 Thermodynamic parameters derived from DSC on residues on 4:1 DPPC (d-62):POPG LUVs with SP-B_{59-80}.

%SP-B (59-80)	T_m (^oC)	ΔH_{cal} (kcal/mol)	ΔH_{vH} (energy/mol)	ΔS (cal/mol/K)	$\Delta T_{1/2}$	CU*	C_p^{max} kcal/mol/^oC
no SP-B(59-80)	32.1 ± 0.4	2.50 ± 0.04	102 ± 6	8.1± 0.1	6.7 ± 0.4	39 ± 2	0.34 ± 0.02
0.1%	32.6 ± 0.3	5.5 ± 1.2	98 ± 13	17.9 ± 3.9	6.6 ± 1.4	18 ± 6	0.70 ± 0.06
0.2%	32.8 ± 0.3	5.9 ±1.3	106 ± 6	19.2 ± 4.4	6.3 ± 0.7	19 ± 4	0.8 ± 0.2
0.5%	32.44 ± 0.03	7.1 ±0.3	84 ± 2.6	23.2 ± 1.1	8.6 ± 0.3	12 ± 1	0.80 ± 0.02
1%	32.0 ± 0.2	6.7± 0.2	117 ± 3	21.6 ± 0.7	5.8 ± 0.1	18 ± 1	1.042 ± 0.008
2%	32.32 ± 0.06	7.5 ± 0.6	123 ± 26	24.4 ± 2.1	6.1 ± 0.1	17 ± 5	1.2 ± 0.2
3%	32.44 ± 0.03	7.01 ± 0.07	137 ± 29	23.0 ± 0.2	6.0 ± 0.3	20 ± 4	1.3 ± 0.3

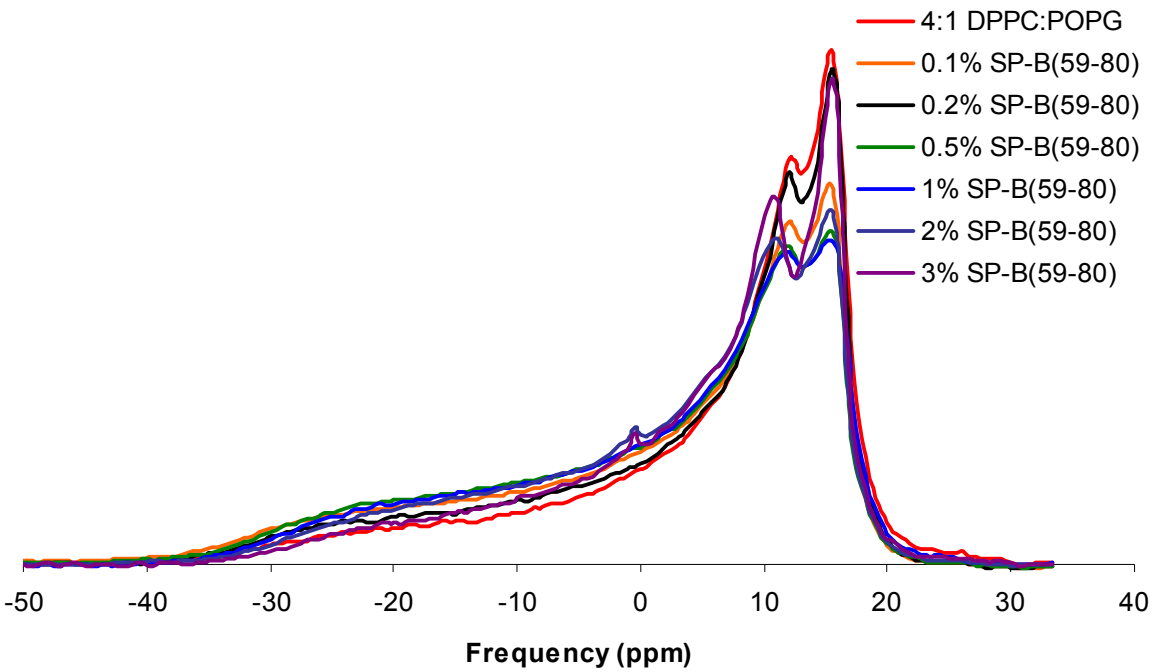

Figure 5-3. 31P NMR data of 4:1 DPPC:POPG MLVs with varying molar percentages of SP-B59-80

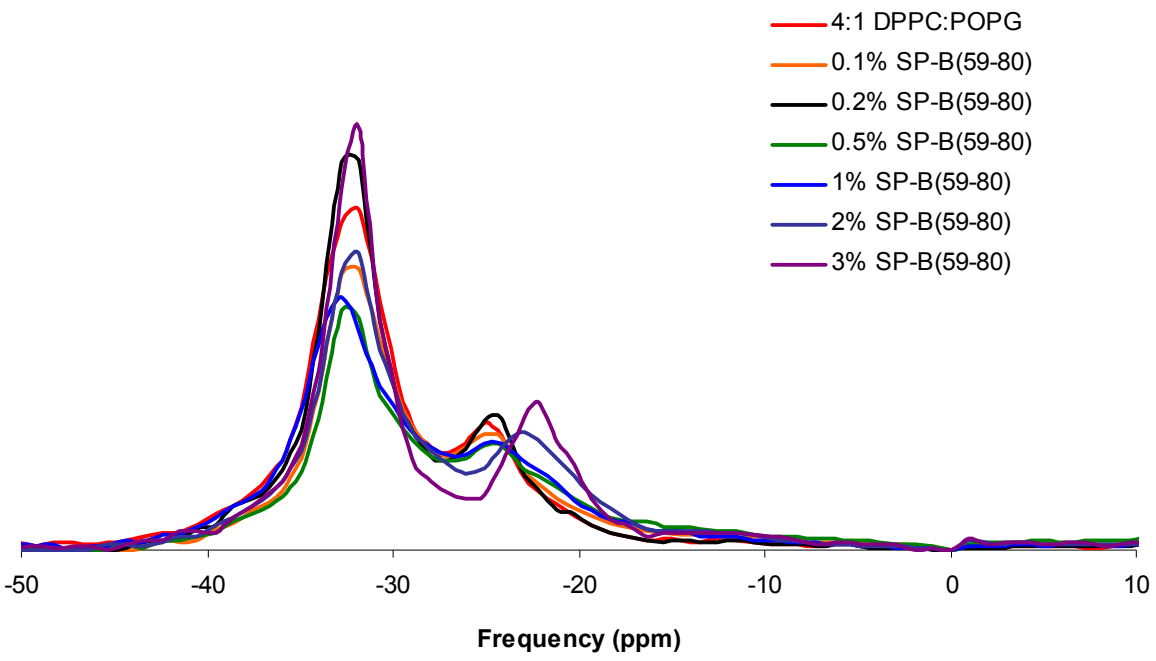

Figure 5-4. DePaked ^{31}P NMR data of 4:1 DPPC:POPG MLVs with varying molar percentages of SP-B_{59-80}

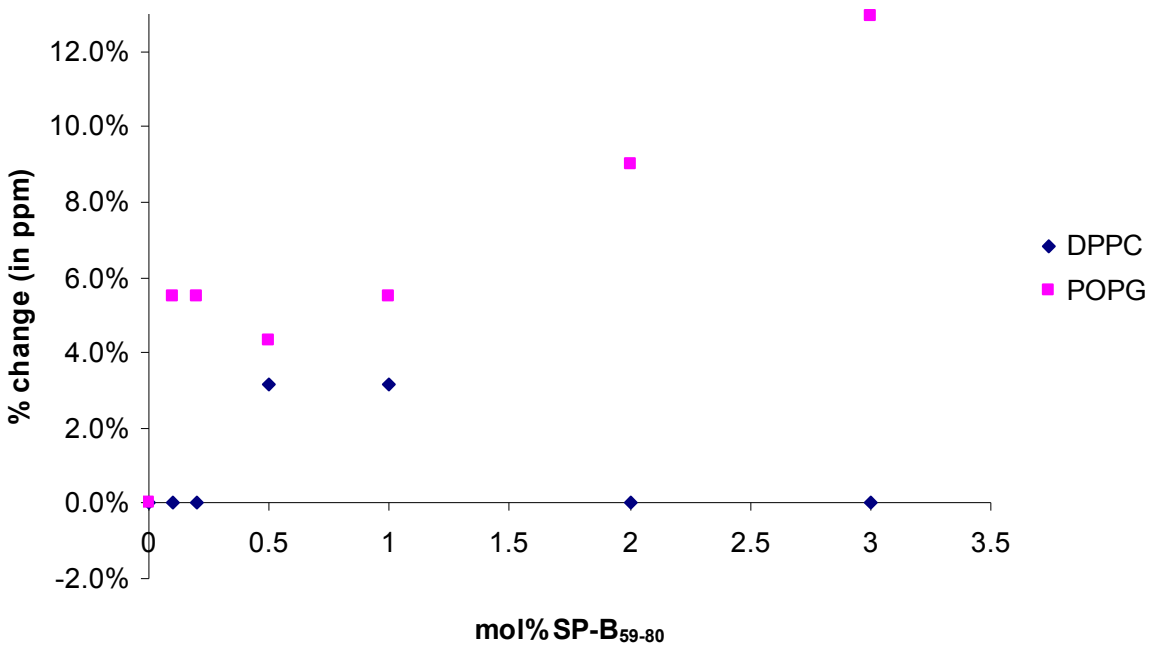

Figure 5-5. Change in ^{31}P CSAs for 4:1 DPPC:POPG MLVs as a result of increasing molar percentages of SP-B_{59-80}

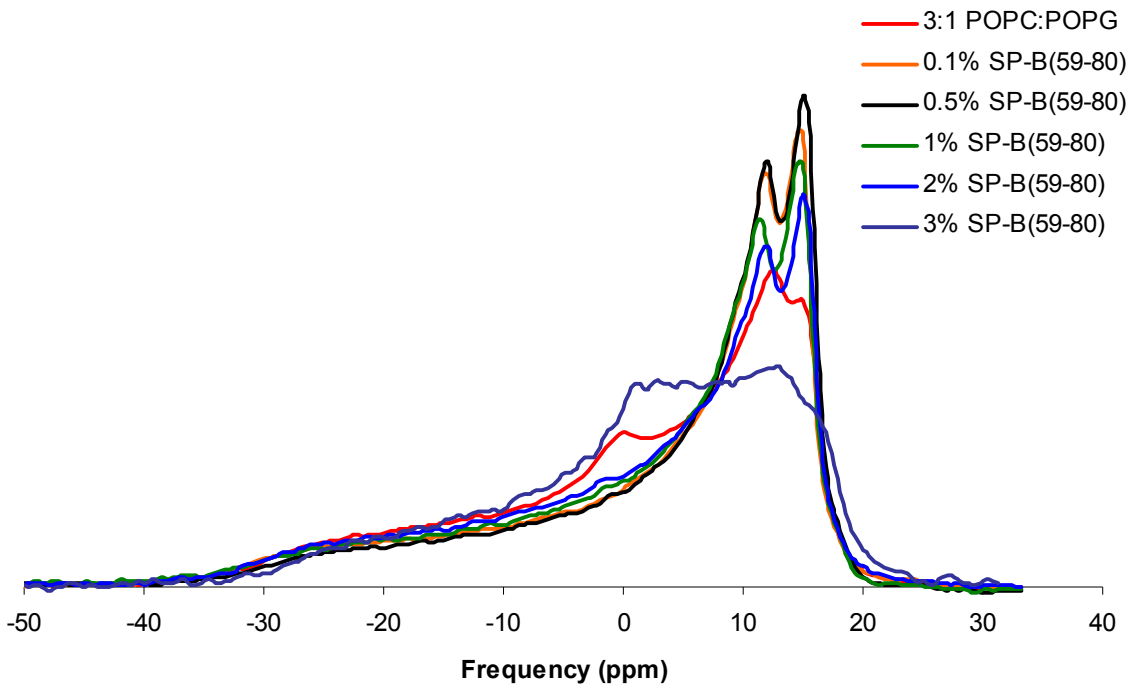

Figure 5-6. Phosphorous NMR data of 3:1 POPC:POPG MLVs with varying molar percentages of SP-B_{59-80}

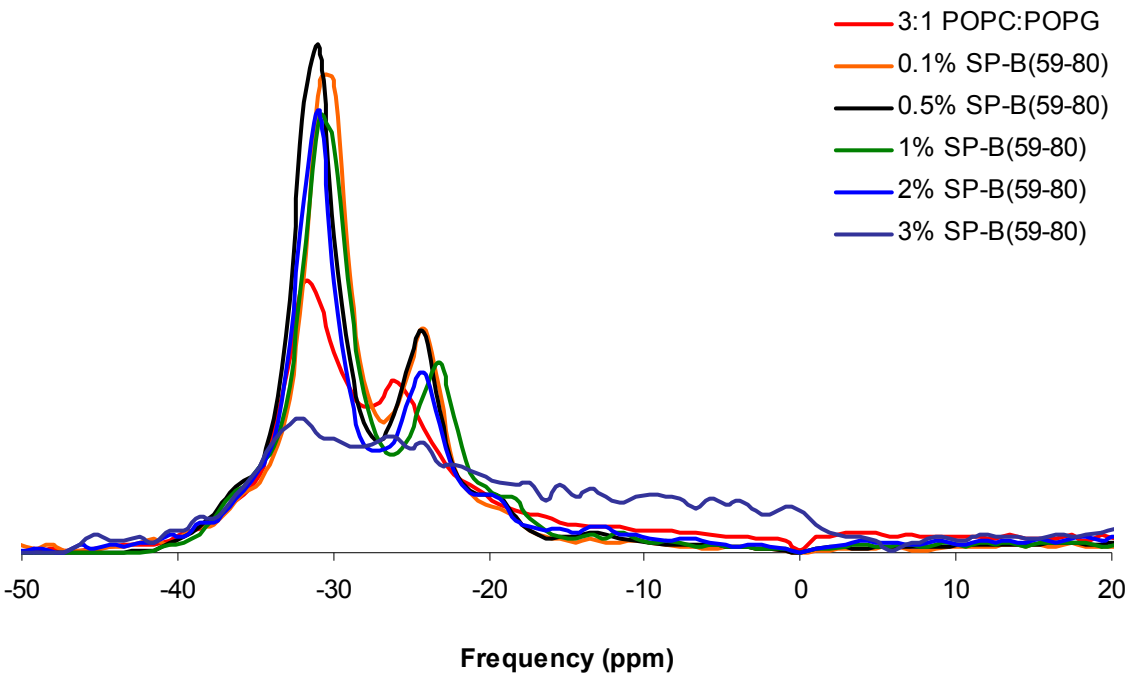

Figure 5-7. DePaked 31PNMR data of 3:1 POPC:POPG MLVs with varying molar percentages of SP-B59-80

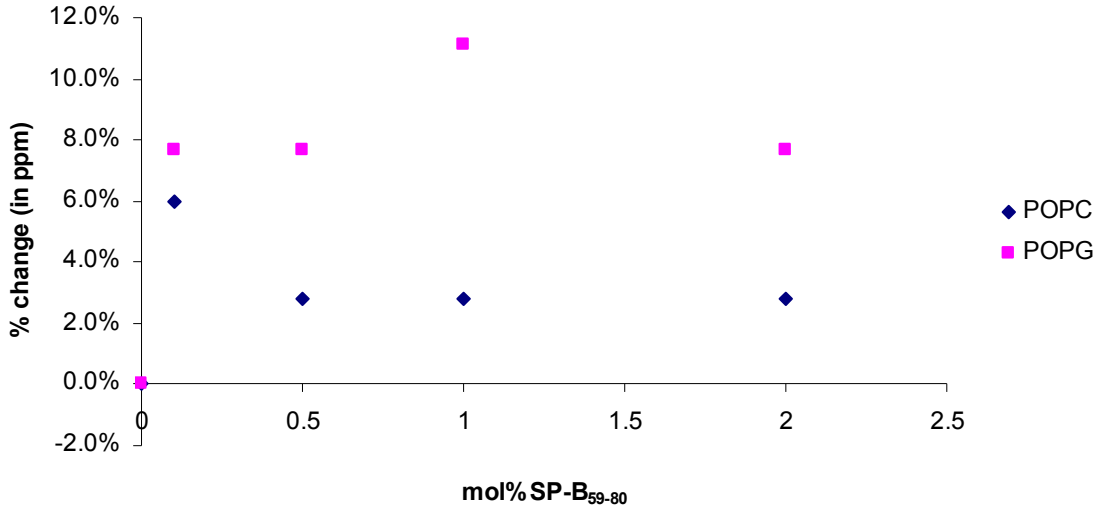

Figure 5-8. Change in ^{31}P CSAs for 3:1 POPC:POPG MLVs as a result of increasing molar percentages of SP-B_{59-80}

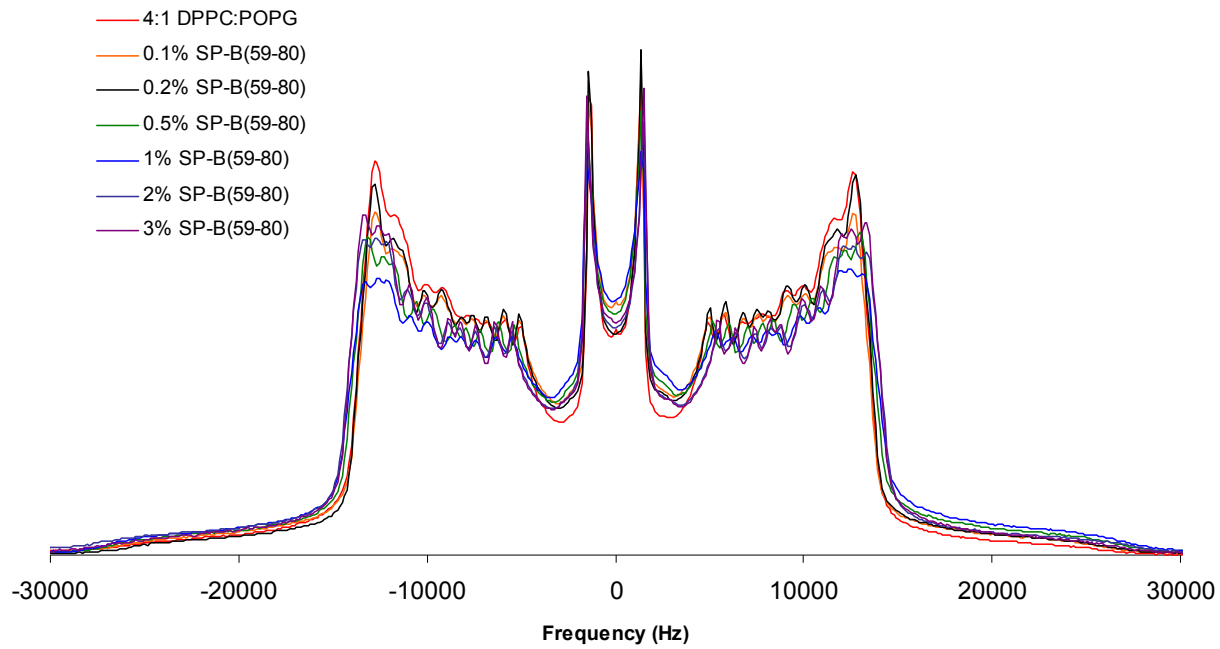

Figure 5-9. Deuterium NMR spectra of 4:1 DPPC(d-62):POPG MLVs with SP-B59-80.

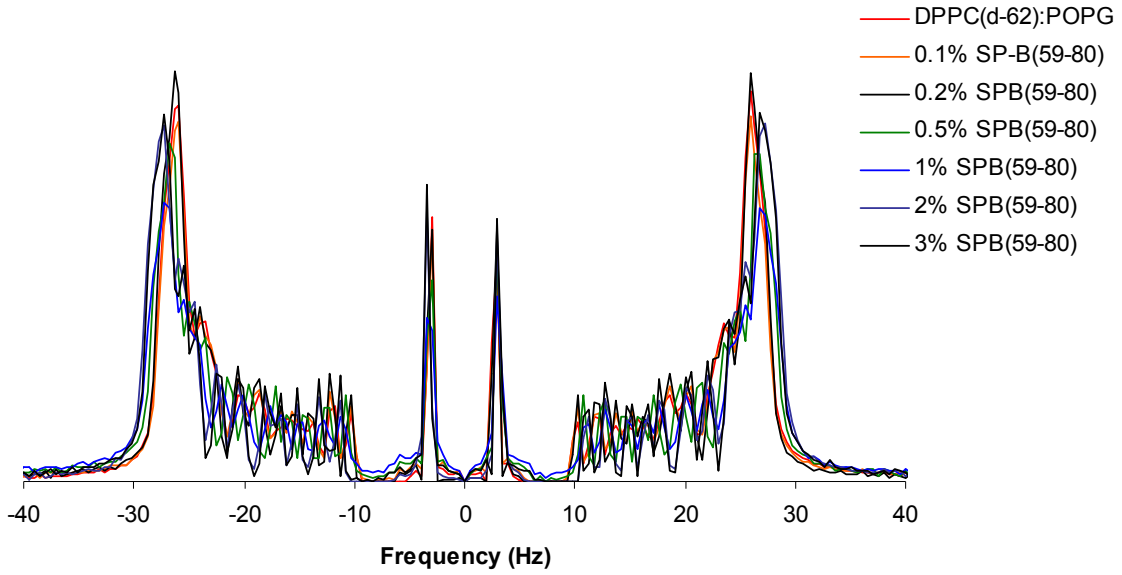

Figure 5-10. Stacked dePaked spectra of 4:1 DPPC(d-62):POPG MLVs with SP-B_{59-80}.

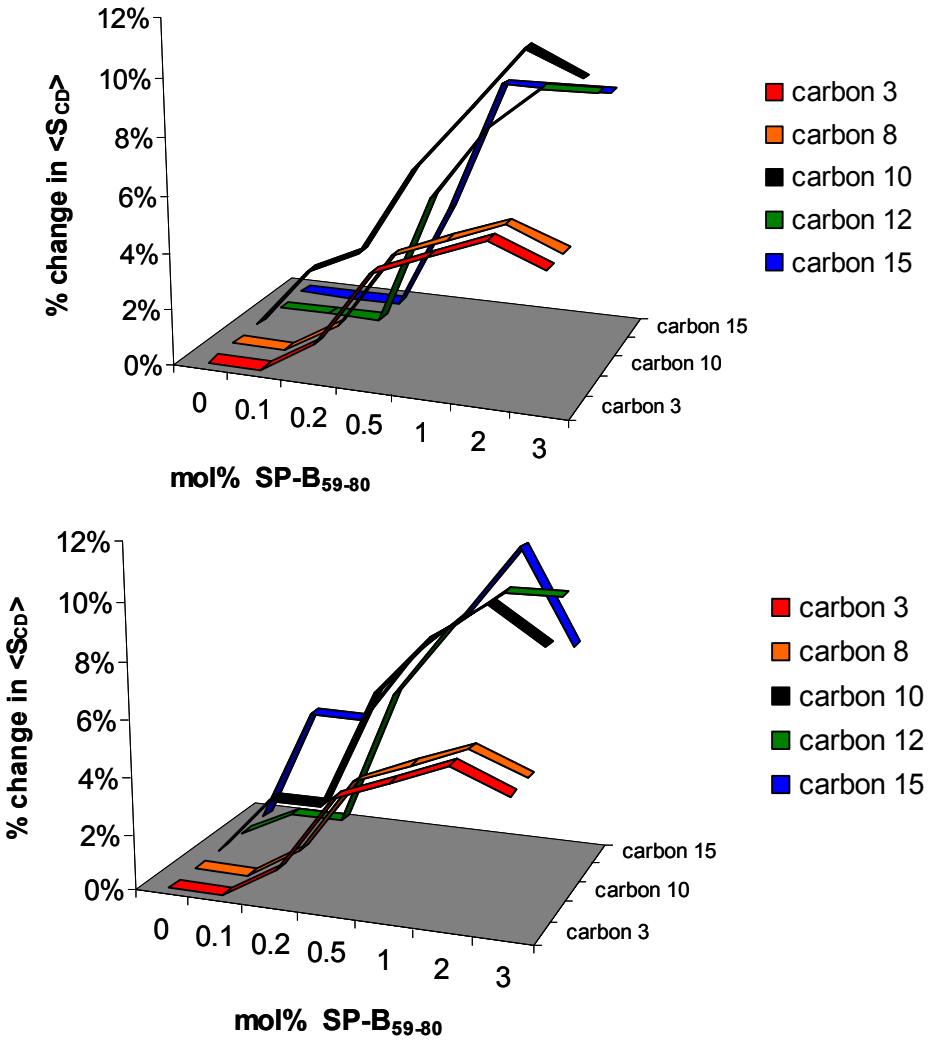

Figure 5-11. Percent change in time averaged order parameter $<\delta S_{CD}>$ for DPPC (d-62) in 4:1 DPPC(d-62):POPG MLVs on addition of SP-B_{59-80}. Top: change shown in the sn-1 and Bottom: the sn-2 chain.

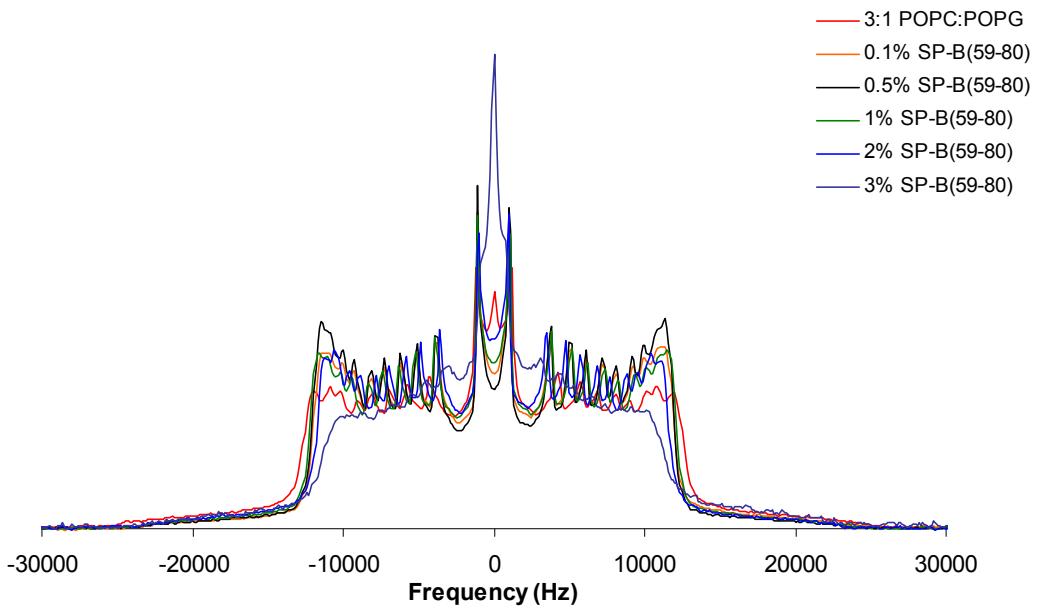

Figure 5-12. ^{2}H NMR spectra of 3:1 POPC(d-31):POPG MLVs with SP-B_{59-80}.

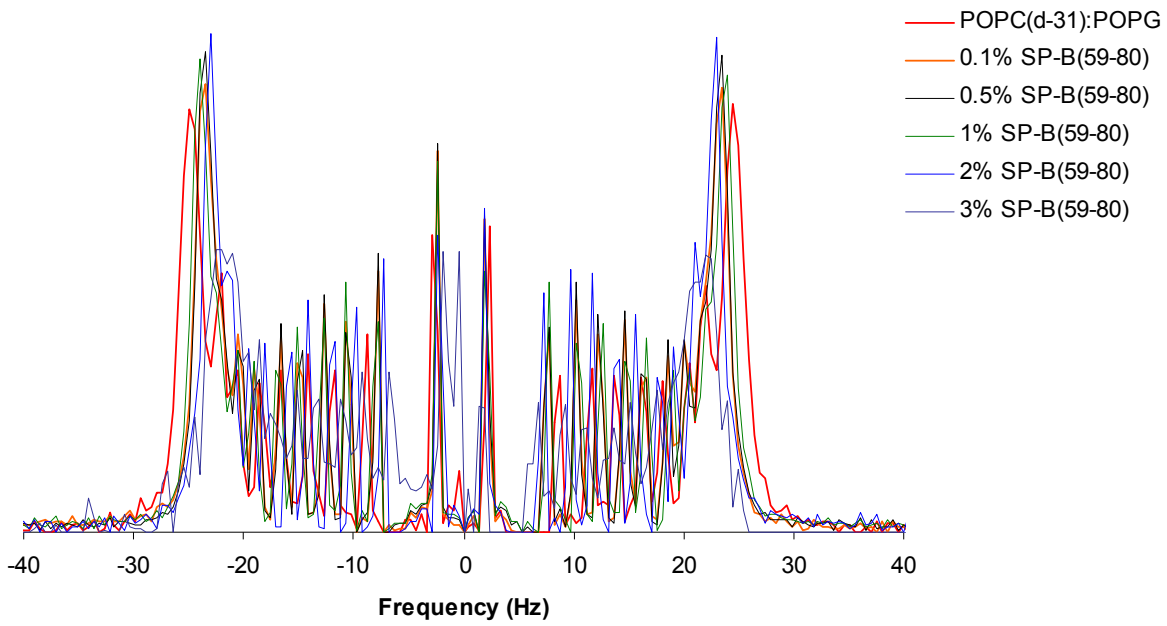

Figure 5-13. Stacked dePaked spectra of 3:1 POPC(d-31):POPG MLVs with SP-B_{59-80}.

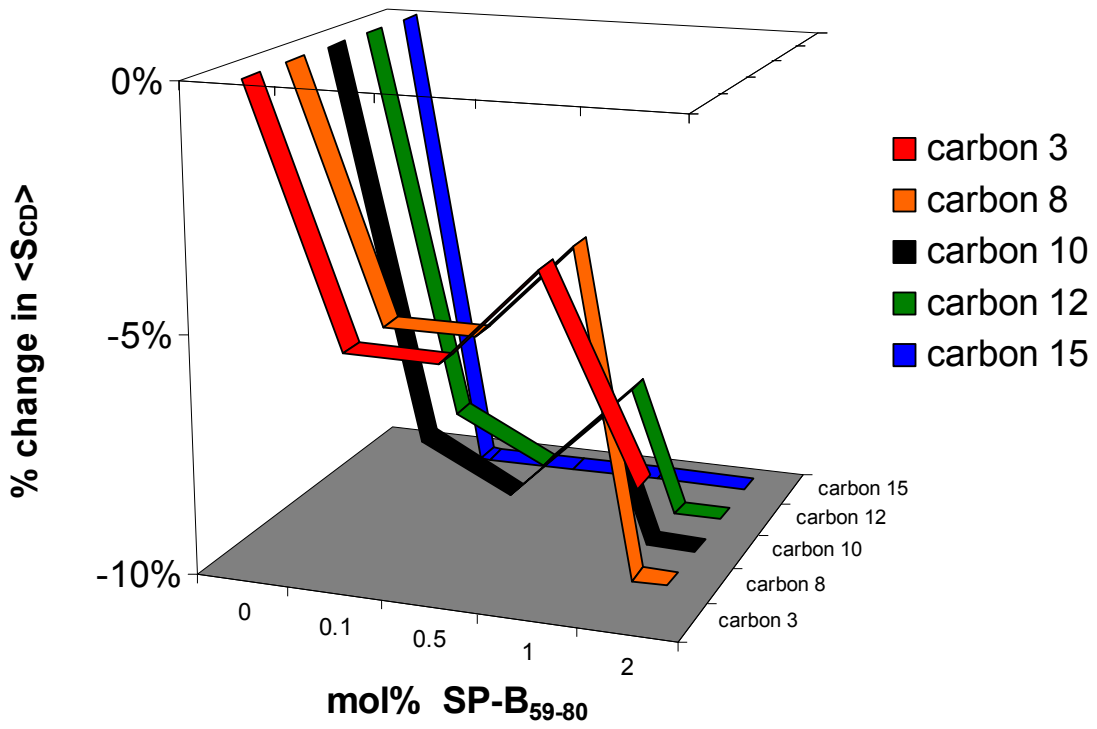

Figure 5-14. Percent change in time averaged order parameter <δSCD> for POPC (d-31) in 3:1 POPC(d-31):POPG MLVs on addition of SP-B59-80. Shown is the change in the sn-1 chain.

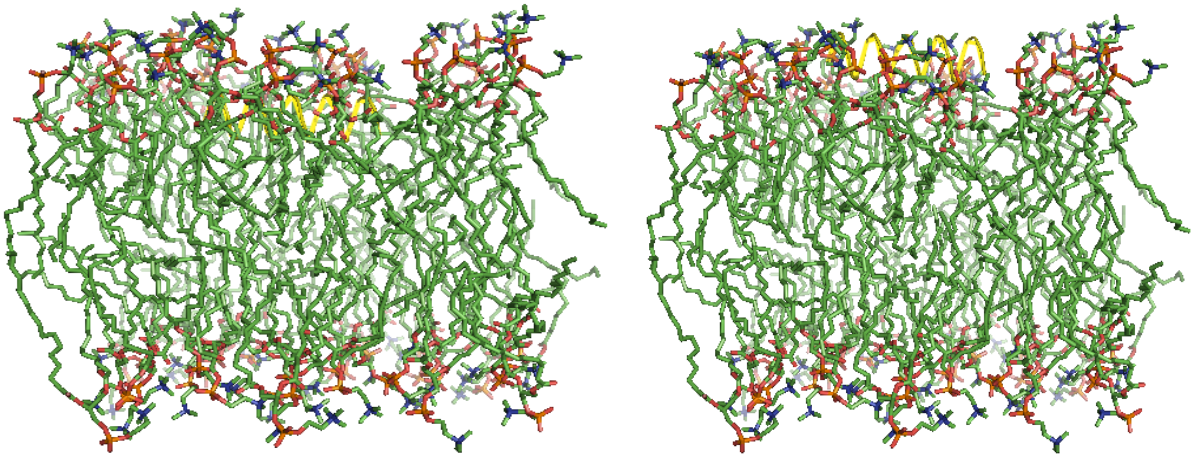

DPPC:POPG POPC:POPG

Figure 5-15. Hypothesized orientational model of SP-B_{59-80} in two different lipid MLV systems. SP-B_{59-80} is assumed helical based on previous literature findings and is shown as a yellow ribbon. The following models are preliminary and are based on ^{2}H and ^{31}P solid state NMR spectroscopy results.

CHAPTER 6
CONCLUSIONS AND FUTURE EXPERIMENTS

Our data argue that KL_4 has a different binding orientation in 3:1 POPC:POPG and 4:1 DPPC:POPG lipid systems. Deuterium NMR is a powerful tool to study the dynamics of the lipid acyl chains based on the quadrupole splittings and the orientational order parameters calculated therefrom. From these data, it is clear that KL_4 has a perturbing effect on DPPC(d-62):POPG. The addition of KL_4 increases the ordering of the acyl chains near the middle and the tail ends indicating that it is these regions of the fatty acyl chains undergoing the most interaction with KL_4. KL_4 is modeled after the last 21 amino acids of SP-B, particularly residues 59-80, in terms of hydrophilic and hydrophobic distribution of residues. Preliminary measurements done in our lab on SP-B_{59-80} have shown that in DPPC(d-62):POPG, a similar increase in order parameters is seen upon addition of peptide. It is believed that both KL_4 and SP-B_{59-80} lodge similarly in DPPC(d-62):POPG lipids. When the POPG sn-1 acyl chain is deuterated, we find that KL_4 decreases the order parameters for both DPPC:POPG and POPC:POPG lipid systems, arguing for very little interaction with the PG acyl chains. In conjunction with the deuterated DPPC data, a possible scenario can be envisioned of phase separation, with KL_4 "snorkeling" with the DPPC acyl chains, and interacting with the phosphate headgroups of POPG. The DSC data strongly argue for the case of lipid phase separation at concentration ranges of 1.5 mol%---such a concentration reported here is dependent on DSC sample preparation.

While the orientation of these peptides may be the same, the question then becomes, what is that orientation? For KL_4, a transmembrane orientation has been proposed based on FT-IR data, but the preparation of the sample warrants some doubt. In those experiments, KL_4 was dried with 7:3 DPPC:DPPG bilayers in non-physiological amounts. The transmembrane

orientation hypothesis contradicts many previous reports that postulated that the evenly spaced charged lysine residues can ionically interact with the phosphate headgroup, thus imparting a more peripheral orientation to the peptide. A second study using IR absorption spectroscopy showed the peptide adapting an anti-parallel beta sheet structure in DPPC/DPPG bilayers while being alpha-helical in DPPC. That work did predict KL_4 to be neither transmembrane nor helical. In light of these findings, our data show KL_4 being helical by circular dichroism, at concentration ranges that negate the effect of potential aggregation. Solid state NMR experiments taken in conjunction with Professor Joanna Long and Dr. Doug Elliott on $^{13}C'$ labeled KL_4 were performed in POPC:POPG and DPPC:POPG lipids. $^{13}C'$-$^{13}C'$ distances and torsion angle measurements show KL_4 to be helical albeit in a non-canonical form as mentioned in Chapter 4. Using DQ-DRAWS, the peptide displayed torsion angles (φ=-105, ψ=-26) that were helical but had the lysines partially aligned along one side of the helix. Similar experiments of $^{13}C'$ labeled KL_4 in DPPC:POPG show that the peptide follows a more π-helical fold with the lysines fully aligned along one face of the helix. In our final model depicted in Chapter 3 and in the submitted manuscript, we model KL_4 as a helix in both DPPC:POPG and POPC:POPG lipids based on the input of the torsion angles generated into the molecular graphics program PYMOL. In light of the data borne out from DSC, and solid-state NMR experiments, it seems that the preferred orientation of KL_4 in 4:1 DPPC:POPG bilayers is to be buried within the bilayer beneath the headgroups. This represents a unique binding orientation of the peptide in lipid compositions modeled after the lung. In model 3:1 POPC:POPG MLVs, we can state with some degree of confidence that KL_4 is bound peripherally to this lipid system at a shallower depth.

^{31}P solid state NMR on static peptide-lipid samples show the peptide decreasing spontaneous macroscopic orientation of the lipids, giving rise to more spherical shapes of the

MLVs. This was found in both lipid systems. As an unintended byproduct of samples run at 14.1Tesla field strength, lipid samples exhibited spontaneous alignment, leading to a loss of the parallel edge of the powder pattern. At a macroscopic level, this can be depicted as normal spherical liposomes being deformed into ellipsoidal shaped vesicles. As part of Professor Edward Sternin's dePaking algorithm, a parameter that reports the extent of orientation caused by magnetic field alignment is reported. Adding KL_4 primarily decreases this parameter indicating the peptide affects the macroscopic ordering of lipids and converting ellipsoidal deformed liposomes into spherical ones. Conversion of an ellipsoidal form of liposomes, as mediated by KL_4, to spherical ones may help in potentiating surface tension but this hypothesis remains to be tested.

The interesting aspect of this work is what KL_4 is doing in the lung. The snorkeling hypothesis presented shows two seemingly conflicting points arising from the NMR data—interaction with POPG headgroup and interaction with DPPC acyl chains at the interfacial region of the tail. One way to reconcile these two results stemming from the ^{31}P and ^{2}H NMR data is phase separation or lipid sequestration. This is seen in the DSC data on DPPC:POPG vesicles, regardless of the method of sample preparation. With phase separation, we envisage a scenario where one population of the peptide can sequester DPPC into a microdomain (of size which cannot be determined from these experiments) and at the same time a second population of the peptide can be interacting with the phosphates of POPG in a POPG-rich domain.

Similar ^{31}P and ^{2}H studies were also performed on SP-B_{59-80}, the native sequence after which KL_4 is modeled, to see if the two peptides orient similarly. Our data show that SP-B_{59-80} presence increases acyl chain ordering in DPPC(d-62):POPG while decreasing it in POPC(d-31):POPG. Similar to KL_4, the ordering or disordering of the acyl chains is dependant on the

saturation status of the phospholipids. ^{31}P NMR data also show SP-$B_{59\text{-}80}$ interacting with PG headgroups as was seen for KL_4. Despite these similarities seen from ssNMR spectroscopy, DSC measurements at increasing levels of SP-$B_{59\text{-}80}$ show no indication of phase separation. This finding implies that the way the two peptides partition between the lipids is different. Hence, SP-$B_{59\text{-}80}$ seems to orient similarly to KL_4 but conveys a different biophysical function to the lipid systems studied in this dissertation.

It was hoped that an inverted H_{II} phase would be seen in our data when KL_4 was added to both our lipid systems. Such a phase can clearly be characterized by ^{31}P NMR and a lipid polymorphism of that arrangement was believed to be important for lung surfactant functioning. Though we did not see such a lipid geometry in both our lipid systems, we believe that snorkeling of KL_4 in DPPC:POPG can induce a curvature strain on the lipids that can make these lipids more prone to alternative geometries (like an inverted H_{II} phase). However, because we did not see an inverted H_{II} phase, we can only speculate that this could be one advantage of lysine snorkeling. Of interesting note, our findings show that at 3mol% SP-$B_{59\text{-}80}$ a potential alternative lipid phase was seen in 3:1 POPC(d-31):POPG lipids but not in 4:1 DPPC(d-62):POPG lipids. This discovery needs to be further investigated to see if indeed the peptide facilitates a concentration dependant change in the geometry that is sensitive to the level of saturation of the lipid chain.

The spectroscopy and calorimetry experiments delineated above were performed on simple binary lipid systems of defined molar ratio. Obviously, lung surfactant is much more heterogeneous than just DPPC and POPG, and a whole host of other minor constituents exist which even include di- and tri-unsaturated fatty acids. Future experiments should involve addition of more layers of complexity to lung surfactant that typify what is found endogenously.

Such experiments have been performed on more native bovine lung surfactant extracts which have been spiked with DPPC(d-62) to measure effect of albumin on phase separation and lipid dynamics (*183*). The studies presented here can also be performed with the addition of palmitic acid to our DPPC:POPG lipid mix to more closely simulate the clinical version marketed by Discovery Labs and Tanaka's original work (*18*). Finally, the studies presented here can be extended to other peptides systems such as RL_4 (lysines replaced with arginine residues), SP-B_{1-25}, and to Mini-B, a surface active fusion peptide of SP-B_{1-25} and SP-B_{59-80} (*184*). By such work, it can be clarified whether peptide mimics based upon SP-B act via a common structural intermediate and interact with lipids in a similar manner. It could also be possible that these peptide mimics can have a substantially different effect of lipid thermodynamics and lipid NMR time-scale dynamics. If so, it would imply more than one mechanism for simple peptides to achieve surface tension lowering capabilities in the lung. Also, it would be interesting to note if the helical secondary structure as reported here for KL_4 (in solution and by solid-state) is essentially the overriding secondary structure needed for proper lung surfactant function. It would be interesting to see whether even more simple peptides that follow the alpha-helical fold can be rationally designed for the treatment of RDS. These short, small molecular weight peptides may also be of aid in solving other problems involving interfacial biology or surface tension minimization.

APPENDIX A
CALCULATED ^{2}H ORDER PARAMETERS (TO 2 SIGNIFICANT FIGURES) FOR DEUTERATED LIPIDS 4:1 DPPC(D-62):POPG WITH KL_4 (MOLAR PERCENTAGES)

Table A-1 Order Parameters for sn-1 and sn-2 chain of DPPC(d-62)

sn-1 chain	Order Parameter						
Carbon number	no KL4	0.09% KL4	0.19% KL4	0.38%KL4	0.76% KL4	1.5% KL4	2.3% KL4
2	0.21	0.22	0.22	0.22	0.22	0.22	0.21
3	0.21	0.21	0.21	0.21	0.21	0.21	0.21
4	0.21	0.22	0.22	0.22	0.22	0.22	0.21
5	0.21	0.21	0.21	0.21	0.21	0.21	0.21
6	0.21	0.21	0.21	0.21	0.21	0.21	0.21
7	0.21	0.21	0.21	0.21	0.21	0.21	0.21
8	0.21	0.21	0.21	0.21	0.21	0.21	0.21
9	0.19	0.19	0.19	0.19	0.19	0.20	0.20
10	0.18	0.18	0.18	0.18	0.19	0.19	0.19
11	0.16	0.16	0.17	0.17	0.17	0.18	0.18
12	0.15	0.15	0.15	0.15	0.15	0.16	0.16
13	0.13	0.13	0.13	0.13	0.13	0.14	0.14
14	0.11	0.11	0.11	0.11	0.11	0.12	0.12
15	0.08	0.08	0.08	0.08	0.08	0.09	0.09
16	0.02	0.02	0.02	0.02	0.02	0.03	0.03
sn -2 chain							
Carbon number	no KL4	0.09% KL4	0.19% KL4	0.38% KL4	0.76% KL4	1.5% KL4	2.3% KL4
2	0.21	0.22	0.22	0.22	0.22	0.22	0.21
3	0.21	0.21	0.21	0.21	0.21	0.21	0.21
4	0.21	0.22	0.22	0.22	0.22	0.22	0.21
5	0.21	0.21	0.21	0.21	0.21	0.21	0.21
6	0.21	0.21	0.21	0.21	0.21	0.21	0.21
7	0.21	0.21	0.21	0.21	0.21	0.21	0.21
8	0.21	0.21	0.21	0.21	0.21	0.21	0.21
9	0.19	0.19	0.19	0.19	0.19	0.20	0.20
10	0.19	0.19	0.19	0.19	0.19	0.20	0.20
11	0.18	0.18	0.18	0.18	0.19	0.19	0.19
12	0.16	0.16	0.17	0.17	0.17	0.18	0.18
13	0.15	0.15	0.15	0.15	0.15	0.16	0.16
14	0.12	0.12	0.12	0.12	0.12	0.13	0.13
15	0.09	0.10	0.10	0.10	0.10	0.10	0.10
16	0.02	0.02	0.02	0.02	0.02	0.03	0.03

APPENDIX B
CALCULATED ^{2}H ORDER PARAMETERS (TO 2 SIGNFICANT FIGURES) FOR DEUTERATED LIPIDS 4:1 DPPC:POPG(D-31) WITH KL_4 (MOLAR PERCENTAGES)

Table B-1 Order Parameters for deuterated sn-1 chain of POPG

palmitoyl chain	Order Parameter		
	No		3.0%
carbon	KL4	1.0% KL4	KL4
2	0.20	0.19	0.18
3	0.20	0.19	0.18
4	0.20	0.19	0.18
5	0.20	0.19	0.18
6	0.20	0.19	0.18
7	0.20	0.19	0.18
8	0.20	0.19	0.18
9	0.18	0.18	0.17
10	0.17	0.17	0.17
11	0.16	0.16	0.16
12	0.14	0.15	0.14
13	0.12	0.13	0.13
14	0.10	0.11	0.11
15	0.08	0.08	0.08
16	0.02	0.02	0.02
	0.16	0.16	0.15

APPENDIX C

CALCULATED ^{2}H ORDER PARAMETERS (TO TWO SIGNIFICANT FIGURES) FOR DEUTERATED LIPIDS 3:1 POPC(D-31):POPG WITH KL_4 (MOLAR PERCENTAGES)

Table C-1 Order Parameters for deuterated sn-1 chain of POPC

palmitoyl chain	Order Parameter						
Carbon number	no KL4	0.09% KL4	0.19% KL4	0.38% KL4	0.76% KL4	1.5% KL4	2.3% KL4
2	0.20	0.19	0.19	0.19	0.19	0.19	0.19
3	0.20	0.19	0.19	0.19	0.19	0.19	0.19
4	0.20	0.19	0.19	0.19	0.19	0.19	0.19
5	0.20	0.19	0.19	0.19	0.19	0.19	0.19
6	0.20	0.19	0.19	0.19	0.19	0.19	0.19
7	0.20	0.19	0.19	0.19	0.19	0.19	0.19
8	0.20	0.19	0.19	0.19	0.19	0.19	0.19
9	0.17	0.17	0.17	0.17	0.17	0.17	0.17
10	0.16	0.16	0.16	0.16	0.16	0.16	0.16
11	0.14	0.14	0.14	0.14	0.14	0.14	0.14
12	0.13	0.12	0.12	0.12	0.12	0.12	0.12
13	0.11	0.11	0.11	0.11	0.10	0.11	0.11
14	0.09	0.09	0.09	0.09	0.09	0.09	0.09
15	0.07	0.07	0.06	0.06	0.06	0.07	0.07
16	0.02	0.02	0.02	0.02	0.02	0.02	0.02

APPENDIX D

CALCULATED ^{2}H ORDER PARAMETERS (TO 2 SIGNIFICANT FIGURES) FOR DEUTERATED LIPIDS IN 3:1 POPC:POPG(D-31) WITH KL_4 (MOLAR PERCENTAGES)

Table D-1 Order Parameters for deuterated sn-1 chain of POPG

palmitoyl chain	Order Parameter			
Carbon	no KL4	0.2% KL4	1.0% KL4	3.0% KL4
2	0.19	0.18	0.18	0.17
3	0.19	0.18	0.18	0.17
4	0.19	0.18	0.18	0.17
5	0.19	0.18	0.18	0.17
6	0.19	0.18	0.18	0.17
7	0.19	0.18	0.18	0.17
8	0.18	0.18	0.18	0.17
9	0.17	0.16	0.16	0.15
10	0.15	0.15	0.15	0.14
11	0.14	0.13	0.13	0.12
12	0.12	0.12	0.12	0.11
13	0.10	0.10	0.10	0.09
14	0.08	0.08	0.08	0.08
15	0.06	0.06	0.07	0.06
16	0.02	0.02	0.02	0.01

APPENDIX E
CALCULATED ^{2}H ORDER PARAMETERS (TO 2 SIGNIFICANT FIGURES) FOR DEUTERATED LIPIDS IN 4:1 DPPC(D-62):POPG WITH SP-B(59-80) (MOLAR PERCENTAGES)

Table E-1 Order parameters for sn-1 and sn-2 chain of DPPC with SP-B(59-80)

	Order Parameter						
sn-1 chain carbon	no SP-B	0.1% SP-B	0.2% SP-B	0.5% SP-B	1.0 SP-B	2.0% SP-B	3.0% SP-B
2	0.22	0.22	0.22	0.22	0.23	0.23	0.23
3	0.21	0.21	0.21	0.21	0.22	0.22	0.22
4	0.22	0.22	0.22	0.22	0.23	0.23	0.23
5	0.21	0.21	0.21	0.21	0.22	0.22	0.22
6	0.21	0.21	0.21	0.21	0.22	0.22	0.22
7	0.21	0.21	0.21	0.21	0.22	0.22	0.22
8	0.21	0.21	0.21	0.21	0.22	0.22	0.22
9	0.19	0.19	0.19	0.20	0.20	0.20	0.20
10	0.18	0.18	0.18	0.19	0.19	0.20	0.19
11	0.16	0.16	0.16	0.17	0.18	0.18	0.18
12	0.15	0.15	0.15	0.16	0.16	0.16	0.16
13	0.13	0.13	0.13	0.14	0.14	0.14	0.14
14	0.11	0.11	0.11	0.12	0.12	0.12	0.12
15	0.08	0.08	0.08	0.09	0.09	0.09	0.09
16	0.02	0.02	0.02	0.02	0.03	0.03	0.03
sn-2 chain carbon	no SP-B	0.1% SP-B	0.2% SP-B	0.5% SP-B	1.0 SP-B	2.0% SP-B	3.0% SP-B
2	0.22	0.22	0.22	0.22	0.23	0.23	0.23
3	0.21	0.21	0.21	0.21	0.22	0.22	0.22
4	0.22	0.22	0.22	0.22	0.23	0.23	0.23
5	0.21	0.21	0.21	0.21	0.22	0.22	0.22
6	0.21	0.21	0.21	0.21	0.22	0.22	0.22
7	0.21	0.21	0.21	0.21	0.22	0.22	0.22
8	0.21	0.21	0.21	0.21	0.22	0.22	0.22
9	0.19	0.19	0.19	0.20	0.20	0.20	0.20
10	0.19	0.19	0.19	0.20	0.20	0.20	0.20
11	0.18	0.18	0.18	0.19	0.19	0.20	0.19
12	0.16	0.16	0.16	0.17	0.18	0.18	0.18
13	0.15	0.15	0.15	0.16	0.16	0.16	0.16
14	0.12	0.12	0.12	0.13	0.13	0.13	0.13
15	0.10	0.10	0.10	0.10	0.10	0.10	0.10
16	0.02	0.02	0.02	0.02	0.03	0.03	0.03

APPENDIX F
CALCULATED ^{2}H ORDER PARAMETERS (TO 2 SIGNIFICANT FIGURES) FOR DEUTERATED LIPIDS IN 3:1 POPC(D-31):POPG WITH SP-B(59-80) (MOLAR PERCENTAGES)

Table F-1 Order Parameters for deuterated sn-1 chain of POPC with SP-B(59-80)

Order Parameter

Carbon	no SP-B(59-80)	0.1% SP-B(59-80)	0.5% SP-B(59-80)	1.0% SP-B(59-80)	2.0% SP-B(59-80)	3.0% SP-B(59-80)
2	0.19	0.19	0.19	0.19	0.19	0.18
3	0.19	0.19	0.19	0.19	0.19	0.18
4	0.19	0.19	0.19	0.19	0.19	0.18
5	0.19	0.19	0.19	0.19	0.19	0.18
6	0.19	0.19	0.19	0.19	0.19	0.18
7	0.19	0.19	0.19	0.19	0.19	0.18
8	0.19	0.19	0.19	0.19	0.19	0.18
9	0.16	0.16	0.16	0.17	0.15	0.15
10	0.15	0.15	0.15	0.15	0.14	0.13
11	0.13	0.13	0.13	0.13	0.13	0.13
12	0.12	0.12	0.12	0.12	0.11	0.11
13	0.10	0.10	0.10	0.10	0.10	0.10
14	0.08	0.08	0.08	0.08	0.08	0.08
15	0.06	0.06	0.06	0.06	0.06	0.06
16	0.02	0.02	0.02	0.02	0.02	0.02

LIST OF REFERENCES

1. Obladen, M. (2005) *Biol. Neonate 87*, 308-16.

2. Clements, J. A., and Avery, M. E. (1998) *Am. J. Respir. Crit. Care Med. 157*, S59-66.

3. Haagsman, H. P., and Diemel, R. V. (2001) *Comp. Biochem. Physiol. A Mol. Integr. Physiol. 129*, 91-108.

4. Veldhuizen, E. J. A., and Haagsman, H. P. (2000) *Biochimica et Biophysica Acta-Biomembranes p1467*, 255-270.

5. Creuwels, L. A., van Golde, L. M., and Haagsman, H. P. (1997) *Lung 175*, 1-39.

6. Possmayer, F., Nag, K., Rodriguez, K., Qanbar, R., and Schurch, S. (2001) *Comp. Biochem. Physiol. A Mol. Integr. Physiol. 129*, 209-20.

7. Ware, L. B., and Matthay, M. A. (2000) *N. Engl. J. Med. 342*, 1334-49.

8. Schwartz, R. M., Luby, A. M., Scanlon, J. W., and Kellogg, R. J. (1994) *N. Engl. J. Med. 330*, 1476-80.

9. Lynch, R. G. (2004) *Faseb J. 18*, 1624.

10. Wustneck, R., Perez-Gil, J., Wustneck, N., Cruz, A., Fainerman, V. B., and Pison, U. (2005) *Adv. Colloid Interface Sci. 117*, 33-58.

11. Notter, R. H. (2000) *Lung surfactants : basic science and clinical applications*, Marcel Dekker, New York.

12. Alonso, C., Waring, A., and Zasadzinski, J. A. (2005) *Biophysical Journal 89*, 266-273.

13. Banerjee, R. (2002) *Current Science 82*, 420-428.

14. Klaus, M. H., Clements, J. A., and Havel, R. J. (1961) *Proc. Natl. Acad. Sci. U S A 47*, 1858-9.

15. Gunstone, F. D., Harwood, J. L., and Padley, F. B. (1986) *The Lipid handbook*, Chapman and Hall, London ; New York.

16. Postle, A. D., Heeley, E. L., and Wilton, D. C. (2001) *Comp. Biochem. Physiol. A Mol. Integr. Physiol. 129*, 65-73.

17. Daniels, C. B., and Orgeig, S. (2001) *Comp. Biochem. Physiol. A Mol. Integr. Physiol. 129*, 9-36.

18. Tanaka, Y., Takei, T., Aiba, T., Masuda, K., Kiuchi, A., and Fujiwara, T. (1986) *J. Lipid Res. 27*, 475-85.

19. Power, J. H., Doyle, I. R., Davidson, K., and Nicholas, T. E. (1999) *J. Exp. Biol. 202*, 2543-50.

20. Kishore, U., Greenhough, T. J., Waters, P., Shrive, A. K., Ghai, R., Kamran, M. F., Bernal, A. L., Reid, K. B., Madan, T., and Chakraborty, T. (2006) *Mol. Immunol. 43*, 1293-315.

21. Mason, R. J. (2006) *Respirology 11 Suppl*, S12-5.

22. Fehrenbach, H. (2001) *Respir. Res. 2*, 33-46.

23. Weaver, T. E., and Conkright, J. J. (2001) *Annu. Rev. Physiol. 63*, 555-78.

24. Rodriguez, R. J. (2003) *Respir. Care 48*, 279-86; discussion 286-7.

25. Romero, E. J., Moya, F. R., Tuvim, M. J., and Alcorn, J. L. (2005) *Pediatric Pulmonology 39*, 167-177.

26. Whitsett, J. A., and Weaver, T. E. (2002) *N. Engl. J. Med. 347*, 2141-8.

27. Waragai, A., Yamashita, H., Hosoi, K., Hoshina, H., Noda, E., Yan, K., and Kawano, T. (2007) *Pediatr. Pulmonol. 42*, 440-5.

28. Wustneck, N., Wustneck, R., Perez-Gil, J., and Pison, U. (2003) *Biophys. J. 84*, 1940-9.

29. Johansson, J., and Curstedt, T. (1997) *Eur. J. Biochem. 244*, 675-93.

30. Hawgood, S., Derrick, M., and Poulain, F. (1998) *Biochim. Biophys. Acta 1408*, 150-60.

31. Hermans, C., and Bernard, A. (1999) *Am. J. Respir. Crit. Care Med. 159*, 646-78.

32. Walther, F. J., Gordon, L. M., Zasadzinski, J. A., Sherman, M. A., and Waring, A. J. (2000) *Mol. Genet. Metab. 71*, 342-51.

33. Munford, R. S., Sheppard, P. O., and O'Hara, P. J. (1995) *J. Lipid Res. 36*, 1653-63.

34. Walther, F. J., Waring, A. J., Sherman, M. A., Zasadzinski, J. A., and Gordon, L. M. (2007) *Neonatology 91*, 303-10.

35. Herting, E., Schiffmann, H., Roth, C., Zaltash, S., and Johannsson, J. (2002) *American Journal of Respiratory and Critical Care Medicine 166*, 1292-1294.

36. Johansson, J. (2001) *Biochemical Society Transactions 29*, 601-606.

37. Nogee, L. M. (1997) *Chest 111*, 129S-135S.

38. Wilder, M. A. (2004) *J. Perinat. Neonatal. Nurs. 18*, 61-7.

39. Clark, J. C., Wert, S. E., Bachurski, C. J., Stahlman, M. T., Stripp, B. R., Weaver, T. E., and Whitsett, J. A. (1995) *Proc. Natl. Acad. Sci. U S A 92*, 7794-8.

40. Hamvas, A. (2006) *Semin. Perinatol. 30*, 316-26.

41. Griese, M., Schumacher, S., Tredano, M., Steinecker, M., Braun, A., Guttentag, S., Beers, M. F., and Bahuau, M. (2005) *Respir. Res. 6*, 80.

42. Doyle, I. R., Davidson, K. G., Barr, H. A., Nicholas, T. E., Payne, K., and Pfitzner, J. (1998) *Am. J. Respir. Crit. Care Med. 157*, 658-64.

43. Qi, X., Leonova, T., and Grabowski, G. A. (1994) *J. Biol. Chem. 269*, 16746-53.

44. Ahn, V. E., Faull, K. F., Whitelegge, J. P., Higginson, J., Fluharty, A. L., and Prive, G. G. (2003) *Protein Expr. Purif. 27*, 186-93.

45. Ahn, V. E., Faull, K. F., Whitelegge, J. P., Fluharty, A. L., and Prive, G. G. (2003) *Proc. Natl. Acad. Sci. U S A 100*, 38-43.

46. John, M., Wendeler, M., Heller, M., Sandhoff, K., and Kessler, H. (2006) *Biochemistry 45*, 5206-16.

47. Zaltash, S., Palmblad, M., Curstedt, T., Johansson, J., and Persson, B. (2000) *Biochim. Biophys. Acta 1466*, 179-86.

48. Serrano, A. G., Cabre, E. J., Oviedo, J. M., Cruz, A., Gonzalez, B., Palacios, A., Estrada, P., and Perez-Gil, J. (2006) *Biochim. Biophys. Acta 1758*, 1621-32.

49. Phizackerley, P. J., Town, M. H., and Newman, G. E. (1979) *Biochem. J. 183*, 731-6.

50. Yu, S. H., and Possmayer, F. (1986) *Biochem. J. 236*, 85-9.

51. Ballard, P. L., Nogee, L. M., Beers, M. F., Ballard, R. A., Planer, B. C., Polk, L., deMello, D. E., Moxley, M. A., and Longmore, W. J. (1995) *Pediatrics 96*, 1046-52.

52. Longo, M. L., Bisagno, A. M., Zasadzinski, J. A., Bruni, R., and Waring, A. J. (1993) *Science 261*, 453-6.

53. Hall, S. B., Wang, Z., and Notter, R. H. (1994) *J. Lipid Res. 35*, 1386-94.

54. Baatz, J. E., Zou, Y., Cox, J. T., Wang, Z., and Notter, R. H. (2001) *Protein. Expr. Purif. 23*, 180-90.

55. Curstedt, T., Jornvall, H., Robertson, B., Bergman, T., and Berggren, P. (1987) *Eur. J. Biochem. 168*, 255-62.

56. Gustafsson, M., Curstedt, T., Jornvall, H., and Johansson, J. (1997) *Biochemical Journal 326*, 799-806.

57. Vincent, J. S., Revak, S. D., Cochrane, C. G., and Levin, I. W. (1991) *Biochemistry 30*, 8395-401.

58. Piknova, B., Schief, W. R., Vogel, V., Discher, B. M., and Hall, S. B. (2001) *Biophys. J. 81*, 2172-80.

59. Paschen, C., and Griese, M. (2005) *J. Chromatogr. B Analyt. Technol. Biomed. Life Sci. 814*, 325-30.

60. Piknova, B., Schram, V., and Hall, S. B. (2002) *Curr. Opin. Struct. Biol. 12*, 487-94.

61. Mazela, J., Merritt, T. A., Gadzinowski, J., and Sinha, S. (2006) *Acta. Paediatr. 95*, 1036-48.

62. Fujiwara, T., Maeta, H., Chida, S., Morita, T., Watabe, Y., and Abe, T. (1980) *Lancet 1*, 55-9.

63. Bringezu, F., Ding, J. Q., Brezesinski, G., and Zasadzinski, J. A. (2001) *Langmuir 17*, 4641-4648.

64. Lee, K. Y. C., Gopal, A., von Nahmen, A., Zasadzinski, J. A., Majewski, J., Smith, G. S., Howes, P. B., and Kjaer, K. (2002) *Journal of Chemical Physics 116*, 774-783.

65. Perez-Gil, J., and Keough, K. M. W. (1998) *Biochimica et Biophysica Acta-Molecular Basis of Disease 1408*, 203-217.

66. Baudouin, S. V. (2004) *N. Engl. J. Med. 351*, 853-5.

67. Seurynck, S. L., Patch, J. A., and Barron, A. E. (2005) *Chemistry & Biology 12*, 77-88.

68. Merritt, T. A., Kheiter, A., and Cochrane, C. G. (1995) *Pediatr. Res. 38*, 211-7.

69. Cochrane, C. G., Revak, S. D., Merritt, T. A., Heldt, G. P., Hallman, M., Cunningham, M. D., Easa, D., Pramanik, A., Edwards, D. K., and Alberts, M. S. (1996) *Am. J. Respir. Crit. Care. Med. 153*, 404-10.

70. Cochrane, C. G., Revak, S. D., Merritt, T. A., Schraufstatter, I. U., Hoch, R. C., Henderson, C., Andersson, S., Takamori, H., and Oades, Z. G. (1998) *Pediatr. Res. 44*, 705-15.

71. Ryan, M. A., Akinbi, H. T., Serrano, A. G., Perez-Gil, J., Wu, H., McCormack, F. X., and Weaver, T. E. (2006) *J. Immunol. 176*, 416-25.

72. Kinniry, P., Pick, J., Stephens, S., Jain, D., Solomides, C. C., Niven, R., Segal, R., and Christofidou-Solomidou, M. (2006) *Pediatr. Pulmonol. 41*, 916-28.

73. Wang, Y. D., Rao, K. M. K., and Demchuk, E. (2003) *Biochemistry 42*, 4015-4027.

74. Sreerama, N., and Woody, R. W. (2000) *Anal. Biochem. 287*, 252-60.

75. Sreerama, N., and Woody, R. W. (2004) *Methods Enzymol. 383*, 318-51.

76. Bulheller, B. M., Rodger, A., and Hirst, J. D. (2007) *Phys. Chem. Chem. Phys. 9*, 2020-35.

77. Wallace, B. A., Lees, J. G., Orry, A. J., Lobley, A., and Janes, R. W. (2003) *Protein Sci. 12*, 875-84.

78. White, S. H., Wimley, W. C., Ladokhin, A. S., and Hristova, K. (1998) *Methods Enzymol. 295*, 62-87.

79. Ramamoorthy, A., Thennarasu, S., Lee, D. K., Tan, A., and Maloy, L. (2006) *Biophys. J. 91*, 206-16.

80. Epand, R. F., Lehrer, R. I., Waring, A., Wang, W., Maget-Dana, R., Lelievre, D., and Epand, R. M. (2003) *Biopolymers 71*, 2-16.

81. Kumaran, S., and Roy, R. P. (1999) *J. Pept. Res. 53*, 284-93.

82. Mcelhaney, R. N. (1982) *Chemistry and Physics of Lipids 30*, 229-259.

83. Alberts, B. (1994) *Molecular biology of the cell*, 3rd ed., Garland Pub., New York.

84. Yeagle, P. (2005) *The Structure of biological membranes*, 2nd ed., CRC Press, Boca Raton, Fla.

85. Epand, R. M. (2006) *Biophys. Chem*.

86. Chen, S. C., Sturtevant, J. M., and Gaffney, B. J. (1980) *Proc. Natl. Acad. Sci. U S A 77*, 5060-3.

87. Ye, Q., and Biltonen, R. L. (1994) *Subcell. Biochem. 23*, 121-60.

88. Huang, C., and Li, S. (1999) *Biochim. Biophys. Acta 1422*, 273-307.

89. Sturtevant, J. M. (1987) *Annual Review of Physical Chemistry 38*, 463-488.

90. Kaznessis, Y. N., Kim, S., and Larson, R. G. (2002) *J. Mol. Biol. 322*, 569-82.

91. Papahadjopoulos, D., Moscarello, M., Eylar, E. H., and Isac, T. (1975) *Biochimica et Biophysica Acta 401*, 317-335.

92. McMullen, T. P., Lewis, R. N., and McElhaney, R. N. (1993) *Biochemistry 32*, 516-22.

93. Liu, F., Lewis, R. N. A. H., Hodges, R. S., and McElhaney, R. N. (2002) *Biochemistry 41*, 9197-9207.

94. Seelig, J. (1978) *Biochim. Biophys. Acta 515*, 105-40.

95. Laws, D. D., Bitter, H. M., and Jerschow, A. (2002) *Angew Chem. Int. Ed. Engl. 41*, 3096-129.

96. Drechsler, A., and Separovic, F. (2003) *IUBMB Life 55*, 515-23.

97. Marassi, F. M., and Opella, S. J. (1998) *Curr. Opin. Struct. Biol. 8*, 640-8.

98. Duer, M. J. (2004) *Introduction to solid-state NMR spectroscopy*, Blackwell, Oxford, UK ; Malden, MA.

99. Luca, S., Heise, H., and Baldus, M. (2003) *Acc. Chem. Res. 36*, 858-65.

100. Levitt, M. H. (2001) *Spin dynamics : basics of nuclear magnetic resonance*, John Wiley & Sons, Chichester ; New York.

101. Haacke, E. M. (1999) *Magnetic resonance imaging : physical principles and sequence design*, J. Wiley & Sons, New York.

102. Sternin, E., Bloom, M., and Mackay, A. L. (1983) *Journal of Magnetic Resonance 55*, 274-282.

103. Sternin, E., Schafer, H., Polozov, I. V., and Gawrisch, K. (2001) *J. Magn. Reson. 149*, 110-3.

104. Seelig, A., and Seelig, J. (1974) *Biochemistry 13*, 4839-45.

105. Bloom, M., Davis, J. H., and Mackay, A. L. (1981) *Chemical Physics Letters 80*, 198-202.

106. Bechinger, B., Kinder, R., Helmle, M., Vogt, T. C., Harzer, U., and Schinzel, S. (1999) *Biopolymers 51*, 174-90.

107. Stockton, G. W., Polnaszek, C. F., Tulloch, A. P., Hasan, F., and Smith, I. C. (1976) *Biochemistry 15*, 954-66.

108. Cullis, P. R., and de Kruijff, B. (1979) *Biochim. Biophys. Acta 559*, 399-420.

109. Marassi, F. M., and Crowell, K. J. (2003) *Journal of Magnetic Resonance 161*, 64-69.

110. Bechinger, B. (2001) *FEBS Lett. 504*, 161-5.

111. Bechinger, B., Aisenbrey, C., and Bertani, P. (2004) *Biochim. Biophys. Acta 1666*, 190-204.

112. Bechinger, B. (2005) *Biochim. Biophys. Acta 1712*, 101-8.

113. Bechinger, B., and Lohner, K. (2006) *Biochimica et Biophysica Acta-Biomembranes 1758*, 1529-1539.

114. Dais, P., and Spyros, A. (2007) *Magn. Reson. Chem. 45*, 367-77.

115. Schiller, J., and Arnold, K. (2002) *Med. Sci. Monit. 8*, MT205-22.

116. Hetherington, H. P., Pan, J. W., and Spencer, D. D. (2002) *J. Magn. Reson. Imaging 16*, 477-83.

117. Seelig, J., and Niederbe.W. (1974) *Journal of the American Chemical Society 96*, 2069-2072.

118. Seelig, J., and Seelig, A. (1980) *Q. Rev. Biophys. 13*, 19-61.

119. Pastor, R. W., Venable, R. M., and Feller, S. E. (2002) *Acc. Chem. Res. 35*, 438-46.

120. Schafer, H., Madler, B., and Sternin, E. (1998) *Biophys. J. 74*, 1007-14.

121. Lafleur, M., Fine, B., Sternin, E., Cullis, P. R., and Bloom, M. (1989) *Biophys. J. 56*, 1037-41.

122. Vermeer, L. S., de Groot, B. L., Reat, V., Milon, A., and Czaplicki, J. (2007) *Eur. Biophys. J*.

123. Burnett, L. J., and Muller, B. H. (1971) *Journal of Chemical Physics 55*, 5829-&.

124. Petrache, H. I., Dodd, S. W., and Brown, M. F. (2000) *Biophys. J. 79*, 3172-92.

125. Paddy, M. R., Dahlquist, F. W., Dratz, E. A., and Deese, A. J. (1985) *Biochemistry 24*, 5988-95.

126. Thurmond, R. L., Dodd, S. W., and Brown, M. F. (1991) *Biophysical Journal 59*, 108-113.

127. de Planque, M. R., Greathouse, D. V., Koeppe, R. E., 2nd, Schafer, H., Marsh, D., and Killian, J. A. (1998) *Biochemistry 37*, 9333-45.

128. Curtis, R. D., Tonge, P. J., Smith, I. C. P., and Jarrell, H. C. (1993) *Journal of Magnetic Resonance Series A 102*, 110-113.

129. Yue, J., and Cushley, R. J. (1990) *Biochimica et Biophysica Acta 1047*, 1-10.

130. Qiu, X., Mirau, P. A., and Pidgeon, C. (1993) *Biochim. Biophys. Acta 1147*, 59-72.

131. Brumm, T., Mops, A., Dolainsky, C., Bruckner, S., and Bayerl, T. M. (1992) *Biophysical Journal 61*, 1018-1024.

132. Sanders, C. R., Schaff, J. E., and Prestegard, J. H. (1993) *Biophysical Journal 64*, 1069-1080.

133. Cochrane, C. G., and Revak, S. D. (1991) *Science 254*, 566-8.

134. Cochrane, C. G., and Revak, S. D. (1994) *Chest 105*, 57S-62S.

135. Serrano, A. G., and Perez-Gil, J. (2006) *Chem. Phys. Lipids 141*, 105-18.

136. Ghodrat, M. (2006) *Am. J. Health Syst. Pharm. 63*, 1504-21.

137. Gupta, M., Hernandez-Juviel, J. M., Waring, A. J., Bruni, R., and Walther, F. J. (2000) *Eur. Respir. J. 16*, 1129-33.

138. Robertson, B., Johansson, J., and Curstedt, T. (2000) *Mol. Med. Today 6*, 119-24.

139. Perkins, W. R., Dause, R. B., Parente, R. A., Minchey, S. R., Neuman, K. C., Gruner, S. M., Taraschi, T. F., and Janoff, A. S. (1996) *Science 273*, 330-2.

140. Moya, F. R., Gadzinowski, J., Bancalari, E., Salinas, V., Kopelman, B., Bancalari, A., Kornacka, M. K., Merritt, T. A., Segal, R., Schaber, C. J., Tsai, H., Massaro, J., and d'Agostino, R. (2005) *Pediatrics 115*, 1018-29.

141. Ma, J. W., Koppenol, S., Yu, H. U., and Zografi, G. (1998) *Biophysical Journal 74*, 1899-1907.

142. Saenz, A., Canadas, O., Bagatolli, L. A., Johnson, M. E., and Casals, C. (2006) *Febs J. 273*, 2515-27.

143. Seelig, J., Borle, F., and Cross, T. A. (1985) *Biochimica et Biophysica Acta 814*, 195-198.

144. Siminovitch, D. J. (1998) *Biochem. Cell Biol. 76*, 411-22.

145. Nagle, J. F. (1993) *Biophysical Journal 64*, 1476-1481.

146. Strandberg, E., Morein, S., Rijkers, D. T. S., Liskamp, R. M. J., van der Wel, P. C. A., and Killian, J. A. (2002) *Biochemistry 41*, 7190-7198.

147. Vogt, B., Ducarme, P., Schinzel, S., Brasseur, R., and Bechinger, B. (2000) *Biophysical Journal 79*, 2644-2656.

148. Gustafsson, M., Vandenbussche, G., Curstedt, T., Ruysschaert, J. M., and Johansson, J. (1996) *FEBS Lett. 384*, 185-8.

149. Long, J. R., Oyler, N., Drobny, G. P., and Stayton, P. S. (2002) *J. Am. Chem. Soc. 124*, 6297-303.

150. Degrado, W. F., and Lear, J. D. (1985) *Journal of the American Chemical Society 107*, 7684-7689.

151. Kiyota, T., Lee, S., and Sugihara, G. (1996) *Biochemistry 35*, 13196-204.

152. Speyer, J. B., Sripada, P. K., Das Gupta, S. K., Shipley, G. G., and Griffin, R. G. (1987) *Biophys. J. 51*, 687-91.

153. Lu, J. X., Blazyk, J., and Lorigan, G. A. (2006) *Biochim. Biophys. Acta. 1758*, 1303-13.

154. Pott, T., and Dufourc, E. J. (1995) *Biophys. J. 68*, 965-77.

155. Naito, A., Nagao, T., Obata, M., Shindo, Y., Okamoto, M., Yokoyama, S., Tuzi, S., and Saito, H. (2002) *Biochimica et Biophysica Acta-Biomembranes 1558*, 34-44.

156. Marcotte, I., Wegener, K. L., Lam, Y. H., Chia, B. C., de Planque, M. R., Bowie, J. H., Auger, M., and Separovic, F. (2003) *Chem. Phys. Lipids 122*, 107-20.

157. Hwang, P. M., and Vogel, H. J. (1998) *Biochemistry and Cell Biology-Biochimie Et Biologie Cellulaire 76*, 235-246.

158. Lu, J. X., Caporini, M. A., and Lorigan, G. A. (2004) *Journal of Magnetic Resonance 168*, 18-30.

159. Tiburu, E. K., Dave, P. C., and Lorigan, G. A. (2004) *Magn. Reson. Chem. 42*, 132-8.

160. Killian, J. A. (1998) *Biochim. Biophys. Acta. 1376*, 401-15.

161. Smondyrev, A. M., and Berkowitz, M. L. (1999) *Biophys. J. 77*, 2075-89.

162. Hofsass, C., Lindahl, E., and Edholm, O. (2003) *Biophys. J. 84*, 2192-206.

163. Xu, X., and London, E. (2000) *Biochemistry 39*, 843-9.

164. de Lange, M. J., Bonn, M., and Muller, M. (2007) *Chem. Phys. Lipids 146*, 76-84.

165. Strandberg, E., and Killian, J. A. (2003) *FEBS Lett. 544*, 69-73.

166. Cai, P., Flach, C. R., and Mendelsohn, R. (2003) *Biochemistry 42*, 9446-52.

167. Pare, C., Lafleur, M., Liu, F., Lewis, R. N., and McElhaney, R. N. (2001) *Biochim. Biophys. Acta. 1511*, 60-73.

168. Harzer, U., and Bechinger, B. (2000) *Biochemistry 39*, 13106-13114.

169. Rohl, C. A., and Baldwin, R. L. (1997) *Biochemistry 36*, 8435-42.

170. Fernandez-Vidal, M., Jayasinghe, S., Ladokhin, A. S., and White, S. H. (2007) *J. Mol. Biol. 370*, 459-70.

171. Fodje, M. N., and Al-Karadaghi, S. (2002) *Protein Eng. 15*, 353-8.

172. Creighton, T. E. (1993) *Proteins : structures and molecular properties*, 2nd ed., W.H. Freeman, New York.

173. Brändén, C.-I., and Tooze, J. (1999) *Introduction to protein structure*, 2nd ed., Garland Pub., New York.

174. Kaiser, E. T., and Kezdy, F. J. (1983) *Proc. Natl. Acad. Sci. U S A 80*, 1137-43.

175. Gordon, L. M., Mobley, P. W., Lee, W., Eskandari, S., Kaznessis, Y. N., Sherman, M. A., and Waring, A. J. (2004) *Protein Sci. 13*, 1012-30.

176. Kandasamy, S. K., and Larson, R. G. (2005) *Biophys. .J 88*, 1577-92.

177. Booth, V., Waring, A. J., Walther, F. J., and Keough, K. M. (2004) *Biochemistry 43*, 15187-94.

178. Kang, J. H., Lee, M. K., Kim, K. L., and Hahm, K. S. (1996) *Biochem. Mol. Biol. Int. 40*, 617-27.

179. Dico, A. S., Hancock, J., Morrow, M. R., Stewart, J., Harris, S., and Keough, K. M. (1997) *Biochemistry 36*, 4172-7.

180. Morrow, M. R., Perez-Gil, J., Simatos, G., Boland, C., Stewart, J., Absolom, D., Sarin, V., and Keough, K. M. (1993) *Biochemistry 32*, 4397-402.

181. Morrow, M. R., Temple, S., Stewart, J., and Keough, K. M. (2007) *Biophys. J. 93*, 164-75.

182. Morrow, M. R., Stewart, J., Taneva, S., Dico, A., and Keough, K. M. (2004) *Eur. Biophys. J. 33*, 285-90.

183. Nag, K., Keough, K. M., and Morrow, M. R. (2006) *Biophys. J. 90*, 3632-42.

184. Waring, A. J., Walther, F. J., Gordon, L. M., Hernandez-Juviel, J. M., Hong, T., Sherman, M. A., Alonso, C., Alig, T., Braun, A., Bacon, D., and Zasadzinski, J. A. (2005) *J. Pept. Res. 66*, 364-74.

BIOGRAPHICAL SKETCH

Vijay C. Antharam got his Bachelor of Science degree in microbiology and cell science at the University of Florida, where he graduated in 3 years. He joined the PhD program in biomedical sciences at the University of Florida in the Fall of 2002 and joined the lab of Joanna R.Long in 2003. His interests include biophysics, structural biology, medicine, and playing chess.